Inaugural dissertation

for

obtaining the doctoral degree

of the

Combined Faculty of Mathematics, Engineering and Natural Sciences

of the

Ruprecht - Karls - University Heidelberg

Presented by: Monami Roy Chowdhury (M.Sc.)
Born in: Kolkata, India
Oral examination: 16.05.2025

Studying the role of Thrombospondin-related protein 1 (TRP1) in sporozoite motility and its journey through the mosquito

Referees:

1. Prof. Dr. Ulrich Schwarz
2. Prof. Dr. Friedrich Frischknecht

Affidavit

I hereby declare that the experiments for the presented work were conducted between April 2021 and December 2024 in the laboratory of Prof. Dr. Friedrich Frischknecht at the parasitology unit of the centre of infectious diseases at the Ruperto-Carola University in Heidelberg.

Furthermore, I declare that I used no resources other than those indicated in my thesis.
Heidelberg, 28.02.2025

Monami Roy Chowdhury

Oral presentation:

First examiner: Prof. Dr. Ulrich Schwarz

Second examiner: Prof. Dr. Friedrich Frischknecht

Examination date: 16.05.2025

For My beloved family
And Dominik

Acknowledgement

I would like to express my deepest gratitude to Prof. Dr. Friedrich Frischknecht for giving me the opportunity to join his laboratory at the Center for Integrative Infectious Disease Research, Heidelberg University, for my doctoral research—especially during the challenging times of the COVID-19 pandemic. I would like to thank Freddy for his patience, trust and for taking a chance on me. Your willingness to grant me independence and flexibility in project planning allowed me to grow as a researcher. Your dedication and commitment to excellence continuously fueled my passion and drive throughout this journey. Being part of the Frischknecht lab was an incredible experience and I truly cherished the opportunity to learn from my peers and colleagues.

I am also immensely grateful to my TAC members, Prof. Dr. Ulrich Schwarz, Dr. Petr Chlanda, Dr. Markus Ganter and Dr. Ada Cavalcanti, for their invaluable insights and guidance throughout my PhD journey. I sincerely thank Prof. Dr. Ulrich Schwarz, Dr. Petr Chlanda and Dr. Viet Loan Dao Thi for agreeing to be a part of my PhD defense committee.

I would like to sincerely thank Dr. Matthias Wagner, Dr. Mirko Singer, and Kevin Walz for proofreading my thesis and providing invaluable insights. The thought-provoking discussions with you all were among the highlights of my PhD journey. I am also deeply grateful to Yvonne Sokolowski, Annika Binder, Lilian Dorner, Dr. Julia Sattler, and Dr. Franziska Hentzschel, as well as all members of AG Frischknecht and AG Hentzschel, for their support, guidance, and stimulating scientific discussions throughout my PhD project.

Matthias- Thank you for checking on me personally when I broke my arm and being a constant guide while I was writing my thesis.

Mirko- Thank you for always giving me your time and suggestions regarding the project. Your constant support while I was writing my thesis was invaluable.

Franzi- Thank you for being a role model for me in science. Your work ethic, grit and passion for research motivates me every day.

Kevin- Thank you for teaching me everything with the patience of a monk about the lab when I first started my journey in the Frischknecht lab.

Yvonne- Thank you for being my first PhD conference mate and a friend in and out of the lab. I cherish every moment with you.
Annika- Thank you for all the meaningful discussions over lunches and making sure the lab was in a Christmas spirit as soon as December came. I learned so much from you through my time in the Frischknecht lab.
Lilian- Thank you for being my first friend in the lab. We started our journey in this lab together and look at us now. Thank you for opening my eyes about french cheese and wine and all the fun times in Alsace.

A special thanks to master's students—Marzia Matejcek, Bea Jagodic, Jacob Kerbl Knapp, and Nina Schmidt—for their dedication and hard work on this project. Your contributions have been truly invaluable, and I deeply appreciate the time and effort you invested in this research.

I would also like to thank members of AG Lanzer, AG Ingham, AG Ganter and former AG Guizetti for all the wonderful discussions we got to have. Dr. Guillermo Gomez, Dr. Jessica Kehrer, Dr. Anja Klemmer, Antonia Böhmert, Natalie Portwood, Carlos Lol, Kim Carlstedt and Violetta Pancakova thank you for all the great discussions we had over Radler and coffee.

I am grateful to the HBIGS PhD Program for creating such an enriching and enjoyable environment during my PhD. The diverse courses—both within and beyond the academic curriculum—helped broaden my perspectives and prepared me for the next stage of my career. A big thanks also to Deutsche Forschungsgemeinschaft (DFG, German Research Foundation): SFB 1129 for generously funding my PhD research and making this work possible.

I would like to take a special moment to thank my partner, Dominik Häußermann, who has been my unwavering rock throughout this challenging yet rewarding journey. Your love, patience, and constant support, along with the warmth and kindness of the entire Häußermann family, have been my greatest source of strength.

My deepest gratitude goes to my incredible family and friends back in India—your boundless enthusiasm and positivity carried me through the tough days. Dr. Soham Basu and Dr. Poulami

Kumar- thank you for over a decade of friendship and the countless adventures we shared; growing up alongside you has been a privilege. Little Cappuccino- thank you for being my companion during late study nights and for all the emotional support—you made this journey a little lighter and my heart a lot fuller.

Lastly, A special thanks to my father Uttam Roy Chowdhury, my greatest pillar of strength, for never clipping my wings, even when my dreams seemed outlandish to others. Thank you for always reminding me of my capabilities, for pushing me to never settle, and for keeping the fire within me alive. This is just the beginning.

Summary

Malaria remains one of the most devastating parasitic diseases, affecting millions worldwide and accounting for the highest mortality among parasitic infections. Caused by unicellular eukaryotic parasites of the genus *Plasmodium* and transmitted by various mosquito species within the *Anopheles* genus. While the disease manifests through the parasite's asexual replication in red blood cells, sexual reproduction occurs within the mosquito. This stage is critical for ensuring genetic diversity and facilitating the parasite's transmission to new hosts.

Plasmodium has evolved a complex life cycle consisting of distinct developmental stages, traversing between a mosquito vector and a mammalian host. The transmissive stage of the parasite and the final developmental stage within the mosquito is the sporozoite, a crescent-shaped, chiral, single celled organism with a highly specialized proteome evolved for efficient host cell invasion and disease transmission. From a single oocyst beneath the basal lamina of the mosquito midgut, thousands of sporozoites develop, uniquely adapted for migration to the salivary glands. There, they undergo further maturation and await transmission during the mosquito's next blood meal. Sporozoite motility is a crucial factor in accomplishing this journey, as their incredible speed, powered by gliding motility, is essential for successful transmission to the host. In this study I investigated the role of Thrombospondin related protein 1 (TRP1) in sporozoite's journey through the mosquito and transmission to the host. TRP1 is a TRAP-related protein, expressed in the late oocyst and salivary gland sporozoite stages and has been identified to be playing a key role in activating sporozoite motility within the oocyst and facilitating its egress. The N-terminus of the TRP1 protein was found to play a role in salivary gland invasion whereas the C-terminus was determined to be crucial for both egress from the oocyst and salivary gland invasion. In this study, I have dissected the roles of different domains of *Plasmodium berghei* TRP1 to better understand the molecular mechanisms through which the protein plays a role in sporozoite motility, egress and invasion via various genetic approaches.

Firstly, I have generated several C-terminus deletion mutants and C-terminus domain swap mutants at the TRP1 C-terminus to identify the key residues involved in sporozoite motility and salivary gland invasion. These studies revealed that contrary to the previous studies, the TRP1 C-terminus is not involved in sporozoite egress but rather plays a crucial role in sporozoite

motility and salivary gland invasion. Perturbation of the C-terminus domain resulted in the loss of productive motility in sporozoites and resulted in no transmission to host. Interestingly, the C-terminal domain of *Plasmodium berghei* TRAP—a well-characterized sporozoite surface protein crucial for motility and invasion—failed to rescue TRP1 function. In contrast, the much shorter C-terminal tail of *Plasmodium falciparum* TRP1 fully restored TRP1 functionality, highlighting the specificity of TRP1's C-terminal interactions in sporozoite motility and invasion.

Next, I investigated the role of the N-terminus and the adjacent highly conserved Thrombospondin repeat (TSR) domain in the TRP1 function. To do this, I generated several TSR domain mutants, including a complete TSR domain deletion, point mutations in conserved tryptophan residues, and a TSR domain swap with the *P. berghei* TRAP TSR domain. These experiments demonstrated the critical role of the TSR domain in sporozoite motility and salivary gland invasion, with the conserved tryptophan residues being essential for its function. Interestingly, despite its high conservation, the TRAP TSR domain was unable to rescue the function of the TRP1 TSR domain, highlighting the specificity of TRP1's TSR interactions in these processes.

I also successfully generated a functional C-terminal GFP-tagged TRP1 by inserting the tag upstream of the C-terminal domain. Building on this, I developed a dual-tagged TRP1 by introducing an N-terminal FLAG tag in the C-terminal GFP-tagged TRP1-expressing parasites. This approach provided deeper insights into the localization of TRP1 in sporozoites and the fate of its N- and C-terminal regions within the parasite.

Lastly, building on the successful tagging of TRP1 upstream of the C-terminus with GFP, I generated tagged versions of TRP1 for proximity biotinylation by fusing it with APEX or miniTurbo to identify C-terminal interaction partners using proximity-dependent biotinylation. Due to time constraints, I conducted biotinylation experiments exclusively with TRP1-APEX, leading to the identification of 307 unique proteins through three independent experiments and subsequent MS analysis. Among these, we identified nine uncharacterized proteins, six of which exhibit high expression levels during the mosquito stages of the parasite. This experiment

provided valuable insights into the potential interaction partners of TRP1 and its critical role in sporozoite motility, salivary gland invasion, and host transmission.

In conclusion, TRP1 plays a crucial role in sporozoite motility, salivary gland invasion, and transmission to the host. Contrary to previous findings, my study revealed that the TRP1 C-terminus is not required for sporozoite egress but is essential for motility and invasion, with its function being highly specific and not interchangeable with the TRAP C-terminus. Similarly, the highly conserved TSR domain at the N-terminus was found to be indispensable for these processes, with conserved tryptophan residues playing a key role. Localization studies using dual-tagged TRP1 provided further insights into the spatial dynamics of the protein in sporozoites. Additionally, proximity biotinylation experiments identified a set of potential interaction partners, including several uncharacterized proteins highly expressed in the mosquito stages, shedding light on the molecular network in which TRP1 operates. Collectively, these findings enhance our understanding of TRP1's unique and indispensable role in *Plasmodium* sporozoite biology and its contribution to parasite transmission.

Zusammenfassung

Malaria bleibt eine der verheerendsten parasitären Krankheiten, betrifft weltweit Millionen von Menschen und weist die höchste Sterblichkeitsrate unter parasitären Infektionen auf. Die Krankheit wird durch einzellige eukaryotische Parasiten der Gattung *Plasmodium* verursacht, die von verschiedenen Stechmückenarten innerhalb der Gattung *Anopheles* übertragen werden. Während die Krankheit durch die asexuelle Replikation des Parasiten in roten Blutzellen hervorgerufen wird, findet die sexuelle Fortpflanzung in der Mücke statt. Dieses Stadiumist entscheidend, da sie die genetische Vielfalt sicherstellt und die Übertragung des Parasiten auf neue Wirte ermöglicht.

Um diese Anpassungen zu erreichen, hat *Plasmodium* einen komplexen Lebenszyklus mit verschiedenen Entwicklungsstadien entwickelt, in dem es zwischen einem Moskito-Vektor und einem Säugetierwirt wechselt. Das übertragungsfähige Stadium des Parasiten und die letzte Entwicklungsphase im Moskito ist der Sporozoit – eine halbmondförmiger, chiraler, einzelliger Organismus mit einem hochspezialisierten Proteom, das für eine effiziente Wirtszellinvasion und Krankheitsübertragung optimiert ist. Aus einer einzigen Oozyste, die sich unter der Basallamina des Moskitomitteldarms befindet, entwickeln sich Tausende von Sporozoiten, die einzigartig an die Migration zu den Speicheldrüsen angepasst sind. Dort reifen sie weiter und warten auf die Übertragung während der nächsten Blutmahlzeit des Moskitos. Die Motilität der Sporozoiten ist ein entscheidender Faktor für diesen Weg, da ihre enorme Geschwindigkeit, die durch „gleitende Motilität“ (Gliding Motility) angetrieben wird, für eine erfolgreiche Übertragung auf den Wirt unerlässlich ist.

In dieser Studie habe ich die Rolle des “Thrombospondin-related protein 1” (TRP1) bei der Wanderung der Sporozoiten durch den Moskito und ihrer Übertragung auf den Wirt untersucht. TRP1 ist ein TRAP-verwandtes Protein, das in späten Oozysten- und Speicheldrüsen-Sporozoiten exprimiert wird und eine Schlüsselrolle bei der Aktivierung der Sporozoitenmotilität innerhalb der Oozyste sowie bei deren Austritt spielt. Während das N-terminale Ende von TRP1 eine Rolle bei der Invasion der Speicheldrüse spielt, ist das C-terminale Ende sowohl für den Austritt aus der Oozyste als auch für die Speicheldrüseninvasion entscheidend. In dieser Studie habe ich die Funktionen verschiedener

Domänen von *Plasmodium berghei* TRP1 untersucht, um die molekularen Mechanismen besser zu verstehen, durch die das Protein an der Sporozoitenmotilität, am Austritt und an der Invasion beteiligt ist, wobei ich verschiedene genetische Herangehensweisen verwendet habe.

Zunächst habe ich mehrere Mutanten erzeugt in denen ich den C-terminus von TRP1 deletiert oder ausgetauscht habe, um die Schlüsselsequenzen zu identifizieren, die an der Sporozoitenmotilität und der Speicheldrüseninvasion beteiligt sind. Diese Untersuchungen ergaben, dass entgegen früheren Studien der TRP1-C-Terminus nicht an der Freisetzung der Sporozoiten beteiligt ist, sondern eine entscheidende Rolle bei der Motilität und Invasion spielt. Eine Störung der C-terminalen Domäne führte zum Verlust produktiver Motilität in Sporozoiten und verhinderte deren Übertragung auf den Wirt. Interessanterweise konnte die C-terminale Domäne von *Plasmodium berghei* TRAP – einem gut charakterisierten Sporozoiten-Oberflächenprotein, das für Motilität und Invasion essenziell ist – die Funktion von TRP1 nicht ersetzen. Im Gegensatz dazu konnte die wesentlich kürzere C-terminale Domäne von *Plasmodium falciparum* TRP1 die Funktion vollständig wiederherstellen, was die Spezifität der C-terminalen Interaktionen von TRP1 bei der Sporozoitenmotilität und Invasion unterstreicht.

Anschließend habe ich die Rolle des N-Terminus und der angrenzenden hochkonservierten TSR-Domäne für die Funktion von TRP1 untersucht. Dazu habe ich verschiedene TSR-Domänenmutanten erzeugt, darunter eine vollständige Deletion der TSR-Domäne, Punktmutationen in konservierten Tryptophanresten und einen Austausch mit der TSR-Domäne von *P. berghei* TRAP. Diese Experimente zeigten die entscheidende Rolle der TSR-Domäne für die Sporozoitenmotilität und die Speicheldrüseninvasion, wobei die konservierten Tryptophanreste für ihre Funktion essenziell sind. Interessanterweise konnte die TSR-Domäne von TRAP trotz ihrer hohen Konservierung die Funktion der TSR-Domäne von TRP1 nicht ersetzen, was auf die Spezifität von Interaktionen der TRP1-TSR-Domäne in diesen Prozessen hinweist.

Ich habe außerdem erfolgreich ein funktionelles C-terminal GFP-getaggtes TRP1 erzeugt, indem ich das GFP vor der C-terminalen Domäne eingefügt habe. Aufbauend auf diesem Erfolg habe ich ein doppelt getaggtes TRP1 entwickelt, indem ich ein N-terminales FLAG-Tag in die C-terminal GFP-getaggten TRP1-exprimierenden Parasiten integriert habe. Dieser Ansatz

ermöglichte tiefere Einblicke in die Lokalisation von TRP1 in Sporozoiten und in das Schicksal seiner N- und C-terminalen Regionen innerhalb des Parasiten.

Schließlich habe ich auf Basis des erfolgreichen GFP-Taggings stromaufwärts des C-Terminus TRP1 mit APEX oder miniTurbo für Proximity-Biotinylierung fusioniert, um C-terminale Interaktionspartner mittels proximity-abhängiger Biotinylierung zu identifizieren. Aufgrund von Zeitbeschränkungen führte ich die Biotinylierungsexperimente ausschließlich mit TRP1-APEX durch, wodurch in drei unabhängigen Experimenten insgesamt 307 einzigartige Proteine mittels MS-Analyse identifiziert wurden. Darunter fanden wir neun nicht charakterisierte Proteine, von denen sechs eine hohe Expressionsrate in den Moskito-Stadien des Parasiten aufweisen. Dieses Experiment lieferte wertvolle Einblicke in die potenziellen Interaktionspartner von TRP1 und seine entscheidende Rolle in der Sporozoitenmotilität, der Speicheldrüseninvasion und der Übertragung auf den Wirt.

Zusammenfassend spielt TRP1 eine entscheidende Rolle bei der Sporozoitenmotilität, der Speicheldrüseninvasion und der Übertragung auf den Wirt. Entgegen früheren Erkenntnissen zeigte meine Studie, dass der TRP1-C-Terminus nicht für den Austritt der Sporozoiten erforderlich ist, sondern essenziell für ihre Motilität und Invasion bleibt, wobei seine Funktion hochspezifisch und nicht mit der des TRAP-C-Terminus austauschbar ist. Ebenso erwies sich die hochkonservierte TSR-Domäne am N-Terminus als unverzichtbar für diese Prozesse, wobei konservierte Tryptophanreste eine Schlüsselrolle spielten. Lokalisationsstudien mit doppelt getaggtem TRP1 lieferten weitere Erkenntnisse über die räumliche Dynamik des Proteins in Sporozoiten. Zusätzlich identifizierten Proximity-Biotinylierungsexperimente potenzielle Interaktionspartner, darunter mehrere nicht charakterisierte Proteine, die in den Moskito-Stadien hoch exprimiert sind, und gaben damit neue Einblicke in das molekulare Netzwerk, in dem TRP1 operiert. Insgesamt vertiefen diese Erkenntnisse unser Verständnis der einzigartigen und unverzichtbaren Rolle von TRP1 in der -Sporozoitenbiologie von *Plasmodium* und seiner Bedeutung für die Parasitenübertragung.

Table of Contents

1. Introduction

1.1 Apicomplexa

1.1.1 Unique features of Apicomplexans

Apicomplexans are a diverse group of parasitic protozoa with a unique evolutionary history and complex phylogenetic relationships due to its ancient evolutionary origins, rapid sequence divergence, and extensive gene loss. Horizontal gene transfer, cryptic diversity, and complex life cycles further complicate classification. Additionally, the presence of the apicoplast, derived from endosymbiosis, adds another layer of evolutionary complexity. Apicomplexans include some of the most significant pathogens affecting human and animal health, such as *Plasmodium spp.*, which causes malaria and *Toxoplasma gondii*, the causative agent of toxoplasmosis. Members of Apicomplexa are obligate intracellular parasites, specialized in invading host cells and multiplying within them. Their defining feature is the presence of an apical complex, a structure containing secretory organelles essential for host cell attachment and invasion, which has led to their naming. Apicomplexans along with chromerids/colpodellids, dinoflagellates and ciliates are clustered under the phylogeny of alveolates and share a characteristic feature of a flattened vesicle like organelle located underneath the plasma membrane. These flattened vesicles are called ‘alveoli’, from which the name alveolates was derived.

Studies indicate that apicomplexans underwent divergent evolution from their free-living ancestors, possibly dinoflagellate-like organisms, adapting to a parasitic lifestyle with unique morphological and genetic features suited to its new life style (Morrison 2009). Molecular analyses of ribosomal RNA sequences, mitochondrial DNA, and plastid genomes have shed light on the evolutionary relationships between Apicomplexa and with other alveolates. These studies indicate that Apicomplexa and dinoflagellates possibly shared a common ancestor during their evolution, marked by genetic similarities and structural features like alveoli, despite the stark differences in lifestyle and habitat. (Mathur et al. 2019; Janouskovec et al. 2010).

Apicomplexa is divided into two major subgroups: the Coccidia and the Haemosporida. The Coccidia subgroup includes genera such as *Toxoplasma sp.* and *Eimeria sp.*, which are not host specific and infect the epithelial cells of various host organisms (Kwong et al. 2019; Borner et al.

2016). Haemosporida includes the *Plasmodium* genus that is dependent on insect vectors for its transmission to vertebrate hosts. Another group within Apicomplexa is the Gregarines, which are primarily invertebrate parasites and have comparatively simpler life cycles than most apicomplexans.

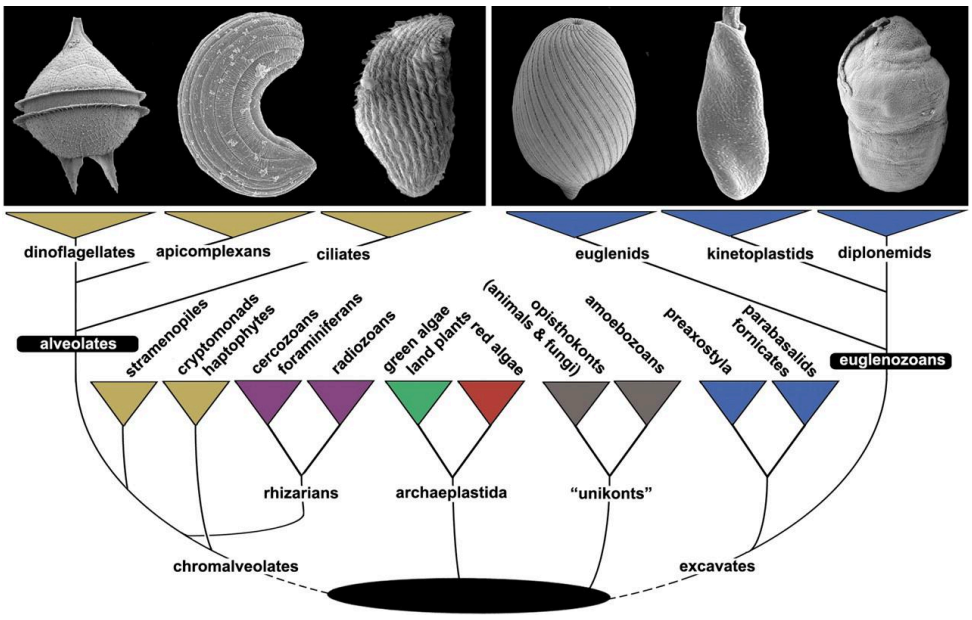

Figure 1.1. Phylogeny of alveolates.

Alveolates comprise several phyla, including Apicomplexa, Dinoflagellata, Chromerida, Colpodellida, and Ciliata. The eukaryotic phylogenetic tree depicts the relative positions of Alveolata. Alveolata is primarily composed of three main groups: dinoflagellates, apicomplexans, and ciliates (illustrated in the upper left with scanning electron micrographs of Protoperidinium, Selenidium, and an unidentified ciliate). Figure taken from (Lukeš, Leander, and Keeling 2009)

Apicomplexans possess various structural and molecular adaptations that facilitate their parasitic lifestyle. The most defining features include, apical cytoskeletal structures: apical polar ring and conoid, secretory organelles such as rhoptries, micronemes, and dense granules that are tailored for motility, invasion and egress and continuation of their life cycle. *Toxoplasma gondii* additionally harbors a specialized, cone-shaped structure called conoid within the apical complex of the cell, serving crucial roles such as host cell attachment and invasion. A conoid has recently also been identified in *Plasmodium spp*. (Dos Santos Pacheco et al. 2022; Koreny et al. 2021).

Micronemes secrete crucial factors including adhesins for motility and invasion in the invasive stages of the parasite and are abundantly present at the apical tip of the parasite. These proteins, including both membrane-bound and soluble factors, serve as key parasite-side binding partners during host cell invasion. Among these, adhesins play a crucial role in triggering rhoptry secretion. Rhoptry proteins, which include both soluble and membrane-associated components, are subsequently delivered into the host cell cytoplasm and plasma membrane. The interaction between micronemal and rhoptry proteins facilitates the formation of the tight junction, a static structure through which the parasite actively invades. This invasion is driven by the parasite's actin-myosin motor, which powers its movement into the host cell. As the parasite enters, it forms the parasitophorous vacuole from the host plasma membrane, incorporating some rhoptry-derived proteins while selectively excluding most host transmembrane proteins (Valleau et al. 2023; Loubens et al. 2023; Suarez et al. 2019; Cova, Lamarque, and Lebrun 2022).

To Summarize, the synchronous and orderly release of the proteins from the apical vesicles is essential in the invasive stages of the parasite's life cycle as microneme secretion primes the parasite for invasion, while rhoptry secretion enables the establishment of a suitable environment for replication within the host.

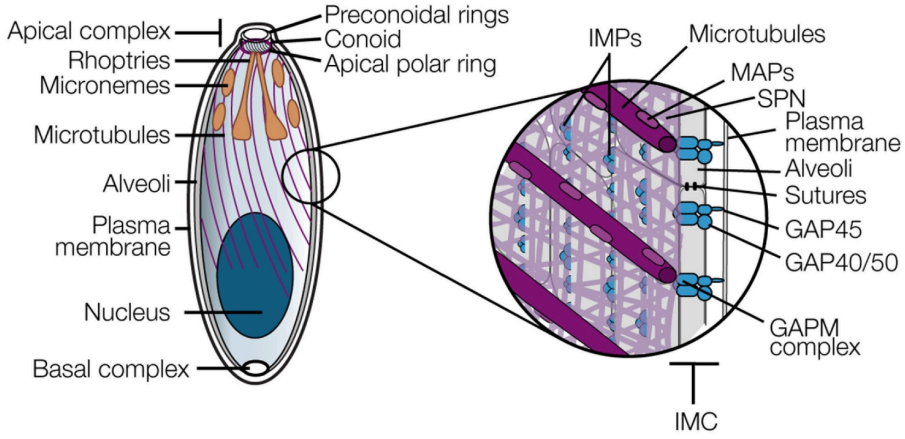

Figure 1.2. Unique features of apicomplexans

Schematic representation of an apicomplexan model, highlighting the apical complex comprising secretory organelles, e.g. micronemes, rhoptries, apical polar ring & conoid (present only in coccidians). Apicomplexans harbor flattened sac-like vesicles, known as alveoli, underneath the plasma membrane and provide structural integrity to the parasite while acting as a scaffold for the proteins involved in motility and cell invasion. IMC: Inner membrane complex, IMP,

inner-membrane particle, MAPs: Microtubule associated proteins, SPN: Subpellicular network, GAP: Glideosome associated protein(s). Figure taken from (Harding and Frischknecht 2020).

Apicomplexans also harbor a unique organelle, i.e. apicoplast, which has evolved from typical plastids into a non-photosynthetic organelle that plays essential roles in lipid and isoprenoid synthesis and are now considered important drug targets for blockage of disease transmission (Nair et al. 2011; Okada et al. 2022; Bulloch et al. 2024). Genetic evidence indicates that the apicoplast originated from an ancient secondary endosymbiosis event, likely involving a red algae ancestor (Janouškovec et al. 2015; 2019). These unique adaptations in apicomplexa ensured their survival and propagation through millions of years. The evolutionary history and biological mechanisms of apicomplexans offer critical insights into host-parasite interactions and potential strategies for disease control (Janouškovec et al. 2019; Wasmuth et al. 2009; Shunmugam et al. 2022).

1.1.2 Life cycle of *Plasmodium* spp.

Plasmodium spp. parasites have a complex life cycle, constantly shuttling between a mosquito vector and an intermediate host. Mosquitoes act as definitive hosts for *Plasmodium spp.* as sexual reproduction occurs here which ensures parasite transmission (Figure 1.3). While usually the intermediate hosts are mammals, *Plasmodium spp.* can also infect birds and reptiles (Borner et al. 2016).

When an infected female *Anopheles* mosquito takes a blood meal, the transmissive stage of the parasite, i.e. the sporozoites, are injected into the skin of the mammal (Sidjanski and Vanderberg 1997; Jerome P. Vanderberg and Frevert 2004; Ménard et al. 2013; Frischknecht and Matuschewski 2017; Ripp et al. 2021). Sporozoites are injected during each bite and start probing for blood capillaries from which they can be transported into the liver where they eventually invade the hepatocytes (Amino et al. 2006). Recent studies show that the number of sporozoites expelled in the skin is directly correlated with the extent of mosquito infection, with a median of 1035 sporozoites in naturally circulating strains in Burkina Faso (Andolina et al. 2024; Kanatani et al. 2024). Only about 35% of sporozoites find blood vessels, while the rest enter the lymphatic system, where they are degraded by white blood cells (Amino et al. 2006; Yamauchi et al. 2007). Sporozoite motility in the host skin is a crucial factor in transmission of

the disease as they need to evade the immune cells present in the dermis of the host (Montagna et al. 2012). Genetically modified motility impaired sporozoites were unable to establish a successful infection in the host and hence transmission of the disease was blocked (A. Ghosh et al. 2024; Heiss et al. 2008; Kehrer et al. 2022; Jerome P. Vanderberg and Frevert 2004; Montagna et al. 2012).

Sporozoites are passively transported to the liver into the hepatic sinusoids, where they interact with hepatocyte receptors enabling their invasion into hepatocytes (Gabriele Pradel, Garapaty, and Frevert 2002; Jethwaney et al. 2005; Ishino et al. 2004; Ishino, Chinzei, and Yuda 2005). Within this environment, sporozoites interact with heparan sulfate proteoglycans (HSPGs) on hepatocytes, which serve as molecular cues indicating their presence in the liver (Sinnis et al. 2007). This interaction facilitates sporozoite adhesion and migration but does not directly trigger immediate hepatocyte invasion (Loubens et al. 2021). The term "receptor" in the context of parasite invasion can be misleading, as it implies a specific ligand-receptor interaction. Parasites like *Plasmodium* often exploit general surface markers on host cells rather than engaging with receptors evolved explicitly for parasite detection. In the hepatic sinusoids, sporozoites do not immediately interact with specific receptors such as CD81; instead, they sense the liver environment and initiate movement to locate suitable entry points (Manzoni et al. 2017). This does of course not rule out that a specific receptor will eventually be identified.

Although sporozoites were initially thought to enter the hepatocytes through the liver resident kupffer cells, recent studies suggest that the sporozoites might be using endothelial cells to make their way into the liver (Tavares et al. 2013; M. M. Mota et al. 2001; G. Pradel and Frevert 2001). Upon successful invasion in the hepatocytes through the formation of a parasitophorous vacuole, sporozoites undergo prolific replication known as schizogony, resulting in the formation of thousands of merozoites (Risco-Castillo et al. 2015).

Liver stage parasites in some species of *Plasmodium,* e.g. *Plasmodium vivax* can persist for years in dormant state, known as hypnozoites, before being reactivated after months or even years after the initial infection (Dembélé et al. 2014). After completing development the merozoites are released from the hepatocytes via the formation of so called merosomes (Sturm et al. 2006).

After being released from ruptured schizonts, *Plasmodium* merozoites rapidly invade red blood cells (RBCs) by initially attaching to the RBC surface, reorienting to align their apical end, and

forming a parasitophorous vacuole (PV) that facilitates their entry and development within the host cell. Inside the PV, the parasite progresses through distinct stages: The ring stage, characterized by a ring-like appearance, where the young parasite begins to metabolize host resources; The trophozoite stage, where the parasite enlarges and actively consumes hemoglobin, leading to the formation of hemozoin pigment and the schizont stage, where the parasite undergoes multiple rounds of nuclear division, resulting in RBC rupture and release of new merozoites infect additional erythrocytes, perpetuating the asexual replication cycle (Matz et al. 2020; Dvorak et al. 1975).

During the schizont stage, *Plasmodium falciparum* modifies red blood cells by inducing the formation of 'knob-like' structures on their surface, which enhance adhesion to blood vessel walls and aid in evading splenic clearance. Malaria-infected RBCs exhibit cytoadherence, allowing them to attach to various host cells, including endothelial cells and uninfected erythrocytes. This adhesion is largely mediated by *Pf*EMP1 (*Plasmodium falciparum* erythrocyte membrane protein 1), which interacts with endothelial receptors, promoting sequestration within the microvasculature. This process plays a crucial role in the development of severe malaria pathogenesis (Hughes, Biagini, and Craig 2010; Pegoraro et al. 2017). Cytoadherence plays a central role in the parasite's immune evasion strategies and is a key factor in the development of severe malaria complications (Lee, Russell, and Rénia 2019; Ho and White 1999). In rodent models, such as *Pb* ANKA, infected RBCs have been observed to cytoadhere to microvascular endothelial cells, providing insights into the mechanisms of sequestration and pathogenesis (Franke-Fayard et al. 2005; El-Assaad et al. 2013).

Upon development the schizonts burst from the RBSs, releasing a new wave of merozoites into the circulation along with *Plasmodium* antigens, toxins, and waste products such as hemozoin into the bloodstream, causing high fever and other disease symptoms (Tilley, Dixon, and Kirk 2011). The ongoing rupture of red blood cells (RBCs) during malaria infection diminishes the blood's oxygen-carrying capacity and leads to hemolytic anemia. This condition arises from the destruction of both infected and uninfected RBCs, as well as suppressed erythropoiesis. The parasite not only lyses infected erythrocytes but also induces the removal of uninfected ones, exacerbating anemia. Additionally, malaria infection suppresses the production of new RBCs in the bone marrow, further contributing to the anemic state (Haldar and Mohandas 2009; White 2018). The cyclic invasion, replication and rupture cycle results in creating patterns of periodic

fevers, where the period is species specific, e.g. *P. falciparum, P. vivax* and *P. ovale* have a 48-hour cycle, while *P. malariae* has a 72-hour cycle, whereas *P. knowlesi* as well as the rodent infecting parasites *P. berghei* and *P yoelii* have a 24-hour cycle (Janse et al. 1989; Cowman et al. 2017).

A fraction of blood stages commit to be differentiated into gametocytes and is regulated by the transcription factor AP2-G (Kafsack et al. 2014; Sinha et al. 2014). AP2-G was also shown to be involved in the regulation of genes involved in RBC invasion (Josling et al. 2020).

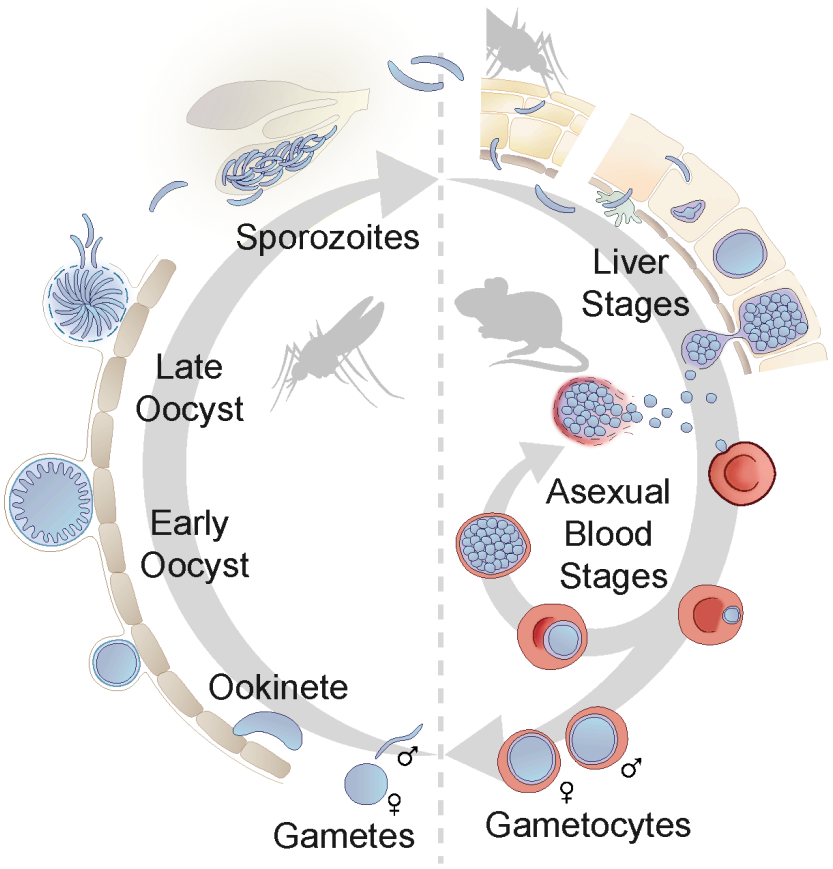

Figure 1.3. Life cycle of *Plasmodium spp.*

When an infected female *Anopheles* mosquito bites, it injects sporozoites into the host's skin while taking a blood meal, from where they migrate to enter blood capillaries. Through the bloodstream, they reach the liver, where they invade hepatocytes and produce thousands of merozoites, which are released back into the blood. These merozoites invade red blood cells and mainly develop into either merozoite-containing schizonts or gametocytes. During a subsequent mosquito bite, gametocytes are taken up by the mosquito. In the mosquito's gut, they activate,

fertilize, and develop into motile ookinetes, which cross the midgut epithelium to establish infection on the gut wall while evading the mosquito immune system, where they transform into oocysts. These oocysts enable the formation of thousands of sporozoites, which, once mature, are released into the mosquito's hemolymph, eventually reaching the salivary glands to await transmission back into a host. Figure adapted from Hentzschel et al. 2023 (Hentzschel et al. 2023).

When a mosquito takes a blood meal from an infected host, male and female gametocytes are taken up as well. The change in the physical parameters like the sudden drop of temperature, an increase of pH, and mosquito specific components such as xanthurenic acid activates the development of male and female gametocytes (O. Billker et al. 1998). In male gametocytes, replication of the genome results in the formation of eight microgametes via three rounds of rapid DNA replication (Sinden and Croll 1975). The male and female gametocytes readily fuse to form a zygote that subsequently develops into a motile zygote, termed as ookinetes in about 20-24 hours post fertilization. Ookinetes traverses through the viscous environment of the blood meal inside the mosquito midgut and invades the midgut epithelium to be finally arrested underneath the basal lamina (Vinetz 2005; Dessens et al. 1999). Ookinetes are thereafter transformed into oocysts where the transmissive stage of the parasite, sporozoites are developed by repeated nuclear division and replication known as sporogony (Singer and Frischknecht 2023).This follows a pattern similar to schizogony, with distinct growth, nuclear division, and cell formation stages. Unlike blood-stage schizogony, where nuclear division occurs primarily in the final stage, oocyst development involves early DNA replication and nuclear division, leading to the formation of large polyploid nuclei. This allows for the production of sufficient mRNA to support rapid parasite growth and differentiation (J. Vanderberg and Rhodin 1967; Thathy 2002). Over approximately 10 days, the oocyst expands as nuclear division continues. Once growth is complete, sporulation occurs rapidly, generating thousands of infectious sporozoites that are eventually released into the mosquito hemocoel and migrate to the salivary glands, ready for transmission to a new host (Saeed, Tremp, and Dessens 2023; Q. Wang, Fujioka, and Nussenzweig 2005; Frischknecht and Matuschewski 2017) . The development of sporozoites is an asynchronous process and varies in time anywhere from 10-21 days post infection depending on the species of *Plasmodium,* hence making oocysts the longest stage of *Plasmodium* life cycle. Thousands of sporozoites are developed within each oocyst and upon complete development, they egress from the oocyst (Klug and Frischknecht 2017; Hentzschel and Frischknecht 2022). It

has been shown that the sporozoites are already moving within the oocysts, even prior to their exit. even prior to their exit (Aly and Matuschewski 2005; Klug and Frischknecht 2017). Although it is unsure if it is a productive motility and whether it contributes to sporozoite egress from the oocyst is not completely understood (Aly and Matuschewski 2005; Klug and Frischknecht 2017; Thieleke-Matos et al. 2024). Upon release, sporozoites are then transported via mosquito hemolymph to the salivary gland where they possibly interact with certain receptors that facilitates their invasion into the salivary gland (Frischknecht et al. 2004; Anil Kumar Ghosh and Jacobs-Lorena 2009; Anil K. Ghosh et al. 2009). Recent studies with three-dimensional electron microscopy showed that sporozoites invade salivary gland cells through the formation of a ring-like structure and a transient vacuole, where they reside until they are ready to be transmitted via next mosquito bite and the cycle continues (Rodriguez and Hernández-Hernández 2004) (Fernandes et al. 2022).

1.1.3 Malaria

Malaria, an ancient and life-threatening disease caused by *Plasmodium* parasites, remains a significant global health challenge. Transmitted through the bites of infected female *Anopheles* mosquitoes, the disease continues to affect millions worldwide. In 2023, an estimated 263 million malaria cases and 597,000 deaths were reported across 83 countries (WHO, 2023).

The World Health Organization (WHO) African Region bears the highest malaria burden, accounting for 94% of global cases (246 million) and 95% of malaria-related deaths (569,000) in 2023. Children under five years old represented approximately 76% of all malaria deaths in this region. In the WHO South-East Asia Region, eight countries remain malaria-endemic. India reported over two million cases in 2023, making up half of all cases in the region, followed by Indonesia with nearly 1.1 million cases. Notably, malaria-related deaths in this region have declined by 82.9%—from approximately 35,000 in 2000 to 6,000 in 2023. In the Americas, malaria remains a concern in 18 countries and one territory. In 2023, approximately 505,600 cases and 116 deaths were reported in the region (WHO, 2023).

Despite decades of efforts to control and eradicate the disease, malaria remains endemic in many parts of the world. According to the World Malaria Report 2023 by WHO, there were approximately 249 million malaria cases worldwide in 2022, an increase from 244 million cases

in 2021. Malaria deaths, however, remained relatively steady at around 608,000 in 2022, just slightly down from 610,000 in 2021. About 95% of these cases and deaths occurred in the African region, with children under the age of five making up nearly 80% of all malaria-related fatalities (WHO, 2023).

The clinical presentation of malaria varies from mild symptoms to severe, depending on factors such as the *Plasmodium* species involved, the host's immunity, and access to healthcare. The most common symptoms include fever, chills, headache, fatigue, and muscle aches. Severe cases, particularly caused by *P. falciparum*, may progress to anemia, cerebral malaria, organ failure, and death. One of the most serious consequences of malaria is hemolytic anemia, caused by the destruction of RBCs during parasite replication. The immune response to malaria can damage both infected and uninfected RBCs, resulting in anemia. Cerebral malaria, another severe manifestation, occurs when *P. falciparum* parasites adhere to the endothelial cells lining the brain's blood vessels, leading to inflammation, impaired blood flow, and sometimes coma or death (Haldar and Mohandas 2009; White 2018; Michinaga and Koyama 2015). Pregnant women and children under five are especially vulnerable, as their immune systems are less capable of mounting an effective defense against the parasite (Milner 2018).

Despite significant progress in malaria control, eradicating the disease remains challenging. Vector control, primarily through insecticide-treated bed nets and indoor residual spraying, has proven effective in reducing transmission, but resistance to insecticides is an increasing problem (Oxborough et al. 2024; Pryce, Medley, and Choi 2022). Additionally, *Plasmodium* has shown remarkable adaptability in developing resistance to antimalarial drugs, particularly in regions where treatments like chloroquine and artemisinin are widely used (Cui et al. 2015). The socio-economic and environmental factors in malaria-endemic regions further complicate control efforts. Poverty, limited access to healthcare, lack of education, and inadequate infrastructure hinder effective malaria management and prevention. Climate change also plays a role, as it influences the habitat and behavior of mosquito populations, potentially expanding the range of malaria transmission (WHO, 2023).

Efforts to eliminate malaria have seen promising advances, including the development of the RTS,S/AS01 vaccine, the first malaria vaccine approved for widespread use (Gordon et al. 1995;

Osoro et al. 2024; Hanboonkunupakarn et al. 2024). This vaccine, although only moderately effective, marks a milestone in malaria prevention. Research is ongoing to develop more effective vaccines, explore gene-editing technologies like CRISPR to create malaria-resistant mosquitoes, and develop novel drugs that target different stages of the parasite's life cycle. (Cui et al. 2015; Richie et al. 2023; Defo et al. 2021).A new vaccine approach with R21/Matrix-M malaria vaccine demonstrated efficacy in Phase III clinical trials, achieving up to 75% efficacy after a booster dose over an 18-month period and targets young children, the group most vulnerable to malaria (Datoo et al. 2024). Also attenuated parasites are being developed (Julia M Sattler et al. 2024; Lamers et al. 2024).

Despite the tireless research efforts from the global malaria research community, societal engagement, along with public health education, remains critical for malaria control. Individuals in high-risk areas benefit from understanding preventative measures, recognizing symptoms, and seeking timely treatment. Global partnerships, such as the Roll Back Malaria Partnership and funding from organizations like the Bill & Melinda Gates Foundation, continue to drive the fight against malaria by supporting research, providing resources, and implementing control measures. Sustained efforts and continued innovation will be essential to achieve this goal and ensure that malaria becomes a disease of the past.

1.1.4 *Plasmodium berghei* as a rodent malaria model

Plasmodium berghei, one of the members of rodent malaria infecting species of *Plasmodium,* is a widely studied, invaluable model in malaria research. Originally isolated from the wild rodent *Thamnomys rutilans* by Ignace and Marcel lips in central Africa, *P. berghei* has become instrumental to study various aspects of malaria biology including immune responses, and drug development (Vincke and Lips 1948). Despite certain differences in pathology between rodent and human infections, the ability of *P. berghei* to model severe malaria syndromes makes it a valuable model for studying disease mechanisms and immune responses to parasite invasion. Ease of genetic manipulation allows for better understanding the mechanisms of drug resistance, identification of new gene functions and potential drug targets and as a foundation for preclinical drug and vaccine testing (Vincke and Lips 1948). (Mendes et al. 2018; Simwela and Waters 2022). Studies on cytokine responses, immune cell recruitment, and antibody development have

enhanced our understanding of how malaria evades and modulates host immunity (Claser et al. 2017). Thus despite certain limitations in emulating human malaria, *Plasmodium berghei* continues to provide a robust and ethical alternative to studying malaria in human and non-human primates (Matz and Kooij 2015).

1.2 Cell migration

1.2.1 Cell motility and its importance

Motility at cellular level is crucial for numerous physiological processes in both single-celled and multicellular organisms. During embryonic development, cell motility is essential for morphogenesis, the process by which cells move to specific locations to form tissues and organs. (Scarpa and Mayor 2016). For example, neural crest cells migrate to different parts of the embryo to form the peripheral nervous system, facial cartilage, and other structures (Vaglia and Hall 1999). Cell motility helps establish spatial patterns in tissues by allowing cells to rearrange and position themselves, which is necessary for forming the correct anatomical structures (Heller and Fuchs 2015). During tissue damage, cells like fibroblasts and epithelial cells migrate to the wound site to repair it. This process is crucial for reconstructing damaged tissue by laying down a new extracellular matrix and proliferating to cover the wound. This process, known as wound healing, relies on the coordinated movement of these cells to close the wound and regenerate the tissue (Blanpain and Fuchs 2014). Immune cells, such as neutrophils, macrophages, and lymphocytes, rely on motility to patrol the body, detect pathogens, and migrate to infection sites. This directed movement, known as chemotaxis, allows immune cells to reach infected or inflamed tissues rapidly, playing a crucial role in the body's defense mechanisms (Mantovani, Bonecchi, and Locati 2006). The ability of cancer cells to migrate from the primary tumor site to distant tissues is a key characteristic of cancer metastasis, the spread of cancer to other parts of the body. Cancer cells often acquire enhanced motility to invade surrounding tissues, enter the bloodstream, and colonize distant organs by moving through the ECM, allowing them to invade neighboring tissues and disseminate (Stuelten, Parent, and Montell 2018). Within cells, motility is critical for the transport of organelles, vesicles, and molecules. For instance, motor proteins move cargo along the cytoskeleton to various parts of the cell, ensuring the proper distribution of nutrients and removal of waste (Stamnes 2002). Motile cells often exhibit polarity, meaning they

have a distinct front (leading edge) and back (trailing edge). This polarization is essential for directional movement, enabling cells to respond to external signals such as chemical gradients (chemotaxis) or mechanical forces (Kozlov and Mogilner 2007). For pathogenic organisms like bacteria and parasites, motility is crucial for invading host tissues and establishing infections (Josenhans and Suerbaum 2002). Also viruses use cellular mechanisms for the intra- and intercellular spread (Miller and Krijnse-Locker 2008). Understanding cell motility is a fundamental aspect of cellular biology and tissue function and key in medical fields such as cancer treatment, tissue engineering, and regenerative medicine.

1.2.2 Gliding motility of apicomplexan parasites

Protozoans consist of a diverse group of single-celled eukaryotic organisms that exhibit a wide range of characteristics in terms of morphology, ecology, and physiology. Protozoans have developed a diverse range of motility systems that is crucial for their survival and dissemination. Unlike most members of the group who use pseudopodia, cilia and flagella for movement, Apicomplexans use a unique form of substrate based motility, known as gliding motility (Baum et al. 2006). Invasive stages of the Apicomplexan parasites utilize gliding motility for successful invasion of host cells and propagation (Frénal et al. 2017a).

Most apicomplexans are obligatory intracellular parasites, and their life cycle requires periodic switching between a carrier vector and a definitive host. However, there are some exceptions or unique cases, e.g. Cryptosporidium species, which cause cryptosporidiosis, can reside within a specialized parasitophorous vacuole at the host cell surface rather than deeply penetrating the host cytoplasm. Gregarines, a group of apicomplexan parasites that infect invertebrates, often remain extracellular in the gut of their hosts (Salomaki et al. 2021; Greigert et al. 2024).

To complete their life cycle, these parasites must invade host cells for their development and replication, but they also need to exit the host cells successfully to continue their progression. Motility plays a crucial role in this journey and is powered by the actomyosin cytoskeletal system located underneath the plasma membrane of the parasite. The complex machinery, known as ‘glideosome’ comprises the actomyosin motor, present in between the plasma membrane and the inner membrane complex (IMC) (Baum et al. 2006). IMC provides the necessary structure and scaffold to the parasite along with the subpellicular microtubules (SPM) and subpellicular

network (SPN) (Kudryashev et al. 2010; Harding and Frischknecht 2020). SPN comprises a network of intermediate filament-like filamentous structures and It interacts closely with the parasite's cytoskeleton, particularly with the SPMs and alveolin proteins present in IMC, and is crucial during parasite development and host cell invasion, as it enables structural stability and flexibility needed for movement through host tissues (Douglas, Moon, and Frischknecht 2024; Gould et al. 2008; Ferreira et al. 2021).

The IMC and PM also act as anchors for the glideosome associated proteins that help in generating the traction force necessary for propelling the parasite forward (Khater, Sinden, and Dessens 2004; Frénal et al. 2017b). The IMC is also essential for cell division as it organizes the cortical cytoskeleton, providing a framework that supports the formation and separation of organelles, ensuring proper partitioning during division (Nishi et al. 2008).

The motor proteins that drive the motility are short single headed heavy chain myosin A (MYOA) that generate traction force required to propel the parasite forward. MYOA is part of the Class XIV myosin family. This family of myosins is highly adapted for apicomplexan specific gliding motility and is distinct from conventional myosins found in other organisms (such as Class II myosins responsible for muscle contraction in animals) (M. B. Heintzelman and Schwartzman 1997). The interaction of MYOA with actin filaments are optimized for rapid movements that are crucial for cell traversal and invasion, unlike conventional myosins that generate force through repeated contraction-relaxation cycles (Meissner, Schlüter, and Soldati 2002; Schüler and Matuschewski 2006). MYOA is associated with myosin light chain 1 (MLC1) in *Toxoplasma gondii* whereas in *Plasmodium spp.* It is known as MYOA tail domain interacting protein (MTIP) (Herm-Götz et al. 2002; Bergman et al. 2003). MYOA is linked to the inner membrane complex (IMC) through the glideosome-associated protein 45 (GAP45), which firmly anchors MYOA by binding to both GAP50 and GAP40, thus bridging the gap between the IMC and the plasma membrane (Fig. 1.4) (Ridzuan et al. 2012; Frénal et al. 2010).

To generate the traction force necessary for forward propulsion of the parasite, the actomyosin motor must be firmly anchored onto the IMC, which is made possible by GAP40 and GAP50 (Gaskins et al. 2004; He et al. 2023; Bosch et al. 2012). Depletion of MYOA completely abrogates ookinete motility in *Plasmodium berghei*, resulting in no oocyst formation and no transmission to the host (Siden-Kiamos et al. 2011). Mutation at serine 19 (S19A) of MYOA significantly reduces the motility of both ookinetes and sporozoites in *P. berghei*, thereby

impairing the parasite's ability to infect host cells, that suggests that the phosphorylation cycle at serine 19 is key to force generation and efficient parasite migration during transmission stages (Ripp et al. 2022; Moussaoui et al. 2020). MYOA interacts with the short and highly dynamic actin filaments present in the apicomplexan parasites (Vahokoski et al. 2014; Douglas et al. 2018; Julia Magdalena Sattler et al. 2011).

Apicomplexans actin filaments differ widely from other eukaryotes, where the actin filaments are longer and stable. The actin filament exists as mostly globular or G-Actin instead of the filamentous or F-Actin, unlike in most eukaryotes (Skillman et al. 2011; Vahokoski et al. 2014). They also contain fewer actin binding proteins and actin was thought to only be polymerized by formins, however recently a non canonical actin related protein 2/3 (ARP 2/3) complex was identified in *Plasmodium berghei* (Hentzschel et al. 2023). Recent studies highlight that apicomplexan motility is driven by actin filaments interacting with the glideosome, generating coordinated, directional movement. Actin dynamics, involving polymerization and depolymerization, create forces that propel the parasite forward. The gliding motility is not solely dependent on myosin motors but also arises from complex, collective behaviors of actin filaments and their regulatory proteins, i.e. emergent actin flow, allowing efficient host cell invasion (Hueschen et al. 2024).

1.2.3 The *Plasmodium spp.* actomyosin motor

Gliding motility is extensively studied in the invasive stages of the parasite i.e. ookinete and the sporozoites in *Plasmodium spp.* (Frischknecht and Matuschewski 2017; Singer et al. 2024) and recently in merozoites (Yahata et al. 2021; Andrews et al. 2023).Sporozoites, the transmissive stage of the parasite, when activated by host derived factors (e.g. BSA), can move at a speed of 2 μm/s on average (J. P. Vanderberg 1974). Motility is not only crucial in host cell invasion and propagation but also essential for successful immune evasion inside the host (Aguirre-Botero et al. 2023; Han and Barillas-Mury 2002). In 2-D in vitro motility assays, sporozoites move counterclockwise in a circular manner, however in a 3-D environment they move in a helical fashion (Muthinja et al. 2018; Amino et al. 2006; 2008; Ripp et al. 2021; Hopp et al. 2021). This can be explained by the chiral shape of the sporozoites, due to its unique asymmetrical cytoskeletal structure. The subpellicular microtubules, which are connected to the apical polar rings, exhibit a left handed directional shift or tilt (Ren et al. 2024). In *Plasmodium* sporozoites,

the apical polar ring (APR) exhibits an inclination, contributing to the parasite's dorso-ventral polarity. This structural arrangement is essential for the parasite's directional motility and invasion capabilities. This asymmetry leads to the formation of a chiral structure, influencing the parasite's motility pattern which might aid the sporozoites in navigating through the extracellular matrix of the host tissues, improving their efficiency in invading host cells (Kudryashev et al. 2012). This incredible feat in motility is achieved by the macromolecular 'glideosomal complex' present underneath the plasma membrane of the parasite (Matthew B. Heintzelman 2015).

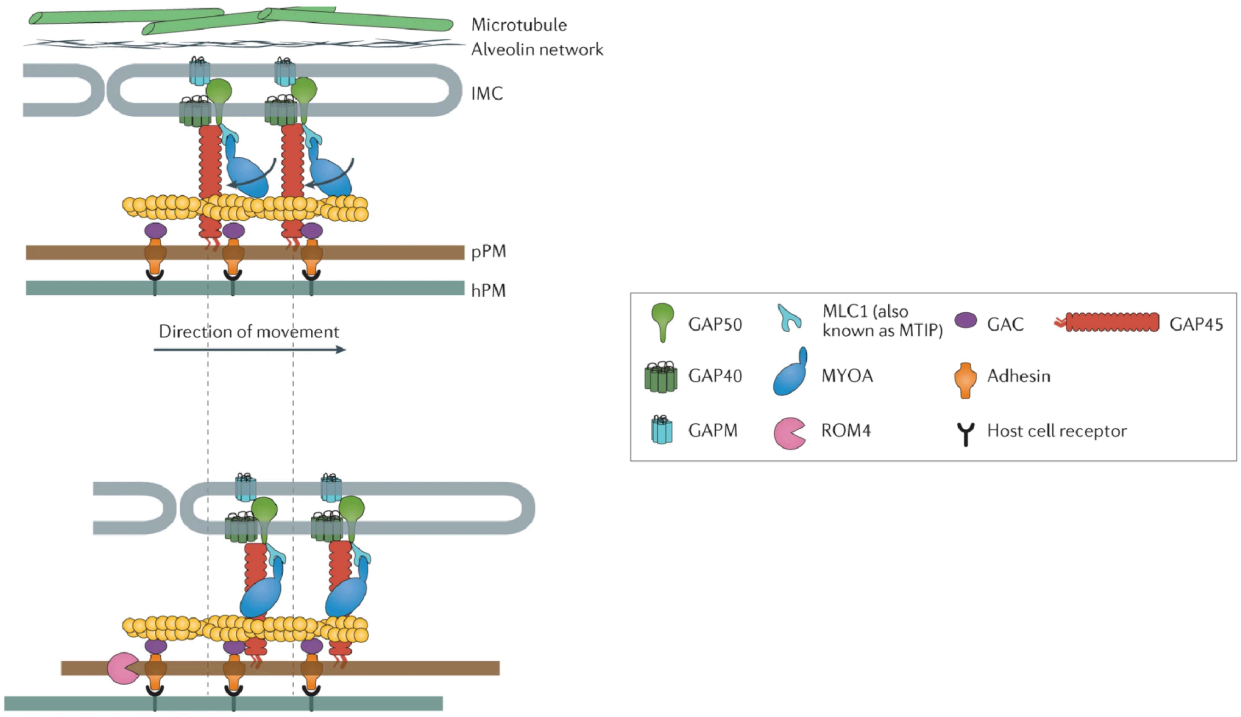

Figure 1.4. Glideosomal complex in apicomplexans

The glideosomal complex in apicomplexans comprises the myosin A (MYOA) motor, which is associated with the myosin light chain (MLC1 in *Toxoplasma gondii* and MTIP in *Plasmodium spp*. This motor complex is anchored to the inner membrane complex (IMC) via interactions with GAP45, GAP40, and GAP50. The glideosome-associated connector (GAC) links F-actin to surface adhesins, while the GAPM family proteins connect the motility complex to the cytoskeleton, facilitating traction force generation. MYOA activity involves conformational changes in its head domain upon ATP hydrolysis, enabling forward parasite movement. Rhomboid proteases (ROM4) cleave the transmembrane domain of adhesins, detaching them from host receptors to complete the motility cycle (Figure taken from Frénal et al. 2017, Nature reviews microbiology).

Plasmodium spp, like other Alveolates, contain a unique structure, consisting of interconnected, flattened vesicle-like structures called alveoli, subtending the plasma membrane (PM), called the inner membrane complex (IMC) (Ferreira et al. 2021). The IMC functions as the anchoring point for the major proteins in the glideosomal complex, providing specific stiffness and structural integrity to the parasite. GAP 45 and likely other proteins maintain the supra-alveolar space between the IMC and the PM (Frénal et al. 2010; Kehrer et al. 2022). The glideosomal complex residing in this supra-alveolar space, consists of class XIV myosin A heavy chain (MyoA) and the myosin light chain (myosin tail-interacting protein, MTIP), that are securely anchored within the outer inner membrane complex (IMC) by the integral membrane protein GAP50 and the lipid-anchored protein GAP45. Myosin interacts with the short and dynamic actin filaments that generate the power stroke, leading to the retrograde flow of the actin filaments towards the rear end of the parasite. The interaction between membrane-spanning adhesins and actin filaments converts the generated force into a propelling movement that drives the parasite forward (Frénal et al. 2017a; Matthew B. Heintzelman 2015). How the adhesins interact with the actin filaments however, still remains poorly understood.

1.2.4 Adhesins in *Plasmodium spp.*

Adhesins are specialized surface proteins found spanning the plasma membrane of the parasites. In the invasive stages of the parasite they facilitate attachment to host cells and tissues, playing a critical role in the transmission of the parasite (Sultan et al. 1997; Heiss et al. 2008; Moreira et al. 2008; Beyer et al. 2021; Dessens et al. 1999; Combe et al. 2009; Morahan, Wang, and Coppel 2009). By binding to specific receptors on host cells, adhesins enable motility and invasion. Adhesins are secreted from micronemes at the parasite's apical end, where they integrate into the plasma membrane. From there, adhesins are translocated toward the posterior end of the parasite by the actin filaments, creating a link between the motor complex and the adhesion sites, enabling the parasite to generate the force needed for movement and invasion (Baum et al. 2006; Quadt et al. 2016).

Major adhesin family in *Plasmodium spp.* includes the TRAP family proteins. The first protein identified as essential for sporozoite motility and host cell invasion was thrombospondin-related

anonymous protein (TRAP) (Sultan et al. 1997). TRAP is crucial for efficient movement and successful host cell entry. Due to its unique domain structure and significant role, other proteins with similar domain compositions are now classified as TRAP-family proteins. TRAP-family proteins share key structural elements, e.g. a signal peptide, a transmembrane domain (TMD), and an extracellular thrombospondin type-I repeat (TSR) in the N-terminal region. They also contain a Von Willebrandt factor A-like domain, commonly found in surface proteins for cell guidance (Whittaker and Hynes 2002). All TRAP family proteins possess a cytoplasmic tail domain (CTD) that interacts with the acto-myosin motor present underneath the plasma membrane through a yet unknown interacting partner(s) (Heiss et al. 2008; Stefan Kappe et al. 1999). The CTD contains a conserved tryptophan residue at the penultimate position in its C-terminus. Mutating the tryptophan or changing the charge in the CTD disrupts the protein's secretion on the sporozoite surface (Stefan Kappe et al. 1999; Bhanot et al. 2003). The complete deletion of TRAP resulted in the full inhibition of salivary gland invasion by sporozoites, along with a loss of effective gliding motility. Without TRAP, sporozoites exhibited a form of unproductive motility, characterized by a back-and-forth movement from a single attachment point to the surface, referred to as ‘patch gliding’, instead of the typical gliding movement required for efficient host cell invasion (Sultan et al. 1997; Münter et al. 2009; Stefan Kappe et al. 1999). Deletion of the entire TRAP CTD phenocopies the disruption in motility, salivary gland invasion and infectivity of TRP1 KO mutant. Deletion of the last 14 amino acids in the CTD resulted in similar effects as well, further highlighting the importance of the TRAP C-terminus (Stefan Kappe et al. 1999). Interestingly, the CTD from other TRAP-family proteins can partially restore its function, including the homolog in *Toxoplasma gondii* MIC2, where CTD resulted in complete restoration of TRAP’s function, indicating a somewhat conserved nature of the CTD amongst the TRAP family proteins and its homolog (Stefan Kappe et al. 1999; Heiss et al. 2008).

Tagging TRAP at the C-terminus remained futile as it disrupted the function of the protein but tagging at the N terminus of the protein after the signal peptide was possible (Kehrer et al. 2016). TRAP interacts extracellularly with the host cells via its N-terminus resident domains, characteristic features in secreted and surface resident proteins, i.e. the Von Willebrandt factor like A-domain and the thrombospondin type-I repeat (TSR) domain (Morahan, Wang, and Coppel 2009). The function of the VWA and TSR domain in TRAP remains elusive as the

perturbations in this region show a range of phenotypes. Replacing within the VWA the conserved threonine (Thr 126) into alanine resulted in severe defect in salivary gland infection and hepatocyte invasion, however it did not interfere with the gliding ability of the sporozoites. Replacing the distal tryptophan of the conserved 'WSXW' motif in the TSR domain only slightly affects the salivary gland and hepatocyte invasion capacity. Interestingly, mutating the basic amino acid clusters at the C-terminus of TSR (256KIRKRK261) domain resulted similarly in mild invasion defects, indicating that both VWA and TSR domain in TRAP is not involved in gliding motility but plays a role in salivary gland and hepatocyte invasion (Matuschewski et al. 2002). Contradictingly, in a study involving the A-domain of TRAP, the endogenous *Pbtrap* gene was replaced with *Pftrap*. Mutations within the A-domain impaired salivary gland invasion but did not affect sporozoite gliding motility or hepatocyte invasion.

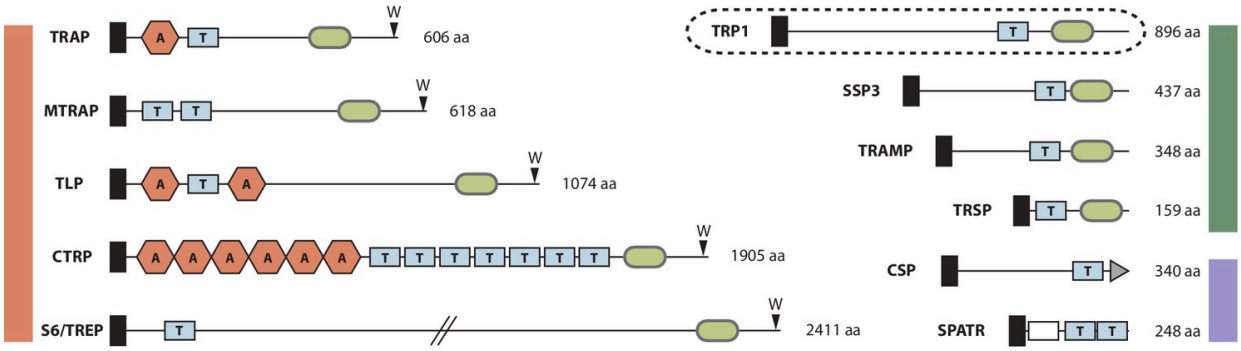

Figure 1.5. : Characteristic features of TRAP family proteins and TRAP-like proteins

Plasmodium spp. contain various TSR containing proteins, that play a range of important roles in invasion and motility in the invasive stages of the parasite. TRAP-family proteins are indicated by an orange bar, TRAP-related proteins by a green bar, and other TSR-containing proteins by a purple bar. TRP1 is highlighted with a dashed outline (top right). Thrombospondin repeats (TSR) are displayed as blue boxes (marked with T), while Von Willebrand factor-like A-domains (VWA) appear as orange hexagons (marked with A). Signal peptides (SP) are represented by black boxes, and transmembrane domains (TMD) by light green ovals. CSP includes a GPI-anchor (gray triangle), whereas SPATR contains an EGF-domain (white box). Conserved tryptophans are labeled as W. Amino acid numbers referring to *P. berghei* proteins. Figure taken from Klug et al. 2017.

Conversely, mutations in the TSP (or TSR) domain disrupted both gliding motility and salivary gland invasion but had no impact on hepatocyte invasion, highlighting the domain-specific roles of TRAP in sporozoite function and tissue targeting (Wengelnik et al. 1999; Matuschewski et al. 2002). However, recent studies indicate that the A-domain of TRAP is crucial for salivary gland invasion, gliding motility and infection and was effectively replaced by the A-domain of MIC2, suggesting that the function of the A domain did not rely so much on the amino acid sequence of the domain but instead on the proper folding of the domain (Klug et al. 2020). Conversely, abrogation of the TSR domain resulted in no issue in the life cycle of the sporozoite (Frischknecht lab, unpublished data). The Von Willebrand factor-like A-domain (I domain) and the thrombospondin type-I repeat (TSR) at the N-terminus of TRAP play crucial roles in force transduction during gliding motility. Recent structural and functional studies have demonstrated that the TRAP I domain exists in both closed and open conformations, with dynamic transitions between these states being essential for ligand binding, gliding motility, and organ invasion. Mutations stabilizing the I domain in either conformation impair sporozoite movement, salivary gland entry, and transmission, highlighting the necessity of conformational flexibility (Braumann et al. 2023).

The other proteins in the TRAP family include CTRP, containing seven TSR domains, is expressed in the ookinete stage and its disruption resulted in a complete block of parasite transmission to mosquitoes due to immotile ookinetes (Dessens et al. 1999). MTRAP is expressed in blood stages and gametocytes and is essential in gametogenesis (Kehrer, Frischknecht, and Mair 2016; Bargieri et al. 2016). TLP is expressed in salivary gland sporozoites however disruption of the gene does not interfere with salivary gland invasion but shows decreased capacity of sporozoites to traverse and infect hepatocytes (Heiss et al. 2008; Moreira et al. 2008; Hellmann et al. 2011; Hegge et al. 2010). S6 or TREP is expressed mostly in midgut sporozoites and plays a mild role in motility and invasion in salivary gland invasion (Combe et al. 2009; Steinbuechel and Matuschewski 2009; Hegge et al. 2012).

1.3 Thrombospondin-related protein 1 (TRP1)

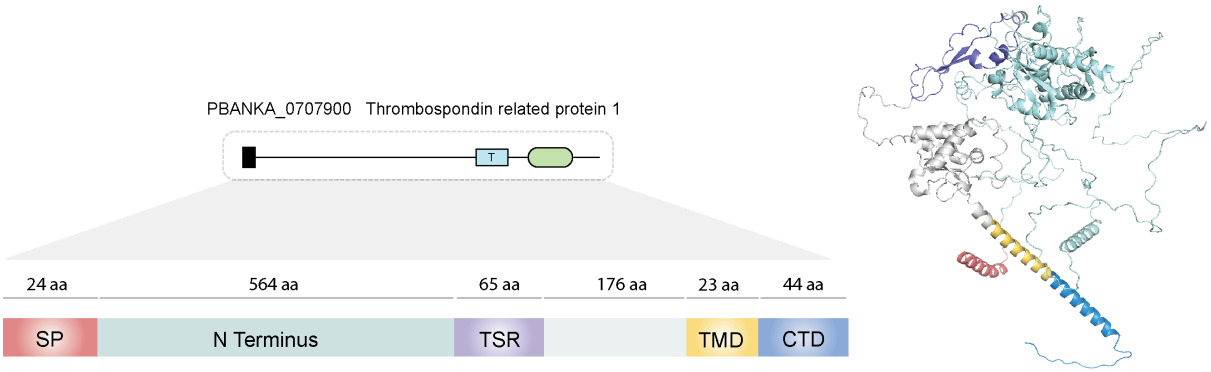

Figure 1.6. : A. Protein model of *Plasmodium berghei* Thrombospondin-related protein 1 (TRP1) **B.** ColabFold prediction of PbTRP1 structure.

Thrombospondin-related protein 1 (TRP1) is a TRAP related protein comprising some of the typical features of a TRAP family protein, such as a signal peptide (SP), an unstructured N-terminus, thrombospondin repeat domain (TSR), a transmembrane domain (TMD) and a C-terminus domain (CTD). However it also lacks some characteristic features of the TRAP family such as the penultimate tryptophan at the C terminus and Von Willebrandt factor like A domain at the N-terminus of the protein.

TRP1 is expressed only in late stage oocyst and salivary gland sporozoites and plays a crucial role in initiating motility in late stage sporozoites while they are still developing within the oocyst and is essential for egress from the oocyst (Klug and Frischknecht 2017). Hence without TRP1, the sporozoites cannot invade the salivary gland and thus have no transmission to the host. However, in the absence of TRP1, sporozoites continue to mature within the oocysts. Mechanically released midgut sporozoites were able to infect the host as well as wild type midgut sporozoites when injected intravenously and showed comparable gliding ability (Klug and Frischknecht 2017).

TRP1 is also present in other *Plasmodium* species, however it is not very well conserved. The N-terminus of the protein is quite unstructured and shows almost no conservation among its orthologs. In the absence of the N-terminus, although the sporozoites are able to egress from the oocyst, they cannot enter the salivary gland of the mosquito. The C-terminus on the other hand, was found to be crucial in both sporozoite egress from the oocyst and in salivary gland invasion.

The C-terminus is not very well conserved among its homologs either and shows quite a variability in its length and isoelectric point of the amino acids (Klug and Frischknecht 2017).
TRP1 also entails a micronemal targeting sequence of F/Y/WXXΦ (Φ: Hydrophobic amino acid) on the cytosolic face of the TMD which is known to be crucial in targeting proteins to the microneme. This indicates potential localization and function of the protein in the sporozoite microneme. However, confirming the localization of the protein has proven to be challenging as all the attempts at tagging the protein with a GFP tag rendered the function of the protein disrupted (Klug and Frischknecht 2017).
GFP tagging attempts at the N-terminus of the protein resulted in no observable GFP signal, although *gfp::trp1* fusion transcript was successfully expressed, indicating heavy processing at the N-terminus at post translational level. Interestingly, GFP signal was observed in *gfp-trp1ΔN* and *trp1-gfp* parasites, however in different localization patterns. *trp1-gfp* parasites showed a unique localization of the protein in the oocyst wall and a peripheral localization in the sporozoites, whereas *gfp-trp1ΔN* parasites showed an internal localization both in oocyst and sporozoites, potentially suggesting ER localization (Klug and Frischknecht 2017).
Western blot results for *trp1-gfp* salivary gland sporozoites indicate that TRP1 undergoes a heavy post translational modification resulting in a cleavage in between the TSR and TMD region of the protein. However, as mentioned before all the attempts at tagging the protein with GFP disrupted the function of TRP1, hence the localization and the cleavage pattern observed might not represent the reality. On the other hand, inability of tagging the protein at the N-terminus region results in a lack of understanding in the localization and potential function of the N-terminus and the TSR domain (Klug and Frischknecht 2017). Thus, further investigation is needed regarding the different domains of TRP1 for a further understanding of the role of TRP1 in sporozoite's journey from the oocyst to the salivary gland and furthermore in the transmission of the disease.

2. Aim of the thesis

Sporozoite motility is crucial for *Plasmodium* transmission and progression through its life cycle. Once deposited in the dermis by an infected *Anopheles* mosquito, sporozoites must rapidly migrate through the skin, enter the bloodstream, and reach the liver, where they invade hepatocytes to establish infection (Ménard et al. 2013). This active movement, known as gliding motility, allows sporozoites to efficiently traverse biological barriers, including the dermal extracellular matrix and endothelial cell layers. Unlike mammalian cells that rely on cytoskeletal rearrangements for movement, *Plasmodium* sporozoites use an actin-myosin motor complex and surface adhesins to propel themselves forward (Matthew B. Heintzelman 2015; Singer and Frischknecht 2023). Disruptions in sporozoite motility led to defects in salivary gland invasion, host skin traversal, reduced liver infection rates, and impaired disease transmission (Frischknecht and Matuschewski 2017). Therefore, understanding the molecular mechanisms regulating sporozoite motility is essential for identifying potential targets for malaria intervention strategies.

Sporozoites exhibit motility even before egress, as they have been observed actively moving within late-stage oocysts. Thrombospondin-related protein 1 (TRP1), a TRAP-related protein expressed in late oocyst and salivary gland sporozoite stages, plays a pivotal role in initiating this intra-oocyst motility and facilitating subsequent egress. Previous studies have highlighted the importance of TRP1's N-terminus in oocyst egress, while the C-terminus appears to have a dual function in both egress and salivary gland invasion (Klug and Frischknecht 2017).

This thesis aims to further investigate TRP1's role in the sporozoite's journey from the mosquito to the host. Specifically, I aim to identify key amino acid residues within the C-terminus that contribute to egress and invasion by generating a series of C-terminal deletion mutants. Additionally, I will create C-terminal swap mutants in which the TRP1 C-terminus is replaced with the C-terminus of *P. berghei* TRAP or the shorter *P. falciparum* TRP1 tail to assess functional differences.

While the N-terminus has been shown to be essential for oocyst egress, the adjacent thrombospondin type-1 repeat (TSR) domain remains unexplored. The TSR domain is well known for its roles in protein-protein interactions, stability, folding, and trafficking, and it is conserved across TRAP family proteins, where it mediates a range of functions (Morahan, Wang,

and Coppel 2009). To better understand its contribution to TRP1 function, I plan to generate point mutations, domain swap with the TSR domain with *P. berghei* TRAP and complete TSR domain deletions.

Another objective of this study is to generate functionally tagged TRP1 at both the N- and C-terminus, as previous attempts at tagging have been unsuccessful. If successful, I will leverage proximity-dependent biotinylation assays to identify potential interaction partners of the TRP1 C-terminus. Given that TRAP family proteins are known to associate with the actomyosin cytoskeleton beneath the parasite's plasma membrane, this approach may reveal novel molecular interactions critical for sporozoite motility and invasion (Morahan, Wang, and Coppel 2009; Frénal et al. 2017b).

Overall, this study aims to provide a comprehensive understanding of TRP1's functional domains and their roles in sporozoite motility, egress, and invasion, shedding light on key molecular mechanisms that drive *Plasmodium* transmission.

3. Material and methods

3.1 Material

3.1.1 Chemicals, enzymes, consumables

1 kb DNA ladder
100 bp DNA ladder
10x Taq buffer with (NH4)2SO4 24-well culture plates
96-well optical bottom plates
AB-1100 Thermo-Fast 96 PCR Detection Plates
Accudenz
Acetic acid, CH3COOH
Agarose Serva research grade
Alkaline phosphatase (CIP)
Aluminum foil 150m
Alsever's solution
Amaxa human T cell Nucleofector Kit
Ampicillin sodium salt
Calcium chloride, (CaCl2) · 2 H2O
Cling film
Beakers (various sizes)
Bepanthen cream
Bovine Serum Albumin, BSA fraction V
Cell culture flask, Cellstar 250 ml
Cover slips 24 x 60 mm
Cryovials CRYO.S
D(+)-Glucose
Diethyl ether
Dimethylsulfoxide (DMSO)
dNTP mix, 10 mM
DNeasy Blood & Tissue Kit
Dulbecco's Modified Eagle Medium (DMEM)
EDTA
EGTA
Eppendorf tubes (1.5 ml, 2.0 ml)
Erlenmeyer flasks (various sizes)
Ethanol 100%
Ethanol 96%

Ethidium bromide 1%
Falcon tube (15 ml, 50 ml)
FBS 16000 (USA)
FCS
Gentamicin (10 mg/ml)
Giemsa's solution Glass-Bottom dish (10 mm) Gloves nitrile
Gloves latex
Glycerol 99%, water-free
Hank's BSS w/o Ca, Mg and Phenol Red
Heparin-Natrium 25000 U
HEPES
Hoechst 33342
Immersion oil, ne = 1.482
Immersol 518F, ne = 1.518
Immersol W, ne = 1.334
Ketamine hydrochloride solution
Loading dye purple (6x, for agarose gels)
Magnesium chloride, (MgCl2) · 2 H2O
Mercurochrome disodium salt
Methanol 100%
MgCl2, reaction buffer
Microscope slides
Midori Green
Mini-PROTEAN TGX Precast Gels MitoTracker Green FM
(Na2EDTA) · 2 H2O
Needles
Nycodenz
Nonidet P-40
2-Propanol
Paraffin 50-52°C
Parafilm
Paraformaldehyde (PFA)
Pasteur capillary pipettes PBS with Ca & Mg
PCR tubes Quali, 8-strips Penicillin/Streptomycin 100x Petri dish
PCR Product Purification Kit
Plastic pipettes (5 ml, 10 ml, 25 ml)
Plastic pestle
5x Phusion GC & HF buffer
Phusion polymerase
Pipette tips

Potassium chloride, KCl
Pyrimethamine
Restriction enzymes
Restriction buffers
RPMI-1640 with L-Glutamine w/o Phenol Red
Saponin
Sea salt, NaCl
Sodium acetate, Na(CH3COO) 3 H2O
Sodium chloride, NaCl
Sodium dihydrogen phosphate NaH2PO4
Sodium hydroxide, NaOH
Sterile filter
Sterile filter unit (1000 ml)
SuperSignal West Pico Chemiluminescent Substrate
SuperSignal West Femto Maximum Sensitivity Substrate
Syringe cannula microlance 3 (20G, 27G)
Syringe Plastipak (1 ml, 5 ml)
T4-DNA-Ligase
T4-DNA-Ligase buffer
Tape 3M Scotch 9545 red
Tape (various colors)
Taq DNA polymerase
Trans-Blot Turbo Mini 0,2 μm Nitrocellulose Transfer Packs
TRIS
Triton X-100
Trypsin / EDTA 10x
Tween20
Xylazine hydrochloride solution Bacto-Yeast extract

3.1.2 Media, Buffer, Solutions

Accudenz solution	17% (w/v) Accudenz in dd H2O
Agar-LB medium	15 g/l Agarose in LB-medium
Ampicillin stock (1000x)	100 mg/ml Ampicillin in dd H2O
Biotin phenol (BP) (100×)	MW BP: 363.5 g/mol

	Dissolve 90.875 mg/mL in DMSO Prepare 150 µL aliquots Store at −80°C
Blocking solution	2% (w/v) BSA in PBS
Complete cell culture medium	0.18% (v/v) Gentamicin 9% (v/v) FCS 0.9% (v/v) Glutamine in DMEM
CAA stock solution (1mL)	400 mM in Urea solution (MW 93.51 → 37.4mg/ml)
Fixation solution	4% (v/v) PFA in PBS
Freezing solution	10% (v/v) Glycerol in Alsever's solution
Giemsa staining solution	14% (v/v) Giemsa in Sörensen staining buffer
KX solution	10% (v/v) Ketamine 2% (v/v) Xylazine in PBS
LB-medium	10 g/l NaCl 10 g/l Bacto-Tryptone 5 g/l Bacto-Yeast extract dissolve in dd H2O pH 7.0
Lys-C stock solution	200 ng/µl solution (in 0.01% TFA) store at -20°C 20µg in 100µL 0.01% TFA
Mercurochrome solution	0.1% (w/v) Mercurochrome in PBS
NP-40	1% (v/v) Nonidet P-40 in PBS
Nycodenz stock solution	0.788 g/l TRIS 0.224 g/l KCl 0.112 g/l Na2EDTA

	276 g/l Nycodenz dissolve in dd H2O pH 7.5
Permeabilization solution	0.2% (v/v) Triton X-100 in blocking solution
Phosphate buffered saline (PBS)	137 mM NaCl 2.7 mM KCl 8 mM Na2HPO4 1.8 mM KH2PO4 in dd H2O pH 7.4
Pyrimethamine stock solution	28 mM Pyrimethamine in DMSO
Pyrimethamine drinking water	Stock 1:100 diluted in tap water (280 μM Pyrimethamine) pH 5.0
Quenching solution (1X)	5.5 mL PBS 100uL 50mM MgCl2 100uL 100mM CaCl2 100uL 100X Trolox 100uL 100X Sodium ascorbate 100uL 100X Sodium azide
RPMI-1640 + Pen/Strep	500 ml RPMI-1640 5 ml Penicillin/Streptomycin (100x)
Saponin stock solution	2.8% (w/v) Saponin in PBS
Sodium ascorbate (100X)	MW sodium ascorbate: 198 g/mol Dissolve 198 mg/mL in MQ water
Sodium azide (100X)	MW Sodium azide: 65 g/molDissolve 65 mg/mL in MQ water

Sporozoite activation buffer	3% (w/v) BSA in RPMI-1640 + Pen/Strep
T-Medium	20% (v/v) FCS (USA) 0.03% (v/v) Gentamicin in RPMI 1640
TCEP stock solution (1mL)	100 mM in 50 mM TEAB, pH 8.5 (MW 286.65 → 28.7mg/ml)
TEAB solution	100 mM TEAB, pH 8.5 1:10 from 1M stock (Sigma, at 4°C)
TFA stock solution	10% Trifluoroacetic acid in distilled water
Tris-Acetate-EDTA buffer (TAE) 50x	484 g/l TRIS 200 ml (v/v) 0.5 M Na2EDTA (pH 8.5) 114.2 ml (v/v) CH3COOH in dd H2O
Trolox (100X)	MW Trolox: 250.3 g/mol Dissolve 125.15 mg/mL in DMSO Prepared fresh and kept on ice
Trypsin stock solution	200 ng/µl solution (in 0.01% TFA), store at -20°C 20µg in 100µL 0.01% TFA
Urea solution (100ml)	6 M Urea (MW 60.06 → 36 g/100 ml) in 100 mM TEAB, pH 8.5. Add buffer until 100mL of powder.
Urea dilution solution	50 mM TEAB pH 8.5
Urea Reduction/Alkylation solution (1 ml):	100 µl TCEP solution

3.1.3 Devices

10x Apoplan objective (NA 0.25, water)	Carl Zeiss, Jena, Germany
25x Objective (NA 0.8, water)	Carl Zeiss, Jena, Germany
63x Objective (NA 1.4, oil)	Carl Zeiss, Jena, Germany
Amaxa Nucleofector II	Lonza, Köln, Germany
Analytic scale TE1245-OCE	Sartorius, Göttingen, Germany
Autoclave	Holzner, Nußloch, Germany
Axiostar plus	Carl Zeiss, Jena, Germany
Axiovert 200 with XL-3 incubator	Carl Zeiss, Jena, Germany
CCD camera EASY 440 K	Herolab, Wiesloch, Germany
Centrifuge 5417 R (cooled)	Eppendorf, Hamburg, Germany
Centrifuge Heraeus BioFuge pico	DJB Labcare, Buckinghamshire, UK
Centrifuge Heraeus Laborfuge 400e	Thermo Fisher Scientific, Waltham, USA
Centrifuge Heraeus Multifuge 1 S-R	DJB Labcare, Buckinghamshire, UK
Counter DeskTally mechanical 4 Gang	TRUMETER, Manchester, UK
Freezer -80°C	New Brunswick Scientific, Edison, USA
Freezers -20°C	Liebherr, Ochsenhausen, Germany
Heating block MBT 250	Kleinfeld Labortechnik, Gehrden, Germany
Heating block, Thermomixer compact	Eppendorf, Hamburg, Germany
Ice machine	Scotsman, Pogliano Milanese, Italy
Incubator CO2 MCO-17AI	Sanyo, München, Germany
Incubator Innova 400 shaker Incubator	New Brunswick Scientific, Edison, USA
Multitron 2 Liquid Nitrogen tank	Air Liquide, Düsseldorf, Germany
ARPEGE 170 MAC5000	
Magnetic stirrer	Carl-Roth, Karlsruhe, Germany
Microwave oven	Medion, Essen, Germany
Mini-PROTEAN Electrophoresis Cell	Bio-Rad Laboratories GmbH, München, Germany
Neubauer chamber improved	Brand, Wertheim, Germany
Nikon coolpix 5400	Nikon, Tokyo, Japan
Pipettes (L20, L200, L1000)	Labmate, St. Albans. UK
Pipette 0,2-2 µl	Gilson, Middleton, USA
PH-meter	Hanna Instruments, Kehl, Germany
Power supply (Electrophoresis) EV231	Consort, Turnhout, Belgium
Power supply (Electrophoresis) EV831	Consort, Turnhout, Belgium
Safety cabinet FWF 90	Düperthal, Kleinostheim, Germany
Scale EW600-2M	Kern, Balingen, Germany
Sterile Workbench Herasafe	Thermo Fisher Scientific, Waltham, USA
Sterile Workbench BSB 6	Gelaire, Sydney, Australia
Mastercycler ep Gradient	Eppendorf, Hamburg, Germany

Mosquito cages	BioQuip Products, Rancho Dominguez, USA
Timer	Oregon Scientific, Neu-Isenburg, Germany
Trans-Blot Turbo Transfer System	Bio-Rad Laboratories GmbH, München, Germany
UV-table UVT-28 L	Herolab, Wiesloch, Germany
Vacuum pump N86KN.18	KNF Neuberger GmbH, Freiburg, Germany
Vortex-Genie 2	Scientific Industries, Bohemia, USA
Water Bath Isotemp 210	Fischer Scientific, Swerte, Germany

3.1.4 Softwares

Adobe Illustrator
Axiovision 4.6. Software
E.A.S.Y Win 32
GraphPad Prism 9, GraphPad Software (San Diego, USA)
ImageJ
Pymol, DeLano Scientific LLC, Schrödinger Inc.
Volocity 5.2.1. LE, software Volocity Demo 6.1.1., Perkin Elmer (Waltham, USA)
Zeiss Axiocam HRm
Zotero

3.2 Molecular Biology

3.2.1 Transformation of E. coli

Transformation was performed using NEB 5-alpha Competent E. coli cells (C2987H) according to the following protocol. Approximately 35 uL of the competent cell was thawed on ice. 10 uL of the ligation mixture or Gibson assembly mix was added in a 1.5 mL microcentrifuge tube and thawed competent cells were added to it without agitation and kept on ice for 20 min. The DNA uptake was initiated by heat shocking the competent cells at 42℃ for 45 seconds immediately followed by placing them back on ice for 5 minutes. Transformed cells were plated directly on LB plates pre warmed at 37℃ containing Ampicillin since all my plasmid constructs contain Ampicillin resistance markers. In case of low transformation efficiency, 950 uL of NEB 10-beta/Stable Outgrowth Medium was added directly after the heat shock step and placed at 37℃ for 1 hour at 250 rpm. Subsequently cells were centrifuged at 13,000 rpm for 1 min and the supernatant was discarded. The remaining pellet was resuspended in 50 uL of the remaining

medium and plated on LB plates pre warmed at 37℃ containing Ampicillin. Plates were incubated overnight at 37℃.

3.2.2 Extraction of plasmid DNA from E. coli

Plasmid DNA was extracted with the Macherey Nagel Miniprep kit following the manufacturer's protocol. Purified DNA was eluted with 35 uL dd H_2O instead of the elution buffer provided in the kit and this step was repeated twice.

3.2.3 Polymerase chain reaction (PCR)

PCRs for qualitative processes like amplifying DNA fragments from plasmids, wild type PbANKA genomic DNA or sequencing were performed using a high fidelity polymerase like Phusion (NEB). For quantitative analysis, e.g. genotyping of the transgenic parasite lines, Taq polymerase (NEB) was used. Primers were designed using Snapgene software. Primers were designed to be 18-20 bp long and designed to be a melting temperature of around 55℃. PCRs were performed using the following conditions.

Reaction mix for *Taq* Polymerase		PCR Program		
Primer 1	1 uL	95℃	1 min 30 sec	
Primer 2	1 uL	95℃	30 sec	x 30
10X standard Taq Buffer	2.5 uL	55-60℃	30 sec	
2mM $MgCl_2$	1.5 uL	60℃	1 min per kb	
2mM dNTPs	2.5 uL	60℃	10 min	
Taq Polymerase	0.25 uL	4℃	hold	
Template	1 uL			
ddH_2O	15.25 uL			
Final volume	25 uL			

Reaction mix for Phusion Polymerase		PCR Program		
Primer 1	1 uL	98℃	1 min 30 sec	
Primer 2	1 uL	98℃	30 sec	
5x Phusion HF Buffer	10 uL	55-70℃	30 sec	x 30
2mM dNTPs	5 uL	72℃	1 min per kb	
Phusion Polymerase	0.50 uL	72℃	10 min	
Template	1 uL	4℃	hold	
ddH_2O	31.50 uL			
Final volume	50 uL			

3.2.4 Purification of DNA

Purification of PCR amplified products along with DNA from agarose gel was obtained with the Macherey Nagel NucleoSpin Gel and PCR Clean-up, mini kit for gel extraction and PCR clean up kit following the manufacturer's protocol. For DNA extraction from agarose gel, UV light was used to visualize the desired DNA band. Gel area containing the DNA band was cut with a scalpel and transferred into a 1.5uL microcentrifuge tube and was processed according to the manufacturer's protocol. Purified DNA was eluted with 20 uL dd H_2O instead of the elution buffer provided in the kit and this step was repeated twice.

3.2.5 Agarose gel electrophoresis

Agarose gels for electrophoresis were prepared using a 1x TAE buffer (40 mM TRIS, 20 mM acetic acid, and 1 mM EDTA, with a pH of 8.5). Agarose concentrations of 0.8% or 2% (w/v) were utilized. The agarose solution was heated in the microwave until complete dissolution, maintained at 60°C until required and poured in a gel caster. After solidification for 15-30

minutes, the gels were placed in an electrophoresis chamber filled with a 1x TAE buffer. Samples were mixed with DNA loading dye (NEB) and pipetted into the gel pockets. Electrophoresis was conducted at 120 V for 20 minutes. The separated DNA fragments were visualized under UV light imaged using a CCD camera. Reference for estimating the size and amount of loaded DNA was provided by the "1 kb-DNA-ladder" and the "100 bp-DNA-ladder" by NEB.

3.2.6 Construction of transfection vectors using Gibson assembly

Gibson assembly allows for the seamless joining of multiple DNA fragments in an isothermal reaction without the need for restriction enzymes or ligases. Its high efficiency and versatility makes it useful for a wide range of cloning applications, including the construction of plasmids, gene fusions, and incorporating point mutations. It can accommodate multiple DNA fragments of varying lengths and sequences, making it suitable for complex cloning projects. For this purpose, primers were designed with overlapping regions between adjacent DNA fragments. Overlaps were approximately 20-40 base pairs in length. DNA fragments to be assembled were amplified and purified to remove any primer dimers, nucleotides and enzymes. NEBioCalculator was used to calculate the number of pmols of each fragment for optimal assembly, based on fragment length and weight. The mass of each fragment was measured using the NanoDrop instrument, (absorbance at 260 nm).
For optimum yield, 100 ng of vector was used with 2-3 fold molar excess of each insert fragment. The following protocol was used for the assembly process.

	2-3 Fragment Assembly	4-6 Fragment Assembly
Total Amount of Fragments	X uL	X uL
Gibson Assembly Master Mix (2X)	10 uL	10 uL
Deionized H_2O	10-X uL	10-X uL
Total volume	20 uL	20 uL

The Gibson Assembly reaction mixture was incubated at 50°C for 1 hour and transformed according to the aforementioned protocol.

3.2.7 Construction of transfection vectors using ligation

Vector construction followed established protocols (Sambrook et al., 1989). Prior to cloning, genes, gene fragments, or regulatory sequences were amplified using Phusion polymerase (NEB) as per the aforementioned protocol. For the traditional cloning method, Plasmids and PCR products underwent digestion with restriction enzymes followed by ligation using T4-DNA ligase, following protocols provided by New England Biolabs. DNA fragments were separated via agarose gel electrophoresis and purified using previously described methods. Ligated plasmids were transformed into NEB 5-alpha Competent E. coli cells (C2987H) cells and selected on LB plates supplemented with Ampicillin. Plasmids were subsequently purified and subjected to restriction enzyme mapping. Finally, the correct design of the resulting plasmids was confirmed through sequencing conducted by Eurofins Genetics.

Restriction digestion (preparative)		Restriction digestion (analytical)	
Restriction enzyme 1	1 uL	Restriction enzyme 1	0.3 uL
Restriction enzyme 2	1 uL	Restriction enzyme 2	0.3 uL
Restriction buffer	5 uL	Restriction buffer	1 uL
DNA (Mini Prep)	43 uL	DNA (Mini Prep)	3 uL
dd H_2O		dd H_2O	5.4 uL
Final volume	50 uL	Final volume	50 uL
Incubation time:	overnight at 37°C	Incubation time:	2-3 hours at 37°C

3.3 Parasite Biology

3.3.1 Bioinformatic analysis

Plasmodium sequences were obtained from PlasmoDB (https://plasmodb.org/plasmo/app) and multiple sequence alignments were conducted using Clustal Omega (https://www.ebi.ac.uk/jdispatcher/msa/clustalo). Potential signal peptides and transmembrane domains were predicted utilizing SignalP

(https://services.healthtech.dtu.dk/services/SignalP-5.0/) and TMHMM (https://services.healthtech.dtu.dk/services/TMHMM-2.0/). Other known domains were identified using SMART (http://smart.embl-heidelberg.de/) and HHpred (https://toolkit.tuebingen.mpg.de/tools/hhpred). Cytoplasmic tail domains (CTDs) pI values and protein molecular weights were calculated using Expasy (https://www.expasy.org/). For visualizing of predicted protein structures, AlphaFold, developed by Deepmind was used (https://deepmind.google/technologies/alphafold/). For predicting the structures of different protein domains or interaction between different domains, CollabFold was used (https://colab.research.google.com/github/sokrypton/ColabFold/blob/main/AlphaFold2.ipynb).

3.3.2 Determination of parasitemia

To quantify the parasitemia in infected mice, a small amount of blood from the tail was placed onto a microscope slide and spread thinly using another slide. The blood smears were air-dried at room temperature and then briefly fixed in 100% methanol followed by dipping in Hemacolor stain for approximately 5 seconds. Next, the slides were immersed in Giemsa staining solution (Merck) and left to stain for 3 minutes. After staining, the blood smears were rinsed with distilled water and air-dried at room temperature. Evaluation of the blood smears was conducted using a light microscope (Carl Zeiss) equipped with a counting grid, with a magnification of 100-fold. The percentage of infected red blood cells was calculated using the following formula:

$$\frac{\text{Counted parasites in all fields}}{\text{Counted erythrocytes in 1 field X Numbers of fields}} \text{ X } 100$$

3.3.3 Blood sampling by cardiac puncture

To collect the entire blood volume,mice with a parasitemia of ≥2% were anesthetized via intraperitoneal injection with a mixture of ketamine and xylazine (87.5 mg/kg ketamine and 12.5

mg/kg xylazine). Blood (800-1,000 µl) was then drawn via cardiac puncture using a 10 ml syringe (BD). Subsequently, mice were euthanized by cervical dislocation.

3.3.4 Transfection of *P. berghei*

Transgenic *Plasmodium spp.* were created through double homologous recombination, a highly effective method due to the absence of non-homologous end-joining (NHEJ) capability in these parasites. Transfections into *Plasmodium berghei* were conducted during the schizont stage using standard protocols. Initially, a naïve NMRI or swiss mouse was infected with wild type parasite line via intraperitoneal injection. Parasites were allowed to proliferate until reaching a parasitemia of approximately 1.5-2%, typically occurring 4-5 days post infection. Infected blood was then obtained via cardiac puncture and mixed with pre-warmed (37°C) T-medium containing heparin for approximately 20 hours. Schizont enrichment in the culture was confirmed microscopically. Subsequently, the culture was centrifuged using density gradient centrifugation with a 55% Nycodenz solution to concentrate schizonts, which were then collected, resuspended with fresh T medium, and prepared for transfection. 100 uL Nucleofector solution (Provided with the Amaxa kit, LONZA) was added to the DNA prepared for the transfection and was mixed with the Schizonts for Transfection. Transfected parasites were electroporated and injected intravenously into the tail vein of naïve NMRI or Swiss mice. Selection pressure was applied approximately 24 hours post-transfection, and mice positive for parasites were maintained until reaching a parasitemia of approximately 2%, at which point blood was collected for stabilate preparation and parasite purification.

3.3.5 Storage and injection of intraerythrocytic stages

To preserve blood stage parasites, 100 µl of infected blood with a parasitemia of ≥2% was transferred into cryotubes and combined with 200 µl of a freezing solution (containing 10% glycerol in Alsever's solution). The tubes were promptly frozen and stored in liquid nitrogen (for long term storage) or at -80°C (For temporary storage). To infect mice anew, the frozen parasites containing stabilates were thawed and administered via intraperitoneal injection into naïve NMRI or Swiss mice.

3.3.6 Generation of isogenic parasite populations

To generate isogenic transfected parasite lines, a donor NMRI or Swiss mouse was infected via intraperitoneal injection with frozen parasite stabilates obtained from transfections (parental population). Approximately 24 hours after injection, selection pressure was initiated by adding pyrimethamine (0.7 mg/ml) to the drinking water. When parasitemia reached 0.5-1%, the donor mouse was bled via cardiac puncture. The collected blood was diluted with PBS to achieve a concentration of 0.8 - 1 parasites per 100 µl solution and then intravenously injected into the tail vein of 9 naive NMRI or Swiss mice. Once infected mice reached a parasitemia of about 2%, they were sacrificed, and one fraction of the blood was frozen as stabilates (as described previously) for future uses and the rest of the blood was used to isolate genomic DNA of the parasite. Genotyping PCR and sequencing were performed for evaluating the Isogenicity of the parasite lines.

3.3.7 Extraction of genomic DNA and genotyping of parasites

To extract genomic DNA (gDNA) from blood stage parasites, mice infected with a parasitemia of ≥2% were subjected to cardiac puncture to collect blood. The collected blood was combined with PBS in an 1.5 mL microcentrifuge tube for a final volume of 1 mL and erythrocytes were lysed by adding 50 uL saponin. After the samples became transparent, the tubes were centrifuged for 2 minutes at 11,000 rpm. The supernatants were then discarded, and the pellets were resuspended in 1 ml, following a second centrifugation step for 1 minute at 11,000 rpm to get rid of the residual erythrocytes, the supernatant was again discarded, and the remaining pellet was resuspended in 200 µl. The purified blood stage parasites were either directly utilized for gDNA isolation or stored at -20°C. Genomic DNA extraction was carried out using the Dneasy Blood & Tissue Kit (Qiagen) according to the manufacturer's protocol. Elution of gDNA was performed with 200 µl of double-distilled water (ddH2O), and the gDNA was either used immediately for PCR or stored at -20°C.

For parasite genotyping, gDNA was employed in a standard PCR reaction with *Taq* polymerase following the aforementioned protocol. To assess correct integration of the transfected DNA, four different PCRs were conducted. Integration at the 5' and 3' ends of the integration site was assessed using PCRs with primers binding upstream and downstream of the integration locus, as well as primers near the 5' and 3' ends of the integrated DNA sequence. Products, comprising a mix of wild-type and integrated sequence, were amplified only if successful DNA integration occurred. Additionally, primers binding near the integration site but not within the transfected DNA sequence were used in a single PCR. In this scenario, products were significantly longer if DNA integration occurred compared to the unmodified locus. Furthermore, a PCR was conducted to confirm the presence of the selection marker by utilizing primers binding within regulatory sequences of the selection cassette. PCR products from transgenic parasites were sequenced to further ensure the presence of a mutation or the absence of a removed sequence.

3.3.8 Exflagellation assay

Before conducting a mosquito infection, exflagellation of the gametocytes were insured. A drop of infected mouse blood from the tail vein was placed on a glass slide and a cover slip was placed directly on top to spread out the blood drop evenly. The slide was placed in an incubator set at 21 degree celsius temperature. The drop in blood temperature initiates the response to exflagellate in gametocytes. The slide was checked for any exflagellation event with a light microscope using phase contrast at 40X magnification exactly after 12 minutes of placing the slide in the incubator.

3.3.9 Mosquito infection

For infecting a mosquito cage, a donor mouse was infected by intraperitoneally injecting them with desired parasite stabilates. The amount injected depended on the timing and number of mosquitoes fed. For an infection with one whole stabilate, parasites were allowed to grow for 4-5 days, followed by bleeding the donor mouse via cardiac puncture once parasitemia reached ~2%. The fresh blood was used for a transfer of 20,000,000 parasites into two naïve mice. Mice receiving a blood transfer were kept for a further 3-4 days depending on the content of gametocytes, which was assessed by the extent of exflagellation events. In case of a satisfactory

amount of exflagellation (at least 3-5 exflagellation events per field), mice were fed to mosquitoes. For feeding a full cage of mosquitoes (around 600 mosquitoes), fresh blood transfer was done in 2 mice and for feeding half a cage (around 300 mosquitoes), only 1 mouse was fed. Mice with the appropriate density of gametocytes were anesthetized with a mixture of ketamine and xylazine (87.5 mg/kg ketamine and 12.5 mg/kg xylazine), placed on top of mosquito cages, and covered with paper tissues to dim the light and encourage biting. Mosquitoes were allowed to feed for 20-30 minutes to ensure most mosquitoes had the opportunity to feed, making sure that the mice were turned and shifted from their initial position every 10 minutes. Subsequently, infected mosquitoes were kept at 80% humidity and 21°C in an incubator for optimum survival.

3.3.10 Counting of oocysts

To know the infection rate of mosquito midguts infected with *Plasmodium,* midguts were dissected between day 10-14 and stained with mercurochrome. Mercurochrome helps create contrast in the oocyst wall and the smooth muscles of mosquito midgut that facilitates in their detection.The midguts post dissection in PBS, are permeabilized in 1% NP 40 solution (in PBS) for 30 minutes.

Eventually, the supernatant was discarded and the permeabilized midguts were incubated in 0.1% mercurochrome solution (in PBS) for at least 1 hour. Post staining, the midguts were washed carefully with PBS 2-3x until the solution becomes clear. The stained midguts were transferred with a pasteur pipette onto a glass slide and covered with a cover slip and sealed with wax. The midguts were then imaged using an Axiovert 200M (Carl Zeiss) fluorescence microscope with 10x magnification.

3.3.11 Preparation of hemolymph, midgut and salivary gland sporozoites

Sporozoites were harvested from the midguts, hemolymph, and salivary glands of infected mosquitoes between day 11 and day 24 post-infection. The timing of dissection depended on the planned experiments: midgut sporozoites were dissected between day 10 and 14, hemolymph sporozoites between day 14 and 16, and salivary gland sporozoites between day 17 and 24 post-infection. In cases of parasite lines with defects in egress from the oocyst or salivary gland

invasion, a time course was conducted by counting sporozoites on day 14, 17/18, 20, and 22 to validate the phenotype.

For counting experiments, midguts and salivary glands from at least 10 mosquitoes were dissected in PBS or RPMI medium, crushed with a pestle, and free sporozoites were counted using a Neubauer counting chamber.In case of midgut sporozoites, sporozoites were diluted 10 times before counting in the Neubauer chamber for the ease of counting. Sporozoites were allowed to settle for 5 minutes before counting, which was done using a light microscope (Carl Zeiss) at 40-fold magnification with a phase contrast.

To isolate hemolymph sporozoites, mosquitoes were anesthetized by cooling on ice for at least 30 minutes. Once immobilized, the last segment of the abdomen was cut with the sharp end of a needle, and mosquitoes were flushed by inserting a long-drawn Pasteur pipette into the lateral side of the thorax and injected with PBS. Hemolymph was drained from the abdomen, collected on a piece of paraffin wax film, and transferred to a 1.5 mL microcentrifuge tube (Eppendorf). Hemolymph sporozoites were then centrifuged at 11,000 rpm for 3 minutes and the supernatant was discarded. The pellet was then resuspended with 100 uL fresh PBS and counting was carried out as described previously for midgut and salivary formula:

3.3.12 Gliding assays of sporozoites

To perform sporozoite gliding motility assays, salivary glands from 20–30 infected mosquitoes were dissected in 50 µl of ice cold RPMI or PBS medium. The tissues were then crushed with a pestle to release the sporozoites, which were subsequently purified using density gradient centrifugation with 17% Accudenz (Kennedy et al. 2012). The purified sporozoite pellets were resuspended in 200 µl of room temperature RPMI or PBS medium supplemented with 3% BSA and transferred to a non coated 96-well plate with an optical bottom. The sporozoites can also be prepared by directly squashing a few cleanly dissected salivary gland tissues in 100 uL of RPMI or PBS medium which was then mixed with an equal volume of RPMI or PBS medium containing 6% bovine serum albumin (BSA). Hemolymph sporozoites from approximately 20 infected mosquitoes were isolated following a previously described method and centrifuged for 3

minutes at 13,000 rpm at room temperature. The excess supernatant was discarded, and the sporozoites were resuspended in 200 µl of RPMI or PBS medium supplemented with 3% BSA and transferred into a 96 well plate. Regardless of the sporozoites origin, the plates were centrifuged for 3 minutes at 1500 rpm and immediately imaged using an Axiovert 200M (Carl Zeiss) fluorescence microscope. Movies were recorded in differential interference contrast (DIC) with a 25x magnification and one frame every 3 seconds and analyzed using FIJI.

3.3.13 Live cell microscopy of *P. berghei*

Imaging of oocysts and salivary gland sporozoites was performed between 11-14 days and 17-24 days post-infection of the mosquitoes, respectively. Midguts or salivary glands were dissected and placed on a microscope slide in a drop of RPMI, PBS supplemented with Hoescht 33342 (1:1000 dilution of 10 mg/ 1 ml stock solution in DMSO) . The sample was sealed and imaged directly with a spinning disc confocal microscope (Perkin Elmer) at 100X magnification (Frénal et al. 2017a). Salivary gland sporozoites were extracted 17-21 days post-infection, transferred to a 8-well non coated optical-bottom plate (Ibidi), and mixed with an equal volume of RPMI containing 6% BSA and Hoechst 33342 (1:1000 dilution). The plate was centrifuged for 3 minutes at 1500 rpm (Heraeus Multifuge S1) and imaged immediately at 100X magnification.

3.3.14 Infection by mosquito bites and sporozoite injections

To evaluate the transmission potential of generated parasite lines, mice were infected by either the natural transmission via mosquito bites or by bypassing the barrier of skin via direct sporozoite injections. For studying native transmission, mosquitoes infected 17-24 days earlier were separated into cups of 10 each and starved for 6-8 hours. Naive C57Bl/6 mice were then anesthetized with an intraperitoneal injection of ketamine and xylazine (87.5 mg/kg ketamine and 12.5 mg/kg xylazine), and placed ventral side down on the cups for about 20 minutes. Mosquitoes that took a blood meal were dissected afterward or the next day to determine sporozoite numbers in their salivary glands. For salivary gland sporozoite injection, salivary glands from mosquitoes infected 17-24 days earlier were dissected in RPMI medium. Sporozoites were released and diluted with RPMI to 10,000 sporozoites per 100 µl. Sporozoite solutions were injected intravenously into the tail vein of naive C57Bl/6 mice. Parasitemia in

infected mice was monitored by daily blood smears from day 3 to day 20 post-infection, and survival was monitored up to 30 days. Blood smears were stained with Giemsa solution and counted using a light microscope (Carl Zeiss) with a counting grid. The time from infection to the first observed blood stage was recorded as the prepatent period.

3.3.15 Western Blotting

For probing protein expression in sporozoites, infected salivary glands or midguts were dissected in ice cold PBS medium supplemented with a protease inhibitor cocktail (containing 50,000 units/L penicillin and 50 mg/L streptomycin). The midguts or salivary glands were crushed with a pestle to release sporozoites. Midgut sporozoites were then purified using density gradient centrifugation with 17% Accudenz solution. Approximately 300,000 purified midgut sporozoites and unpurified salivary gland sporozoites were centrifuged for 5 minutes at 13,000 rpm. The supernatant was discarded and the pellets were stored indefinitely in -80 degree celsius. Before performing the western blot, the samples were lysed with 30-50 µl RIPA buffer and then mixed with Laemmli buffer (containing 10% β-mercaptoethanol), denatured at 95°C for 10 minutes, and centrifuged for 1 minute at 13,000 rpm. Sporozoite samples were frozen for 5 minutes at -20°C after denaturation and before loading onto the gel and only the supernatant was loaded. The gel was run with 120 Volts and 90 Watts for about 2 hours until the protein ladder was visually well separated. The proteins were transferred to nitrocellulose membranes using the Trans-Blot Turbo Transfer System (Bio-Rad), blocked with TBST containing 0.05% Tween20 and 5% milk powder for 1 hour, and incubated with specific antibodies overnight at 4°C. After incubation, the blots were washed three times with TBST containing 0.05% Tween20 for 5 minutes each, followed by at least 1-hour incubation with secondary antibodies (diluted 1:10,000). Signals were detected using SuperSignal West Pico Chemiluminescent Substrate and/or SuperSignal West Femto Maximum Sensitivity Substrate (Thermo Fisher Scientific).
If a second primary antibody was needed, such as for a loading control, the membranes were treated with a mild stripping buffer and re-blocked before applying the second primary antibody (following company protocols).

3.3.16 Immunofluorescence assays with sporozoites

To visualize protein expression on sporozoites using immunofluorescence, infected midguts or salivary glands were dissected either in ice cold PBS or RPMI in a plastic reaction tube (Eppendorf). The sporozoites were then mechanically released with a pestle and purified using density gradient centrifugation as mentioned earlier. The purified sporozoites were resuspended in PBS and pipetted onto 8 well non coated Ibidi dishes with an optical bottom . Sporozoite solutions were activated with an equal volume of PBS containing 6% BSA and centrifuged down for 3 minutes at 13,000 rpm at room temperature. The sporozoites were allowed to glide for 20 minutes to 1 hour at room temperature . Afterward, the supernatant was discarded, and sporozoites were fixed with 4% PFA (diluted in PBS). Fixation was always carried out for 1 hour at RT. The fixed samples were washed three times with PBS for 5 minutes each. Subsequently, sporozoites were blocked (PBS containing 2% BSA) or blocked and permeabilized (PBS containing 2% BSA and 0.5% Triton X-100) for at least 1 hour at room temperature or overnight at 4°C. Samples were then incubated with primary antibody solutions for at least 1 hour at RT in the dark and washed three times with PBS. After the last washing step, samples were incubated with secondary antibody solutions for 1 hour at RT in the dark. Stained samples were washed three times in PBS, and 200 uL fresh PBS was added. The sample was either imaged immediately or stored in the fridge overnight or until next use.

Antibody/ Dye	**Dilution ratio**	**Source**
Anti CS (mouse)	1/ 3000	(Yoshida et al., 1980)
Anti GFP (mouse) for WB	1/ 1000	Roche
Anti GFP (rabbit) for IFA	1/ 40	Invitrogen, Thermo Fisher Scientific
Anti rabbit Alexa 488/ 546/ 594	1/ 500	Invitrogen, Thermo Fisher Scientific
Anti rabbit HRP	1/ 10000	Bio-Rad
Anti mouse Alexa 488/ 546/ 594	1/ 500	Invitrogen, Thermo Fisher Scientific

Hoechst 33342 (10mg/ml)	1/ 500	Sigma, München, Germany
Streptavidin- 594	1/ 1000	Sigma, München, Germany
Anti FLAG (mouse) for IFA	1/50	Abfinity

3.3.17 Proximity dependant biotinylation assay using APEX:

Sporozoite sample preparation:

1. Well infected t*rp1-apex* mosquitoes were dissected as clean as possible to collect only the salivary glands, barring mosquito debris.
2. Salivary gland sporozoites were purified through accudenz purification.
3. Sporozoites were counted and 1.5 million sporozoites were incubated with 2.5 mM Biotin-Phenol solution and 3% BSA for 2 hours.
4. After 2 hours of incubation, freshly prepared Hydrogen peroxide solution was added so that the final concentration is 1mM. For control samples, this step was skipped.
5. Freshly prepared quenching solution was added immediately after 1 min and the sporozoites were centrifuged at 1000 g for 3 minutes. The supernatant was discarded and fresh quenching solution was added to resuspend the sporozoite pellet. This step was repeated twice more.
6. Finally the sporozoite pellet was collected and the supernatant was discarded. The pellet was frozen immediately at -80 degree celsius until further use.

Protocol was optimized from (Tan et al. 2020)

Protein Extraction, Streptavidin Enrichment, and Digestion Protocol:

1. Cell pellets were lysed in 600 µL cold RIPA buffer for 1 hour at room temperature (RT) with continuous shaking/rotation.
2. Lysates were centrifuged at 15,000g for 10 minutes at 4°C, then the supernatant was transferred to fresh 1.5-mL microcentrifuge tubes. Non-autoclaved tubes were used and were kept sealed.

3. Streptavidin-coated Dynabeads C1 magnetic beads were washed twice with RIPA buffer.
4. Each sample was incubated with 50 µL bead slurry in separate microcentrifuge tubes for 1 hour at RT with rotation.
    - Note: Bead volume was reduced from 100 µL to minimize excess streptavidin binding.
5. Beads were washed twice with 1 mL RIPA buffer.
6. 10 stringent washes were performed with 1 mL Urea solution (6M Urea, 100mM TEAB) to completely remove detergents.
    - Note: Mix thoroughly by removing tubes from the magnet, shaking, spinning briefly, and placing back on the magnet to prevent detergent carryover.
    - If beads stick to the tube walls after multiple washes, reconstitute in RIPA, transfer to low-binding tubes, and continue washing.
7. The supernatant was removed and beads were resuspended in 50 µL Urea-Reduction/Alkylation solution, scraping beads off tube walls as needed.
8. Incubation was done for 30 minutes at RT.
9. Beads were washed with 100 µL Urea solution, supernatant was removed and resuspended in 25 µL Urea solution.
10. 300 ng Lys-C (1.5 µL from stock) was added and incubated for 4 hours at 37°C in a Thermoshaker (2000 rpm).
11. 75 µL TEAB solution was added.
12. 300 ng Trypsin (1.5 µL from stock) was added and digested overnight at 37°C in a Thermoshaker (2000 rpm).
13. Centrifugation was done at 2000 rpm for 2 minutes and the supernatant was collected.
14. The sample was acidified by adding 8 µL of 10% TFA to reach a final concentration of 0.4% (vol/vol).
15. It was verified that the pH is <2.
16. Proceeded with peptide desalting using C18-StageTips (at MS facility platform).

3.3.17 Image processing and data analysis

Images were processed and adjusted with FIJI (Schindelin et al. 2012). Fluorescence images were mostly acquired as Z-Stack. Final images from these data were obtained by projecting all

focal planes with the ‘Z-Projection’ function. Speeds of moving sporozoites were tracked with the ‘Manual tracking’ function. Generated data were exported as an excel file and further processed in GraphPad Prism and R.

3.3.18 Statistical analysis

Statistical analysis was performed using GraphPad Prism (GraphPad, San Diego, CA, USA) and R software. The normality of the datasets was assessed using a Kolmogorov-Smirnov test. If the data exhibited a normal distribution, significance was evaluated using a One-way ANOVA test for more than two datasets, or a paired t-test for two datasets. Conversely, if the data did not follow a normal distribution, significance was assessed using a Kruskal-Wallis test for more than two datasets, or a Mann-Whitney test for two datasets. The p-values are provided in the legends corresponding to the graphs.

3.3.19 Ethics statement

All animal studies adhered to the GV-SOLAS and FELASA standard protocols and were authorized by the relevant German regulatory bodies (Regierungspräsidium Karlsruhe). Plasmodium parasites were sustained in Swiss and NMRI mice sourced from Charles River Laboratories or JANVIER. Prepatency following sporozoite infection and parasite growth were assessed using C57Bl/6 mice obtained from Charles River Laboratories or JANVIER. All transfections and genetic alterations were conducted in the *Plasmodium berghei* ANKA strain (Vincke and Bafort 1968).

4. Parasite lines

4.1 Generation of *trp1* C-terminal deletion parasites: *trp1Δ3, trp1Δ14, trp1Δ19*

A series of C-terminal domain mutants were generated for understanding the role of C-terminus in egress, invasion and motility. Parasites lacking various lengths of C-terminus domain were generated for identifying the key residues of the domain. For this purpose, TRP1 C-term GFP vector generated by previous PhD student Dennis Klug was used (Klug and Frischknecht 2017). Parasites containing various TRP1 C-terminus deletions were generated by PCR amplifying the *trp1* ORF containing the desired C-terminus length and cloned into the already existing TRP1 C-term GFP vector in a way where *gfp* was excised from the plasmid. The final vector containing a *hdhfr-yfcu* positive-negative selection marker was digested (*Sac*II and *Xho*I) to generate a linear DNA fragment that was transfected into wild type parasites (*wt*) using double homologous recombination. The final construct containing the selection marker was surrounded by around 1000 bp upstream of the intended deletion site at the C-terminus, that was used as the 5' homologous region and the 3' homologous region was comprised of the last 609 bp of the C-terminus along with about 500 bp downstream of the *trp1* ORF, since the distance between *trp1* and its neighboring gene (PbANKA_070800) was very little (291 bp), disrupting which could lead to potential perturbation in the protein expression of both genes. Following this method three different isogenic parasite lines were generated with 3 (*trp1Δ3*), 14 (*trp1Δ14*) and 19 (*trp1Δ19*) amino acid deletions respectively in the C-terminus domain of *trp1*. Parasites were selected using pyrimethamine post transfection. Isogenic parasite lines were generated using limiting dilution (See 'Materials and methods' section).

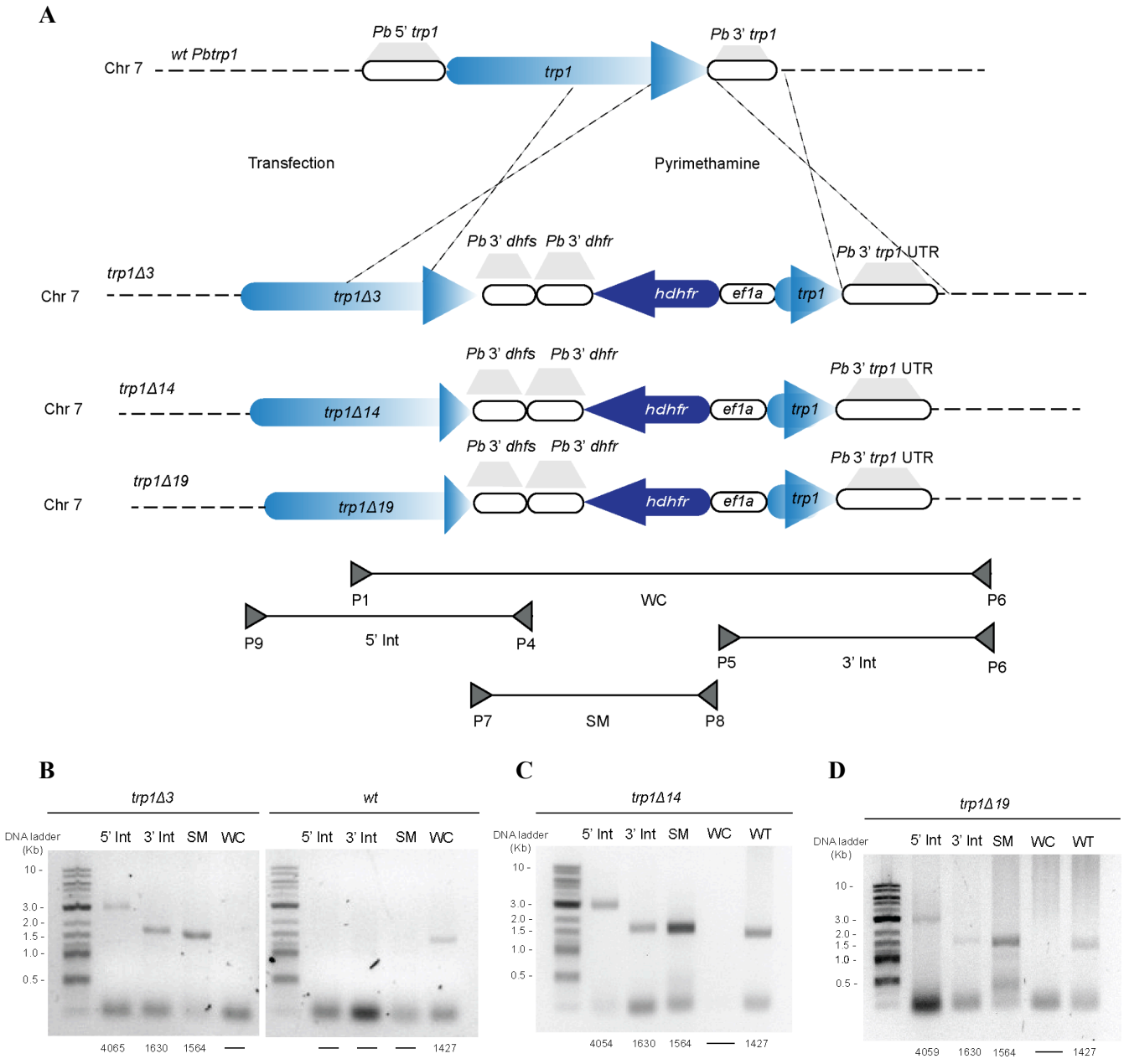

Figure: 4.1. Generation of *trp1Δ3, trp1Δ14, trp1Δ19* parasites.

A. Illustration of the generation of various C-terminal deletion mutants for TRP1. The integration of transfected DNA into the wild-type parasite led to the generation of C-terminal deletion mutants via double crossover homologous recombination. The binding sites of the primers, along with the approximate lengths of the PCR products used for genotyping, are indicated by arrowheads and lines positioned above and below the schematic representation. **B-D.** Genotyping of isogenic *trp1Δ3, trp1Δ14, trp1Δ19* parasite lines were conducted, with the expected PCR product sizes indicated below the gel images (in bp length). Notably,

amplification of the complete constructs were unsuccessful, likely due to the sequence's length and high AT content. PCR analyses were also performed on the wild-type (*wt*) recipient line for comparison. (5' int: 5' integration; 3' int: 3' integration; SM: Selection marker; WC: Whole construct, WT: Wild type *trp1* construct).

4.2 Generation of *trp1* C-terminal swap parasites: *Pbtrp1-Pftrp1 ctd swap, Pbtrp1-Pbtrap ctd swap*

To better understand the function of the CTD in sporozoites journey from the oocyst to the salivary gland better, I swapped the C-terminus of *Pb trp1* with the much shorter C-terminus (98 bp) of *Pf trp*1 to generate *Pbtrp1-Pftrp1 ctd swap*. For generating this parasite line the TRP1 C-term GFP vector was used as the backbone. A four fragment Gibson assembly was used to assemble the three PCR fragments amplifying about 1000 bp of the *Pbtrp1* ORF until the transmembrane domain (TMD), the 98bp long C-terminus domain of *Pftrp1,* and 396 bp of the 3'UTR of *Pbdhfs* that was instead of the native 3' UTR to express TRP1 respectively.

To assess if the C-terminus of *Pb*TRAP can rescue the function of *Pb* TRP1, another C-terminus swap mutant, *Pbtrp1-Pbtrap ctd swap* was generated. For generation of this parasite line I used the TRP1 C-term GFP vector as the backbone for gibson assembly. A four fragment assembly was conducted, where three fragments consisting of 1000 bp of the *Pbtrp1* ORF until the transmembrane domain (TMD), the 178bp long C-terminus domain of *Pbtrap* and 396 bp of the 3'UTR of *Pbdhfs, all* containing complementary overhang were PCR amplified and cloned into the original vector. Double homologous recombination was used to transfect the digested linear plasmid DNA fragments (*Sac*II and *Xho*I) in both cases into *wt* parasites. Isogenic parasite populations were selected by using a limiting dilution method. Note that the final plasmids for both the swap mutants were designed to exclude the gene coding for *gfp.*

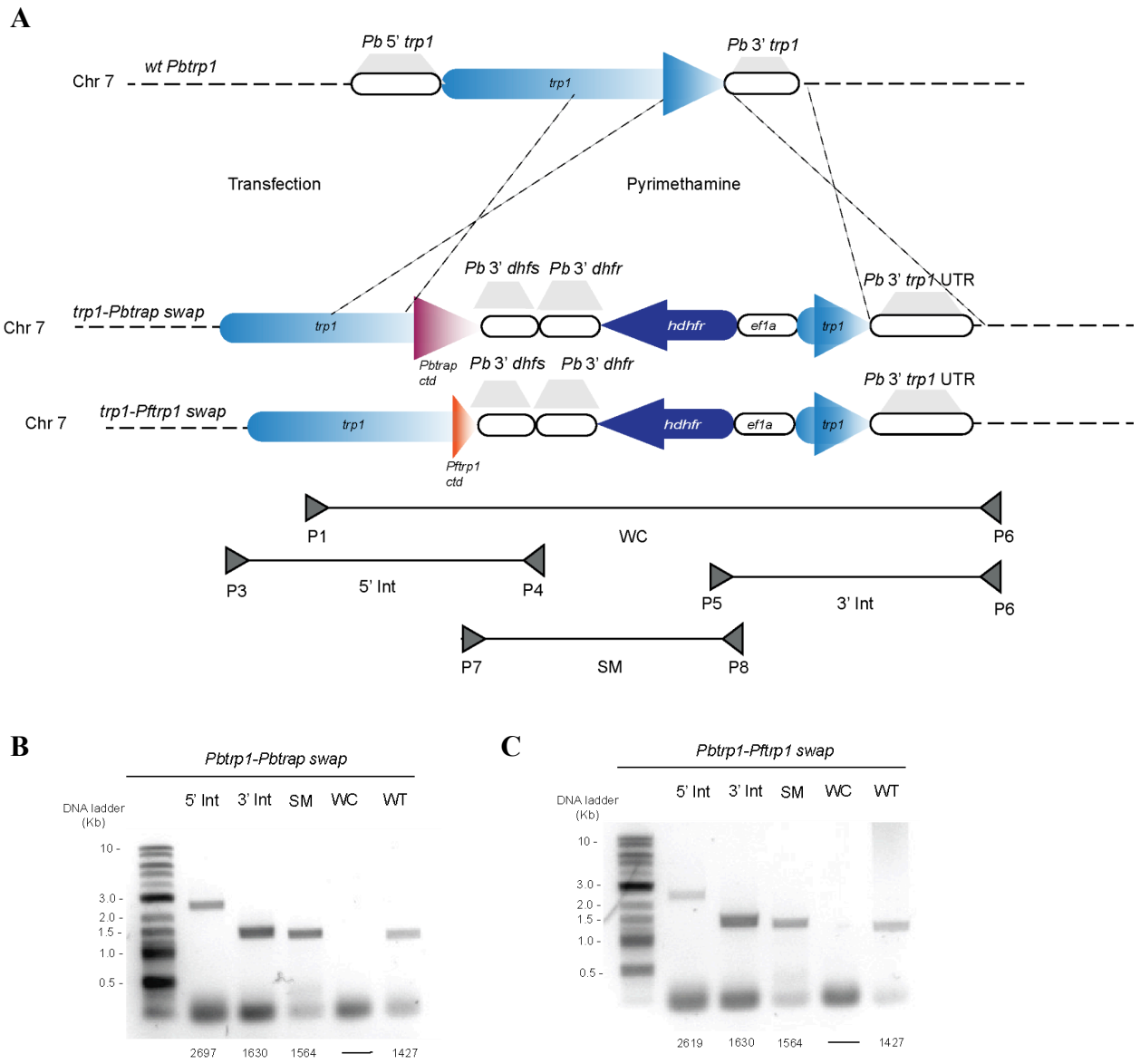

Figure: 4.2. Generation of *Pbtrp1-Pbtrap ctd swap, Pbtrp1-Pftrp1 ctd swap* parasites.

A. Illustration of the generation of various C-terminal swap mutants for TRP1. The integration of transfected DNA into the wild-type parasite led to the generation of C-terminal swap mutants via double crossover homologous recombination. The binding sites of the primers, along with the approximate lengths of the PCR products used for genotyping, are indicated by arrowheads and lines positioned above and below the schematic representation. **B-C.** Genotyping of isogenic *Pbtrp1-Pbtrap ctd swap, Pbtrp1-Pftrp1 ctd swap* parasite lines were conducted, with the expected PCR product sizes indicated below the gel images (in bp length). Notably, amplification of the complete constructs were unsuccessful, likely due to the sequence's length and high AT content. PCR analyses were also performed on the wild-type (*wt*) recipient line for

comparison. (5’ int: 5’ integration; 3’ int: 3’ integration; SM: Selection marker; WC: Whole construct, WT: Wild type *trp1* construct).

4.3 Generation of *trp1 tsr* domain mutant parasites: *trp1Δtsr, trp1-tsr-point, trap-tsr-swap*

To understand the role of the TSR domain in the function of TRP1, with the help of Master students Bea Jagodic and Marzia Matejcek I generated parasites lacking the *trp1tsr* domain (*trp1Δtsr*) and parasites containing point mutations in the conserved tryptophans (W591A,W594A) of the TSR domain (*trp1-tsr-point*). For generation of this parasite line, I first constructed an intermediate vector containing the whole length of *trp1* ORF, Pb238::TRP1gDNA using the TRP1 C-term GFP vector as the backbone. The whole ORF of *trp1* was amplified and restriction sites (*Sac*II and *Bam*HI) were added to its 5’ and 3’ end by PCR. Meanwhile the vector backbone was digested with the same restriction enzyme (*Sac*II and *Bam*HI) and the PCR amplified product was cloned into the construct using T4 ligase. Note that the intermediate vector did not contain any *gfp* coding gene sequence.

Pb238::TRP1gDNA vector was used as a template and backbone to generate PCR fragments required for generating both TSR mutant constructs. For generating the *trp1Δtsr* parasite line, a three fragment gibson assembly was conducted, including a 1845 bp long fragment of *trp1* ORF until right before the *tsr* domain and a 1143 bp sequence encoding *trp1* ORF post *tsr* domain and part of the 3’*dhfs* sequence including complementary overhangs. For generating the *trp1-tsr-point* parasite line, I used a three fragment gibson assembly where two PCR amplified fragments of complementary trp1 ORFs containing overhangs that included the point mutations in the conserved tryptophan residues at position 591 and 594 were cloned into the donor vector backbone. The resulting vectors were digested (*Sac*II and *Xho*I), purified and transfected into *wt* parasites. Isogenic parasite lines were selected via limiting dilution of the transfected parasites.

Similarly, for the generation of *trap-tsr-swap* parasite line Pb238::TRP1gDNA vector was used as a template and backbone to generate PCR fragments required for generating the constructs for gibson assembly. TRAP- TSR domain was amplified from *wt* genomic DNA and was assembled using gibson assembly. The resulting vectors were digested (*Sac*II and *Xho*I), purified and

transfected into *wt* parasites. Isogenic parasite lines were selected via limiting dilution of the transfected parasites.

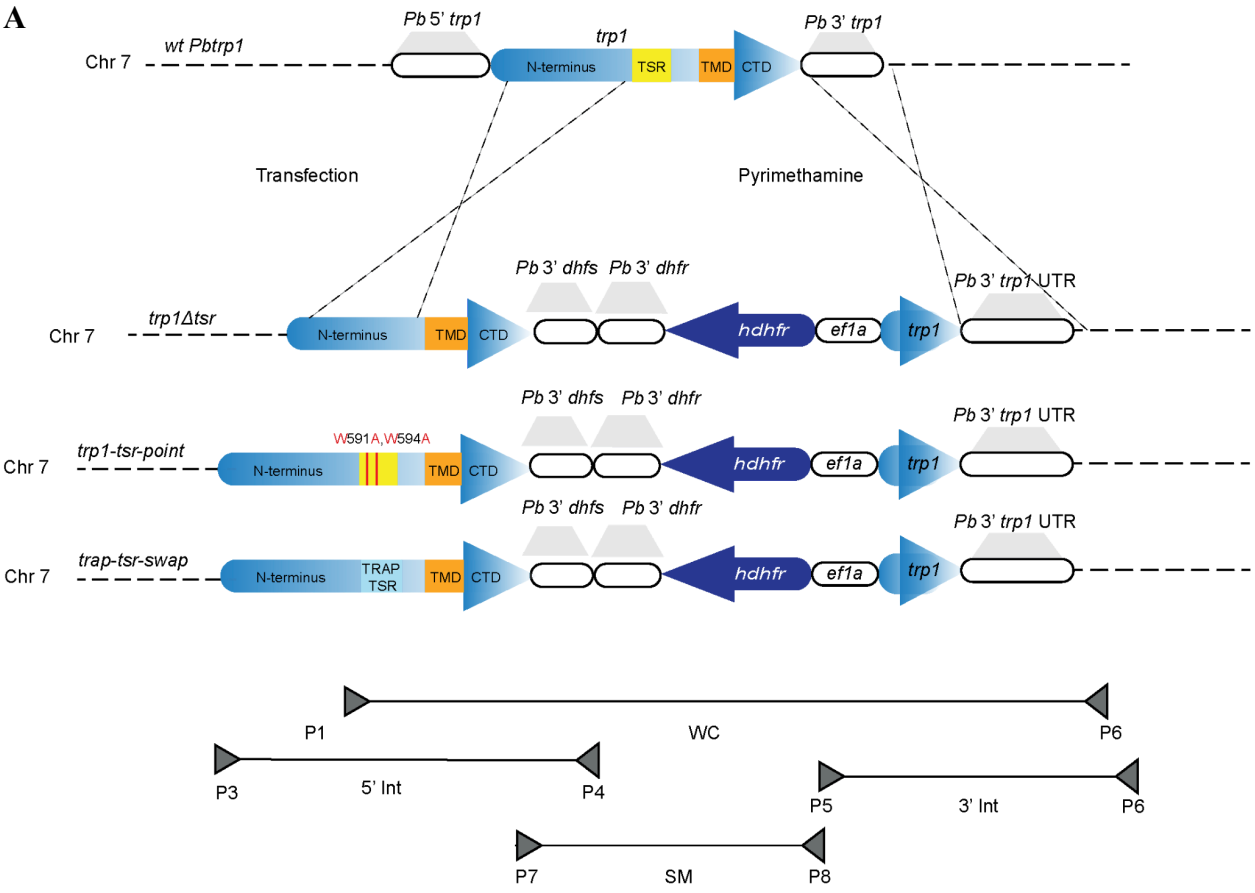

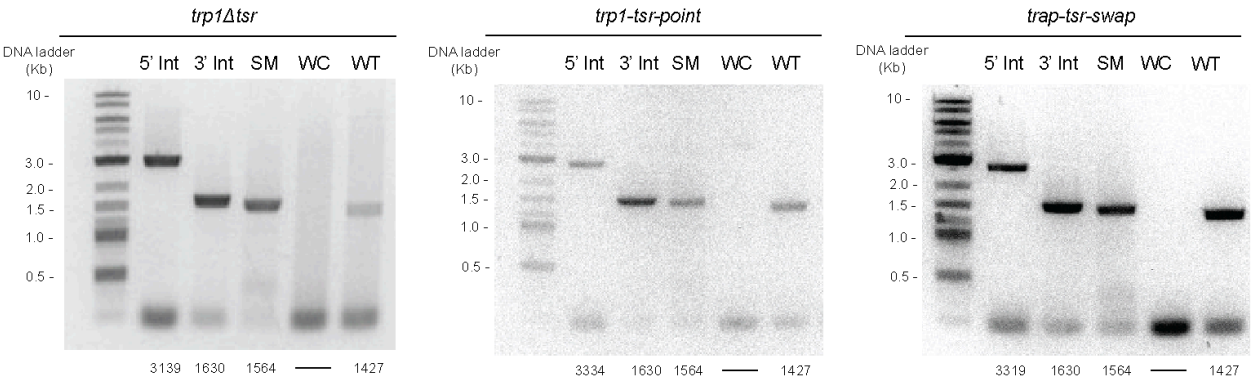

Figure: 4.3. Generation of *trp1Δtsr*, *trp1-tsr-point*, *trap-tsr-swap* parasites.

A. Illustration of the generation of various TSR domain mutants for TRP1. The integration of transfected DNA into the wild-type parasite led to the generation of TSR domain mutants via double crossover homologous recombination. The binding sites of the primers, along with the approximate lengths of the PCR products used for genotyping, are indicated by arrowheads and lines positioned above and below the schematic representation. **B-D.** Genotyping of isogenic *trp1Δtsr, trp1-tsr-point, trap-tsr-swap* parasite lines were conducted, with the expected PCR product sizes indicated below the gel images (in bp length). Notably, amplification of the complete constructs were unsuccessful, likely due to the sequence's length and high AT content. PCR analyses were also performed on the wild-type (*wt*) recipient line for comparison. (5' int: 5' integration; 3' int: 3' integration; SM: Selection marker; WC: Whole construct, WT: Wild type *trp1* construct).

4.4 Generation of *trp1-gfp-tsr, trp1-tmd-gfp, trp1-flag10-gfp, trp1-flag20-gfp* parasites:

I used the intermediate vector Pb238::TRP1gDNA to generate parasite lines *trp1-gfp-tsr, trp1-tmd-gfp, trp1-flag10-gfp and trp1-flag20-gfp.* For generating *trp1-gfp-tsr* and *trp1-tmd-gfp* parasites, a four fragment gibson assembly was implemented. A 767 bp long *egfp* sequence including a short linker region comprised of two glycines surrounding it, amplified from the TRP1 C-term GFP vector, was either cloned upstream of the *tsr* domain or upstream of the *c-terminus* to form two versions of internally tagged *trp1* gene. Final constructs were generated by digesting the Pb238::TRP1-TMD-GFP and Pb238::TRP1-GFP-TSR vectors (*Sac*II and *Xho*I) and transfecting the linear fragments of DNA into *wt* parasites. Isogenic parasite lines were selected via limiting dilution of the transfected parasites.

For generating the *trp1-flag10-gfp and trp1-flag20gfp parasites* I used the Pb238::TRP1 TMD-GFP vector as the source of both the donor vector for cloning and template for amplification of the fragments needed for the assembly of the vectors Pb238::TRP1-FLAG10-GFP and Pb238::TRP1-FLAG20-GFP. A four fragment gibson assembly was conducted that included either a 1702 bp or a 1732 bp long fragment of *trp1* ORF right upstream of the *tsr* domain, a 118 bp long fragment of 3X *flag* encoding gene and a 2091 bp long fragment encoding the rest of *trp1* ORF including *egfp* upstream of the *c-terminus* and a part of the 3'*dhfs*. The *flag* encoding sequence was amplified from pbat-sil6-ef1a-cas13x vector

borrowed from Dr. Franziska Hentschel and was placed either 10 or 20 amino acids upstream of the *trp1*-TSR domain . The resulting vectors were digested to generate linear DNA fragments (*Sac*II and *Xho*I) and were transfected into *wt* parasites. Isogenic parasite lines were selected via limiting dilution of the transfected parasites as described before.

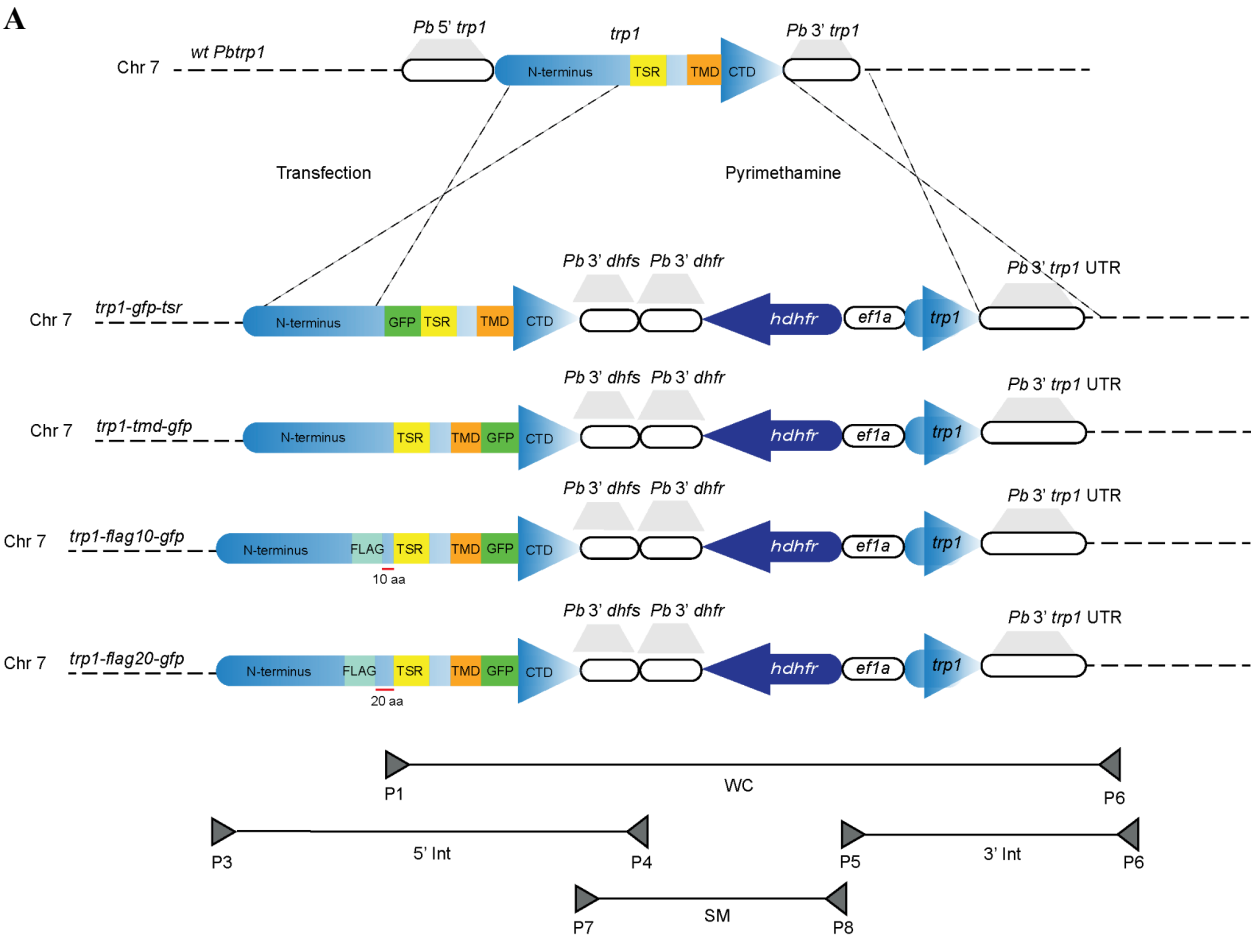

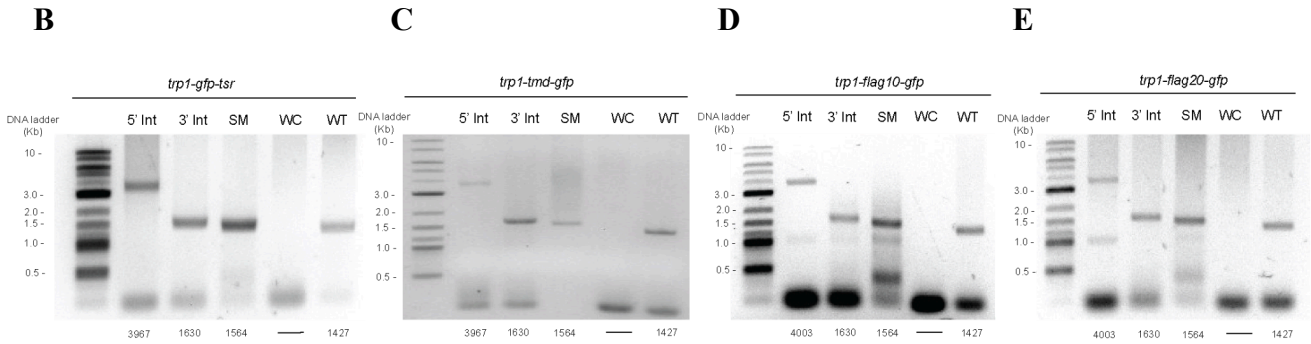

Figure: 4.4. Generation of *trp1-gfp-tsr*, *trp1-tmd-gfp, trp1-flag10-gfp, trp1-flag20-gfp* parasites.

A. Illustration of the generation of various GFP and FLAG tagged mutants of TRP1. The integration of transfected DNA into the wild-type parasite led to the generation of various tagged versions of TRP1 protein via double crossover homologous recombination. The binding sites of the primers, along with the approximate lengths of the PCR products used for genotyping, are indicated by arrowheads and lines positioned above and below the schematic representation. **B-E.** Genotyping of *trp1-gfp-tsr, trp1-tmd-gfp, trp-flag10-gfp, trp-flag20-gfp* isogenic parasite lines were conducted, with the expected PCR product sizes indicated below the gel images (in bp length). Notably, amplification of the complete constructs were unsuccessful, likely due to the sequence's length and high AT content. PCR analyses were also performed on the wild-type (*wt*) recipient line for comparison. (5' int: 5' integration; 3' int: 3' integration; SM: Selection marker; WC: Whole construct, WT: Wild type *trp1* construct).

4.5 Generation of proximity biotinylation tagged *trp1* parasites: *trp1-apex, trp1-miniturbo*

For generating the *trp1-apex* and *trp1-miniturbo* parasites, I used the Pb238::TRP1 TMD-GFP vector as the backbone and template for cloning the final constructs. A four fragment gibson assembly was implemented to generate the constructs. Three fragments were PCR amplified similar to the construction of the *trp1-tmd-gfp* parasites, including a 2635 bp long sequence of *trp1* ORF, 802 bp long *apex* or 830 bp long *miniturbo* encoding gene and a 543 bp long sequence including the rest of the *trp1* gene and a part of the 3'*dhfs*. The sequence encoding apex and miniturbo were amplified from vectors pl 121 and pl 129 respectively and were borrowed from Dr. Jessica Kehrer and a short linker region of two glycine residues were added on both ends of the genes and placed upstream of the c-terminus, similar in position to the *gfp* gene in Pb238::TRP1-TMD-GFP vector. The resulting vectors were digested to generate linear DNA fragments (*Sac*II and *Xho*I) and were transfected into *wt* parasites following the aforementioned method. Isogenic parasite lines were selected via limiting dilution for further experiments.

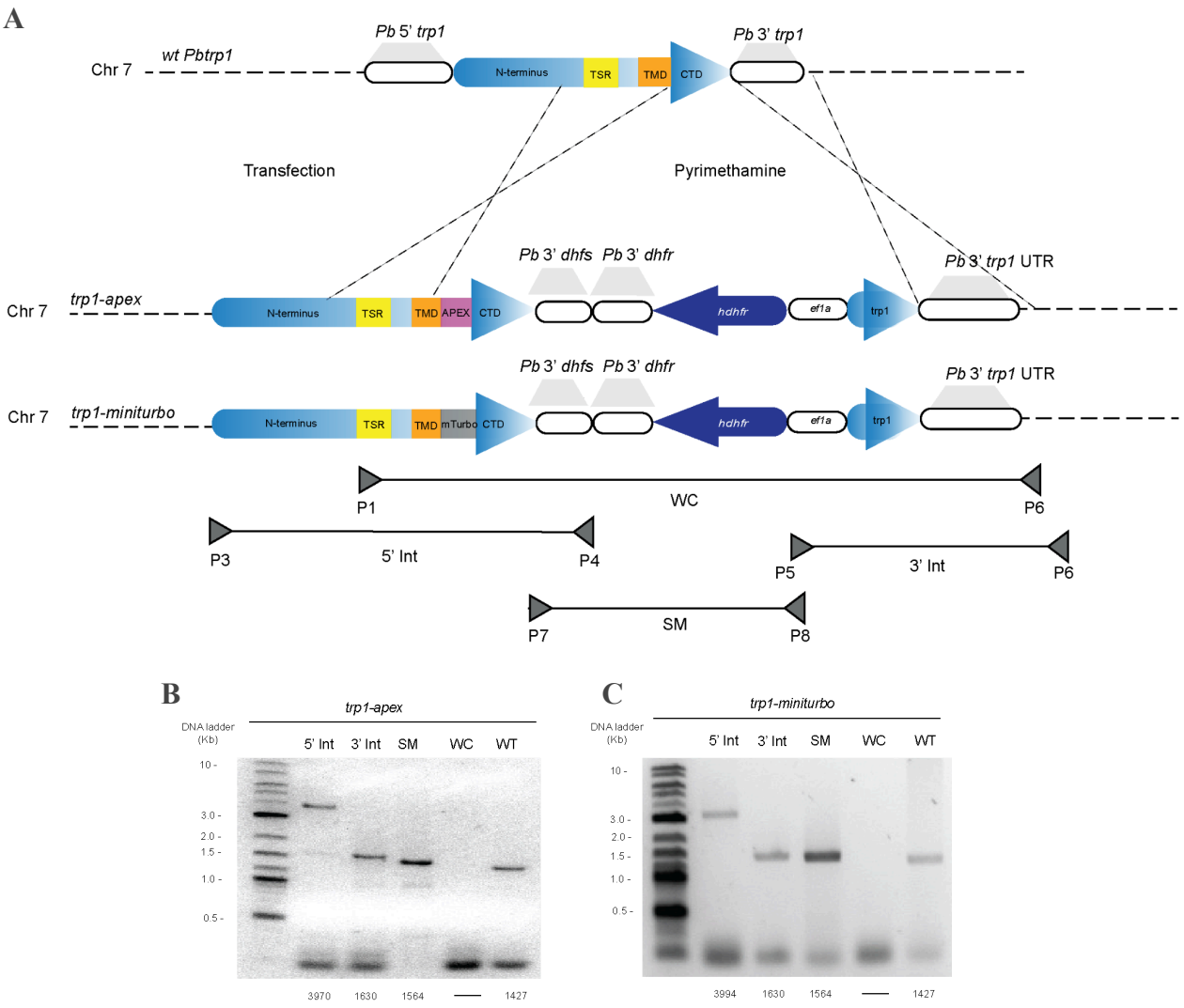

Figure: 4.5. Generation of *trp1-apex*, *trp1-miniturbo* parasites.

A. Schematic representation of the generation of TRP1 mutants with various proximity biotinylation tags.. The integration of transfected DNA into the wild-type parasite led to the generation of various tagged versions of TRP1 protein via double crossover homologous recombination. The binding sites of the primers, along with the approximate lengths of the PCR products used for genotyping, are indicated by arrowheads and lines positioned above and below the schematic representation. **B-C.** Genotyping of *trp1-apex* and *trp1-miniturbo* isogenic parasite lines were conducted, with the expected PCR product sizes indicated below the gel images (in bp length). Notably, amplification of the complete constructs were unsuccessful, likely due to the sequence's length and high AT content. PCR analyses were also performed on the wild-type (*wt*) recipient line for comparison. (5' int: 5' integration; 3' int: 3' integration; SM: Selection marker; WC: Whole construct, WT: Wild type *trp1* construct).

5. Results

5.1 C-terminus of Thrombospondin related protein 1 (TRP1) plays crucial role in salivary gland invasion and motility in sporozoites.

Previous studies on TRP1 indicated a crucial dual role of the C-terminus in sporozoite egress from oocyst and invasion in the salivary gland (Klug and Frischknecht 2017). Thus, in order to identify the key residues in the C-terminus, I generated a series of mutants including a series of deletion mutants that entailed various lengths of deletion in the C-terminus, i.e. *trp1Δ3, trp1Δ14, trp1Δ19* parasite lines containing 3, 14 and 19 amino acid deletions at the C-terminal end respectively. Apart from generation of the new C-terminus deletion mutants, I re-characterized *gfp-trp1Δctd* (from now on introduced as *trp1Δctd*) and *trp1 ko* mutants previously generated by, Dr. Dennis Klug, lacking the C-terminus or the entire *trp1* gene respectively (Fig. 5.1.1. B).

Disruption of the C-terminus did not result in any defect in the development of the sporozoites, reflected in the infectivity rate of the mosquito midgut and the midgut sporozoite numbers (Fig. 5.1.1. C). TRP1 mutants are not expected to have any defects in the sporozoite development stage as TRP1 is only expressed in the late oocyst and salivary gland stages. Sporozoite numbers of midgut, hemolymph and salivary gland within the same mosquitoes were counted to calculate oocyst egress and salivary gland invasion ratios. Compared to control infections, only *trp1 ko* showed reduced haemolymph sporozoites indicating impaired egress while *trp1 ko, trp1Δctd* and *trp1Δ14* show reduced salivary gland numbers, indicating impaired salivary gland invasion (Fig. 5.1.1. D).

Although the C-terminus domain has low conservation amongst the TRP1 homologs, both *P. berghei* and *P. falciparum* TRP1 contain several lysine residues at the end of the CTD (Fig. 5.1.2.). However, when the last 3 amino acids of the *Pb* TRP1 CTD containing two lysines were deleted, no effect was observed in the ability of the sporozoite to egress the oocyst and invade the salivary gland. Interestingly, deletion of the last 14 amino acids at the C-terminus resulted in almost 2.5-fold reduction in the ability of the sporozoites to invade the salivary gland, although the ability of the sporozoites to egress the oocyst remained unaffected. However, deletion of the last 19 amino acids resulted in comparable egress and invasion capacity of the sporozoites into the salivary gland as wild type parasites (Fig. 5.1.1. D).

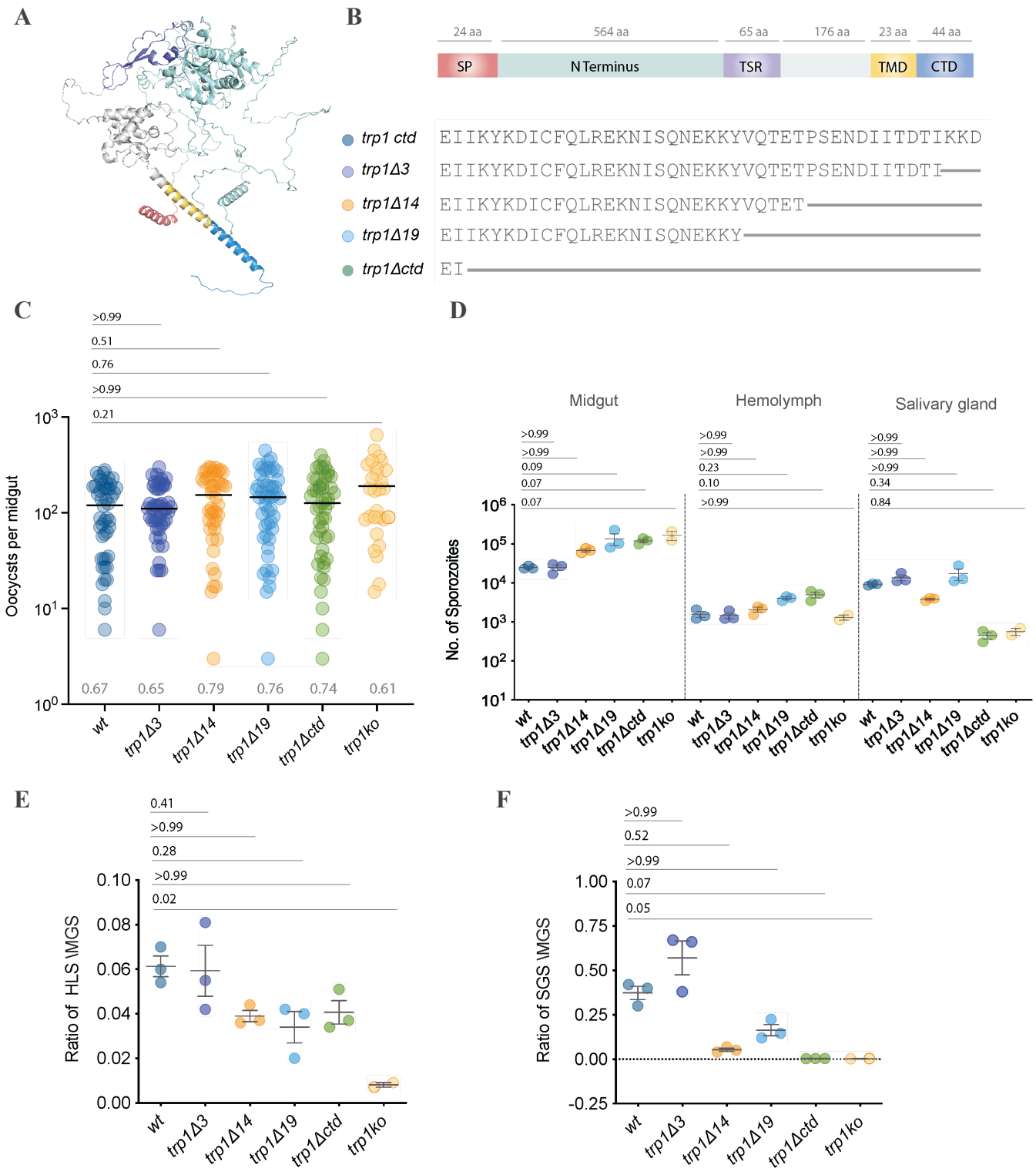
A
B
24 aa
564 aa
65 aa
176 aa
23 aa
44 aa
SP
N Terminus
TSR
TMD
CTD
trp1 ctd
trp1Δ3
trp1Δ14
trp1Δ19
trp1Δctd
EIIKYKDICFQLREKNISQNEKKYVQTETPSENDIITDTIKKD
EIIKYKDICFQLREKNISQNEKKYVQTETPSENDIITDTI
EIIKYKDICFQLREKNISQNEKKYVQTET
EIIKYKDICFQLREKNISQNEKKY
EI
C
Oocysts per midgut
>0.99
0.51
0.76
>0.99
0.21
0.67
0.65
0.79
0.76
0.74
0.61
wt
trp1Δ3
trp1Δ14
trp1Δ19
trp1Δctd
trp1ko
D
Midgut
Hemolymph
Salivary gland
No. of Sporozoites
>0.99
>0.99
0.09
0.07
0.07
>0.99
>0.99
0.23
0.10
>0.99
>0.99
>0.99
>0.99
0.34
0.84
E
Ratio of HLS \MGS
0.41
>0.99
0.28
>0.99
0.02
F
Ratio of SGS \MGS
>0.99
0.52
>0.99
0.07
0.05

Figure: 5.1.1. TRP1 C-terminus plays a crucial role in salivary gland invasion.

A. ColabFold prediction of PbTRP1 structure. **B.** Schematic representation of PbTRP1 (Various domains are color coordinated with the ColabFold prediction of TRP1) and amino acid sequence of the C-terminus domain deletion mutants. **C.** Oocyst numbers per midgut, where each dot represents one midgut. Black dash over each group represents the mean. Percentage of infection rates are indicated below the graph. **D.** Total numbers of sporozoites in midgut, hemolymph and salivary gland of various C-terminus deletion mutants; Each dot represents an average number of sporozoites calculated from mosquitoes dissected from 1 cage feed. **E.** Ratio of hemolymph and midgut sporozoites. **F.** Ratio of salivary gland and midgut sporozoites;
Statistical significance calculated by Kruskal-Wallis with Dunn's multiple comparisons test (Data from three cage feeds except 2 cage feeds for *trp1ko* parasite line).

To compare the abilities of the C-terminus deletion mutants, previously generated *trp1Δctd* and *trp1 ko* parasites were used as controls and re-characterized. Contrary to the previous observations by Dennis Klug, *trp1Δctd* parasites could indeed egress from the oocyst but were unable to enter the salivary glands (Fig. 5.1.1. D-F) (Klug and Frischknecht 2017). Indeed, only the *trp1 ko* affected the sporozoites ability to egress from the oocyst, as observed in the ratio of hemolymph and corresponding midgut sporozoites, collected on day 16 post infection (Fig. 5.1.1. E). The numbers of salivary gland sporozoites in some of the C-terminus deletion mutants are lower than controls thus indicating that the C-terminus is essential in salivary gland invasion, Strong reduction in the numbers of sporozoites in the salivary gland was observed in *trp1Δctd* mutants, whereas *trp1Δ14* sporozoites showed an intermediate ability between the wild type and *trp1Δctd* mutants to invade the salivary gland (Fig. 5.1.1. F).
To determine whether deleting the C-terminus domain in TRP1 disrupts its overall structure, ColabFold was utilized to predict the structure of the TRP1ΔCTD (Fig. 5.1.2. C-E). The predicted structure revealed subtle changes in the positions of secondary structural elements near the C-terminus domain. Structural alignment between the C-terminal domain-deleted protein and the original protein yielded a root-mean-square deviation (RMSD) value of 22.67 Å. RMSD is a quantitative measure of the difference between two protein structures, typically calculated after aligning their backbone atoms (or, in some cases, all atoms). This value summarizes the average deviation between corresponding atoms in the two structures, with the observed RMSD (>5Å) indicating a significant structural deviation in the vicinity of the deletion, that might be responsi-

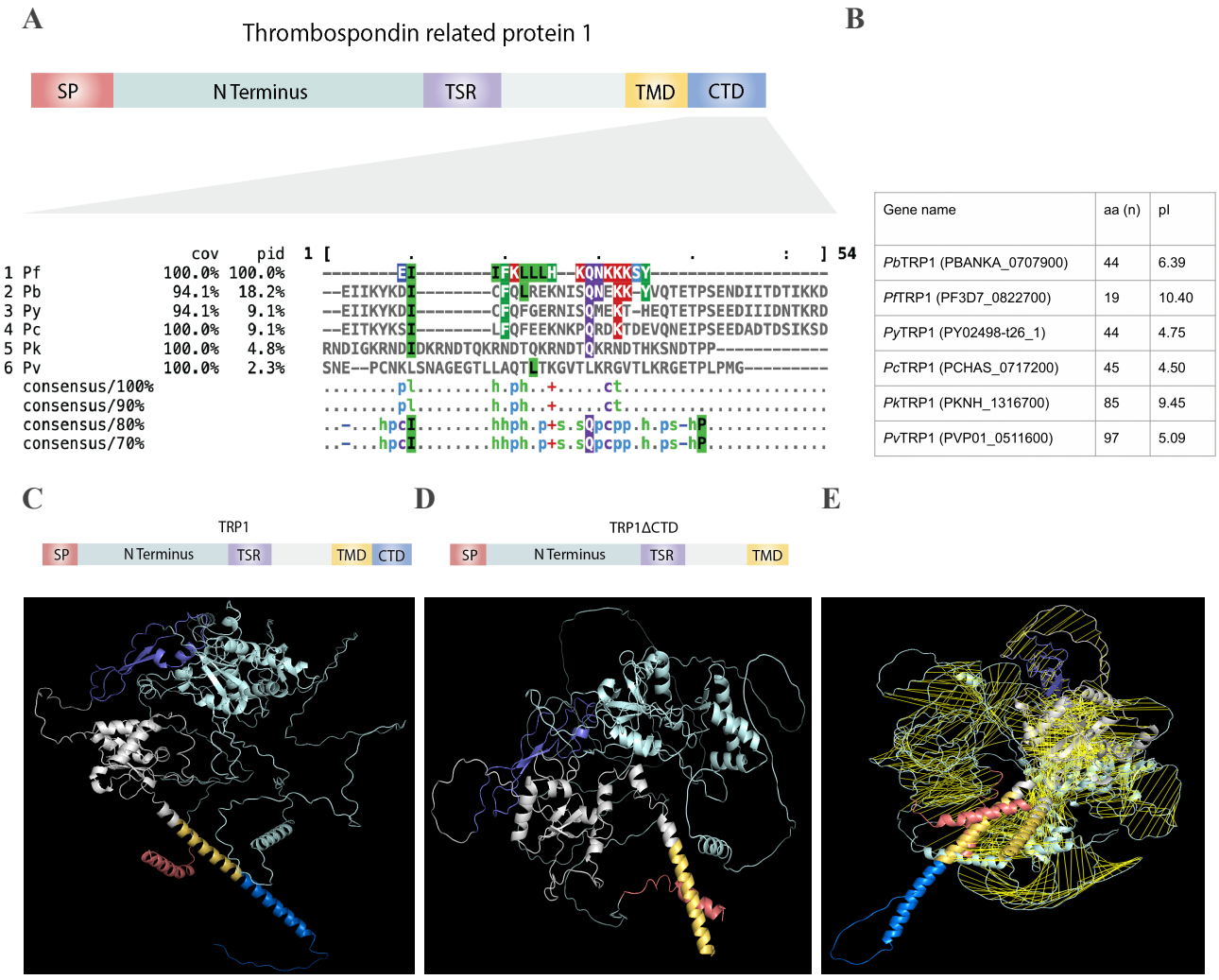

Gene name	aa (n)	pI
*Pb*TRP1 (PBANKA_0707900)	44	6.39
*Pf*TRP1 (PF3D7_0822700)	19	10.40
*Py*TRP1 (PY02498-t26_1)	44	4.75
*Pc*TRP1 (PCHAS_0717200)	45	4.50
*Pk*TRP1 (PKNH_1316700)	85	9.45
*Pv*TRP1 (PVP01_0511600)	97	5.09

Figure: 5.1.2. TRP1 C-terminus is not well conserved among its homologs in *Plasmodium*.

A. Multiple sequence alignment of the C-terminus of *Pb*TRP1 with the CTDs of *Pf*TRP1, *Py*TRP1, *Pc*TRP1, *Pk*TRP1 and *Pv*TRP1 using Clustal Omega. **B.** Isoelectric points and the corresponding amino acid lengths of different TRP1 homologs in *Plasmodium*. **C-D.** ColabFold predictions of TRP1 and TRP1ΔCTD structure (color coded according to the figure legend) **E.** Structural alignment of TRP1 and TRP1ΔCTD using PyMOL.

-le for the functional perturbations we observe with the C-terminus deletion mutant. It is important to note that the transmembrane (TM) domain effectively shields the C-terminus from interactions with the main extracellular region of the protein. As a result, modifications at the C-terminus are likely to impact only the C-terminal region itself, potentially extending to the TM domain and, to a lesser extent, the adjacent extracellular domain.

A

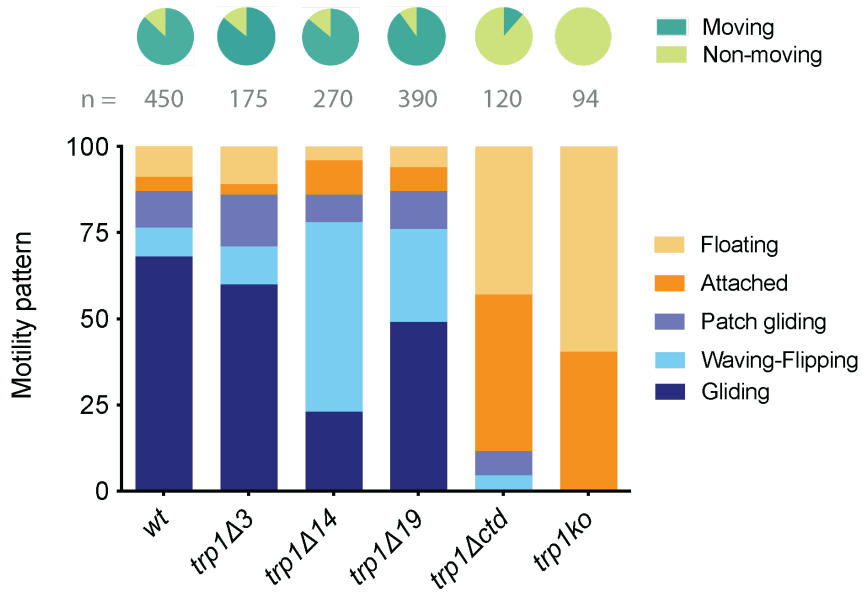
Moving
Non-moving
n = 450 175 270 390 120 94
100
75
50
25
0
Motility pattern
Floating
Attached
Patch gliding
Waving-Flipping
Gliding
wt
trp1Δ3
trp1Δ14
trp1Δ19
trp1Δctd
trp1ko

B

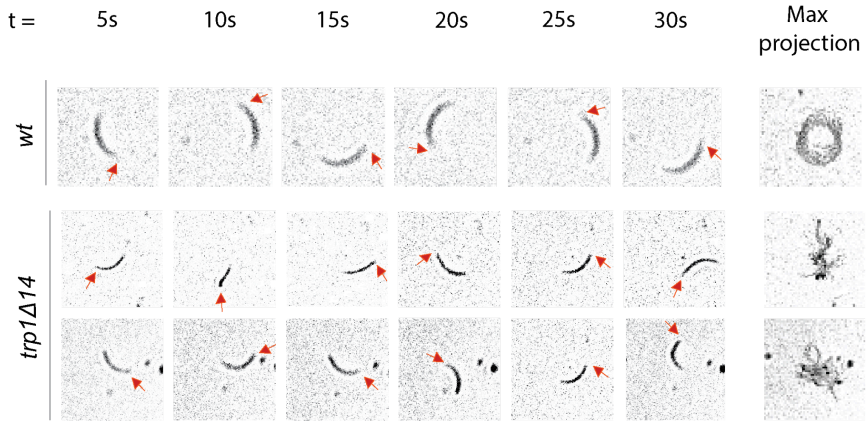
t =
5s
10s
15s
20s
25s
30s
Max projection
wt
trp1Δ14

C

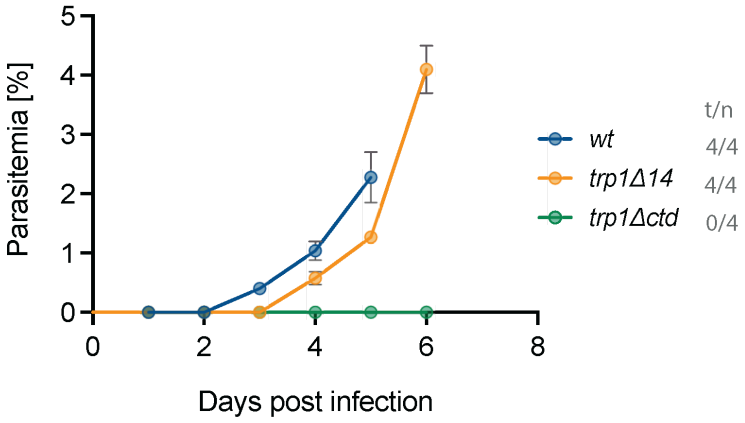
Parasitemia [%]
0
1
2
3
4
5
0
2
4
6
8
Days post infection
wt
trp1Δ14
trp1Δctd
t/n
4/4
4/4
0/4

Figure: 5.1.3. TRP1 C-terminus is crucial in sporozoite motility and transmission to host.

A. Motility patterns observed in various TRP1 C-terminus domain mutant salivary gland sporozoites compared to wild type. 'n' equals the total number of sporozoites quantified from each parasite line. Data collected from two cage feed experiments. The pie chart in green depicts the proportion of moving and non-moving sporozoites overall in each parasite line, where both productive and unproductive motility accounts for the 'moving' sporozoites. Attached and floating sporozoites were joined together into the 'non moving' category. **B.** Motility pattern montage of 'waving-flipping' *trp1Δ14* sporozoites vs normal gliding motility in *wt* sporozoites. Red arrowheads indicate the tip of the sporozoite in each panel. **C.** Natural transmission assay comparing parasitemia in mice infected via 'bite-back' method with *trp1Δ14* and *trp1Δctd* infected mosquitoes compared to *wt Pb*ANKA infected mosquitoes. 't' indicates the number of mice that became positive with malaria, whereas 'n' indicates the total number of mice infected.

It is important to note that structure prediction tools like ColabFold do not inherently account for the presence of the TM domain. Consequently, these models may incorrectly predict interactions between intracellular and extracellular regions, leading to structural artifacts and false-positive results. Furthermore, significant deviations observed in predicted structures are often localized within unstructured loop regions, which are inherently less reliable in prediction models. Since these loops are not well-resolved, their variability might not provide meaningful insights for RMSD-based structural comparisons.

To investigate if the ability of salivary gland invasion is correlated with the productive motility of the sporozoites, in vitro motility assays were performed on the salivary gland sporozoites of C-terminus deletions mutants. *trp1Δ14* parasites showed a peculiar defect in their motility, where sporozoites were unable to continue gliding in a regular fashion. Instead, the sporozoites exhibited a combination of gliding, waving and flipping motion, which is labeled henceforth as 'waving-flipping' motility (Fig. 5.1.3. A, B).

Interestingly, the majority of the *trp1Δ14* sporozoites showed such a pattern in the motility assays. Although *trp1Δ19* sporozoites had no difficulty invading the salivary gland, around 25% of the salivary gland sporozoites showed similar motility patterns as *trp1Δ14* sporozoites, which indicate a dual importance of the C-terminus in salivary gland invasion and motility. *gfp-trp1Δc* salivary gland sporozoites however were completely unable to perform any form of productive motility in the in-vitro motility assays, further reinstating the importance of the C-terminus in salivary gland invasion and motility (Fig. 5.1.2. A).

To determine whether the *trp1Δ14* and *trp1Δctd* sporozoites can penetrate the host skin barrier and infect mice, I performed a natural transmission assay (bite back assay) where 4 anesthetized mice where bitten by ten infected mosquitoes each and the parasitemia was measured in the mice from day 3 onwards post infection. The mice infected with *trp1Δ14* parasites showed 1 day delay in prepatency compared to wild type parasites. *trp1Δctd* sporozoites however could not infect any mice via natural transmission, further reinforcing C-terminus domain's importance in motility and transmission to the host (Fig. 5.1.2. C).

Table 5.1.1: Absolute numbers and ratios for sporozoite counts in the midgut, hemolymph and salivary glands of all C-terminus domain mutants.

Parasite line	Midgut sporozoite no.	Hemolymph sporozoite no.	Salivary gland sporozoite no.	HLS/MGS	SGS/MGS
wt	25000 ± 2200	1600 ± 470	9100 ± 530	0.064	0.36
trp1Δ3	24600 ± 7000	1500 ± 440	13600 ± 3900	0.060	0.55
trp1Δ14	67600 ± 9500	2100 ± 500	3800 ± 360	0.031	0.056
trp1Δ19	136300 ± 79700	4000 ± 580	17200 ± 9400	0.029	0.13
trp1Δctd	119300 ± 22000	5000 ± 1400	450 ± 140	0.042	0.0034
trp1 ko	165000 ± 45000	1300 ± 200	565 ± 115	0.007	0.0034

Table 5.1.2: Transmission assay summary

The transmission potential of all generated parasite lines was assessed using C57BL/6 mice. In each experiment, four naïve mice were infected. The prepatent period, defined as the time from infection to the first detection of blood-stage parasites, is reported as the mean for all mice that became blood-stage positive. For comparison, similar experiments were conducted with wild-type parasites.

Parasite line	Inoculation route	Mice infected/Total	Prepatency
wt	By mosquito bite	4/4	3
trp1Δ14	By mosquito bite	4/4	4
trp1Δctd	By mosquito bite	0/4	∞

5.2 TRAP C-terminus cannot rescue the function of TRP1 C-terminus domain

The C-terminus of the TRAP family proteins are known to interact with the acto-myosin cytoskeleton present underneath the plasma membrane of the parasite, which generates the force that powers gliding motility (Frénal et al. 2017a; S. Kappe et al. 1999; Münter et al. 2009). Although TRP1 shares many characteristic features with TRAP family proteins, the C-terminus of *Pb*TRP1 shows little homology with that of *Pb*TRAP (Fig. 5.2.1 A). Notably, *Pb*TRP1 lacks the penultimate tryptophan at its C-terminus, a residue demonstrated to be critical for motility and salivary gland invasion (Sultan et al. 1997; Baum et al. 2006; Bhanot et al. 2003).

To determine whether the C-terminus of TRAP can rescue the function of TRP1, the C-terminus of *Pb*TRP1 was replaced with the C-terminus of *Pb*TRAP and an isogenic line was generated for further characterization. Mosquito tissues were dissected post infection from *Pbtrp1-Pbtrap ctd* swap parasite line for determining the number of sporozoites in midgut, hemolymph and salivary glands according to previously mentioned protocol.

Swapping the C-terminus of *Pb*TRP1 with *Pb*TRAP did not result in any defect in infectivity of the mosquito midgut, as observed in the comparable number of oocysts per midgut and midgut sporozoite numbers with wild type parasite infected mosquitoes (Fig. 5.2.1 B-C).

However, the number of hemolymph sporozoites were significantly elevated in *Pbtrp1-Pbtrap ctd swap* parasite infected mosquitoes compared to the wild type. Correspondingly, the number of salivary gland sporozoites indicated severe reduction in the ability of the sporozoites to invade salivary glands. These results indicate that the *Pbtrp1-Pbtrap ctd swap* sporozoites have no difficulty in egressing the oocyst, however they have severe defects in invading the salivary glands (Fig. 5.2.1 C). These findings are further emphasized by the increased hemolymph-to-midgut sporozoite ratio observed in the *Pbtrp1-Pbtrap ctd* swap mutants compared to the wild type, coupled with a markedly lower salivary gland-to-midgut sporozoite ratio (Fig. 5.2.1 D-E). Interestingly, these parasites mimic the phenotype observed in the *trp1Δctd* sporozoites, where they lack the entire C-terminus indicating, *Pb*TRAP C-terminus cannot successfully rescue the function of *Pb*TRP1 C-terminus (Fig. 5.1.1 D-F). To probe the *Pbtrp1-Pbtrap ctd swap* sporozoites ability to effectively move, in vitro motility assays were performed on salivary gland sporozoites. No sporozoites were observed to be productively moving in the in vitro motility assay. Most of the sporozoites seemed to be floating while a few

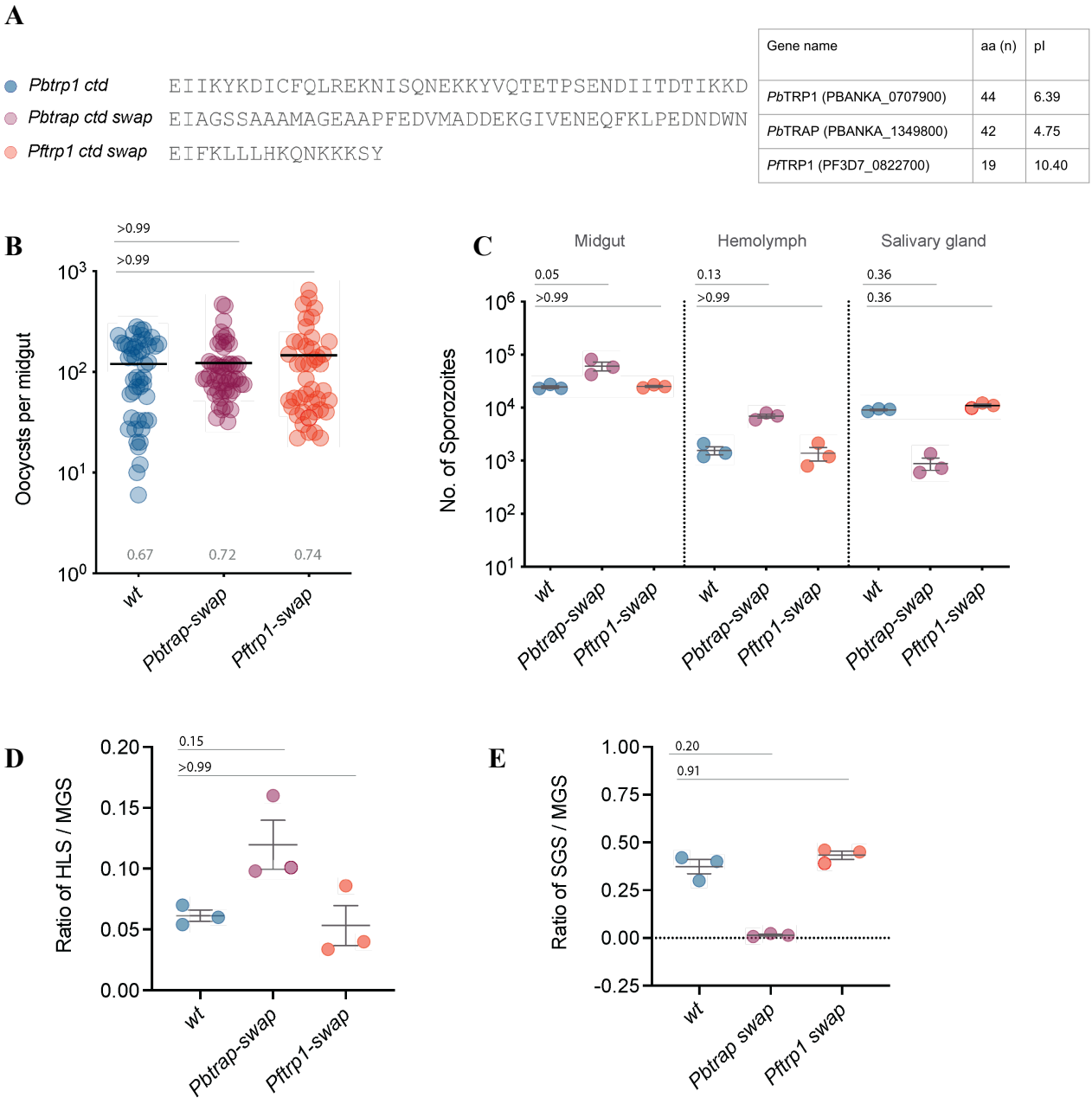

Figure: 5.2.1. TRAP C-terminus cannot rescue the function of TRP1 C-terminus however the short C-terminus tail of *Pf*TRP1 complements TRP1 function completely.

A. Amino acid sequence of the C-terminus domain swap mutants compared to wild type and comparison of the isoelectric charges and lengths of the C-terminus domain of *Pb*TRP1, *Pb*TRAP and *Pf*TRP1 **B.** Oocyst numbers per midgut. Data collected from three cage feeds, where each dot represents one midgut. Black dash over each group represents the mean. Percentage of infection rates are indicated below the graph. **C.** Total numbers of sporozoites in midgut, hemolymph and salivary gland of various C-terminus deletion mutants; Each dot

represents an average number of sporozoites calculated from mosquitoes dissected from 1 cage feed. **D.** Ratio of hemolymph and midgut sporozoites; **E.** Ratio of salivary gland and midgut sporozoites.
Statistical significance calculated by Kruskal-Wallis with Dunn's multiple comparisons test (Data from three cage feeds).

remained attached to the bottom of the imaging dish, similar to the *gfp-trp1Δctd* sporozoites (Fig. 5.2.2 B). To determine whether the *Pbtrp1-Pbtrap ctd swap* hemolymph sporozoites cannot enter the salivary gland due to any defect in motility, in-vitro motility assays were performed on the hemolymph sporozoites following similar protocol as the salivary gland sporozoites. Interestingly, the percentage of moving sporozoites in the hemolymph were much higher in the *Pbtrp1-Pbtrap ctd swap* mutants compared to wt, including a fraction of sporozoites showing gliding motility. This highlights the presence of several key factors in salivary gland invasion other than sporozoite motility (Fig. 5.2.2 A).

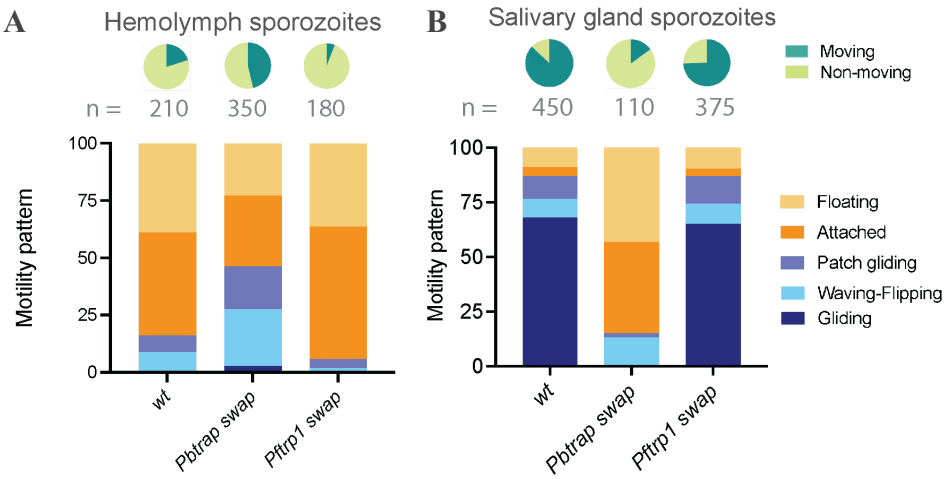

Figure: 5.2.2. *Pb*TRAP C-terminus swap disrupts sporozoite motility

A. Motility patterns observed in various TRP1 C-terminus domain swap mutant hemolymph sporozoites compared to wild type. Data collected from two cage feed experiments. **B.** Motility patterns observed in various TRP1 C-terminus domain swap mutant salivary gland sporozoites compared to wild type. 'n' equals the total number of sporozoites quantified from each parasite line. Data collected from three cage feed experiments. The pie chart in green depicts the proportion of moving and non-moving sporozoites overall in each parasite line, where both productive and unproductive motility accounts for the 'moving' sporozoites. Attached and floating sporozoites were clubbed together into the 'non moving' counterpart.

To probe for *Pbtrp1-Pbtrap ctd swap* salivary gland sporozoite's ability to transmit disease into the host, transmission assays were conducted. To determine if the sporozoites can be transmitted

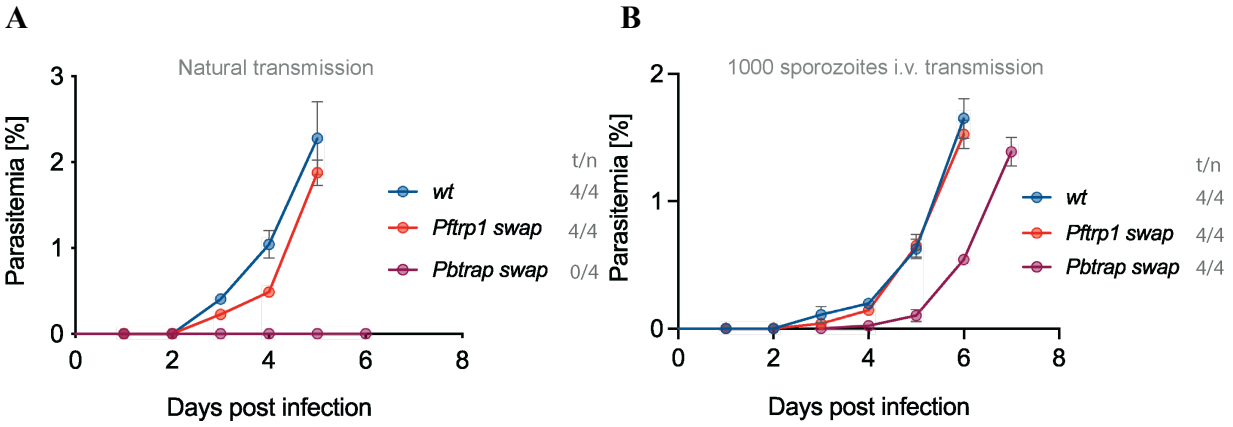

Figure: 5.2.3. *Pbtrp1-Pbtrap ctd swap* sporozoites cannot successfully transmit disease to host via natural transmission

A. Natural transmission assay comparing parasitemia in mice infected via 'bite-back' method with *Pbtrp1-Pbtrap ctd swap* and *Pbtrp1-Pftrp1ctd swap* infected mosquitoes compared to wt PbANKA infected mosquitoes. **B.** Intravenous transmission assay comparing parasitemia in mice infected with 1000 salivary gland sporozoites from *Pbtrp1-Pbtrap ctd swap* and *Pbtrp1-Pftrp1ctd swap* mutants compared to wt. 't' indicates the number of mice that became positive with malaria, whereas 'n' indicates the total number of mice infected.

via mosquito bites, a natural transmission assay (bite back assay) was performed according to aforementioned protocol using 4 C57BL/6 mice. The mice infected with *Pbtrp1-Pbtrap ctd swap* did not become positive with blood-stage parasitemia (30+ days). Whereas, in i.v. transmission assay where 1000 salivary gland sporozoites from each experimental setup was injected intravenously bypassing the skin route altogether, resulted in 1.5 days (on average for 4 mice) delay in prepatency in *Pbtrp1-Pbtrap ctd swap* infected mice compared to wild type and *Pbtrp1-Pftrp1ctd swap* infection.

To determine if the functional perturbations observed in *Pbtrp1-Pbtrap ctd swap* sporozoites in salivary gland invasion and productive motility is due to structural changes incurred on TRP1 by the C-terminus domain swap, I compared the structural alignment of TRP1 and TRP1-*Pb*TRAP CTD using PyMOL revealing structural differences, particularly in the C-terminal region where

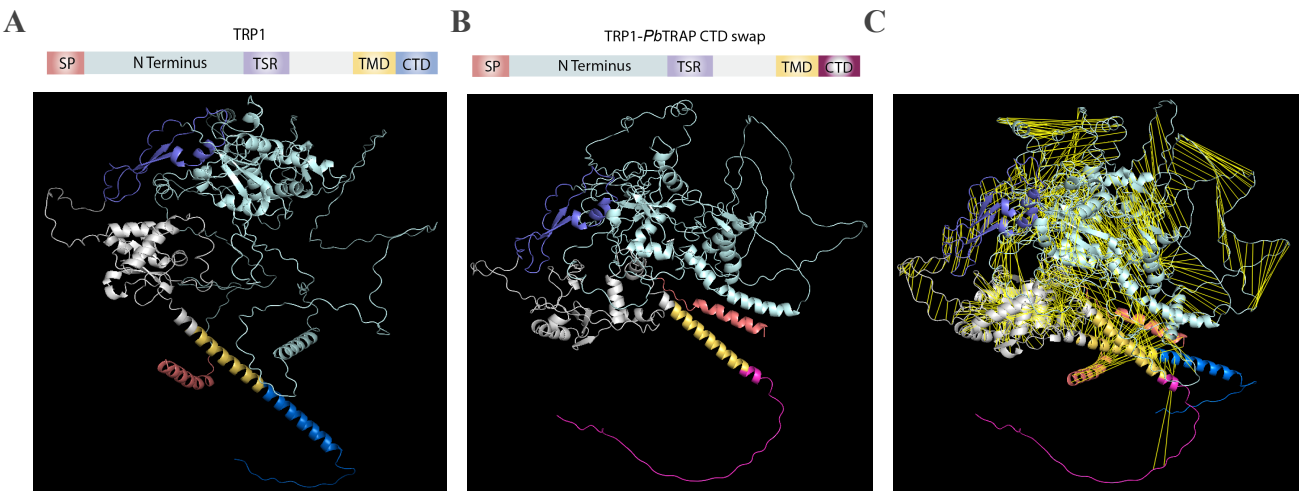

Figure: 5.2.4 Structural alignment of TRP1 and TRP1-*Pb*TRAP CTD swap visualized using PyMOL.

A. ColabFold prediction of TRP1 and **B.** TRP1-*Pb*TRAP CTD swap structure (color coded according to the figure legend) **C.** Structural alignment of TRP1 and TRP1-*Pb*TRAP CTD swap using PyMOL.

the domain swap occurs (Fig: 5.2.4 A-C). Perturbations in the secondary structural elements near the mutation site highlight the impact of the C-terminal swapping on the overall protein conformation, further highlighted by the RMSD value of 23.75 Å. However it is important to note here that the transmembrane (TM) domain (in Yellow) seems to be shielding the C-terminus from interacting with the main extracellular region of the protein. As a result, alterations at the C-terminus primarily affect this region itself, with potential but limited influence on the TM domain and the neighboring intracellular or extracellular segment. Structural prediction models, such as ColabFold, do not inherently recognize the presence of the TM domain, which can lead to inaccuracies.

5.3 *Pf*TRP1 C-terminus can restore the function of *Pb*TRP1 C-terminus domain

The amino acid sequence of C-terminus is not well conserved among TRP1 homologs, showing a high variance in amino acid numbers in the C-terminus along with varying isoelectric points (Fig: 5.1.2 A-B). To assess if the much shorter C-terminus of *Pf*TRP1 can replace the function of the *Pb*TRP1, I generated a isogenic C-terminus swap parasite line, *Pbtrp1-Pftrp1ctd swap* by replacing the *Pb*TRP1 C-terminus with *Pf*TRP1 C-terminus.

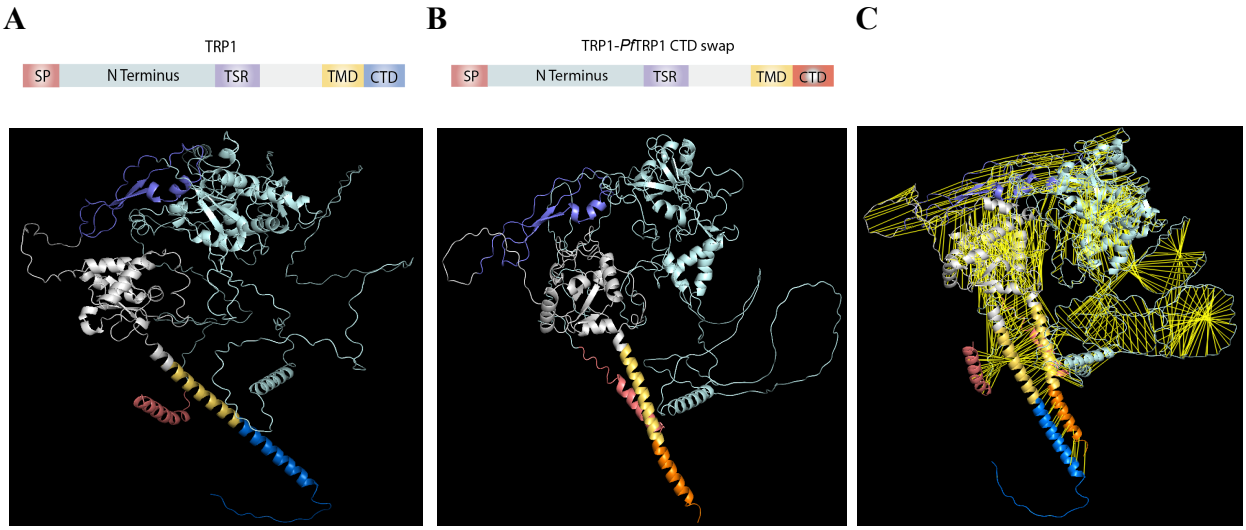

Figure: 5.3.1 Structural alignment of TRP1 and TRP1-*Pf*TRP1 CTD swap visualized using PyMOL.

A. ColabFold prediction of TRP1 and **B.** TRP1-*Pf*TRP1 CTD swap structure (color coded according to the figure legend) **C.** Structural alignment of TRP1 and *Pb*TRP1-*Pf*TRP1 CTD swap using PyMOL.

Interestingly, *Pbtrp1-Pftrp1ctd swap* sporozoites showed no difficulty egressing the oocyst or invading the salivary gland (Fig: 5.2.1 B-F). This could be resulting from the relative structural similarity shared between *Pb*TRP1 and *Pb*TRP1-*Pf*TRP1 CTD swap in the vicinity of the C-terminus domain (Fig: 5.3.1). Although structural alignment of TRP1 and *Pb*TRP1-*Pf*TRP1 CTD swap suggests slight changes in the overall structure of TRP1 as indicated by the RMSD value of 22.36 Å. Similar to TRP1ΔCTD , TRP1-*Pb*TRAP CTD swap structure, the transmembrane (TM) domain seems to be shielding the C-terminus in TRP1-*Pf*TRP1 CTD swap

structure as well, limiting its interactions to nearby regions and thus resulting in inaccuracies in RMSD value calculation.

To determine if the *Pbtrp1-Pftrp1ctd swap* sporozoites have any defect in exhibiting productive motility, I performed in vitro motility assays on the salivary gland and hemolymph sporozoites. Majority of the salivary gland sporozoites exhibited productive motility comparable to *wt* sporozoites (Fig. 5.2.2 B).

Pbtrp1-Pftrp1ctd swap hemolymph sporozoites also showed similar motility pattern as *wt* hemolymph sporozoites (Fig. 5.2.2 A). To determine the sporozoites ability to infect hosts, I performed transmission assays where I either infected 4 C57BL/6 mice via mosquito bites or I injected 1000 sporozoites into 4 C57BL/6 mice intravenously, bypassing the skin and monitored their blood smear to check the parasitemia. *Pbtrp1-Pftrp1ctd swap* sporozoites had no difficulty in transmission of the disease as all the mice infected with the mutant parasites showed prepatency and infection rates comparable as the wild type parasites (Fig. 5.2.3).

Table 5.3.1

Absolute numbers and ratios for sporozoite counts in the midgut, hemolymph and salivary glands of all C-terminus swap mutants.

Parasite line	Midgut sporozoite no.	Hemolymph sporozoite no.	Salivary gland sporozoite no.	HLS/MGS	SGS/MGS
wt	25000 ± 2200	1600 ± 470	9100 ± 530	0.064	0.36
Pbtrap ctd swap	60600 ± 16100	7000 ± 860	890 ± 330	0.115	0.014
Pftrp1 ctd swap	25200 ± 1400	1380 ± 570	11000 ± 1000	0.054	0.43

Table 5.3.2

Transmission assay summary:

The transmission potential of all generated parasite lines was assessed using C57BL/6 mice. In each experiment, four naïve mice were infected. The prepatent period, defined as the time from infection to the first detection of blood-stage parasites, is reported as the mean for all mice that became blood-stage positive. For comparison, similar experiments were conducted with wild-type parasites.

Parasite line	Inoculation route	Mice infected/Total	Prepatency
wt	By mosquito bite	4/4	3
wt	1000 spz i.v.	4/4	3
Pbtrap ctd swap	By mosquito bite	0/4	∞
Pbtrap ctd swap	1000 spz i.v.	4/4	4
Pftrp1 ctd swap	By mosquito bite	4/4	3
Pftrp1 ctd swap	1000 spz i.v.	4/4	3

5.4 Generation of a functionally tagged TRP1 protein

Previous attempts to tag TRP1 with GFP at either the N-terminus or the C-terminus were unsuccessful as it interfered with the function of the protein (Klug and Frischknecht 2017). Tagging at the N-terminus resulted in an undetectable GFP signal, while C-terminal tagging disrupted the protein's function. In an attempt to generate a functional tagged variety of TRP1 protein, here two parasite lines were generated, *trp1-tmd-gfp* and *trp1-gfp-tsr* where GFP was tagged between the transmembrane domain (TMD) and the C-terminal domain (CTD) or directly upstream of the thrombospondin repeat (TSR) domain respectively with a short linker consisting of two glycines on either side of GFP (Fig. 5.4.1 A).

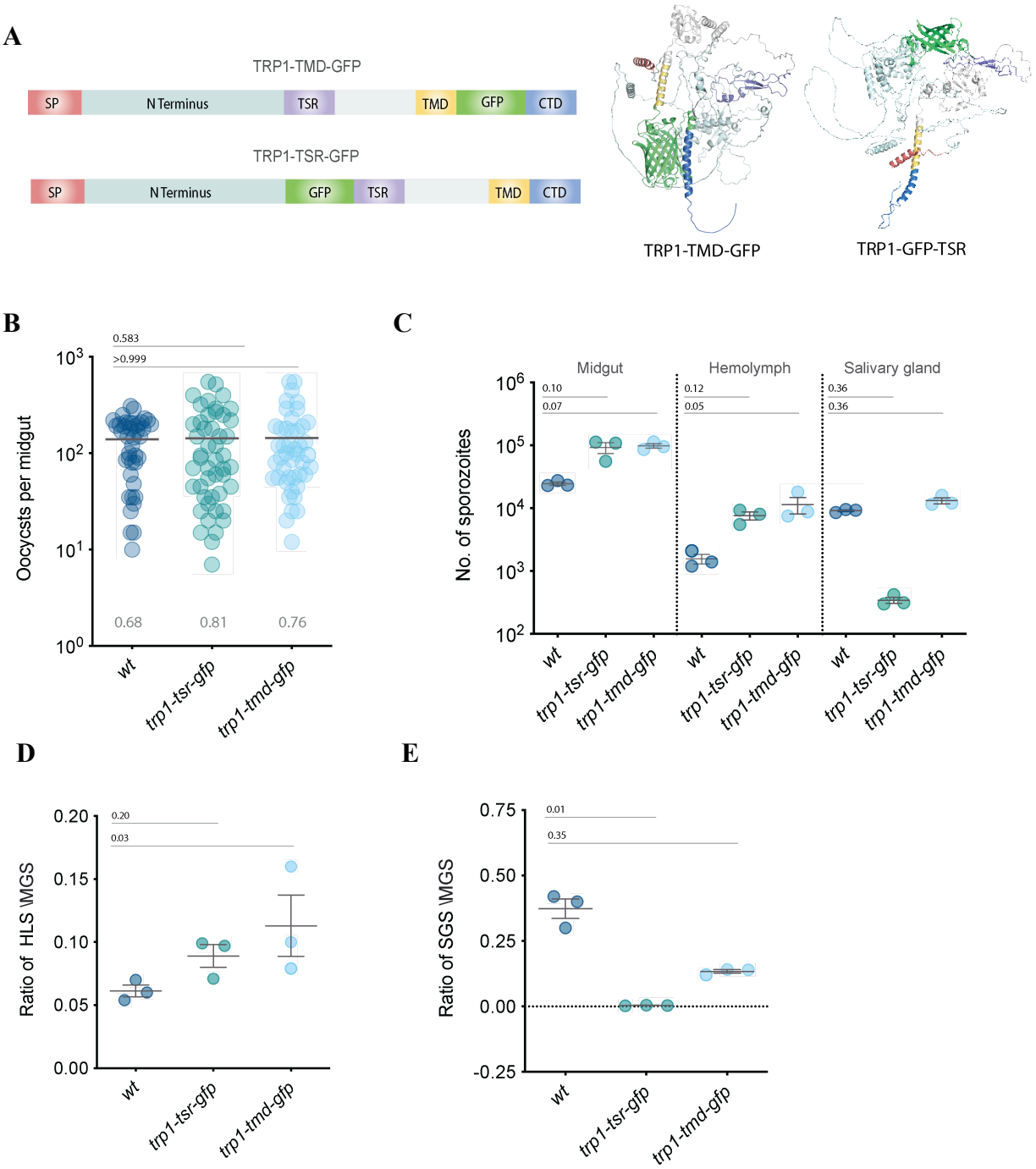

Figure: 5.4.1. TRP1 can be successfully tagged upstream of the C-terminus.

A. Schematic representation of TRP1-TMD-GFP and TRP1-GFP-TSR and ColabFold prediction of the structures (Various domains in the schematic representations are color coordinated with the ColabFold predictions). **B.** Oocyst numbers per midgut. Data collected from three cage

feeds, where each dot represents one midgut. Black dash over each group represents the mean. Percentage of infection rates are indicated below the graph. **C.** Total numbers of sporozoites in midgut, hemolymph and salivary gland of various C-terminus deletion mutants; Each dot represents an average number of sporozoites calculated from mosquitoes dissected from 1 cage feed. **D.** Ratio of hemolymph and midgut sporozoites. **E.** Ratio of salivary gland and midgut sporozoites;
Statistical significance calculated by Kruskal-Wallis with Dunn's multiple comparisons test (Data from three cage feeds).

The *trp1-gfp-tsr* sporozoites had no difficulty in development and egress from the oocyst as reflected by the the oocyst number per midgut and the number of sporozoites in the midgut and hemolymph (Fig. 5.4.1 B). However, they show severe defects in salivary gland invasion as observed in the total number of the salivary gland sporozoites and the ratio of sporozoites in hemolymph and salivary gland compared to midgut (Fig. 5.4.1 C-E).

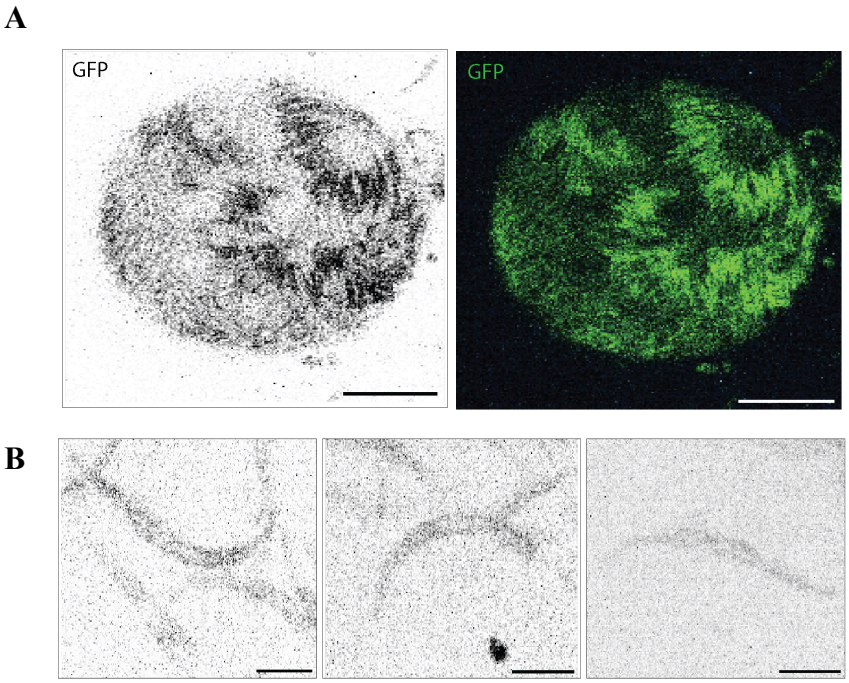

Figure: 5.4.2 GFP localization in TRP1-GFP-TSR

A. Localization of GFP in *trp1-gfp-tsr* oocyst (scale bar: 10 µm) **B.** Localization of GFP in *trp1-tsr-gfp* midgut sporozoites (scale bar: 3 µm).

To check the localization of GFP in *trp1-gfp-tsr* parasites, oocysts and midgut sporozoites were imaged live with confocal microscopy on day 14 post infection. The oocysts showed a signal

indicating an internal localization of TRP1-GFP-TSR in the sporozoites, whereas in the midgut sporozoites the signal observed was very faint and indicated a peripheral localization (Fig. 5.4.2 A-B).

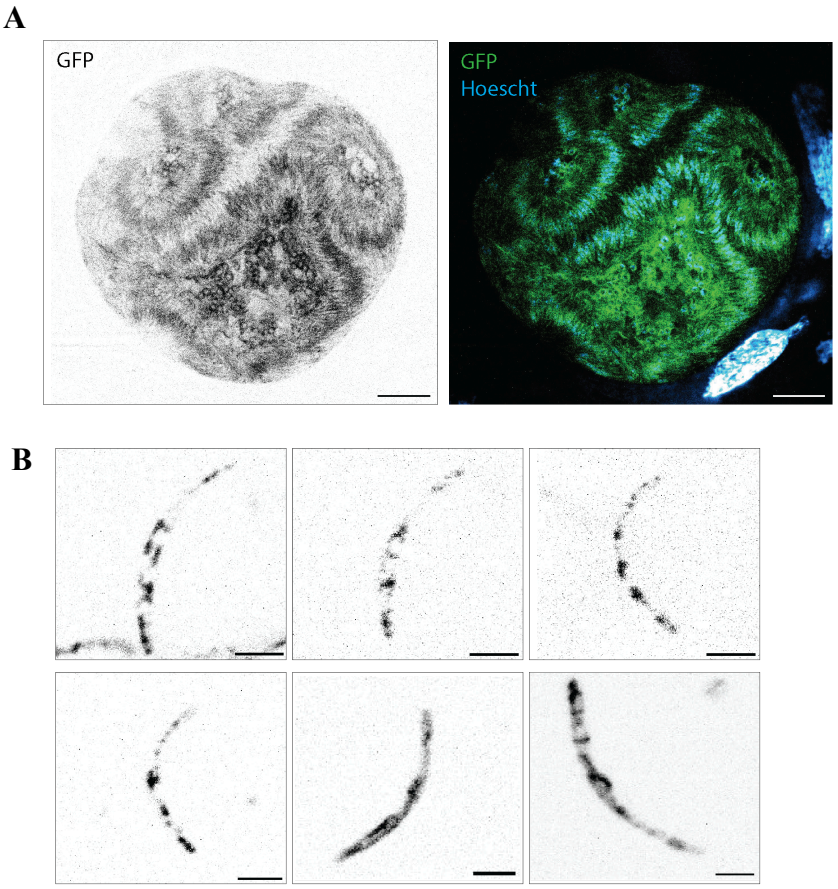

Figure: 5.4.3 GFP localization in TRP1-TMD-GFP

A. Localization of GFP in *trp1-tmd-gfp* oocyst (scale bar: 5 µm) **B.** Localization of GFP in *trp1-tmd-gfp* midgut sporozoites (live) showing "patchy localization" (scale bar: 3 µm).

The *trp1-tmd-gfp* sporozoites exhibited no defects during development or egress from the oocyst, as indicated by the oocyst count per midgut and the number of sporozoites observed in the midgut and hemolymph (Fig. 5.4.1 B-C). To determine whether *trp1-tmd-gfp* sporozoites can effectively invade salivary glands, sporozoites were collected from salivary glands and corresponding midguts and compared with *wild type* parasite infected mosquitoes. These results indicate that the *trp1-tmd-gfp* sporozoites could invade the salivary gland as well as the *wild type* sporozoites, indicating that the GFP tag upstream of the C-terminus does not inhibit the ability of sporozoites to invade salivary gland (Fig. 5.4.1 C-E).

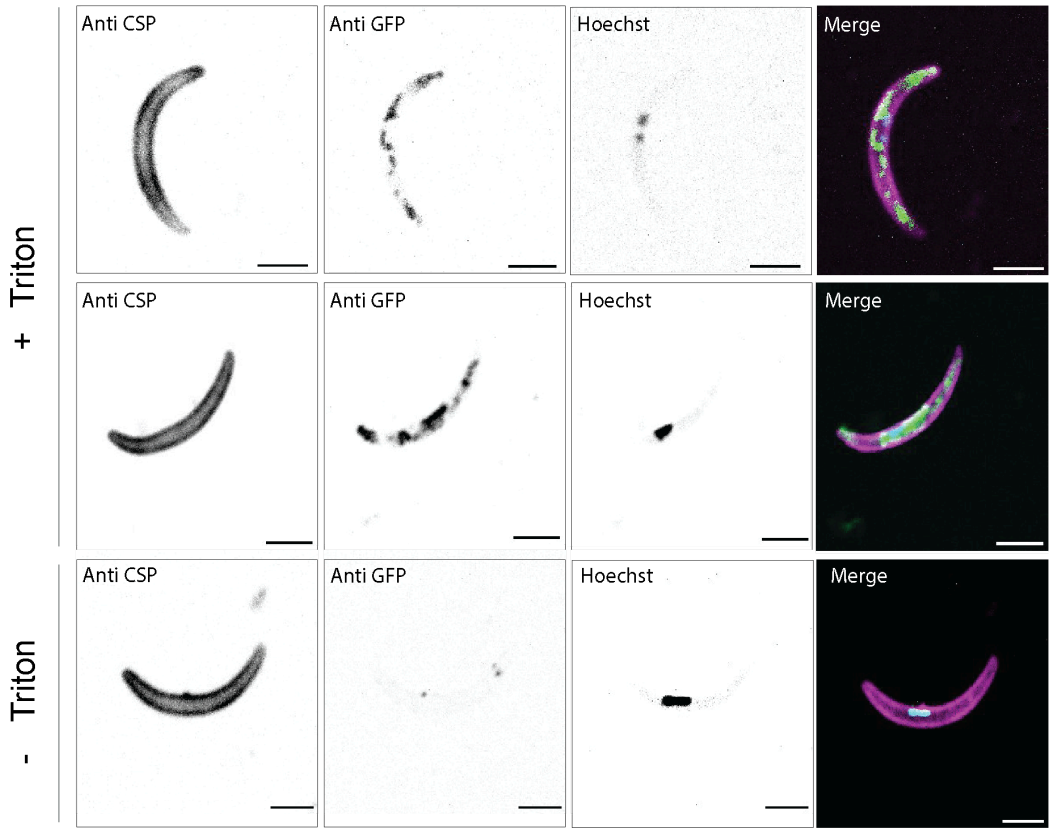

Figure: 5.4.4 GFP localization in *trp1-tmd-gfp* salivary gland sporozoites

A. Localization of GFP in *trp1-tmd-gfp* salivary gland sporozoites in the presence or absence of Triton X-100, indicating a "patchy" localization throughout the sporozoites (scale bar: 3 μm).

The *trp1-tmd-gfp* oocysts were imaged on day 14 post infection to determine the localization of GFP in the parasite. The oocysts showed no signal at the oocyst wall, as observed previously in *trp1-gfp* mutants (Klug and Frischknecht 2017) (Constructs generated previously by Dennis Klug). The salivary gland sporozoites however showed a "patchy" GFP localization, where each sporozoite exhibited a unique pattern of "patchiness". The variety of patchiness indicates a potential range of localization in sporozoite periphery, (subset of) micronemes and ER.

Immunofluorescence assay performed on the salivary gland sporozoites indicated a similar pattern of "patchy" localization of GFP in the periphery, microneme and in the ER of the sporozoites. However the signal was only observed in cell membrane permeabilized sporozoites,

indicating an internal localization of the TRP1 C-terminus als suggested by the protein topology prediction by TMMH-server (https://services.healthtech.dtu.dk/services/TMHMM-2.0/) (Fig: 5.4.4).

To determine if the *trp1-tmd-gfp* sporozoites could perform productive motility, in-vitro motility assays were performed on salivary gland sporozoites. These results indicated a comparable productive motility as *wt* salivary gland sporozoites. Interestingly, the GFP localization in moving sporozoites stayed fixed relative to its respective position within the sporozoite, indicating non-dynamic nature of the TRP-TMD-GFP localization in moving sporozoites (Fig: 5.4.5 A).

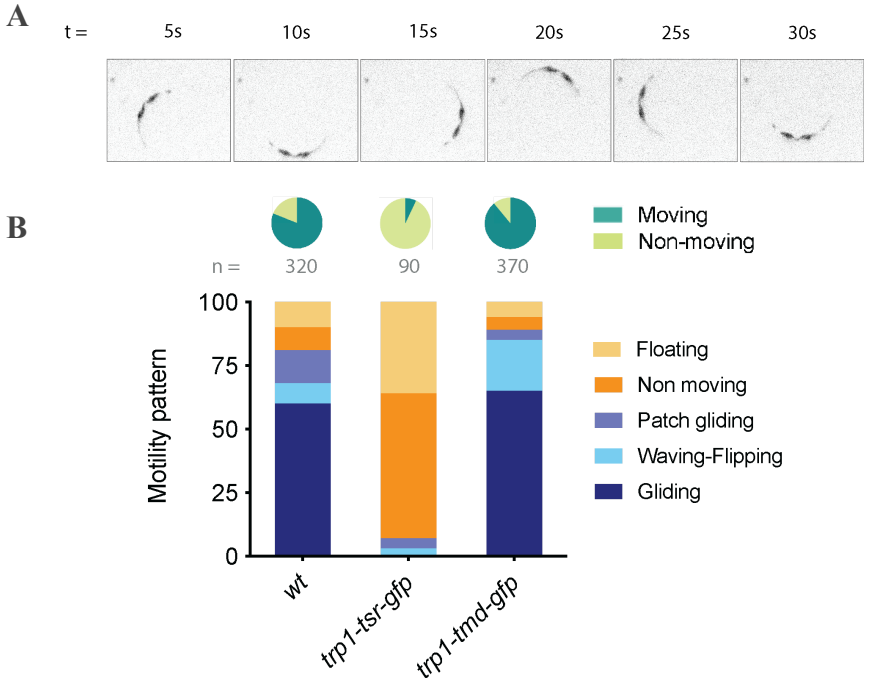

Figure: 5.4.5. ***trp1-gfp-tsr*** **salivary gland sporozoites are unable to move productively**

A. Motility pattern montage of *trp1-tmd-gfp* salivary gland sporozoites indicating that the GFP signal is not dynamic in moving sporozoites. **B.** Motility patterns observed in various TRP1 GFP-tagged mutant salivary gland sporozoites compared to wild type. 'n' equals the total number of sporozoites quantified from each parasite line. Data collected from three cage feed experiments. The pie charts depict the proportion of moving and non-moving sporozoites overall in each parasite line, where both productive and unproductive motility accounts for the 'moving' sporozoites. Attached and floating sporozoites were clubbed together into the 'non moving' counterpart.

Table 5.4

Absolute numbers for sporozoite counts in the midgut, hemolymph and salivary glands of all TRP1-GFP tagged mutants.

Parasite line	Midgut sporozoite no.	Hemolymph sporozoite no.	Salivary gland sporozoite no.	HLS/MGS	SGS/MGS
wt	25000 ± 2200	1600 ± 470	9100 ± 530	0.064	0.36
trp1-gfp-tsr	92000 ± 25900	7600 ± 1580	340 ± 70	0.082	0.0037
trp1-tmd-gfp	97800 ± 11400	11400 ± 4700	13170 ± 2500	0.12	0.14

5.5 Deciphering the role of N terminus extracellular domains in the function of TRP1

Previous studies on TRP1 indicated the crucial role of the N-terminus in salivary gland invasion (Klug and Frischknecht 2017). However, all attempts to tag the N-terminus were unsuccessful, as no GFP signal was observed despite detecting the *gfp::trp1* transcript. To further investigate the function of the N-terminus, two N-terminally 3X FLAG-tagged parasite lines, *trp1-flag10-gfp* and *trp1-flag20-gfp*, were generated using the *trp1-tmd-gfp* parasite line, where the C-terminal GFP tag is functional. This resulted in the creation of dual-tagged parasite lines.

Isogenic parasite lines were generated for both *trp1-flag10-gfp* and *trp1-flag20-gfp* mutants where a 3X FLAG-tag was placed 10 and 20 amino acids upstream of the TSR domain respectively and characterized according to previously described manner.

Presence of the FLAG tag at the N-terminus did not result in any defects regarding sporozoite development and egress from the oocyst as observed from the number of sporozoites in the midgut and hemolymph (Fig. 5.5.1 B-C). However, in *trp1-flag10-gfp* mutants the capacity to

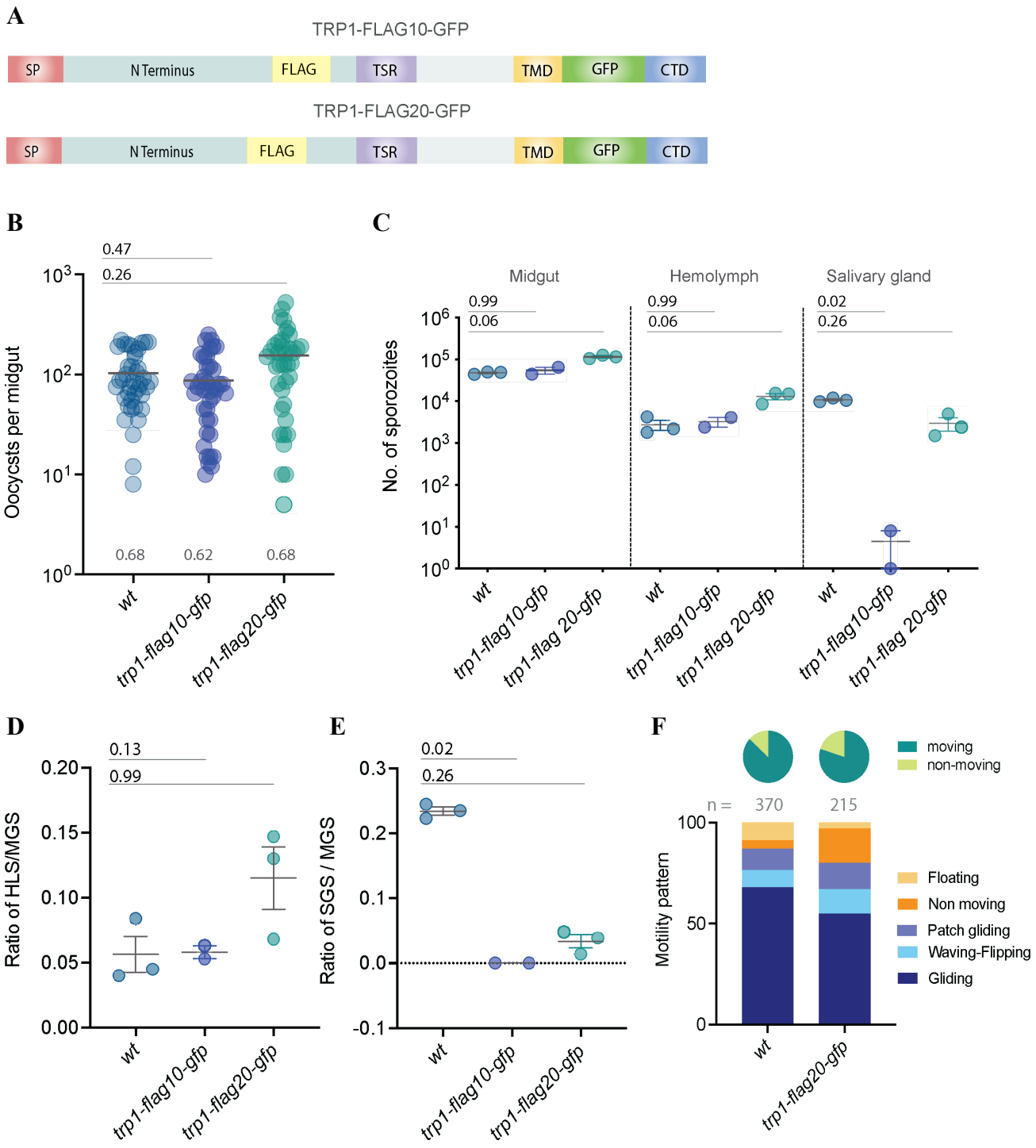

Figure: 5.5.1. Tagging upstream of the TSR domain disrupts the function of TRP1

A. Schematic representation of TRP1-FLAG10-GFP and TRP1-FLAG20-GFP. **B.** Oocyst numbers per midgut, where each dot represents one midgut. Black dash over each group represents the mean. Percentage of infection rates are indicated below the graph. **C.** Total

numbers of sporozoites in midgut, hemolymph and salivary gland of various C-terminus deletion mutants; Each dot represents an average number of sporozoites calculated from mosquitoes dissected from 1 cage feed. **D.** Ratio of hemolymph and midgut sporozoites **E.** Ratio of salivary gland and midgut sporozoites Data from three cage feeds for *wt* and *trp1-flag20-gfp;* 2 cage feeds for *trp1-flag10-gfp*. Statistical significance calculated by Kruskal-Wallis with Dunn's multiple comparisons test. **F.** Motility patterns observed in *trp1-flag20-gfp* salivary gland sporozoites compared to *wt* salivary sporozoites during in-vitro motility assay. Data from two cage feeds.

invade the salivary gland was completely disrupted (Fig. 5.5.1 C-E). Interestingly, placing the FLAG tag just 10 amino acids upstream of the *trp1-flag10-gfp* mutants, improves the salivary gland invasion capacity significantly, as observed in the case of the *trp1-flag20-gfp* mutants (Fig. 5.5.1 C-E).

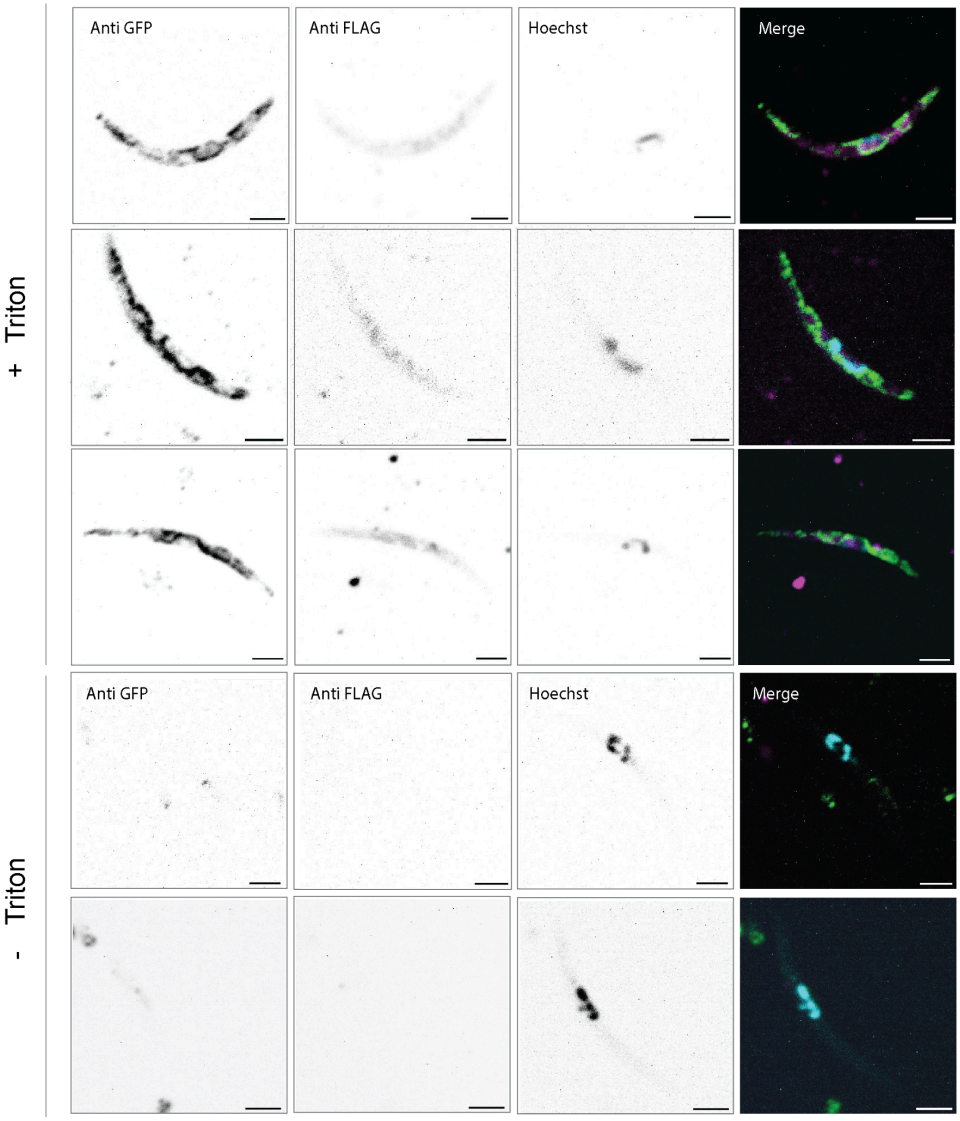

Figure: 5.5.2 GFP and FLAG localization in *trp1-flag20-gfp* salivary gland sporozoites.

A. Localization of FLAG and GFP in *trp1-flag20-gfp* permeabilized salivary gland sporozoites (scale bar: 3 μm) **B.** Localization of FLAG and GFP in *trp1-flag20-gfp* non permeabilized salivary gland sporozoites (scale bar: 3 μm).

In order to probe for the *trp1-flag20-gfp* salivary gland sporozoite's ability to move productively, in vitro motility assays were performed. The *trp1-flag20-gfp* salivary gland sporozoites showed comparable ability to move as well as the *wt* sporozoites, with a small decrease in the number of gliding sporozoites (Fig. 5.5.1 F).

Since the *trp1-flag20-gfp* sporozoites were able to invade the salivary gland, I wanted to probe the localization of the FLAG tagged N-terminus in sporozoites. Thus, Immunofluorescence assay was performed on permeabilized and non-permeabilized salivary gland sporozoites. This resulted in similar 'patchy' GFP localization as observed in *trp1-tmd-gfp* sporozoites (Fig. 5.4.4). However, the FLAG signal was only detected very faintly and only in permeabilized sporozoites, diffused in the cytoplasm (Fig. 5.5.2).

Table 5.5

Absolute numbers for sporozoite counts in the midgut, hemolymph and salivary glands of *trp1-flag10-gfp* and *trp1-flag20-gfp*.

Parasite line	Midgut sporozoite no.	Hemolymph sporozoite no.	Salivary gland sporozoite no.	HLS/MGS	SGS/MGS
wt	48000 ± 3200	2700 ± 1300	10800 ± 1100	0.056	0.22
trp1-flag10-gfp	109500 ± 14500	3250 ± 1200	5 ± 5	0.029	0.00004
trp1-flag20-gfp	115300 ± 10500	13000 ± 3900	2300 ± 1800	0.11	0.019

5.6 TSR domain plays a crucial role in the function of TRP1

The TSR domain is a characteristic feature found in several proteins crucial for the invasive stages of the *Plasmodium*, including all TRAP family and TRAP-related proteins, playing a significant role in protein-protein interactions, identification of receptors on host cells, thus

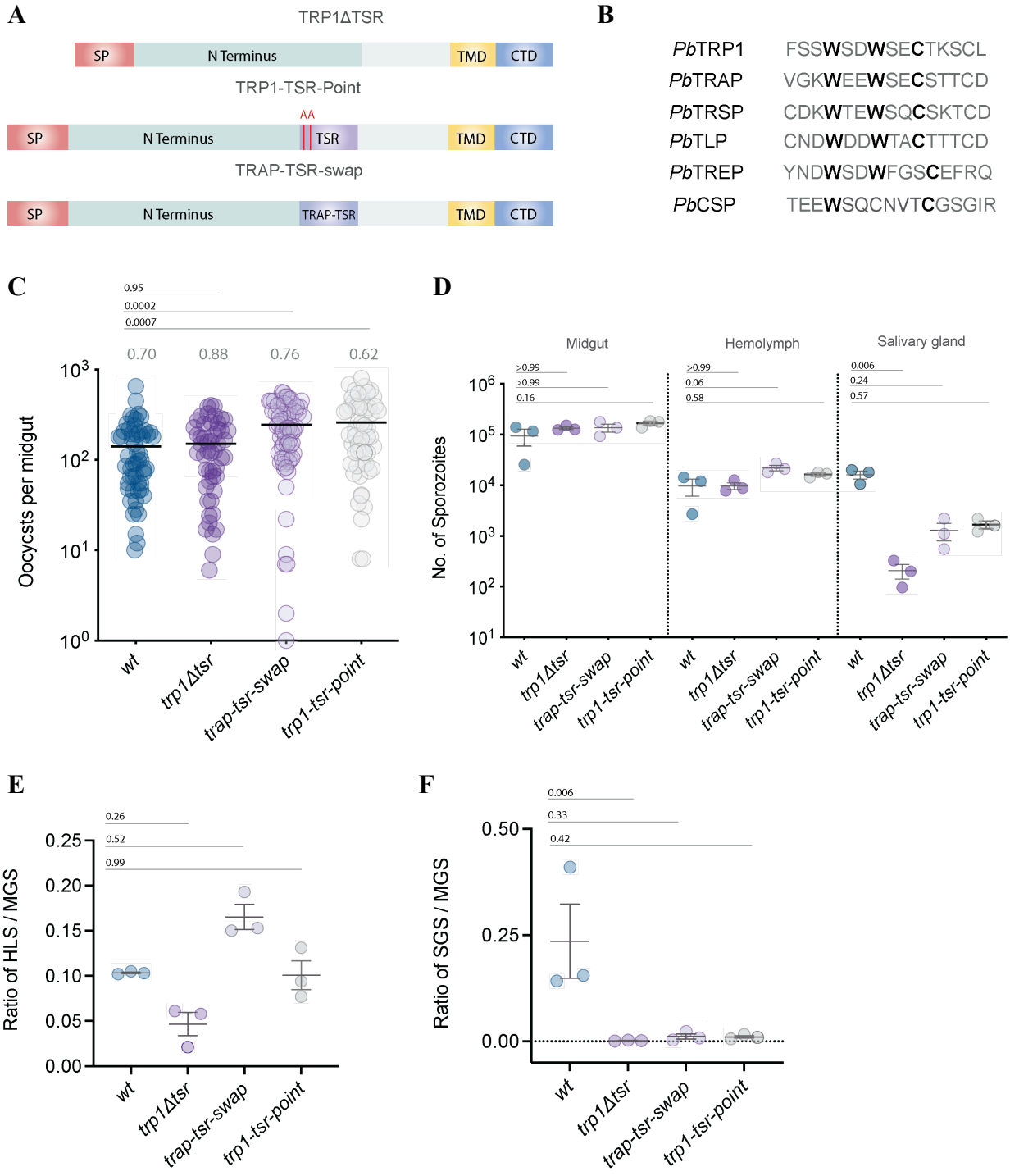

Figure: 5.6.1 TRP1 TSR domain is crucial in salivary gland invasion.

A. Schematic representation of TRP1 TSR-domain mutants **B**. Schematic representation of TSR domain across various proteins expressed in sporozoites, highlighting the conserved tryptophan residues. **C.** Oocyst numbers per midgut. where each dot represents one midgut. Black dash over each group represents the mean. Percentage of infection rates are indicated above the graph. **D**. Total numbers of sporozoites in midgut, hemolymph and salivary gland of various C-terminus deletion mutants; Each dot represents an average number of sporozoites calculated from mosquitoes dissected from 1 cage feed. **E.** Ratio of hemolymph and midgut sporozoites **F.** Ratio of salivary gland and midgut sporozoites
Statistical significance calculated by Kruskal-Wallis with Dunn's multiple comparisons test (Data from three cage feeds).

facilitating invasion and motility (Matuschewski et al. 2002; Ramakrishnan et al. 2011; Tewari et al. 2002; Klug et al. 2020). This domain contains a highly conserved 'WxxWxxC' motif, where the tryptophan residues are known to undergo post translational modifications, specifically C-mannosylation, a modification crucial for providing structural stability and ensuring proper folding and trafficking of TSR-containing proteins (Lopaticki et al. 2022). In the sporozoite stage, perturbations in the TSR domain of TSR domain containing proteins result in a wide range of phenotypes, particularly affecting the ability of sporozoites to invade salivary glands and exhibit productive motility, underscoring the diverse functions of this domain (Tewari et al. 2002; Lopaticki et al. 2022; Klug et al. 2020).

To investigate the TSR domain's role in TRP1 function, several TSR domain mutants were generated, including a complete deletion of the TSR domain. An isogenic *trp1Δtsr* parasite line was generated with help from master rotation student Bea Jagodic and characterized with the help of master thesis student Marzia Matejcek.

Sporozoites were collected from the hemolymph and salivary glands of infected mosquitoes 16 and 18 days post-infection, along with the corresponding midguts and characterized in the aforementioned fashion. The results showed that although the sporozoites had no difficulty in egressing from the oocyst, subsequently had a strong defect in salivary gland invasion (Fig. 5.6.1 D-F).

In order to investigate the effect on motility of the TSR domain mutants, in vitro motility assays were conducted on salivary gland and hemolymph sporozoites. No gliding sporozoites could be detected in the salivary gland for *trp1Δtsr* sporozoites. Hemolymph sporozoites also exhibited severe defects in motility when compared with *wt* sporozoites, where most sporozoites seemed to be simply attached to the surface or showing very little movement., signifying the importance of the TSR domain in the function of TRP1 (Fig. 5.6.2).

To investigate the role of the conserved tryptophan residues in the function of the TSR domain, isogenic population of *trp1-tsr-point* mutants were generated and characterized in similar manner with the help of Marzia Matejcek where both tryptophan residues in the conserved TSR motif were replaced by alanines (Fig. 5.6.1 A-B). As expected, sporozoites showed no defect in development and egress from the oocyst, however they exhibited a strongly reduced ability to invade the salivary gland . Interestingly, the defect in invasion of the salivary gland was less pronounced in *trp1-tsr-point* sporozoites compared to *trp1Δtsr* sporozoites (Fig. 5.6.1 D-F). However, the *trp1-tsr-point* salivary gland sporozoites showed similar defect in motility as in *trp1Δtsr* salivary gland sporozoites in in-vitro motility assays (Fig. 5.6.2).

Since the TSR is a conserved domain present in various TRAP family and TRAP related proteins, the potential of TRAP TSR-domain complementing the function of TRP1 TSR-domain was probed by generating an isogenic *trap-tsr-swap* parasite line where the entire TRP1 TSR-domain was replaced by TRAP TSR-domain with the help of Marzia Matejcek (Fig. 5.6.1 A-B). The *trap-tsr-swap* sporozoites showed no difficulty in development and egress from the oocysts, however they showed similar defects in salivary gland invasion as *trp1-tsr-point* sporozoites (Fig. 5.6.1 D-F). The *trp1-tsr-point* salivary gland sporozoites also showed similar defects in motility during in-vitro motility assays as *trp1-tsr-point* sporozoites, highlighting TRAP TSR-domain's inability to rescue the function of TRP1 TSR-domain. Salivary gland sporozoites showed no gliding motility and in most sporozoites only showed very little movement while being attached to the surface (Fig. 5.6.2). Majority of the hemolymph sporozoites however showed a unique motility pattern where most sporozoites seemed to exhibit a 'flexing' or contractile motility. This motility behaviour however was not seen in the salivary gland sporozoites .

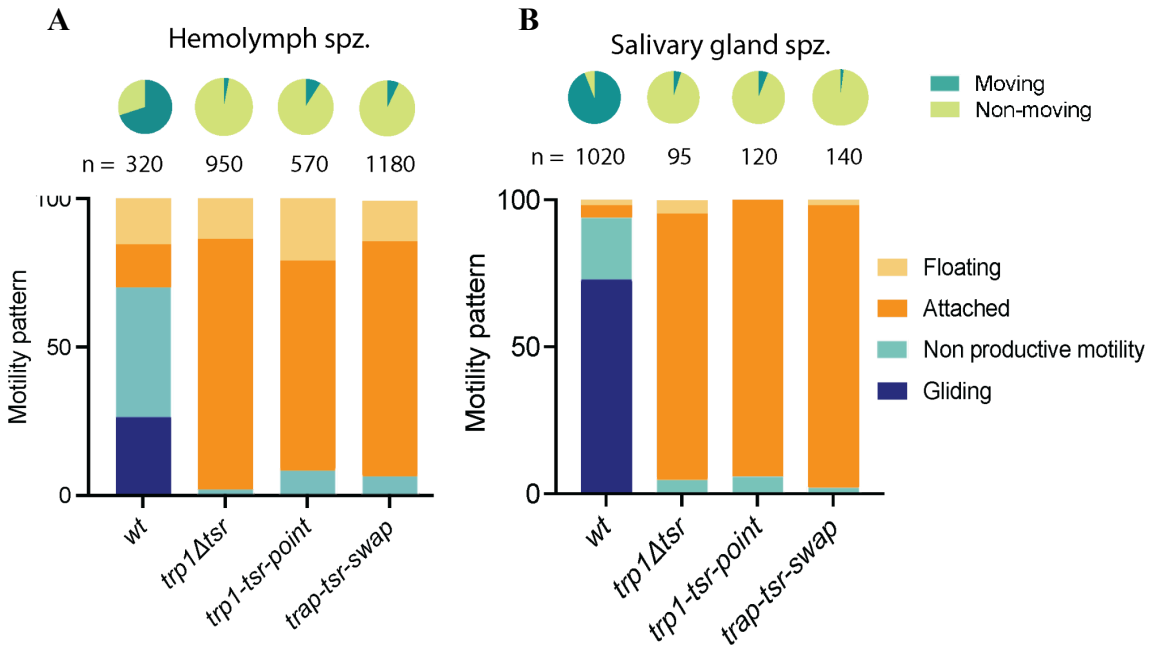

Figure: 5.6.2. TRP1 TSR domain is crucial for sporozoite motility

A. Motility patterns observed in various TRP1 TSR domain mutant hemolymph sporozoites compared to wild type. **B.** Motility patterns observed in various TRP1 TSR domain mutant salivary gland sporozoites compared to wild type.
'n' equals the total number of sporozoites quantified from each parasite line. Data collected from three cage feed experiments. The pie chart in green depicts the proportion of moving and non-moving sporozoites overall in each parasite line, where both productive and unproductive motility accounts for the 'moving' sporozoites. Attached and floating sporozoites were clubbed together into the 'non moving' counterpart.

Since the TSR domain mutant sporozoites had a severe defect in motility and invasion, transmission assays were conducted with the salivary gland sporozoites to probe for the mutants' ability to transmit malaria. For this purpose, both natural transmission and intravenous transmission assay was conducted. In the natural transmission assay, no mice were infected when bit by *trp1Δtsr* sporozoites, showing complete block of transmission. However in the i.v. transmission assay, where 1000 salivary gland sporozoites were injected bypassing the host skin barrier, 3 out of 4 mice became positive with malaria with a delay of 3 days in prepatency. The *trp1-tsr-point* mutants, similar to *trp1Δtsr* mutants, resulted in the infection of no mice, showing complete block of transmission via natural transmission. However in the i.v. transmission assay, 1 out of 4 mice became positive with malaria with a delay of 3 days in prepatency. The

trp1-tsr-swap mutants also showed no transmission of disease In the natural transmission assay, similar to *trp1Δtsr* and *trp1-tsr-point* mutants. However in the i.v. transmission assay, 2 out of 4

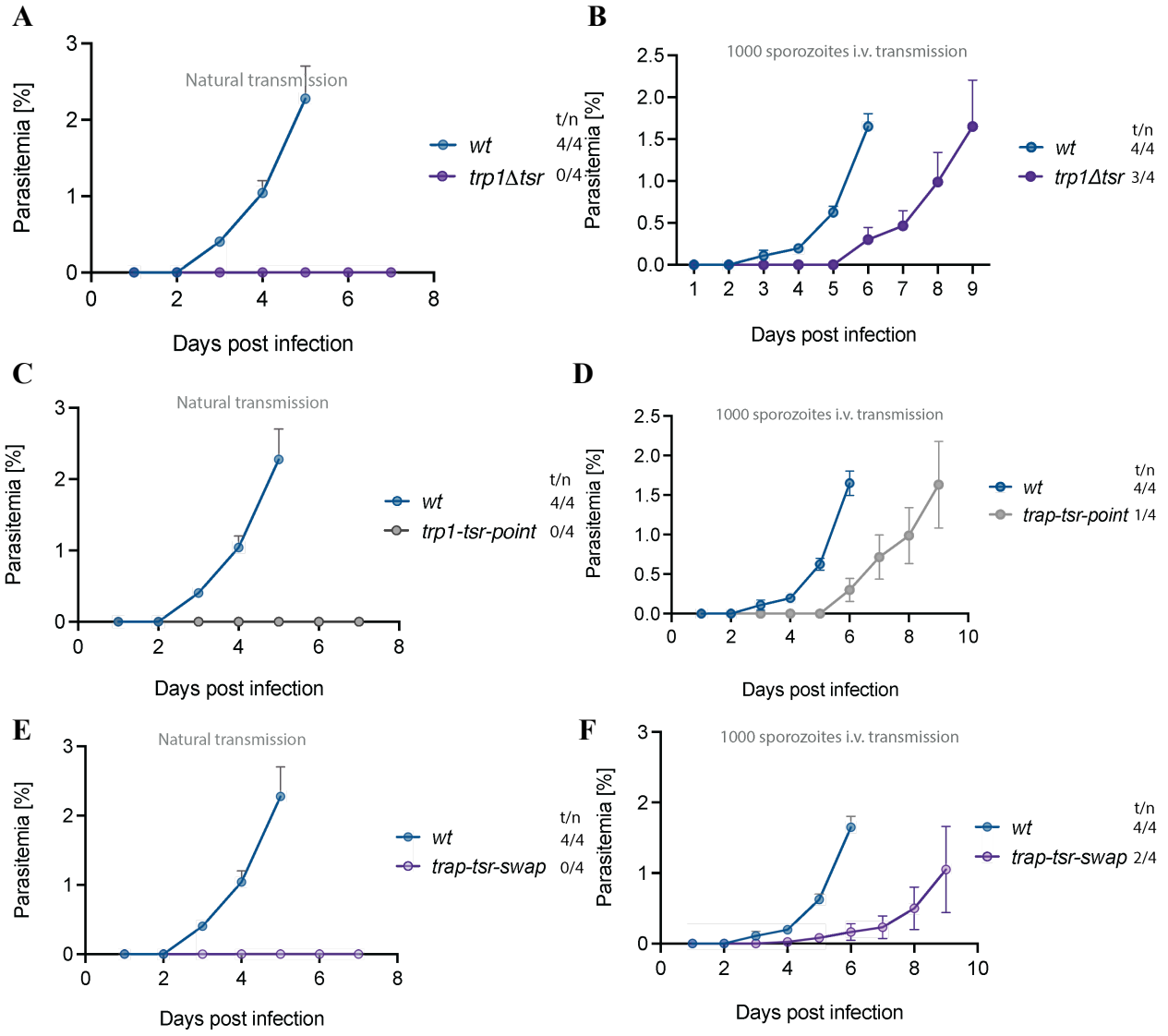

Figure: 5.6.3. TRP1 TSR mutant sporozoites cannot successfully transmit disease to host via natural transmission

A. Natural transmission assay comparing parasitemia in mice infected via 'bite-back' method with *trp1Δtsr* infected mosquitoes compared to wt PbANKA infected mosquitoes. **B.** Intravenous transmission assay comparing parasitemia in mice infected with 1000 salivary gland sporozoites from *trp1Δtsr* mutants compared to wt. **C.** Natural transmission assay comparing parasitemia in mice infected with *trp1-tsr-point* mutants compared to wt **D.** Intravenous transmission assay comparing parasitemia in mice infected with *trp1-tsr-point* mutants to wt. **E.** Natural transmission assay comparing parasitemia in mice infected with *trap-tsr-swap* mutants

compared to wt. **F.** Intravenous transmission assay comparing parasitemia in mice infected with *trap-tsr-swap* mutants to wt. 't' indicates the number of mice that became positive with malaria, whereas 'n' indicates the total number of mice infected.

mice became positive with malaria with a delay of 2 days in prepatency exhibiting significant reduction in parasitemia (Fig: 5.6.3 A-F).

Table 5.6.1: Absolute numbers for sporozoite counts in the midgut, hemolymph and salivary glands of all TRP1 TSR domain mutants.

Parasite line	Midgut sporozoite no.	Hemolymph sporozoite no.	Salivary gland sporozoite no.	HLS/MGS	SGS/MGS
wt	93900 ± 60400	9700 ± 6100	16200 ± 5000	0.10	0.17
trp1Δtsr	134200 ± 15300	9700 ± 2500	210 ± 110	0.07	0.0015
trp1-tsr-point	167000 ± 26200	22000 ± 4600	1300 ± 840	0.13	0.0077
trap-tsr-swap	136300 ± 79700	13400 ± 2000	1670 ± 500	0.09	0.012

Table 5.6.2: Transmission assay summary:

The transmission potential of all generated parasite lines was assessed using C57BL/6 mice. In each experiment, four naïve mice were infected. The prepatent period, defined as the time from infection to the first detection of blood-stage parasites, is reported as the mean for all mice that became blood-stage positive. For comparison, similar experiments were conducted with wild-type parasites.

Parasite line	Inoculation route	Mice infected/Total	Prepatency
wt	By mosquito bite	4/4	3
wt	1000 spz i.v.	4/4	3
trp1Δtsr	By mosquito bite	0/4	∞
trp1Δtsr	1000 spz i.v.	3/4	6
trp1-tsr-point	By mosquito bite	0/4	∞
trp1-tsr-point	1000 spz i.v.	1/4	6
trap-tsr-swap	By mosquito bite	0/4	∞
trap-tsr-swap	1000 spz i.v.	2/4	5

5.7 Generation of functional proximal biotinylation tagged TRP1

In order to find cytoplasmic interaction partners of TRP1 C-terminus, TRP1 was labeled with two different proximity biotinylation tags, i.e. APEX2 and miniTurbo at the C-terminus domain, just downstream of the transmembrane domain., Both methods were used as they have different properties, fast and abundant labeling with a big radius (APEX) and slower labeling in closer proximity (mTurbo) (REFs). In order to generate the constructs, the miniTurbo or APEX2 tags were inserted directly upstream of the C-terminus domain (CTD) and downstream of the

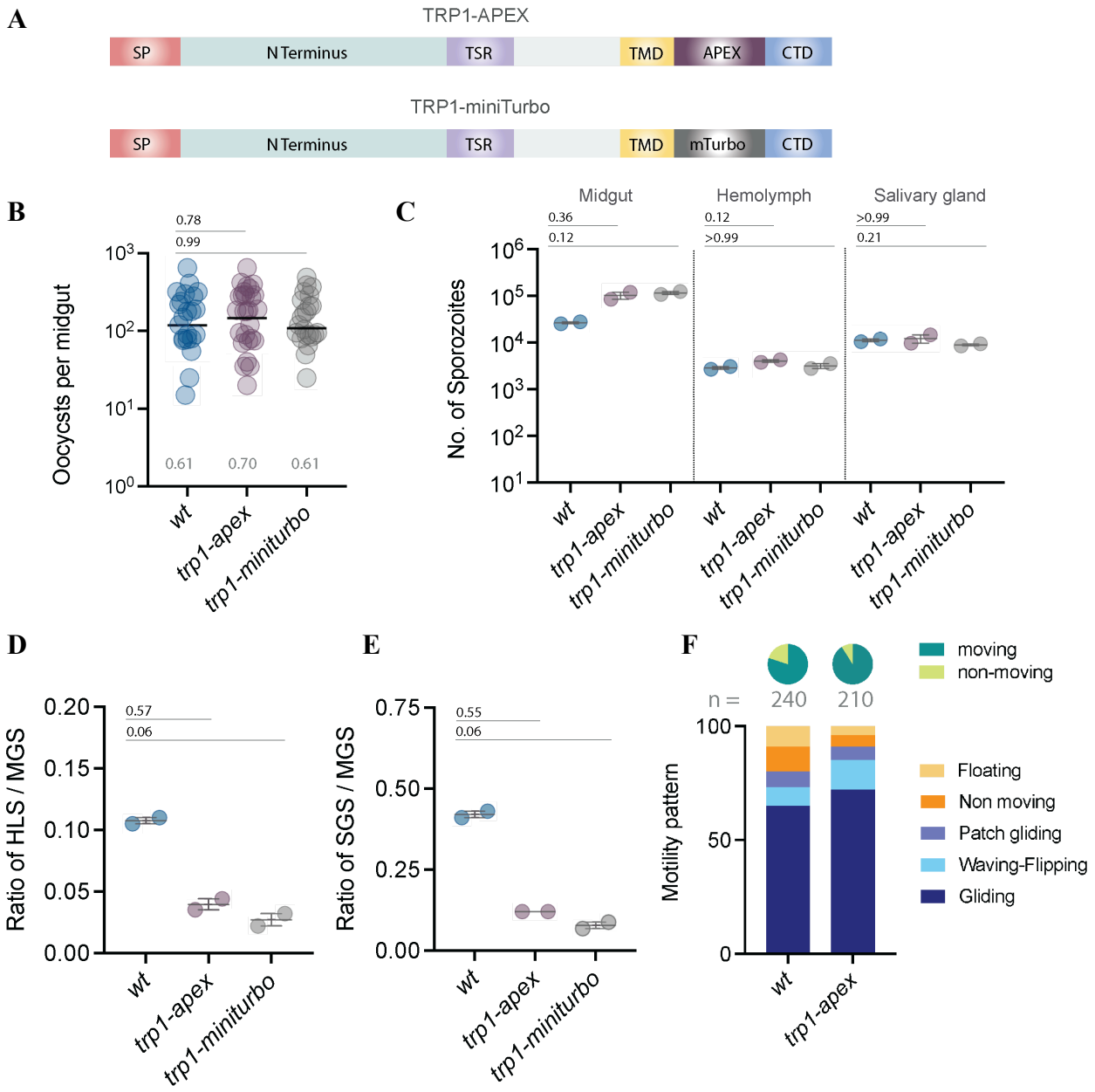

Figure: 5.7.1. TRP1 can be successfully tagged upstream of the C-terminus with APEX2 and miniTurbo.

A. Schematic representation of TRP1-APEX and TRP1-miniTurbo. **B.** Oocyst numbers per midgut. Data collected from two cage feeds, where each dot represents one midgut. Black dash over each group represents the mean. Percentage of infection rates are indicated below the graph. **C.** Total numbers of sporozoites in midgut, hemolymph and salivary gland of various C-terminus deletion mutants; Each dot represents an average number of sporozoites calculated from mosquitoes dissected from 1 cage feed. **D.** Ratio of hemolymph and midgut sporozoites **E.** Ratio of salivary gland and midgut sporozoites **F.** Motility patterns observed in *trp1-apex* salivary gland sporozoites compared to *wt* salivary sporozoites during in-vitro motility assay.
Statistical significance calculated by Kruskal-Wallis with Dunn's multiple comparisons test (Data from two cage feeds).

transmembrane domain (TMD) with a small linker of two glycine residues on both sides of the tag, identical to the location of GFP tag in *trp1-tmd-gfp* parasite line which functionally behaved like wild type (Fig: 5.7.1 A). Isogenic parasite lines were generated for the *trp1-apex* and *trp1-miniturbo* constructs and characterized henceforth.

Sporozoites showed no development defects, as expected as observed from the infectivity rate of mosquito midguts and the number of midgut sporozoites (Fig: 5.7.1 B-C). Hemolymph and salivary gland sporozoites were collected from the dissected mosquito tissue, on day 16 and 18 respectively along with the midgut sporozoites from the corresponding mosquitoes, as mentioned before and counted to assess the sporozoites' ability to egress from the oocyst and invade the

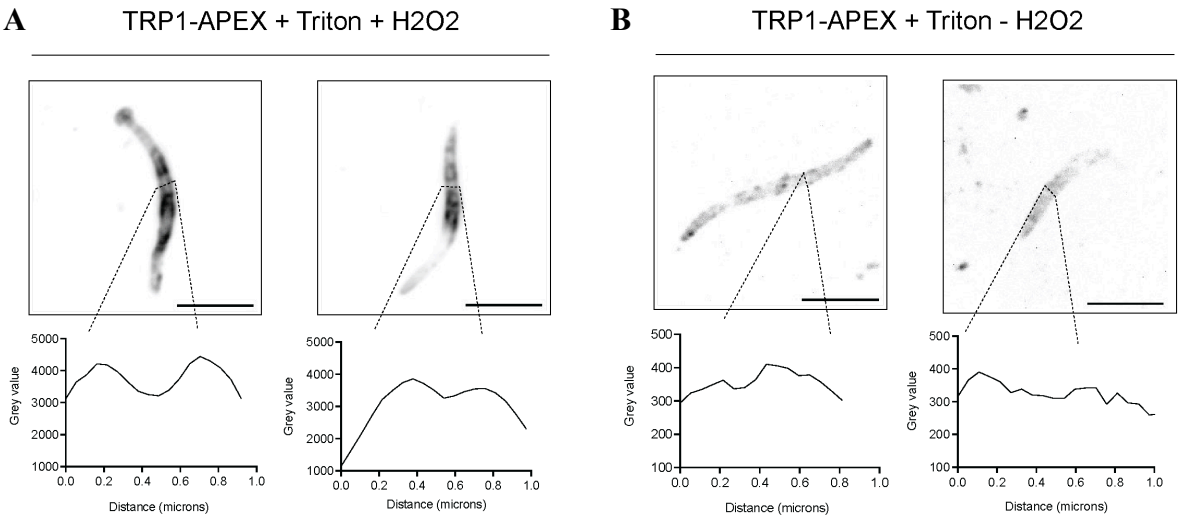

Figure: 5.7.2. TRP1-APEX sporozoites can be specifically biotinylated.

A. IFA on *trp1-apex* salivary gland sporozoites in the presence of triton-X-100 and hydrogen peroxide (H_2O_2) using Alexa Fluor 594 Streptavidin highlighting specific biotinylation. **B.** IFA on *trp1-apex* salivary gland sporozoites in the presence of only triton-X-100 using Alexa Fluor 594 Streptavidin. Scale bar: 5 uM.

salivary gland. The ratio of sporozoite numbers and the total no. of sporozoites in hemolymph and salivary gland clearly indicate that the proximity biotinylation tags don't disrupt the ability of the parasite to egress from the oocyst and invade the salivary gland (Fig: 5.7.1 C-E).

For time constraints, only the *trp1-apex* parasite line was chosen for further characterizations.

To ensure that *trp1-apex* sporozoites can move as efficiently as the wt, motility assays were conducted on salivary gland sporozoites. This showed comparable motility between *wt* and *trp1-apex* sporozoites (Fig: 5.7.1 F).

To assess the localization of TRP1-APEX in salivary gland sporozoites, immunofluorescence assay was performed on *trp1-apex* salivary gland sporozoites using Alexa Fluor 594 Streptavidin to detect biotinylation extent. A strong biotinylation signal was observed exclusively in permeabilized sporozoites treated with biotin-phenol when hydrogen peroxide was present to initiate the reaction. In contrast, permeabilized sporozoites treated with biotin-phenol without hydrogen peroxide showed only the background signal from naturally occurring biotinylated proteins in salivary gland sporozoites (Fig: 5.7.2 A-B). Interestingly, the pattern of biotinylation on the *trp1-apex* sporozoites resembles closely with the GFP signal in *trp1-tmd-gfp* sporozoites. This further indicates the specificity of biotinylation in *trp1-apex* salivary gland sporozoites.

Table 5.7

Absolute numbers and ratios for sporozoite counts in the midgut, hemolymph and salivary glands of proximity biotinylation tagged mutants.

Parasite line	Midgut sporozoite no.	Hemolymph sporozoite no.	Salivary gland sporozoite no.	HLS/MGS	SGS/MGS
wt	26750 ± 1770	2900 ± 280	11250 ± 1060	0.10	0.42
trp1-apex	103000 ± 25450	4050 ± 350	12250 ± 3470	0.039	0.12
trp1-miniturbo	116500 ± 12020	3200 ± 530	9000 ± 670	0.027	0.08

5.8 Identification of TRP1 C-terminus interaction partner proteins

As TRP1 C-terminus plays a crucial role in motility, salivary gland invasion and transmission to the host, I wanted to identify the interaction partners of TRP1 C-terminus. For this purpose, an isogenic population of *trp1-apex* parasite line was generated, that included a proximity biotinylation tag APEX2, a genetically engineered ascorbate peroxidase enzyme fused with TRP1. When provided with hydrogen peroxide and biotin-phenol, APEX2 catalyzes a reaction that biotinylates proteins within a very small radius (typically around 20 nanometers) of the fusion protein. APEX2 catalyzes the oxidation of biotin-phenol into a highly reactive and short lived biotin-phenoxyl radical with the help of Hydrogen peroxide (H_2O_2) as an oxidizing agent. These radicals diffuse only a few nanometers (~20 nm) before reacting with electron-rich residues on nearby proteins (primarily tyrosine, but also cysteine and tryptophan) (Filali-Mouncef et al. 2024; Kimmel et al. 2022). This labeling occurs within seconds to minutes, making APEX2 a highly time-resolved tool for studying dynamic cellular environments. APEX accomplishes much faster labeling than BioID (APEX2 works within 1 minute, whereas BioID requires several hours) and entails improved labeling efficiency and reduced background labeling. APEX mediated proximity biotinylation also results in higher spatial specificity due to the formation of short-lived radicals and is also effective in live cells without the need for external biotin ligase expression. APEX2 was chosen instead of APEX as it shows improved labelling efficiency and higher spatial specificity (Filali-Mouncef et al. 2024).

Once it was established that APEX2 tagging did not interfere with the function of TRP1 and shows specific biotinylation, proximity biotinylation assay was performed on *trp1-apex* salivary gland sporozoites following the protocol mentioned in the ‘materials and methods’ section. Three experimental setups were designed: the first cohort entailed 1.5 million salivary gland sporozoites activated with 3% BSA and treated with biotin phenol and hydrogen peroxide, second cohort entailed 1.5 million sporozoites activated with 3% BSA and only treated with biotin phenol, whereas the third cohort included 1.5 million wildtype sporozoites activated with 3% BSA and treated with biotin phenol and hydrogen peroxide. The second cohort acts as the direct control for the proximity biotinylation experiment, whereas the third cohort serves as an indicator if there are naturally occuring biotinylation events in wildtype salivary gland sporozoites.

Table: 5.8.1

A. Class I proteins: Peptides detected in at least 2 replicates and not in control

No.	Gene ID	Description	Peptide no.	Characteristics/ Function
1	PBANKA_1340100	L-lactate dehydrogenase	17	Dehydrogenase
2	PBANKA_1218200	T-complex protein 1 subunit epsilon, putative	10	Chaperon
3	PBANKA_0929900	Heat shock protein 90, putative	10	Chaperon
4	PBANKA_0916200	T-complex protein 1 subunit alpha	10	Chaperon
5	PBANKA_0310900	T-complex protein 1 subunit theta, putative	10	Chaperon
6	PBANKA_1026200	NADP-specific glutamate dehydrogenase, putative	7	Amino acid dehydrogenase
7	PBANKA_1461800	26S protease regulatory subunit 8, putative	7	Protease
8	PBANKA_0405200	T-complex protein 1 subunit beta, putative	7	Chaperon
9	PBANKA_1031900	eukaryotic translation initiation factor 2 subunit gamma, putative	6	Transcription factor
10	PBANKA_1439200	polyadenylate-binding protein 1, putative	6	RNA binding protein
11	PBANKA_1117700	Malate dehydrogenase	6	Dehydrogenase
12	PBANKA_0703900	Receptor for activated c kinase, putative	5	WD40-repeat containing protein
13	PBANKA_1242300	Hsc70-interacting protein, putative	4	Chaperon
14	PBANKA_1030100	Actin-2	4	Cytoskeletal protein
15	PBANKA_0702800	Protein disulfide-isomerase	4	Isomerase
16	PBANKA_0821700	Inosine-5'-monophosphate dehydrogenase	4	Unknown
17	PBANKA_1103100	actin-depolymerizing factor 1	3	Actin filament regulation
18	PBANKA_1003800	V-type proton ATPase subunit B, putative	3	ATPase
19	PBANKA_1032700	CUGBP Elav-like family member 2, putative	3	RNA binding protein
20	PBANKA_1010600	calmodulin, putative	2	Calcium signalling
21	PBANKA_0938300	heat shock protein HspJ62	2	Chaperon
22	PBANKA_0523900	Glideosome associated protein with multiple membrane spans 2, putative	2	Glideosome associated protein
23	PBANKA_0904100	Ras-related protein Rab-6	2	Chaperon
24	PBANKA_1432300	CelTOS: cell traversal protein for ookinetes and sporozoites	2	Host cell traversal
25	PBANKA_0819900	Nucleosome assembly protein	2	Nucleosome assembly proteins

26	PBANKA_0506600	Serine/arginine-rich splicing factor 4, putative	2	Splicer protein
27	PBANKA_1344400	AMP deaminase	2	Deaminase

B. Class II proteins (Selected): Peptides detected in at least 1 replicate and not in control

No.	Gene ID	Description	Peptide no.	Characteristics/ Function
1	PBANKA_0619200	Secreted ookinete protein, putative	7	Migration through the midgut wall
2	PBANKA_1312700	Gamete egress and sporozoite traversal protein	5	Male and female gamete egress, Sporozoite traversal
4	PBANKA_1464100	Coronin	4	Actin filament regulation
7	PBANKA_1115300	Glideosome-associated protein 40, putative	3	Glideosome associated protein
8	PBANKA_0931100	Uncharacterized protein	3	-
9	PBANKA_1451200	p25-alpha family protein, putative	2	Male gametocyte exflagellation
10	PBANKA_1233700	Uncharacterized protein	2	-
11	PBANKA_0902700	Uncharacterized protein	2	-

C. Class III proteins (Selected): Peptides detected in both test and control

No.	Gene ID	Description	Peptide no.	Characteristics/ Function
1	PBANKA_1137800	Glideosome-associated connector	52	Glideosome associated protein
2	PBANKA_1355700	Myosin A	40	Cytoskeletal protein
3	PBANKA_0402600	Inner membrane complex protein 1a	37	IMC protein
4	PBANKA_1206900	Tubulin beta chain	28	Cytoskeletal protein
5	PBANKA_1464900	Rhoptry neck protein 3, putative	26	Rhoptry protein, host cell invasion
6	PBANKA_0417700	Tubulin alpha chain	23	Cytoskeletal protein
7	PBANKA_1459300	Actin-1	23	Cytoskeletal protein
8	PBANKA_1137000	Bergheilysin	20	Putative role in salivary gland invasion or skin passage
9	PBANKA_0402700	Inner membrane complex protein 1e	20	IMC protein
10	PBANKA_1422900	Concavin	18	Sporozoite shape maintenance, host transmission

11	PBANKA_1342500	Subpellicular microtubule protein 3	17	Sporozoite motility, host transmission
12	PBANKA_1354900	Inner membrane complex protein 1k, putative	17	IMC protein
13	PBANKA_1120400	Inner membrane complex protein 1j, putative	15	IMC protein
14	PBANKA_1349800	Thrombospondin-related anonymous protein	14	Sporozoite motility
15	PBANKA_1006200	Sporozoite invasion-associated protein 1	14	Sporozoite motility, Salivary gland invasion
16	PBANKA_0901300.2	Membrane associated erythrocyte binding-like protein	12	Salivary gland invasion
17	PBANKA_0107300	T-complex protein 1 subunit zeta, putative	12	Chaperon
18	PBANKA_0605900	S14	11	Sporozoite motility and infectivity
19	PBANKA_1436600	Inner membrane complex protein 1h	11	IMC protein
20	PBANKA_1104800	Actin-like protein, putative	10	Actin filament regulation
21	PBANKA_0306600	Uncharacterized protein	9	-
21	PBANKA_1315700	Rhoptry neck protein 2	8	Rhoptry protein, host cell invasion
22	PBANKA_1240600	Inner membrane complex protein 1g, putative	7	IMC protein
23	PBANKA_0304700	SERA5	7	Serine protease, Egress from oocyst
24	PBANKA_0513000	Inner membrane complex protein 1m, putative	7	IMC protein
25	PBANKA_1006300	Sporozoite micronemal protein essential for cell traversal	6	Host cell traversal
26	PBANKA_1025700	Inner membrane complex protein 1l, putative	6	IMC protein
27	PBANKA_1025700	Inner membrane complex protein 1l, putative	6	IMC protein
28	PBANKA_1209400	Inner membrane complex sub-compartment protein 1	5	IMC protein
29	PBANKA_0830400	G2 protein	5	Morphology and motility of ookinetes and sporozoites
30	PBANKA_1120100	Uncharacterized protein	5	-
31	PBANKA_0620800	Uncharacterized protein	5	-
32	PBANKA_1445000	Subpellicular microtubule protein 2, putative	4	Cytoskeleton associated protein
33	PBANKA_1417200	Uncharacterized protein	3	-
34	PBANKA_0204600	Photosensitized INA-labeled protein PHIL1	3	IMC protein
35	PBANKA_0111600	Rhoptry protein ROP14, putative	3	Rhoptry protein, host cell invasion
36	PBANKA_0206700	Uncharacterized protein	3	-

37	PBANKA_1306500	TRAP-like protein	2	Sporozoite motility
38	PBANKA_1338900	Glideosome associated protein with multiple membrane spans 1, putative	2	Glideosome associated protein

In MS analysis of three independent sets of experiments 307 unique proteins were identified. Of these 307 proteins, 27 proteins were detected in all three experiments only in the first cohort and classified as “Class I” proteins. 52 proteins were detected in at least one experiment only in the first cohort and classified as “Class II” proteins. 164 proteins were detected in both the first and second cohort and classified as “Class III” proteins (Table 5.8).

This was interesting as the “Class III” proteins would generally be considered as a contaminant, but in this case showed inner membrane complex (IMC) associated proteins like inner membrane complex protein subunit(s), PHIL1 (PBANKA_0204600), glideosome associated proteins such as, glideosome-associated connector (PBANKA_1137800) and glideosome associated protein with multiple membrane spans 1 (PBANKA_1338900). Surface proteins involved in sporozoite motility like TRAP (PBANKA_1349800), TRAP-like protein (PBANKA_1306500), subpellicular network (SPN) associated proteins like subpellicular microtubule protein 2 (PBANKA_1445000), subpellicular microtubule protein 3 (PBANKA_1342500) were also detected along with 5 uncharacterized proteins. These proteins are known to be located at the IMC, SPN, micronemes, rhoptries, sporozoite surface or soluble components involved in gliding motility and invasion (Table 5.8 C).

The group of 52 “Class II” proteins also entailed some interesting proteins associated with glideosome and motility including GAP 40 (PBANKA_1115300), coronin (PBANKA_1464100), myosin A (PBANKA_1355700) along with 3 uncharacterized proteins (Table 5.8 B).

Out of 27 “Class I” proteins, 3 motility associated proteins such as actin II (PBANKA_1030100), actin-depolymerizing factor 1 (PBANKA_1103100) and the putative Glideosome associated protein with multiple membrane spans 2 (PBANKA_0523900) were identified. It also entailed 8 chaperon proteins and 3 RNA binding-domain containing proteins (Table 5.8 A). Interestingly, “Class I” proteins entailed 4 subunits of T complex protein I, a chaperon that is known to be crucial in development in the asexual stages but is also highly expressed in ookinete, oocyst and

liver stages of the parasite. Its function in mosquito stages of the parasite remains unexplored (Spillman et al. 2017).

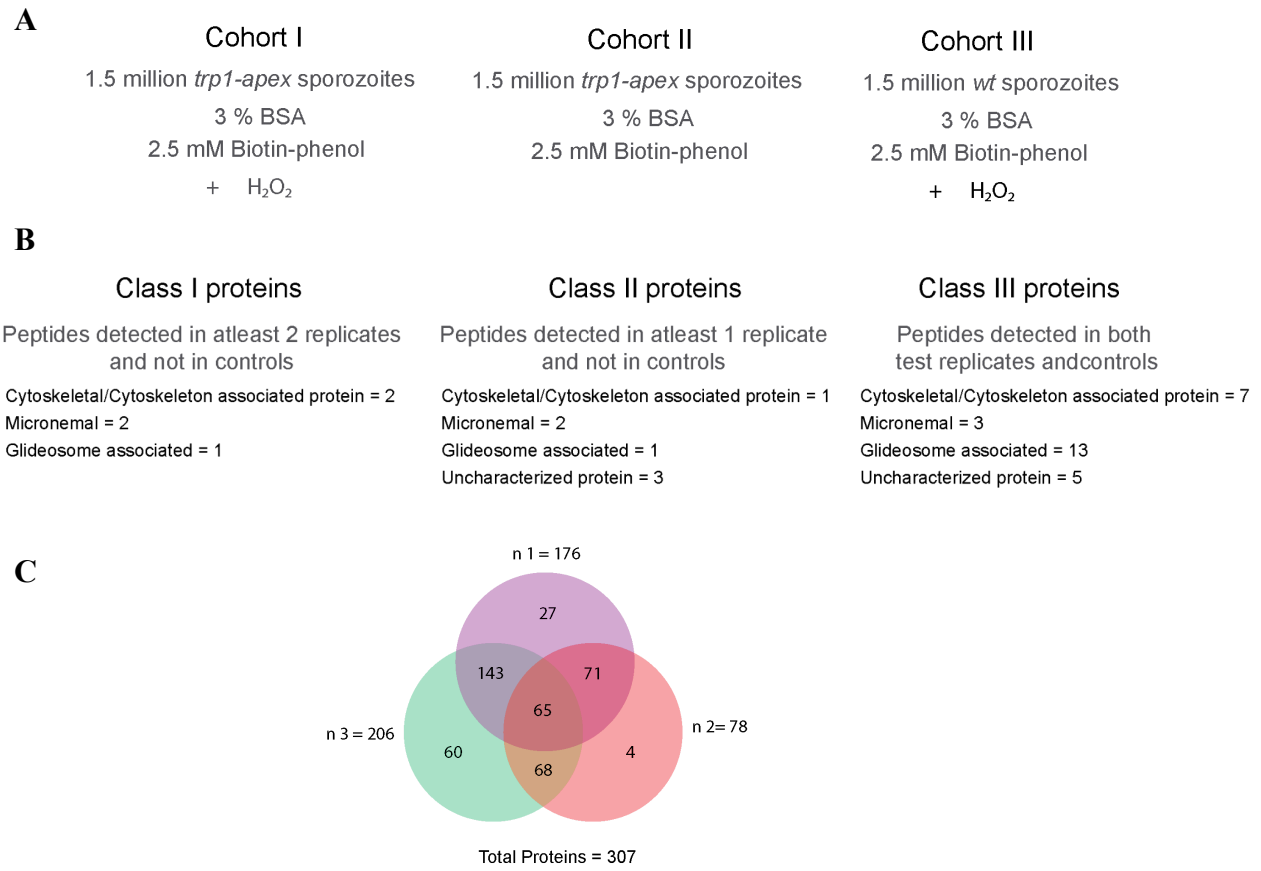

Figure: 5.8.1 Identifying C-terminus interaction partners of TRP1.

A. Experimental setup for APEX2 mediated proximity dependent biotinylation of *trp1-apex* salivary gland sporozoites **B.** MS data is classified into three groups according to their presence in different cohorts. Class I proteins are only identified in cohort I in at least 2 experiments. Class II proteins are only identified in cohort I in at least 1 experiment. Class III proteins are identified in cohort I and also cohort II and III. **C.** Overview of mass- spectrometry analyses identifying total 307 unique proteins in 3 independent experiments including 65 commonly identified proteins in all 3 experiments**.**

In all three experiments, 9 uncharacterized proteins were identified in total, of which 3 proteins belonged in "Class II" and 5 proteins in "Class III" (Table: 5.8.2).

Table: 5.8.2 List of uncharacterized proteins identified:

No.	Gene ID	Class	Peptide no.	Highly expressed in	Plasmogem phenotype
1	PBANKA_0620800	III	11	Mosquito stages, Female gametocyte	-
2	PBANKA_0306600	III	9	Ookinete, Female gametocyte	Dispensable
3	PBANKA_1120100	III	5	Liver, Trophozoite, Schizont, Female gametocyte	Dispensable
4	PBANKA_1417200	III	3	Schizont, Female gametocyte	-
5	PBANKA_0206700	III	3	Male gametocyte	Dispensable
6	PBANKA_0931100	II	3	Ookinete, Sporozoite, Liver, Trophozoite, Schizont, Female gametocyte, Male gametocyte	-
7	PBANKA_1034500	-	3	Ookinete, Sporozoite	Dispensable
8	PBANKA_1233700	II	2	Ookinete, Sporozoite	-
9	PBANKA_0902700	II	2	Oocyst	-

Table: 5.8.3 Closest homologs/orthologs of uncharacterized proteins with identity scores along with AlphaFold 3 structure predictions:

1

PBANKA_0620800

Rank	Protein Name / Accession	Organism	Identity (%)	E-value
1	Conserved Plasmodium protein, unknown function |SCM19946.1|	*Plasmodium berghei*	90.88%	0
2	Conserved Plasmodium protein, unknown function |SCO60006.1|	*Plasmodium berghei*	92.55%	0
3	Uncharacterized protein PY17X_0623500 |XP_729902.1|	*Plasmodium yoelii*	65.50%	0
4	Hypothetical protein YYG_03625	*Plasmodium vinckei petteri*	66.61%	0
5	Plasmodium protein, unknown function |XP_037490285.1|	*Plasmodium vinckei vinckei*	62.82%	0

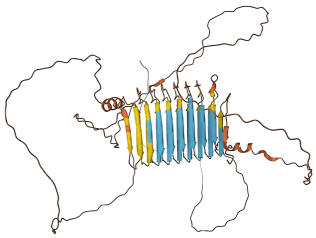

2

PBANKA_0306600

Rank	Protein Name / Accession	Organism	Identity (%)	E-value
1	Conserved Plasmodium protein, unknown function |SCM17159.1|	*Plasmodium berghei*	99.79%	0
2	Conserved Plasmodium protein, unknown function |SCL97414.1|	*Plasmodium chabaudi chabaudi*	75.83%	0
3	Conserved Plasmodium protein, unknown function |SCM04991.1|	*Plasmodium chabaudi adami*	75.88%	0
4	Conserved Plasmodium protein, unknown function |CAD2085275.1|	*Plasmodium vinckei brucechwatti*	75.46%	0
5	Hypothetical protein |EAA22739.1|	*Plasmodium yoelii yoelii*	70.07%	0

3

PBANKA_1120100

Rank	Protein Name / Accession	Organism	Identity (%)	E-value
1	Hypothetical protein YYC_05124	*Plasmodium yoelii* 17X	93.99%	0
2	Conserved Plasmodium protein, unknown function	*Plasmodium yoelii*	93.83%	0
3	Conserved Plasmodium protein, unknown function	*Plasmodium vinckei lentum*	91.56%	0
4	Conserved Plasmodium protein, unknown function	*Plasmodium vinckei*	91.63%	0
5	Conserved Plasmodium protein, unknown function	*Plasmodium chabaudi adami*	91.48%	0

N/A

4

PBANKA_1417200

Rank	Protein Name / Accession	Organism	Identity (%)	E-value
1	Conserved protein, unknown function |XP_729580.2|	Plasmodium yoelii	89.05%	0
2	TATA element modulatory factor |EAA21145.1|	Plasmodium yoelii yoelii	89.14%	0
3	Conserved Plasmodium protein, unknown function |CAD2104180.1|	Plasmodium vinckei brucechwatti	86.20%	0
4	Hypothetical protein YYG_00193	Plasmodium vinckei petteri	84.73%	0
5	Conserved Plasmodium protein, unknown function |CAD2104076.1|	Plasmodium vinckei lentum	84.73%	0

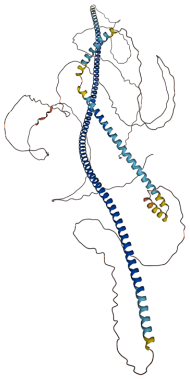

5

PBANKA_0206700

Rank	Protein Name / Accession	Organism	Identity (%)	E-value
1	Conserved Plasmodium protein, unknown function |CAD2084543.1|	*Plasmodium vinckei lentum*	63.97%	7e-69
2	Hypothetical protein |YYC_02286|	*Plasmodium yoelii 17X*	60.99%	3e-66
3	Conserved Plasmodium protein, unknown function |XP_724862.1|	*Plasmodium yoelii*	60.14%	6e-66
4	Conserved Plasmodium protein, unknown function |XP_008626372.1|	*Plasmodium vinckei vinckei*	68.86%	2e-63
5	Conserved Plasmodium protein, unknown function |CAD2096346.1|	*Plasmodium vinckei*	65.07%	2e-63

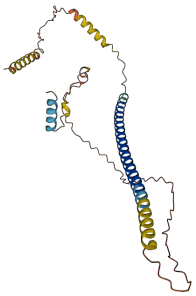

6

PBANKA_0931100

Rank	Protein Name / Accession	Organism	Identity (%)	E-value
1	Hypothetical protein YYC_04629 |ETB57820.1|	*Plasmodium yoelii 17X*	89.50%	1e-143
2	Conserved protein, unknown function |XP_022812238.1|	*Plasmodium yoelii*	89.04%	6e-143
3	Conserved Plasmodium protein, unknown function |CAD2091442.1|	*Plasmodium vinckei brucechwatti*	84.02%	1e-134
4	Conserved Plasmodium protein, unknown function |CAD2103857.1|	*Plasmodium vinckei*	82.19%	2e-131
5	Conserved Plasmodium protein, unknown function |SCM20899.1|	*Plasmodium chabaudi adami*	81.74%	3e-131

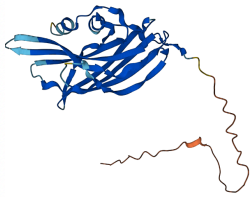

7

PBANKA_1034500

Rank	Protein Name / Accession	Organism	Identity (%)	E-value
1	Conserved Plasmodium protein, unknown function |CAD2093817.1|	Plasmodium vinckei brucechwatti	90.37%	0
2	Hypothetical protein YYG_00764	Plasmodium vinckei petteri	90.12%	0
3	Conserved Plasmodium protein, unknown function	Plasmodium vinckei	89.63%	0
4	Conserved Plasmodium protein, unknown function |XP_008624066.1|	Plasmodium vinckei vinckei	89.63%	0
5	Conserved protein, unknown function |XP_022813394.1|	Plasmodium yoelii	92.84%	0

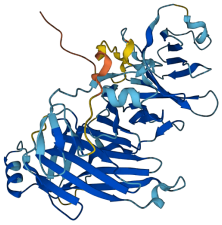

8

PBANKA_1233700

Rank	Protein Name / Accession	Organism	Identity (%)	E-value
1	Conserved protein, unknown function |XP_022812699.1|	*Plasmodium yoelii*	92.89%	8e-136
2	Conserved Plasmodium protein, unknown function |SCM25216.1|	*Plasmodium chabaudi chabaudi*	87.02%	6e-123
3	conserved protein, unknown function |XP_016654324.1|	*Plasmodium chabaudi chabaudi*	87.02%	2e-122
4	conserved Plasmodium protein, unknown function |SCN62337.1|	*Plasmodium chabaudi adami*	87.02%	2e-122
5	Conserved Plasmodium protein, unknown function |SCM23274.1|	*Plasmodium chabaudi adami*	87.02%	2e-122

9

PBANKA_0902700

Rank	**Protein Name / Accession**	**Organism**	**Identity (%)**	**E-value**
1	Conserved Plasmodium protein, unknown function |CXI39502.1|	*Plasmodium berghei*	99.28%	0
2	Conserved Plasmodium protein, unknown function |SCO60045.1|	*Plasmodium berghei*	98.23%	0
3	Conserved Plasmodium protein, unknown function |XP_022812111.1|	*Plasmodium yoelii*	80.50%	4e-123
4	Conserved Plasmodium protein, unknown function |CAD2105166.1|	*Plasmodium vinckei*	72.89%	2e-119
5	Conserved Plasmodium protein, unknown function |CAD2105257.1|	*Plasmodium vinckei petteri*	73.13%	3e-116

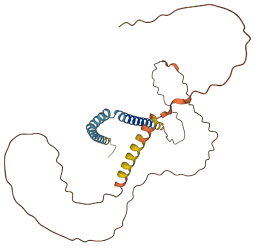

The uncharacterized proteins did not contain any predicted domains identifiable by InterProScan (InterPro), SMART (SMART Database), CDD (Conserved Domain Database) (NCBI CDD), SWISS-MODEL and HMMER, however AlphaFold 3 predicted a highly confident folded core structure in 3 uncharacterized proteins (Table 5.8.3). Interestingly, none of the uncharacterized proteins contained a signal peptide and transmembrane domain. Notably, 6 out of 9 uncharacterized proteins exhibited a high level of expression in the mosquito stages of the parasite and should be explored further to probe their role in motility and invasion (Table 5.8.2).

Notably, none of the experiments identified Circumsporozoite protein (CSP), the most abundant surface proteins on the surface of sporozoites, further indicating the specificity of the biotinylation by TRP1-APEX.

6. Discussion

6.1 TRP1 C-terminus plays a crucial role in salivary gland invasion and motility in sporozoite

Motility is a crucial aspect for *Plasmodium spp.* parasites to successfully complete its life cycle. *Plasmodium* undergoes a complex life cycle, traversing between a mosquito and a vertebrate host. To successfully complete its life cycle, sporozoites need to egress from the oocyst and eventually invade the salivary gland to be transmitted into a host. An assortment of proteins are involved in the parasite's journey from the mosquito to the host and amongst them the adhesins of the TRAP family (TRAP, TLP S6/TREP, CTRP) play crucial roles in effective motility and invasion of the parasite (Sultan et al. 1997; Frénal et al. 2017b; Combe et al. 2009; Beyer et al. 2021)

The N-terminus of the TRAP family adhesins interacts with the surface receptors while the C-terminus interact with the acto-myosin cytoskeleton present underneath the plasma membrane, which in turn generates the traction force needed for the parasite to propel forward (S. Kappe et al. 1999; Song et al. 2012; Klug et al. 2020; Braumann et al. 2023). The Thrombospondin related protein 1 (TRP1) plays an essential role in sporozoite's egress from the oocyst and in activating sporozoite motility within the oocyst, without perturbing their development (Klug and Frischknecht 2017; S. Kappe et al. 1999). A previous study on the deletion of the TRP1 C-terminus indicated a block in sporozoite egress from oocyst and no transmission of the disease to the host. However, my own work now showed that parasites lacking the C-terminus can readily exit from oocytes but are blocked in salivary gland invasion. The C-terminus of TRP1 is not very well conserved among its ortholog as it differs widely in the isoelectric points, overall charges and lengths (Fig. 5.1.2 A). To identify the key amino acid residues in the C-terminus important for salivary gland invasion, I generated a series of C-terminus deletion mutants entailing deletions of various lengths of the C-terminus along with re-characterization of the *trp1Δctd* and *trp1 ko* parasite lines lacking the C-terminus domain and the entire protein respectively.

Interestingly, in the complete absence of the C-terminus, sporozoites showed no difficulty in egressing from the oocyst contrary to what has been seen in previous studies (Klug and Frischknecht 2017). However, *trp1Δctd* sporozoites showed a strong defect in salivary gland invasion showing about 10x reduction in salivary gland sporozoite numbers compared to Wildtype sporozoites, indicating that the TRP1 C-terminus is crucial in salivary gland invasion. The discrepancy in the hemolymph sporozoite numbers observed in my studies compared to past studies, indicating sporozoite's ability to egress from the oocyst could have stemmed from relatively low infection rates in the mosquitoes in the past compared to present day in the lab. The *trp1Δctd* salivary gland sporozoites showed no productive motility in motility assays and the majority of sporozoites seemed to be just attached to the surface or floating, highlighting the importance of the C-terminus in productive motility and might also explain their inability to invade salivary glands in mosquitoes as observed in the cases of several mutants with disrupted motility (Sultan et al. 1997; Beyer et al. 2021; Loubens et al. 2023; Combe et al. 2009; A. Ghosh et al. 2024). TRAP C-terminus deletion mutant sporozoites showed strong invasion defects and were completely unable to exhibit any productive movements and were also unable to transmit disease to the host, similar to what was observed in *trp1Δctd* mutants (S. Kappe et al. 1999). However, disrupted motility does not always result in a defect in salivary gland invasion, resulting in an inability to draw direct correlation between motility defect and salivary gland invasion (Bane et al. 2016; Santos et al. 2017; Engelmann, Silvie, and Matuschewski 2009; Montagna et al. 2012).

Mice infected with *trp1Δctd* salivary gland sporozoites via natural transmission never got infected with malaria. This could be explained either by the presence of very few sporozoites in the salivary gland or by the severe motility defect seen in the absence of the C-terminus, further reinstating the importance of C-terminus in sporozoite motility, salivary gland invasion and transmission to the host. However, in all my experiments, the TRP1 C-terminus was found to not be essential for sporozoite egress from the oocyst. In contrast to this discrepancy with the previous work by Dennis Klug, I could confirm his finding that the *trp1 ko* sporozoites showed a strong defect in egress from the oocyst.

Consistently, none of the other C-terminus deletion mutants showed an egress defect. Interestingly, although only a very small percentage of the midgut sporozoites could make it to

the hemolymph, about 50% of those sporozoites were able to enter the salivary gland, contrary to the *trp1Δctd* parasite line where only about 10% hemolymph sporozoites could enter the salivary gland (Figure: 5.1.1. & Table 5.1.1). The salivary gland sporozoites however showed no movement in the motility assays as they seemed to be either attached to the surface or floating, reinstating the essential role of TRP1 in egress from the oocyst, salivary gland invasion, gliding motility and transmission to the host (S. Kappe et al. 1999).

6.2 Searching for motifs in the C-terminus of TRP1

The C-terminus of the TRAP family proteins are crucial in interacting with the acto-myosin motor present underneath the plasma membrane of the parasite and are well conserved among its orthologs (S. Kappe et al. 1999). The C-terminus of the TRAP family proteins show some common features, such as they are usually rich in acidic amino acids and consist of a tryptophan residue in the penultimate position at the C-terminus. The tryptophan residue has been shown to be crucial in the function of the protein (S. H. I. Kappe et al. 2004). In TRAP, the C-terminus plays a crucial role in salivary gland invasion, productive motility and transmission to host. Abrogation of the last 14 amino acids at the C-terminus already disrupts salivary gland invasion capacity of the sporozoites, however the hemolymph sporozoites are able to perform 'patch gliding' motility where they are able to move back and forth while being attached to a certain point on the surface. Whereas, deletion of the entire C-terminus results in no observable motility in the sporozoites that phenocopies the TRAP knockout sporozoites (S. Kappe et al. 1999).

TRP1 C-terminus domain does not share much similarity with TRAP and other TRAP family proteins, including the absence of a conserved tryptophan residue (Fig. 5.2.1 A). Despite the low conservation of the C-terminus, a conserved "KXD" amino acid motif was observed at the end of the C-terminus of *Plasmodium* species causing rodent malaria (Fig. 5.1.2 A & 6.2). Since lysine and aspartic acid residues are implicated in post-translational modifications, the final three amino acids were deleted in the *trp1Δ3* parasite line to investigate the role of lysine and aspartic acid residues in the overall function of the C-terminus (Z. A. Wang and Cole 2020; Yi et al. 2023). Despite this conservation, *trp1Δ3* sporozoites had no difficulty in egress from the oocyst or in the invasion of the salivary gland. Salivary gland sporozoites also showed no defects in their ability to move in in-vitro motility assays, indicating that the lysine and aspartic acid residues at the end

of C-terminus were not essential for the function of TRP1 and might explain the absence of the "KXD" amino acid motif in other *Plasmodium* species.

The *P. falciparum* ortholog of TRP1 has a significantly shorter tail with little similarity in amino acid sequence to *Pb*TRP1. I created the *trp1Δ19* mutant because its end closely resembles that of *Pf*TRP1, with the *trp1Δ19* C-terminus ending with "QNEKKY" whereas *Pf*TRP1 ends with a "QNKKKSY" (Fig. 6.2 A-B). Additionally, the *trp1Δ14* parasite line was designed with a C-terminus of intermediate length between those of TRP1Δ3 and TRP1Δ19.

A

B

Pftrp1 ctd	KWHIFKLLLHKQNKKKSY
Pbtrp1Δ19	KYKDICFQLREKNISQNEKKY

Fig. 6.2. A. Multiple sequence alignment of the C-terminus of *Pb*TRP1 with the CTDs of *Pf*TRP1, *Py*TRP1, *Pc*TRP1, *Pk*TRP1 and *Pv*TRP1 using Clustal Omega. **B.** Comparison of CTD sequence of *Pftrp1* and *Pbtrp1Δ19*

The *trp1Δ14* sporozoites exhibited a marked reduction in their ability to invade the salivary glands, despite showing no significant defects in oocyst egress. Notably, in in vitro motility assays, these salivary gland sporozoites displayed an unusual motility defect (Figure: 5.1.3.). Approximately 50% of the sporozoites demonstrated a distinctive pattern of movement where they attempted to glide but could not continue to do so as they struggled to maintain surface attachment. This resulted in a continuous flipping and waving motion during their attempts to glide—a previously undescribed motility pattern in sporozoites (J. P. Vanderberg 1974; Hegge et al. 2009). Due to its unique characteristics, this behavior was termed "waving-flipping," reflecting its combination of both movement types. To investigate if this motility defect and reduced salivary gland invasion rate in *trp1Δ14* sporozoites had an impact on disease transmission to the host, a natural transmission assay was performed. Although all mice showed positive infections, the natural transmission resulted in 1 day delay in prepatency in *trp1Δ14* infected mice compared to *wt* infected mice. Notably, one day delay is considered a 90%

reduction in infectivity (J. P. Vanderberg 1975). This suggests that the final 14 amino acids of the TRP1 C-terminus contain critical amino acid residues essential for sporozoite motility and salivary gland invasion. The observed delay in prepatency could be attributed either to the approximately 2.5-fold reduction in *trp1Δ14* sporozoites within the salivary glands compared to wild-type sporozoites, reducing their likelihood of being transmitted via mosquito bites, or due to their impaired ability to traverse the host skin due to motility defects. The "waving-flipping" motility in the *trp1Δ14* salivary gland sporozoites could stem from the inability of the sporozoites to maintain adequate surface attachment during motility assays. This defect could be caused by the disruption in the interaction of the C-terminus with the glideosome apparatus located beneath the plasma membrane due to the deletion of the last 14 amino acids. This disruption likely hinders the formation of secondary adhesion sites after initial surface attachment, a process critical for sustained productive motility (Hegge et al. 2010).

The impact of motility defects observed in *trp1Δ14* sporozoites may be more pronounced during salivary gland invasion than during host transmission. This distinction could arise from the difference in interaction surfaces: the salivary gland presents a largely 2D interface, whereas the host skin provides a more complex 3D environment. In a 3D setting, potential adhesion defects might be mitigated by increased surface contact, leading to a less pronounced effect on transmission. To investigate this hypothesis, *trp1Δ14* sporozoites could be assessed for motility in a 3D polyacrylamide gel (Ripp et al. 2021). However, a key challenge in this approach would be isolating the motility-deficient subpopulation, as the mutant also includes a fraction of normally gliding parasites, potentially complicating data interpretation.

Interestingly, the TRAP C-terminus domain mutant lacking the last 14 amino acids exhibited a similar defect in sporozoite motility although it shares very little homology with the TRP1 C-terminus, where the sporozoites were unable to glide and exhibited mostly a ‘patch gliding’ motility where the sporozoites were moving back and forth being attached to one focal point on the surface as did only the W mutants (S. Kappe et al. 1999; Buscaglia et al. 2003).This suggests that the TRP1 C-terminus end plays a role in transportation of TRAP to the back of the sporozoites and its release for continuous gliding, thus showcasing a mixture of ‘patch gliding’, ‘waving’ and ‘flipping’ motility in *trp1Δ14* sporozoites.

Interestingly, the *trp1Δ19* sporozoites showed no difficulty egressing the oocyst and invading the salivary gland despite encompassing a bigger deletion at the C-terminus than the *trp1Δ14*

parasite line. In vitro motility assays also indicated no significant defect in the ability to glide, even though a larger number of 'waving-flipping' sporozoites were observed in comparison to the *wt* sporozoites, majority of the sporozoites showed gliding motility. This phenotype could be attributed to the fact that the C-terminus of the TRP1Δ19 closely resembles that of *Pf*TRP1 in the amino acid constitution, indicating to the fact that the residual amino acids at the C-terminus of the TRP1Δ19 is enough for TRP1 function and that the "QNEKKY" motif might play a role in sporozoite motility and salivary gland invasion. Further experiments could investigate the importance of the "QNEKKY" motif by adding it at the end of TRP1Δ14 and checking whether it abrogates the defect in motility and salivary gland invasion observed in *trp1Δ14* sporozoites.

6.3 TRAP C-terminus can not restore the function of TRP1 C-terminus

Since contrary to previously published results (Klug et al. 2017), TRP1 not only shows a oocyst egress and salivary gland invasion phenotype but is also crucial for productive motility and thus not only shows structural but also closed functional similarity with TRAP, I wanted to investigate if the TRAP C-terminus can successfully complement the function of the TRP1 C-terminus. TRP1 is crucial for initiating movement in the midgut sporozoites whereas TRAP plays a crucial role in generating productive motility in sporozoites by interacting with the acto-myosin motor present underneath the plasma membrane of sporozoites with its C-terminus. However, how TRAP interacts with the actomyosin motor is not completely understood. The homolog of TRAP in *Toxoplasma gondii,* TgMIC2 is believed to link the parasite's actomyosin system by interacting with GAC (glideosome associated connector) through its cytoplasmic tail. GAC is highly conserved in apicomplexa and aids in linking F-actin with the surface adhesins of the parasite to ensure productive motility (Jacot et al. 2016). The TRAP family proteins including TRAP, share a characteristic feature of an C-terminus tail rich in acidic amino acids and a penultimate tryptophan residue that have been shown to be crucial in the function of TRAP (Morahan, Wang, and Coppel 2009).

TRP1 C-terminus does not share much homology with the TRAP C-terminus besides the small size, including the non acidic C-terminus and the lack of penultimate tryptophan residue suggesting that the two proteins might bind different adaptors. To address this hypothesis, I generated a mutant where the C-terminus of TRP1 was replaced with the TRAP C-terminus. As expected, and confirming my observation that the C-terminus is not important for oocyst egress,

the *Pbtrp1-Pbtrap ctd swap* sporozoites showed no difficulty in egressing the oocyst. However they had a strong defect in invading the salivary gland (Figure: 5.2.1.).

Curiously, *Pbtrp1-Pbtrap ctd swap* hemolymph sporozoites were more motile in comparison to *wt* sporozoites, yet salivary gland sporozoites showed significant defects as no gliding sporozoites were observed. The sporozoites that were able to move exhibited a strongly reduced "waving-flipping" kind of movement although most sporozoites just remained attached to the surface or floating. This is interesting, as though the hemolymph sporozoites did not show any significant defects in motility, they still had severe defects in invasion, further indicating the presence of several crucial factors other than motility, in salivary gland invasion as was also shown for mutants in actin (Douglas et al. 2018). These experiments reinstate the importance of TRP1 C-terminus in salivary gland invasion and gliding motility independent of the function of TRAP in the same.

In the natural transmission assay *Pbtrp-Pbtrap ctd swap* infected mice never became positive, indicating either the sporozoites are unable to cause an infection in the host because of the strong motility defect in salivary gland sporozoites and/or because of the presence of low numbers of sporozoites in the salivary gland in the first place. To investigate if the sporozoites can cause an infection if the route through host skin is bypassed, 1000 salivary gland sporozoites were injected intravenously, resulting in all mice getting positive, albeit with one day delay in prepatency. This partly confirms results by Dennis Klug, who showed that large numbers of midgut derived parasites lacking TRP1 could infect the liver (Klug and Frischknecht 2017).

Similar to *trp1Δ14*, *Pbtrp1-Pbtrap ctd swap* salivary gland sporozoites may also benefit from the 3D environment of the host skin, allowing them to successfully transmit the disease, albeit with some delay. This suggests that the severe defects observed in motility and salivary gland invasion could stem from the inability of *Pbtrp1-Pbtrap ctd swap* sporozoites to establish proper adhesion with surfaces. Thus, the TRP1 C-terminus may play a crucial role in facilitating the function of other sporozoite surface proteins involved in substrate attachment and receptor-ligand interactions like S6, TREP, UOS3, RON4 etc. (Mikolajczak et al. 2008; Steinbuechel and Matuschewski 2009; Combe et al. 2009; Kaiser et al. 2004). TRAP is essential for salivary gland invasion and gliding motility in sporozoites and in the absence of the protein, sporozoites cannot move productively anymore (Sultan et al. 1997) and only show a back-and-forth patch-gliding (Münter et al. 2009). TRAP C-terminus domain deletion mutant also shows similar defects in

motility and invasion, highlighting the crucial role of TRAP C-terminus in salivary gland invasion and motility (S. Kappe et al. 1999). Interestingly, *Pbtrp1-Pbtrap ctd swap* sporozoites also shows a similar phenotype that incidentally phenocopies the *trp1Δctd* sporozoites as well, clearly suggesting that the C-terminus of *Pb*TRAP cannot rescue the function of *Pb*TRP1 C-terminus.

This is intriguing as the *Pb*TRAP C-terminal domain can be functionally replaced, either fully or partially, by the C-terminal domains of TRAP family proteins such as TLP (expressed in salivary gland sporozoites) and CTRP (expressed in ookinetes), as well as MIC2, its homolog in *Toxoplasma gondii* (S. Kappe et al. 1999; Heiss et al. 2008). This demonstrates functional conservation despite limited amino acid sequence similarity among these proteins and highlights the possibility of a different functional pathway for modulating motility with TRP1 in salivary gland sporozoites This can be further reinstated by the lack of the conserved tryptophan residue in TRP1 C-terminus, that is known to play a crucial in sporozoite motility and salivary gland invasion in TRAP (S. H. I. Kappe et al. 2004). These findings underscore the importance of both TRP1 and TRAP in enabling effective salivary gland invasion and ensuring productive sporozoite motility. A good way to test this would be to generate a TRAP-TRP1 CTD swap mutant parasite line where the C-terminus domain of *Pb*TRAP is swapped with the C-terminus domain of *Pb*TRP1 to implore the effect on motility and invasion. Although, considering the importance of the penultimate tryptophan for TRAP this is unlikely to yield a functional TRAP.

Interestingly, *trp1 ko* midgut sporozoites showed comparable gliding ability as *wt* midgut sporozoites (Klug and Frischknecht 2017). This could indicate different modulation of motility in midgut sporozoites as salivary gland sporozoites were completely unable to move in *trp1 ko* mutants.

TRP1 C-terminus could potentially play a role in sporozoite motility by ensuring proper interaction of TRAP C-terminus with the acto-myosin complex present underneath the plasma membrane. Hence, disrupting the C-terminus of TRP1 might in turn disrupt the interaction between TRAP and actomyosin complex. Alternatively, TRP1 and TRAP may have mutually exclusive downstream interaction pathways through which they regulate salivary gland invasion and motility, however these pathways are not complementary or redundant as evident by characterizing the *Pbtrp1-Pbtrap ctd swap* parasite line.

6.4 *Pf*TRP1 C-terminus can successfully rescue the function of TRP1 C-terminus

The *PfTRP1* C-terminus is much shorter than the *Pb*TRP1 counterpart lacking the long alpha helical structure with not much similarity in the amino acid composition. Hence, to investigate if the *Pf*TRP1 C-terminus can rescue the function of *Pb*TRP1 I generated the *Pbtrp1-Pftrp1 ctd swap* parasite line. Interestingly, the *Pbtrp1-Pftrp1 ctd swap* sporozoites had no defect in egressing the oocyst and invading the salivary gland. Motility assays also show the majority of the salivary gland sporozoites were able to perform gliding motility. This parasite line phenocopies the *trp1Δ19* line, where the sporozoites also show no defect in its journey from the oocyst to the salivary gland despite missing 19 amino acids from the C-terminus. In both natural and i.v. transmission assays using the *Pbtrp1-Pftrp1 ctd swap* salivary gland sporozoites the mice showed no delay in prepatency.

This lack of disruption of TRP1 function could be attributed to the fact that the C-terminus in both *Pbtrp1-Pftrp1 ctd swap* and *trp1Δ19* parasite line bear resemblance in their distal end entailing the "QNXKKXY" or "QNXKKY" motif that is enough for the proper function of TRP1 (Fig. 6.2 B). This motif might play a crucial role in recruitment of other interaction partners at the C-terminus domain, thus explaining the inability of *trp1Δ14* sporozoites to invade salivary glands and move productively. Although, it could not be explained why deleting the last three amino acids containing two lysines at the end of the C-terminus did not cause any perturbation in the function of the protein as observed in *trp1Δ3* sporozoites.

6.5 TRP1 can be tagged functionally upstream of the C-terminus domain with GFP

All the previous attempts at tagging TRP1 and obtaining a functional fusion protein in the parasite have been futile as regardless of tagging at the N or the C-terminus of TRP1 disrupted its function. Interestingly, tagging at different termini of the protein resulted in completely different localization in the oocyst and sporozoites. Most notably in the *trp1-gfp* parasite line the parasite showed a unique localization on the oocyst wall and a periphery of the sporozoites (Klug and Frischknecht 2017). However, since the *trp1-gfp* sporozoites were unable to egress the oocysts and complete its life cycle, the proper localization of TRP1 in the parasite could not be determined.

In a new attempt to tag TRAP with GFP I generated the *trp1-gfp-tsr* and *trp1-tmd-gfp* parasite lines where TRP1 was tagged with GFP either upstream (N-terminal) of the TSR domain or downstream (C-terminal) of the transmembrane domain. The *trp1-tmd-gfp* parasite line was designed to keep the C-terminus free to interact with its native interaction partners without perturbing the structure of the protein. This resulted in a GFP tagged parasite line that had no difficulty in completing its life cycle through the mosquito tissues, as indicated by the number of the sporozoites in the hemolymph and the salivary gland (Fig: 5.4.1.). The salivary gland sporozoites also showed no defect in its motility, as comparable numbers of gliding sporozoites were noted as the *wt* parasites (Fig: 5.4.5.).

Interestingly, *trp1-tmd-gfp* parasites showed a completely different localization compared to the previously generated *trp1-gfp* parasites. No signal could be observed in the oocyst wall as observed previously, instead an intrinsic signal could be noted corresponding to a probable ER localization in the oocyst. Whereas, a very peculiar localization was observed in the *trp1-tmd-gfp* sporozoites, where the GFP signal seemed to be distributed in a "patchy" localization either throughout the sporozoites or on the periphery of the sporozoites (Fig: 5.4.3). Curiously, the "patchy" localization has not been described in any other protein in the sporozoites before and seems to be unique for every sporozoite, with a common localization point in the apical end, surrounding the nucleus and at the posterior end of the parasites, while occasionally localizing at the periphery of sporozoites, making it difficult to deduce the actual localization of the protein. To get a better understanding about the TRP1 localization, immunofluorescence assay with an anti GFP antibody was performed on salivary gland sporozoites with or without the presence of triton X-100, i.e. with and without lysing the plasma membrane (Fig: 5.4.4). Using this assay GFP signal was only observed in permeabilized sporozoites, suggesting that the C-terminus of TRP1 is indeed present intracellularly.

Interestingly, and despite the individually highly variable signals, the GFP localization did not seem to be dynamic in the gliding sporozoites, suggesting that the protein is not freely diffusible in the moving parasite but located at a fixed structure (Fig: 5.4.5.A). This could indicate that TRP1 could be a part of a stable structural element at the periphery of the sporozoites, e.g. the inner membrane complex.

TRP1 contains a potential micronemal sorting sequence F/Y/WXXΦ (Φ; hydrophobic amino acid) at the cytoplasmic site of the TMD suggesting its probable localization in the micronemes

and was also detected in the sporozoite surface proteome (Lindner et al. 2013; Di Cristina et al. 2000). However, from the live imaging and IFA on the *trp1-tmd-gfp* salivary gland sporozoites, we could not be sure whether it truly localizes in the micronemal vesicles or not as the signal was much weaker than the signals observed in other microneme secreted proteins like TRAP (S. Kappe et al. 1999). Salivary gland sporozoites harbour a large number of micronemes at the apical end of the parasite as the microneme secreted proteins are crucial for gliding motility, rhoptry discharge and invasion of the host cells (Valleau et al. 2023). Hence the signal of micronemal proteins in the salivary gland sporozoites is expected to be more abundant. The GFP signal observed at the apical end of the *trp1-tmd-gfp* salivary gland sporozoites might stem from the localization at the IMC close to the apical pole, however further experiments are required to confirm this speculation.

6.6 TRP1 cannot be tagged at the TSR domain with GFP

In order to decipher the fate of the TRP1 N-terminus, several attempts were made to successfully tag the protein with GFP at the N-terminus. Interestingly, the GFP signal was not observed in the *gfp-trp1* parasite line even though the *gfp::trp1* transcript could be detected, indicating the possibility of heavy post translational processing at the N-terminus (Klug and Frischknecht 2017).

The *trp1-gfp-tsr* parasite line was generated with the intention of understanding the role of the TSR domain and the N terminus in the function of TRP1 as the GFP tag was placed directly upstream of the TSR domain. Upon development in the oocyst, the *trp1-gfp-tsr* sporozoites had no difficulty egressing from it, however were significantly disrupted from invading the salivary glands (Fig: 5.4.1.). This stark defect in salivary gland invasion might be explained by the GFP tag disrupting the proper folding of the N-terminus or the adjacent TSR domain, N-terminal processing or sterically hindering the interaction partners from binding at these domains, highlighting the importance of the N-terminus in the function of TRP1. Both the N-terminus and the TSR domain are predicted to be inside the lumen of ER and micronemes and after secretion to the plasma membrane on the extracellular side (TMMH prediction) and might be playing an important role in interacting with surface proteins on the salivary gland that regulates invasion.

Curiously, although weak, a GFP signal was observed in the *trp1-gfp-tsr* parasite line. In the oocyst, the signal seemed different from the *trp1-tmd-gfp* parasite line, localizing mostly on only

one half of the sporozoites. However in the isolated midgut sporozoites, the signal seemed to be only coming from the periphery. It should be noted that since the *trp1-gfp-tsr* parasite line was not functional as the sporozoites were unable to invade the salivary gland, hence the GFP localization we see might be an artifact or represent the localization of the N-terminus after some processing event. As the signal of the TRP1-TMD-GFP is much stronger in comparison, this seems likely and the GFP signal of *trp1-gfp-tsr* might represent parts of the protein that are about to be degraded or secreted into the supernatant.

6.7 TRP1 could not be tagged at the N-terminus without perturbing its function

Since the *trp1-gfp-tsr* parasite line indicated the importance of the unperturbed N-terminus and the TSR domain for the proper function of TRP1, *trp1-flag10-gfp* and *trp1-flag20-gfp* parasite lines were generated were a 3X FLAG tag was inserted 10 and 20 amino acids upstream of the TSR domain in the already existing *trp1-tmd-gfp* parasite line, since it can be functionally tagged upstream of the C-terminus. This way the *trp1-flag10-gfp* and *trp1-flag20-gfp* parasite lines were expected to yield a dual reporter line for the N and the C-terminus of TRP1 to dissect when TRP1 is cleaved..

Although the *trp1-flag10-gfp* sporozoites were completely disrupted in their salivary gland invasion capacity, the *trp1-flag20-gfp* sporozoites could somewhat enter the salivary gland, albeit in a reduced number. This indicates the importance of the TSR domain and the surrounding N-terminus region. Although FLAG tag is a small epitope tag and not expected to disrupt the structure of the protein at the N-terminus, close proximity to the TSR domain significantly disrupts the sporozoite's ability to invade the salivary gland, highlighting the role of TSR domain in salivary gland invasion.

Since *trp1-flag20-gfp* sporozoites could invade the salivary gland although in a reduced number, the localization of the FLAG tag along with the GFP tag in the sporozoites was expected to help us understand the fate of the N-terminus along with the TSR domain. In previous studies, TRP1 was shown to be processed heavily post translationally in the region between TSR and TMD. Probing for FLAG and GFP in the *trp1-flag20-gfp* sporozoites could shed light on this processing event.

Immunofluorescence assays were performed on the *trp1-flag20-gfp* salivary gland sporozoites for understanding the localization of FLAG and GFP with or without the presence of Triton X-100 and it highlighted the same localization for GFP in the sporozoites, indicating that the FLAG tag at the N-terminus does not interfere with the localization at the C-terminus. However the FLAG tag signal was only visible in permeabilized sporozoites and did not co-localize with the GFP signal, as the signal was very faint and seemed to be uniformly diffused throughout the sporozoite cytosol. This was unusual since the FLAG tag is expected to be extracellularly located on the sporozoites surface and should be detectable without permeabilizing the parasite. This observation could stem from the possibility that the N-terminus region is heavily processed in TRP1 and hence that part of the protein is lost. This would also explain the absence of the GFP signal in the *gfp-trp1* sporozoites. The most likely explanation is that the FLAG tag is inside secretory vesicles and ER as the GFP signal is also present mainly at those structures and not at the periphery. The N-terminus of TRP1 shows very little conservation among its homologs, which might support the possibility of heavy processing at the N-terminus end. However, I could not resolve how the TRP1 N-terminus plays a role in sporozoite invasion in the salivary gland and warrants further experiments.

6.8 TRP1 TSR domain plays a crucial role in salivary gland invasion and motility in sporozoite

The *trp1-gfp-tsr, trp1-flag20-gfp and trp1-flag10-gfp* parasite lines indicated the importance of the TSR domain in the function of TRP1 as any attempts of tagging the TSR domain disrupted the function of the protein. The TSR domain is a highly conserved domain present in eukaryotes and is known to play an important role in protein-protein interaction and proper folding and trafficking of proteins (Bentley and Adams 2010; Neubauer et al. 2017). The TSR domain entails a conserved consensus motif ‘WxxWxxC’, where the tryptophans are crucial as they serve as the site for glycosylation, specifically C-mannosylation of the TSR domain, an event that is known to be crucial for several functions of the domain. The TSR domain is an important feature in several proteins involved in the invasive stages of *Plasmodium sp.*. In the sporozoite stage, the TSR domain can be found in members of the TRAP family proteins such as TRAP, TLP and

TREP, TRAP related proteins such as TRP1, SSP3 and TRSP, and other proteins such as CSP and SPATR. Although abundantly present, the TSR domain exhibits a range of functions in these proteins (Matuschewski et al. 2002; Tewari et al. 2002; Ramakrishnan et al. 2011; Lopaticki et al. 2022; Klug et al. 2020).

In CSP, the perturbation on the TSR domain resulted in disruption of the parasite life cycle as the sporozoites were unable to egress from the oocyst (Tewari et al. 2002). Whereas in TRAP, we see conflicting data on the importance of the TSR domain. As observed in one report where the mutation of the conserved tryptophans in *Pb*TRAP resulted in reduced salivary gland invasion and gliding motility, whereas in an unpublished data from Dennis Klug, the deletion of the entire TSR domain in *Pb*TRAP resulted in no defect in motility and invasion whatsoever (Matuschewski et al. 2002; Lopaticki et al. 2022). It was also shown that the lack of O-fucosylation in the TSR domain of *Pf*TRAP resulted in disruption of trafficking in salivary gland sporozoites and reduced infectivity of the host (Lopaticki et al. 2017). Whereas, in CTRP, a protein crucial for ookinete invasion in the mosquito midgut, deletion of 7 TSR domains did not result in any disruption of the parasite life cycle, indicating a wide and diverse range of function of the domain (Ramakrishnan et al. 2011).

To explore the role of the TSR domain in TRP1 function, several mutations were introduced: *trp1Δtsr*, *trp1-tsr-point*, and *trp1-tsr-swap* parasite lines, in which the entire TSR domain was deleted, the conserved tryptophan residues were mutated to alanines, or the TSR domain was replaced with that of *Pb*TRAP, respectively.

As expected, TSR domain mutant sporozoites displayed no defects in development or mosquito infection rates, given that TRP1 is expressed in late oocysts and sporozoites. While the mutants showed no impairment in oocyst egress, they exhibited a severe defect in salivary gland invasion. Hemolymph and salivary gland sporozoites also demonstrated significant motility impairments, with most sporozoites remaining attached to the surface with minimal movement. These defects resulted in a complete block of disease transmission via natural mosquito bite. However, when the skin barrier was bypassed, mutant sporozoites successfully infected the host, albeit with an average two-day delay in prepatency. This underscores the TSR domain's critical role in TRP1 function, particularly in salivary gland invasion, sporozoite motility, and malaria transmission.

In *trp1-tsr-point* mutants, altering just two amino acids was sufficient to completely disrupt salivary gland invasion, mirroring the *trp1Δtsr* phenotype. Bioinformatic analyses suggest that these mutations do not destabilize the overall protein structure, indicating that the observed defects are unlikely to result from TRP1 or TSR misfolding. The motility impairments observed in hemolymph and salivary gland sporozoites further highlight the conserved tryptophan residues as key determinants of TSR domain function. However, further studies are needed to confirm potential post-translational modifications, particularly C-mannosylation of the TSR domain's tryptophan residues, which could not be investigated due to time constraints.

The motility defects observed in TRP1-TSR domain mutants during in vitro motility assays suggest impaired adhesion of sporozoites to the substrate. In all three mutants, the majority of salivary gland sporozoites exhibited no productive motility, and hemolymph sporozoites similarly failed to move effectively. Only a few gliding salivary gland sporozoites were observed in the *trp1-tsr-swap* mutants. Given that TSR domain disruption leads to motility defects, this suggests a potential role for the TSR domain in binding to yet unknown salivary gland ligands critical for invasion and furthermore, in providing sufficient adhesion to support gliding motility. Further studies on traction force generated by the TSR-domain mutant sporozoites could shed more light on the nature of adhesion defects.

Similar to *trp1Δctd* mutants, TSR domain mutant sporozoites are unable to be transmitted naturally through mosquito bites but can still establish infection when bypassing the skin barrier. This implies that, once inside the host, defects in TSR domain mediated adhesion may no longer significantly hinder hepatocyte invasion. However, it is also possible that the transmission block results from the low number of sporozoites successfully reaching the salivary gland.

Interestingly, despite the conserved nature of the TSR domain, the *Pb*TRAP TSR domain failed to compensate for the loss of the TRP1 TSR domain in salivary gland invasion, motility, and transmission. This suggests that the TSR domains of TRP1 and TRAP interact with distinct partners, reflecting their roles at different stages of the parasite's life cycle. It is likely that the TRP1 TSR domain plays a more critical role in salivary gland invasion and motility, while the TRAP TSR domain is essential for hepatocyte invasion. This aligns with unpublished findings from Dennis Klug's work on TRAP TSR deletion mutants, which demonstrated no defects in

sporozoite motility, invasion, or transmission, further supporting the idea of divergent TSR domain functions in TRP1 and TRAP.

It is important to consider that the phenotypes observed in the TSR domain mutants may not solely result from TSR domain disruption but could also be influenced by alterations in the adjacent N-terminal domain. To investigate this, generating a functional tag at the N-terminus, proximal to the TSR domain, would be crucial for elucidating the molecular mechanisms through which the N-terminus and/or TSR domain contribute to salivary gland invasion, sporozoite motility, and transmission. Additionally, a functional tag would enable proximity-dependent biotinylation assays at the N-terminus of TRP1, providing insights into potential interaction partners.

6.9 Identification of TRP1 C-terminus interaction partner proteins

In order to identify the interaction partners of the TRP1 C-terminus, APEX2 based proximity biotinylation assay was performed on *trp1-apex* salivary gland sporozoites. Through three independent MS experiments, we identified 307 unique proteins, categorized into three classes. "Class I**"** comprised proteins exclusively detected during biotinylation in the presence of hydrogen peroxide in *trp1-apex* sporozoites across all three experiments. "Class II" included proteins identified under the same conditions but in at least one experiment. "Class III" encompassed proteins found not only in the test cohort (*trp1-apex* sporozoites treated with hydrogen peroxide) but also in the control group, where *trp1-apex* sporozoites were either untreated or detected in wild-type (*wt*) sporozoites exposed to hydrogen peroxide.

Out of 307 proteins detected, 27 proteins were classified as "Class I" proteins, 52 proteins classified as "Class II" proteins and 164 proteins were classified as "Class III" proteins.

Interestingly, Class I proteins exhibit crucial cytoskeleton and glideosomal complex associated proteins like actin II (PBANKA_1030100), actin-depolymerizing factor 1 (PBANKA_1103100) and putative glideosome associated protein with multiple membrane spans 2 (PBANKA_0523900). Microneme resident crucial protein involved in transmission and cell traversal, CelTOS (PBANKA_1432300) was also identified. Crucial proteins that are known to be important in other stages of the parasite but not explored in *P. berghei* mosquito stages, e.g. L-lactate dehydrogenase (PBANKA_1340100), receptor for activated c kinase

(PBANKA_0703900) and T-complex protein 1 subunits alpha (PBANKA_0916200), beta (PBANKA_0405200), theta (PBANKA_0310900), epsilon (PBANKA_1218200) were detected, indicating the importance of probing their roles in the mosquito stages of the parasite, especially as they show high expression levels in the mosquito stages of the parasite.

T-complex protein 1 (TCP-1), also known as the Chaperonin Containing TCP-1 (CCT) or TRiC, is a molecular chaperone complex essential for proper protein folding in eukaryotic cells. This complex is composed of eight distinct subunits, each approximately 60 kDa in size, arranged in two stacked rings to form a barrel-like structure (Kubota, Hynes, and Willison 1995). The primary function of the TCP-1/CCT complex is to assist in the folding of newly synthesized and

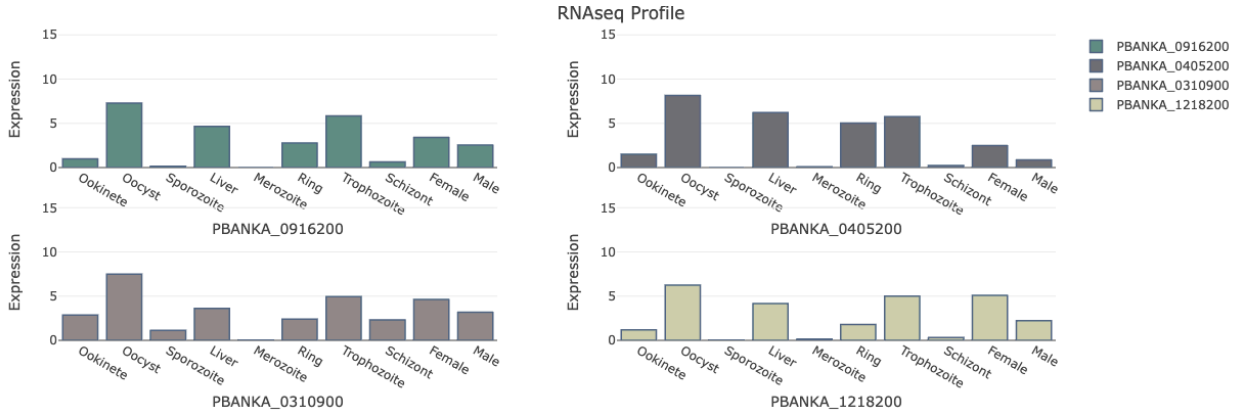

Fig: 6.9. Gene expression profiles of T-complex protein 1 subunits alpha (PBANKA_0916200), beta (PBANKA_0405200), theta (PBANKA_0310900), epsilon (PBANKA_1218200) across different stages of parasite life cycle.
Generated using SPOT (https://frischknechtlab.shinyapps.io/SPOT/) (Farr, Sattler, and Frischknecht 2021)

misfolded proteins, particularly cytoskeletal proteins such as actin and tubulin (Brackley and Grantham 2009). Interestingly, 7 out of 8 TCP-1 subunits were detected in the MS analysis, including four subunits classified as 'Class I' (Figure: 6.9.). Their high expression levels in the oocyst and liver stages of the parasite, along with the detection of actin II, actin-depolymerizing factor 1, and calmodulin in 'Class I' proteins, suggest a potential role for TRP1 in actin regulation in sporozoites.

Interestingly, polyadenylate-binding protein 1 (PBANKA_1439200), that has been shown to be localized on the surface of transmitted salivary gland sporozoites and to be deposited in trails when parasites glide on a substrate, was also identified in the 'Class I' proteins (Minns et al. 2018).

Although 'Class II' entails those proteins detected in the first cohort (*trp1-apex* sporozoites treated with biotin phenol and hydrogen peroxide) which only show up in one or two out of the three experiments, it exhibited interesting candidates, e.g. GAP40 (PBANKA_1115300), Coronin (PBANKA_1464100), Secreted ookinete protein (PBANKA_0619200), Gamete egress and sporozoite traversal protein (PBANKA_1312700) that are crucial in motility, invasion and transmission to host (Bane et al. 2016; Frénal et al. 2010; Tachibana et al. 2021; Talman et al. 2011).

Interestingly, 'Class III' proteins also exhibited many crucial proteins involved in sporozoite motility, salivary gland invasion and transmission to host, including 7 cytoskeletal or cytoskeleton associated proteins, 13 glideosome proteins 3 micronemal and 3 rhoptry proteins.

Notably, these MS results reveal mostly IMC associated or glideosome associated proteins, in contrast to expected micronemal proteins, as TRP1 contains a micronemal sorting sequence and is expected to localize in the micronemes from which it is supposed to be secreted on the surface of the sporozoite. Instead, all three classes mostly entailed crucial components of glideosomal apparatus, that could explain the observed perturbation of motility, salivary gland invasion and transmission to host, when the TRP1 C-terminus is disrupted.

This could indicate a different localization of TRP1 than we previously assumed. TRP1 could potentially be localized or docked on both sides of the IMC as it is a transmembrane domain containing protein, while on one side (proximal to the acto-myosin complex) its C-terminus faces the glideosomal apparatus and on the other side (proximal to the subpellicular network) its C-terminus faces the subpellicular network. This could explain why we observe IMC protein subunits, subpellicular microtubule proteins, tubulin alpha and beta chains, GAPMs, GAC, GAP40 while also observing proteins like actin I, actin II, myosin A, TRAP, TLP, coronin. IMC localization could also explain why TRP1-TMD-GFP localization in motile salivary gland sporozoites is non dynamic, as the protein might be part of a structural unit and don't diffuse readily. IMC localization could also explain the "patchy" localization we observed in *trp1-tmd-gfp* sporozoites, as TRP1 might be present at irregular intervals throughout the IMC,

while showing a predisposition for localization at the apical and posterior ends of the sporozoites. However, how TRP1 can be transported to the IMC is not clear. Also how a mutation in the TSR inhibits salivary gland entry would not be explained by this hypothesis.

TRP1 might contribute to sporozoite motility by supporting the function of TRAP-like protein (TLP), a TRAP family adhesin, by facilitating its interaction with actin filaments beneath the plasma membrane. TLP is specifically expressed in salivary gland sporozoites and plays a critical role in generating the optimal force required for gliding motility through its interaction with actin (Moreira et al. 2008; Ripp et al. 2024). TRP1 may help stabilize this interaction, ensuring efficient motility. This could explain why TRP1 mutants exhibit a milder phenotype in hemolymph sporozoites but show a more pronounced defect in salivary gland invasion and gliding motility. However, the motility phenotype of TRP1 mutants are more pronounced that of the TLP mutant. Notably, TLP was detected in the 'Class III' proteins identified by MS analysis.

Interestingly, coronin and actin depolymerising factor 1 (ADF) are also observed in the MS data within 'Class II' and 'Class I' respectively, which could explain the localization of TRP1 at the posterior end of the sporozoites, where coronin is also known to localize in moving sporozoites. Coronin is thought to coordinate actin assembly at the posterior end of the sporozoite, ensuring efficient force generation for continued movement (Bane et al. 2016). Coronin is known to interact with ADF/cofilin, enhancing actin depolymerization and turnover, which is crucial for rapid cytoskeletal remodeling (Schüler, Mueller, and Matuschewski 2005). Notably, calmodulin was also identified within the Class I proteins. Calmodulin is known to play a role in the regulation of coronin function, particularly in actin cytoskeleton dynamics. Coronin contains calmodulin-binding motifs, suggesting that its activity can be modulated by Ca^{2+}-calmodulin interactions. Since coronin is critical for actin-based gliding motility, calmodulin may regulate its function during host cell invasion and tissue traversal (Matsumoto et al. 1987; Yan et al. 2005). TRP1 C-terminus might play a role in modulating or stabilizing the interaction of coronin and ADF/cofilin with the actin filaments present underneath the plasma membrane of the sporozoites. Thus disrupting the TRP1 C-terminus would result in dysregulation of the actin dynamics and could hence explain the severe motility defect we observe in *Pbtrp1-Pbtrap ctd swap* and *trp1Δctd* sporozoites.

Parallaly, TRP1 might also play a role in modulating or stabilizing the interaction between the actin filaments and TRAP and might explain why we see the 'waving-flipping' defect in *trp1Δ14*

sporozoites. The *trp1Δ14* salivary gland sporozoites seem to exhibit a defect in forming secondary adhesion sites during in-vitro motility assays and hence constantly flip or wave in an attempt to move productively. This defect in motility is reminiscent of the defect we observe in *trapΔ14* salivary gland sporozoites. Whereas, both TRAP and TRP1 C-terminus deletion sporozoites don't show any productive motility at all. These results further indicate the possibility of an interaction between TRAP, TRP1 and the acto-myosin complex where TRP1 might play a role as a moderator of interaction between TRAP and the acto-myosin complex.

7. Bibliography

https://doi.org/10.1080/19420862.2023.2215364

Aguirre-Botero, Manuela C., Lawrence T. Wang, Pauline Formaglio, Eduardo Aliprandini, Jean-Michel Thiberge, Arne Schön, Yevel Flores-Garcia, et al. 2023. "Cytotoxicity of Human Antibodies Targeting the Circumsporozoite Protein Is Amplified by 3D Substrate and Correlates with Protection." *Cell Reports* 42 (7): 112681. https://doi.org/10.1016/j.celrep.2023.112681.

Aly, Ahmed S. I., and Kai Matuschewski. 2005. "A Malarial Cysteine Protease Is Necessary for Plasmodium Sporozoite Egress from Oocysts." *The Journal of Experimental Medicine* 202 (2): 225–30. https://doi.org/10.1084/jem.20050545.

Amino, Rogerio, Donatella Giovannini, Sabine Thiberge, Pascale Gueirard, Bertrand Boisson, Jean-François Dubremetz, Marie-Christine Prévost, Tomoko Ishino, Masao Yuda, and Robert Ménard. 2008. "Host Cell Traversal Is Important for Progression of the Malaria Parasite through the Dermis to the Liver." *Cell Host & Microbe* 3 (2): 88–96. https://doi.org/10.1016/j.chom.2007.12.007.

Amino, Rogerio, Sabine Thiberge, Béatrice Martin, Susanna Celli, Spencer Shorte, Friedrich Frischknecht, and Robert Ménard. 2006. "Quantitative Imaging of Plasmodium Transmission from Mosquito to Mammal." *Nature Medicine* 12 (2): 220–24. https://doi.org/10.1038/nm1350.

Andolina, Chiara, Wouter Graumans, Moussa Guelbeogo, Geert-Jan van Gemert, Jordache Ramijth, Soré Harouna, Zongo Soumanaba, et al. 2024. "Quantification of Sporozoite Expelling by Anopheles Mosquitoes Infected with Laboratory and Naturally Circulating P. Falciparum Gametocytes." *eLife* 12 (March):RP90989. https://doi.org/10.7554/eLife.90989.

Andrews, Mia, Jake Baum, Paul R. Gilson, and Danny W. Wilson. 2023. "Bottoms up! Malaria Parasite Invasion the Right Way Around." *Trends in Parasitology* 39 (12): 1004–13. https://doi.org/10.1016/j.pt.2023.09.010.

Bane, Kartik S., Simone Lepper, Jessica Kehrer, Julia M. Sattler, Mirko Singer, Miriam Reinig, Dennis Klug, et al. 2016. "The Actin Filament-Binding Protein Coronin Regulates Motility in Plasmodium Sporozoites." Edited by Rita Tewari. *PLOS Pathogens* 12 (7): e1005710. https://doi.org/10.1371/journal.ppat.1005710.

Bargieri, Daniel Y., Sabine Thiberge, Chwen L. Tay, Alison F. Carey, Alice Rantz, Florian Hischen, Audrey Lorthiois, et al. 2016. "Plasmodium Merozoite TRAP Family Protein Is Essential for Vacuole Membrane Disruption and Gamete Egress from Erythrocytes." *Cell Host & Microbe* 20 (5): 618–30. https://doi.org/10.1016/j.chom.2016.10.015.

Baum, Jake, Dave Richard, Julie Healer, Melanie Rug, Zita Krnajski, Tim-Wolf Gilberger, Judith L. Green, Anthony A. Holder, and Alan F. Cowman. 2006. "A Conserved Molecular Motor Drives Cell Invasion and Gliding Motility across Malaria Life Cycle Stages and Other Apicomplexan Parasites." *Journal of Biological Chemistry* 281 (8): 5197–5208. https://doi.org/10.1074/jbc.M509807200.

Bentley, A. A., and J. C. Adams. 2010. "The Evolution of Thrombospondins and Their Ligand-Binding Activities." *Molecular Biology and Evolution* 27 (9): 2187–97. https://doi.org/10.1093/molbev/msq107.

Bergman, Lawrence W., Karine Kaiser, Hisashi Fujioka, Isabelle Coppens, Thomas M. Daly, Sarah Fox, Kai Matuschewski, Victor Nussenzweig, and Stefan H. I. Kappe. 2003. "Myosin A Tail Domain Interacting Protein (MTIP) Localizes to the Inner Membrane Complex of Plasmodium Sporozoites." *Journal of Cell Science* 116 (Pt 1): 39–49. https://doi.org/10.1242/jcs.00194.

Beyer, Konrad, Simon Kracht, Jessica Kehrer, Mirko Singer, Dennis Klug, and Friedrich Frischknecht. 2021. "Limited Plasmodium Sporozoite Gliding Motility in the Absence of TRAP Family Adhesins." *Malaria Journal* 20 (1): 430. https://doi.org/10.1186/s12936-021-03960-3.

Bhanot, Purnima, Ute Frevert, Victor Nussenzweig, and Cathrine Persson. 2003. "Defective Sorting of the Thrombospondin-Related Anonymous Protein (TRAP) Inhibits Plasmodium Infectivity." *Molecular and Biochemical Parasitology* 126 (2): 263–73. https://doi.org/10.1016/s0166-6851(02)00295-5.

Billker, O., V. Lindo, M. Panico, A. E. Etienne, T. Paxton, A. Dell, M. Rogers, R. E. Sinden, and H. R. Morris. 1998. "Identification of Xanthurenic Acid as the Putative Inducer of Malaria Development in the Mosquito." *Nature* 392 (6673): 289–92. https://doi.org/10.1038/32667.

Blanpain, Cédric, and Elaine Fuchs. 2014. "Stem Cell Plasticity. Plasticity of Epithelial Stem Cells in Tissue Regeneration." *Science (New York, N.Y.)* 344 (6189): 1242281. https://doi.org/10.1126/science.1242281.

Borner, Janus, Christian Pick, Jenny Thiede, Olatunji Matthew Kolawole, Manchang Tanyi Kingsley, Jana Schulze, Veronika M. Cottontail, et al. 2016. "Phylogeny of Haemosporidian Blood Parasites Revealed by a Multi-Gene Approach." *Molecular Phylogenetics and Evolution* 94 (Pt A): 221–31. https://doi.org/10.1016/j.ympev.2015.09.003.

Bosch, Jürgen, Matthew H. Paige, Akhil B. Vaidya, Lawrence W. Bergman, and Wim G. J. Hol. 2012. "Crystal Structure of GAP50, the Anchor of the Invasion Machinery in the Inner Membrane Complex of Plasmodium Falciparum." *Journal of Structural Biology* 178 (1): 61–73. https://doi.org/10.1016/j.jsb.2012.02.009.

Brackley, Karen I., and Julie Grantham. 2009. "Activities of the Chaperonin Containing TCP-1 (CCT): Implications for Cell Cycle Progression and Cytoskeletal Organisation." *Cell Stress & Chaperones* 14 (1): 23–31. https://doi.org/10.1007/s12192-008-0057-x.

Braumann, Friedrich, Dennis Klug, Jessica Kehrer, Gaojie Song, Juan Feng, Timothy A Springer, and Friedrich Frischknecht. 2023. "Conformational Change of *Plasmodium* TRAP Is Essential for Sporozoite Migration and Transmission." *EMBO Reports* 24 (7): e57064. https://doi.org/10.15252/embr.202357064.

Bulloch, Michaela S., Long K. Huynh, Kit Kennedy, Julie E. Ralton, Malcolm J. McConville, and Stuart A. Ralph. 2024. "Apicoplast-Derived Isoprenoids Are Essential for Biosynthesis of GPI Protein Anchors, and Consequently for Egress and Invasion in Plasmodium Falciparum." *PLoS Pathogens* 20 (9): e1012484. https://doi.org/10.1371/journal.ppat.1012484.

Buscaglia, Carlos A., Isabelle Coppens, Wim G. J. Hol, and Victor Nussenzweig. 2003. "Sites of Interaction between Aldolase and Thrombospondin-Related Anonymous Protein in *Plasmodium*." *Molecular Biology of the Cell* 14 (12): 4947–57. https://doi.org/10.1091/mbc.e03-06-0355.

Claser, Carla, J. Brian De Souza, Samuel G. Thorburn, Georges Emile Grau, Eleanor M. Riley,

Laurent Rénia, and Julius C. R. Hafalla. 2017. “Host Resistance to Plasmodium-Induced Acute Immune Pathology Is Regulated by Interleukin-10 Receptor Signaling.” *Infection and Immunity* 85 (6): e00941-16. https://doi.org/10.1128/IAI.00941-16.

Combe, Audrey, Cristina Moreira, Susan Ackerman, Sabine Thiberge, Thomas J. Templeton, and Robert Ménard. 2009. “TREP, a Novel Protein Necessary for Gliding Motility of the Malaria Sporozoite.” *International Journal for Parasitology* 39 (4): 489–96. https://doi.org/10.1016/j.ijpara.2008.10.004.

Cova, Marta Mendonça, Mauld H. Lamarque, and Maryse Lebrun. 2022. “How Apicomplexa Parasites Secrete and Build Their Invasion Machinery.” *Annual Review of Microbiology* 76 (September):619–40. https://doi.org/10.1146/annurev-micro-041320-021425.

Cowman, Alan F., Christopher J. Tonkin, Wai-Hong Tham, and Manoj T. Duraisingh. 2017. “The Molecular Basis of Erythrocyte Invasion by Malaria Parasites.” *Cell Host & Microbe* 22 (2): 232–45. https://doi.org/10.1016/j.chom.2017.07.003.

Cui, Liwang, Sungano Mharakurwa, Daouda Ndiaye, Pradipsinh K. Rathod, and Philip J. Rosenthal. 2015. “Antimalarial Drug Resistance: Literature Review and Activities and Findings of the ICEMR Network.” *The American Journal of Tropical Medicine and Hygiene* 93 (3 Suppl): 57–68. https://doi.org/10.4269/ajtmh.15-0007.

Datoo, Mehreen S., Alassane Dicko, Halidou Tinto, Jean-Bosco Ouédraogo, Mainga Hamaluba, Ally Olotu, Emma Beaumont, et al. 2024. “Safety and Efficacy of Malaria Vaccine Candidate R21/Matrix-M in African Children: A Multicentre, Double-Blind, Randomised, Phase 3 Trial.” *Lancet (London, England)* 403 (10426): 533–44. https://doi.org/10.1016/S0140-6736(23)02511-4.

Defo, E. T., A. T. Tsapi, M. Fossi, B. D. Dongho, G. Nguefack-Tsague, E. M. Zogning, D. F. Achu, et al. 2021. “MosquirixTM Malaria Vaccine: An Evaluation of Patients’ Willingness to Pay in Cameroon.” *Igiene E Sanita Pubblica* 77 (2): 459–73.

Dembélé, Laurent, Jean-François Franetich, Audrey Lorthiois, Audrey Gego, Anne-Marie Zeeman, Clemens H. M. Kocken, Roger Le Grand, et al. 2014. “Persistence and Activation of Malaria Hypnozoites in Long-Term Primary Hepatocyte Cultures.” *Nature Medicine* 20 (3): 307–12. https://doi.org/10.1038/nm.3461.

Dessens, J. T., A. L. Beetsma, G. Dimopoulos, K. Wengelnik, A. Crisanti, F. C. Kafatos, and R. E. Sinden. 1999. “CTRP Is Essential for Mosquito Infection by Malaria Ookinetes.” *The EMBO Journal* 18 (22): 6221–27. https://doi.org/10.1093/emboj/18.22.6221.

Di Cristina, M., R. Spaccapelo, D. Soldati, F. Bistoni, and A. Crisanti. 2000. “Two Conserved Amino Acid Motifs Mediate Protein Targeting to the Micronemes of the Apicomplexan Parasite Toxoplasma Gondii.” *Molecular and Cellular Biology* 20 (19): 7332–41. https://doi.org/10.1128/MCB.20.19.7332-7341.2000.

Dos Santos Pacheco, Nicolas, Lorenzo Brusini, Romuald Haase, Nicolò Tosetti, Bohumil Maco, Mathieu Brochet, Oscar Vadas, and Dominique Soldati-Favre. 2022. “Conoid Extrusion Regulates Glideosome Assembly to Control Motility and Invasion in Apicomplexa.” *Nature Microbiology* 7 (11): 1777–90. https://doi.org/10.1038/s41564-022-01212-x.

Douglas, Ross G., Robert W. Moon, and Friedrich Frischknecht. 2024. “Cytoskeleton Organization in Formation and Motility of Apicomplexan Parasites.” *Annual Review of Microbiology*, August. https://doi.org/10.1146/annurev-micro-041222-011539.

Douglas, Ross G., Prajwal Nandekar, Julia-Elisabeth Aktories, Hirdesh Kumar, Rebekka Weber, Julia M. Sattler, Mirko Singer, et al. 2018. “Inter-Subunit Interactions Drive Divergent Dynamics in Mammalian and Plasmodium Actin Filaments.” Edited by Laura Machesky.

PLOS Biology 16 (7): e2005345. https://doi.org/10.1371/journal.pbio.2005345.
Dvorak, J. A., L. H. Miller, W. C. Whitehouse, and T. Shiroishi. 1975. "Invasion of Erythrocytes by Malaria Merozoites." *Science (New York, N.Y.)* 187 (4178): 748–50. https://doi.org/10.1126/science.803712.
El-Assaad, Fatima, Julie Wheway, Andrew John Mitchell, Jinning Lou, Nicholas Henry Hunt, Valery Combes, and Georges Emile Raymond Grau. 2013. "Cytoadherence of Plasmodium Berghei-Infected Red Blood Cells to Murine Brain and Lung Microvascular Endothelial Cells *In Vitro*." Edited by J. H. Adams. *Infection and Immunity* 81 (11): 3984–91. https://doi.org/10.1128/IAI.00428-13.
Engelmann, Sabine, Olivier Silvie, and Kai Matuschewski. 2009. "Disruption of Plasmodium Sporozoite Transmission by Depletion of Sporozoite Invasion-Associated Protein 1." *Eukaryotic Cell* 8 (4): 640–48. https://doi.org/10.1128/EC.00347-08.
Farr, Elias B, Julia M Sattler, and Friedrich Frischknecht. 2021. "SPOT: A Web-Tool Enabling Swift Profiling of Transcriptomes." Edited by Jan Gorodkin. *Bioinformatics* 38 (1): 284–85. https://doi.org/10.1093/bioinformatics/btab541.
Fernandes, Priyanka, Manon Loubens, Rémi Le Borgne, Carine Marinach, Béatrice Ardin, Sylvie Briquet, Laetitia Vincensini, et al. 2022. "The AMA1-RON Complex Drives Plasmodium Sporozoite Invasion in the Mosquito and Mammalian Hosts." *PLoS Pathogens* 18 (6): e1010643. https://doi.org/10.1371/journal.ppat.1010643.
Ferreira, Josie Liane, Dorothee Heincke, Jan Stephan Wichers, Benjamin Liffner, Danny W. Wilson, and Tim-Wolf Gilberger. 2021. "The Dynamic Roles of the Inner Membrane Complex in the Multiple Stages of the Malaria Parasite." *Frontiers in Cellular and Infection Microbiology* 10 (January):611801. https://doi.org/10.3389/fcimb.2020.611801.
Filali-Mouncef, Yasmina, Alexandre Leytens, Prado Vargas Duarte, Mattia Zampieri, Jörn Dengjel, and Fulvio Reggiori. 2024. "An APEX2-Based Proximity-Dependent Biotinylation Assay with Temporal Specificity to Study Protein Interactions during Autophagy in the Yeast Saccharomyces Cerevisiae." *Autophagy* 20 (10): 2323–37. https://doi.org/10.1080/15548627.2024.2366749.
Franke-Fayard, Blandine, Chris J. Janse, Margarida Cunha-Rodrigues, Jai Ramesar, Philippe Büscher, Ivo Que, Clemens Löwik, et al. 2005. "Murine Malaria Parasite Sequestration: CD36 Is the Major Receptor, but Cerebral Pathology Is Unlinked to Sequestration." *Proceedings of the National Academy of Sciences of the United States of America* 102 (32): 11468–73. https://doi.org/10.1073/pnas.0503386102.
Frénal, Karine, Jean-François Dubremetz, Maryse Lebrun, and Dominique Soldati-Favre. 2017a. "Gliding Motility Powers Invasion and Egress in Apicomplexa." *Nature Reviews Microbiology* 15 (11): 645–60. https://doi.org/10.1038/nrmicro.2017.86.
———. 2017b. "Gliding Motility Powers Invasion and Egress in Apicomplexa." *Nature Reviews Microbiology* 15 (11): 645–60. https://doi.org/10.1038/nrmicro.2017.86.
Frénal, Karine, Valérie Polonais, Jean-Baptiste Marq, Rolf Stratmann, Julien Limenitakis, and Dominique Soldati-Favre. 2010. "Functional Dissection of the Apicomplexan Glideosome Molecular Architecture." *Cell Host & Microbe* 8 (4): 343–57. https://doi.org/10.1016/j.chom.2010.09.002.
Frischknecht, Friedrich, Patricia Baldacci, Béatrice Martin, Christophe Zimmer, Sabine Thiberge, Jean-Christophe Olivo-Marin, Spencer L. Shorte, and Robert Ménard. 2004. "Imaging Movement of Malaria Parasites during Transmission by Anopheles Mosquitoes." *Cellular Microbiology* 6 (7): 687–94.

https://doi.org/10.1111/j.1462-5822.2004.00395.x.
Frischknecht, Friedrich, and Kai Matuschewski. 2017. “Plasmodium Sporozoite Biology.” *Cold Spring Harbor Perspectives in Medicine* 7 (5): a025478. https://doi.org/10.1101/cshperspect.a025478.
Gaskins, Elizabeth, Stacey Gilk, Nicolette DeVore, Tara Mann, Gary Ward, and Con Beckers. 2004. “Identification of the Membrane Receptor of a Class XIV Myosin in Toxoplasma Gondii.” *The Journal of Cell Biology* 165 (3): 383–93. https://doi.org/10.1083/jcb.200311137.
Ghosh, Anil K., Martin Devenport, Deepa Jethwaney, Dario E. Kalume, Akhilesh Pandey, Vernon E. Anderson, Ali A. Sultan, Nirbhay Kumar, and Marcelo Jacobs-Lorena. 2009. “Malaria Parasite Invasion of the Mosquito Salivary Gland Requires Interaction between the Plasmodium TRAP and the Anopheles Saglin Proteins.” *PLoS Pathogens* 5 (1): e1000265. https://doi.org/10.1371/journal.ppat.1000265.
Ghosh, Anil Kumar, and Marcelo Jacobs-Lorena. 2009. “Plasmodium Sporozoite Invasion of the Mosquito Salivary Gland.” *Current Opinion in Microbiology* 12 (4): 394–400. https://doi.org/10.1016/j.mib.2009.06.010.
Ghosh, Ankit, Aastha Varshney, Sunil Kumar Narwal, null Nirdosh, Roshni Gupta, and Satish Mishra. 2024. “The Novel Plasmodium Berghei Protein S14 Is Essential for Sporozoite Gliding Motility and Infectivity.” *Journal of Cell Science* 137 (11): jcs261857. https://doi.org/10.1242/jcs.261857.
Gordon, D. M., T. W. McGovern, U. Krzych, J. C. Cohen, I. Schneider, R. LaChance, D. G. Heppner, G. Yuan, M. Hollingdale, and M. Slaoui. 1995. “Safety, Immunogenicity, and Efficacy of a Recombinantly Produced Plasmodium Falciparum Circumsporozoite Protein-Hepatitis B Surface Antigen Subunit Vaccine.” *The Journal of Infectious Diseases* 171 (6): 1576–85. https://doi.org/10.1093/infdis/171.6.1576.
Gould, S. B., W.-H. Tham, A. F. Cowman, G. I. McFadden, and R. F. Waller. 2008. “Alveolins, a New Family of Cortical Proteins That Define the Protist Infrakingdom Alveolata.” *Molecular Biology and Evolution* 25 (6): 1219–30. https://doi.org/10.1093/molbev/msn070.
Greigert, Valentin, Iti Saraav, Juhee Son, Yinxing Zhu, Denise Dayao, Avan Antia, Saul Tzipori, et al. 2024. “Cryptosporidium Infection of Human Small Intestinal Epithelial Cells Induces Type III Interferon and Impairs Infectivity of Rotavirus.” *Gut Microbes* 16 (1): 2297897. https://doi.org/10.1080/19490976.2023.2297897.
Haldar, Kasturi, and Narla Mohandas. 2009. “Malaria, Erythrocytic Infection, and Anemia.” *Hematology. American Society of Hematology. Education Program*, 87–93. https://doi.org/10.1182/asheducation-2009.1.87.
Han, Yeon Soo, and Carolina Barillas-Mury. 2002. “Implications of Time Bomb Model of Ookinete Invasion of Midgut Cells.” *Insect Biochemistry and Molecular Biology* 32 (10): 1311–16. https://doi.org/10.1016/s0965-1748(02)00093-0.
Hanboonkunupakarn, Borimas, Mavuto Mukaka, Podjanee Jittamala, Kittiyod Poovorawan, Pongphaya Pongsuwan, Lisa Stockdale, Samuel Provstgaard-Morys, et al. 2024. “A Randomised Trial of Malaria Vaccine R21/Matrix-M™ with and without Antimalarial Drugs in Thai Adults.” *Npj Vaccines* 9 (1): 124. https://doi.org/10.1038/s41541-024-00920-1.
Harding, Clare R., and Friedrich Frischknecht. 2020. “The Riveting Cellular Structures of Apicomplexan Parasites.” *Trends in Parasitology* 36 (12): 979–91.

https://doi.org/10.1016/j.pt.2020.09.001.
He, Lu, Yue Qiu, Geping Pang, Siqi Li, Jingjing Wang, Yonghui Feng, Lumeng Chen, et al. 2023. “Plasmodium Falciparum GAP40 Plays an Essential Role in Merozoite Invasion and Gametocytogenesis.” *Microbiology Spectrum* 11 (3): e0143423. https://doi.org/10.1128/spectrum.01434-23.
Hegge, Stephan, Mikhail Kudryashev, Ashley Smith, and Friedrich Frischknecht. 2009. “Automated Classification of *Plasmodium* Sporozoite Movement Patterns Reveals a Shift towards Productive Motility during Salivary Gland Infection.” *Biotechnology Journal* 4 (6): 903–13. https://doi.org/10.1002/biot.200900007.
Hegge, Stephan, Sylvia Münter, Marion Steinbüchel, Kirsten Heiss, Ulrike Engel, Kai Matuschewski, and Friedrich Frischknecht. 2010. “Multistep Adhesion of Plasmodium Sporozoites.” *FASEB Journal: Official Publication of the Federation of American Societies for Experimental Biology* 24 (7): 2222–34. https://doi.org/10.1096/fj.09-148700.
Hegge, Stephan, Kai Uhrig, Martin Streichfuss, Gisela Kynast-Wolf, Kai Matuschewski, Joachim P. Spatz, and Friedrich Frischknecht. 2012. “Direct Manipulation of Malaria Parasites with Optical Tweezers Reveals Distinct Functions of Plasmodium Surface Proteins.” *ACS Nano* 6 (6): 4648–62. https://doi.org/10.1021/nn203616u.
Heintzelman, M. B., and J. D. Schwartzman. 1997. “A Novel Class of Unconventional Myosins from Toxoplasma Gondii.” *Journal of Molecular Biology* 271 (1): 139–46. https://doi.org/10.1006/jmbi.1997.1167.
Heintzelman, Matthew B. 2015. “Gliding Motility in Apicomplexan Parasites.” *Seminars in Cell & Developmental Biology* 46 (October):135–42. https://doi.org/10.1016/j.semcdb.2015.09.020.
Heiss, Kirsten, Hui Nie, Sumit Kumar, Thomas M. Daly, Lawrence W. Bergman, and Kai Matuschewski. 2008. “Functional Characterization of a Redundant Plasmodium TRAP Family Invasin, TRAP-like Protein, by Aldolase Binding and a Genetic Complementation Test.” *Eukaryotic Cell* 7 (6): 1062–70. https://doi.org/10.1128/EC.00089-08.
Heller, Evan, and Elaine Fuchs. 2015. “Tissue Patterning and Cellular Mechanics.” *The Journal of Cell Biology* 211 (2): 219–31. https://doi.org/10.1083/jcb.201506106.
Hellmann, Janina Kristin, Sylvia Münter, Mikhail Kudryashev, Simon Schulz, Kirsten Heiss, Ann-Kristin Müller, Kai Matuschewski, Joachim P. Spatz, Ulrich S. Schwarz, and Friedrich Frischknecht. 2011. “Environmental Constraints Guide Migration of Malaria Parasites during Transmission.” Edited by Maria M. Mota. *PLoS Pathogens* 7 (6): e1002080. https://doi.org/10.1371/journal.ppat.1002080.
Hentzschel, Franziska, and Friedrich Frischknecht. 2022. “Still Enigmatic: Plasmodium Oocysts 125 Years after Their Discovery.” *Trends in Parasitology* 38 (8): 610–13. https://doi.org/10.1016/j.pt.2022.05.013.
Hentzschel, Franziska, David Jewanski, Yvonne Sokolowski, Pratika Agarwal, Anna Kraeft, Kolja Hildenbrand, Lilian P. Dorner, Mirko Singer, Friedrich Frischknecht, and Matthias Marti. 2023. “A Non-Canonical Arp2/3 Complex Is Essential for *Plasmodium* DNA Segregation and Transmission of Malaria.” https://doi.org/10.1101/2023.10.25.563799.
Herm-Götz, Angelika, Stefan Weiss, Rolf Stratmann, Setsuko Fujita-Becker, Christine Ruff, Edgar Meyhöfer, Thierry Soldati, Dietmar J. Manstein, Michael A. Geeves, and Dominique Soldati. 2002. “Toxoplasma Gondii Myosin A and Its Light Chain: A Fast, Single-Headed, plus-End-Directed Motor.” *The EMBO Journal* 21 (9): 2149–58.

https://doi.org/10.1093/emboj/21.9.2149.
Ho, May, and Nicholas J. White. 1999. “Molecular Mechanisms of Cytoadherence in Malaria.” *American Journal of Physiology-Cell Physiology* 276 (6): C1231–42. https://doi.org/10.1152/ajpcell.1999.276.6.C1231.
Hopp, Christine S, Sachie Kanatani, Nathan K Archer, Robert J Miller, Haiyun Liu, Kevin K Chiou, Lloyd S Miller, and Photini Sinnis. 2021. “Comparative Intravital Imaging of Human and Rodent Malaria Sporozoites Reveals the Skin Is Not a Species‐specific Barrier.” *EMBO Molecular Medicine* 13 (4): e11796. https://doi.org/10.15252/emmm.201911796.
Hueschen, Christina L., Li-av Segev-Zarko, Jian-Hua Chen, Mark A. LeGros, Carolyn A. Larabell, John C. Boothroyd, Rob Phillips, and Alexander R. Dunn. 2024. “Emergent Actin Flows Explain Distinct Modes of Gliding Motility.” *Nature Physics*, October. https://doi.org/10.1038/s41567-024-02652-4.
Hughes, Katie R., Giancarlo A. Biagini, and Alister G. Craig. 2010. “Continued Cytoadherence of Plasmodium Falciparum Infected Red Blood Cells after Antimalarial Treatment.” *Molecular and Biochemical Parasitology* 169 (2): 71–78. https://doi.org/10.1016/j.molbiopara.2009.09.007.
Ishino, Tomoko, Yasuo Chinzei, and Masao Yuda. 2005. “A Plasmodium Sporozoite Protein with a Membrane Attack Complex Domain Is Required for Breaching the Liver Sinusoidal Cell Layer Prior to Hepatocyte Infection.” *Cellular Microbiology* 7 (2): 199–208. https://doi.org/10.1111/j.1462-5822.2004.00447.x.
Ishino, Tomoko, Kazuhiko Yano, Yasuo Chinzei, and Masao Yuda. 2004. “Cell-Passage Activity Is Required for the Malarial Parasite to Cross the Liver Sinusoidal Cell Layer.” Edited by Gary Ward. *PLoS Biology* 2 (1): e4. https://doi.org/10.1371/journal.pbio.0020004.
Jacot, Damien, Nicolò Tosetti, Isa Pires, Jessica Stock, Arnault Graindorge, Yu-Fu Hung, Huijong Han, Rita Tewari, Inari Kursula, and Dominique Soldati-Favre. 2016. “An Apicomplexan Actin-Binding Protein Serves as a Connector and Lipid Sensor to Coordinate Motility and Invasion.” *Cell Host & Microbe* 20 (6): 731–43. https://doi.org/10.1016/j.chom.2016.10.020.
Janouskovec, Jan, Ales Horák, Miroslav Oborník, Julius Lukes, and Patrick J. Keeling. 2010. “A Common Red Algal Origin of the Apicomplexan, Dinoflagellate, and Heterokont Plastids.” *Proceedings of the National Academy of Sciences of the United States of America* 107 (24): 10949–54. https://doi.org/10.1073/pnas.1003335107.
Janouškovec, Jan, Gita G. Paskerova, Tatiana S. Miroliubova, Kirill V. Mikhailov, Thomas Birley, Vladimir V. Aleoshin, and Timur G. Simdyanov. 2019. “Apicomplexan-like Parasites Are Polyphyletic and Widely but Selectively Dependent on Cryptic Plastid Organelles.” *eLife* 8 (August):e49662. https://doi.org/10.7554/eLife.49662.
Janouškovec, Jan, Denis V. Tikhonenkov, Fabien Burki, Alexis T. Howe, Martin Kolísko, Alexander P. Mylnikov, and Patrick J. Keeling. 2015. “Factors Mediating Plastid Dependency and the Origins of Parasitism in Apicomplexans and Their Close Relatives.” *Proceedings of the National Academy of Sciences of the United States of America* 112 (33): 10200–207. https://doi.org/10.1073/pnas.1423790112.
Janse, C.J., E.G. Boorsma, J. Ramesar, Ph. Van Vianen, R. Van Der Meer, P. Zenobi, O. Casaglia, B. Mons, and F.M. Van Der Berg. 1989. “Plasmodium Berghei: Gametocyte Production, DNA Content, and Chromosome-Size Polymorphisms during Asexual Multiplication in Vivo.” *Experimental Parasitology* 68 (3): 274–82.

https://doi.org/10.1016/0014-4894(89)90109-4.
Jethwaney, Deepa, Timothy Lepore, Saria Hassan, Kerrianne Mello, Radha Rangarajan, Willi Jahnen-Dechent, Dyann Wirth, and Ali A. Sultan. 2005. “Fetuin-A, a Hepatocyte-Specific Protein That Binds Plasmodium Berghei Thrombospondin-Related Adhesive Protein: A Potential Role in Infectivity.” *Infection and Immunity* 73 (9): 5883–91. https://doi.org/10.1128/IAI.73.9.5883-5891.2005.
Josenhans, Christine, and Sebastian Suerbaum. 2002. “The Role of Motility as a Virulence Factor in Bacteria.” *International Journal of Medical Microbiology: IJMM* 291 (8): 605–14. https://doi.org/10.1078/1438-4221-00173.
Josling, Gabrielle A., Timothy J. Russell, Jarrett Venezia, Lindsey Orchard, Riëtte van Biljon, Heather J. Painter, and Manuel Llinás. 2020. “Dissecting the Role of PfAP2-G in Malaria Gametocytogenesis.” *Nature Communications* 11 (1): 1503. https://doi.org/10.1038/s41467-020-15026-0.
Kafsack, Björn F. C., Núria Rovira-Graells, Taane G. Clark, Cristina Bancells, Valerie M. Crowley, Susana G. Campino, April E. Williams, et al. 2014. “A Transcriptional Switch Underlies Commitment to Sexual Development in Malaria Parasites.” *Nature* 507 (7491): 248–52. https://doi.org/10.1038/nature12920.
Kaiser, Karine, Kai Matuschewski, Nelly Camargo, Jessica Ross, and Stefan H. I. Kappe. 2004. “Differential Transcriptome Profiling Identifies *Plasmodium* Genes Encoding Pre‐erythrocytic Stage‐specific Proteins.” *Molecular Microbiology* 51 (5): 1221–32. https://doi.org/10.1046/j.1365-2958.2003.03909.x.
Kanatani, Sachie, Deborah Stiffler, Teun Bousema, Gayane Yenokyan, and Photini Sinnis. 2024. “Revisiting the Plasmodium Sporozoite Inoculum and Elucidating the Efficiency with Which Malaria Parasites Progress through the Mosquito.” *Nature Communications* 15 (1): 748. https://doi.org/10.1038/s41467-024-44962-4.
Kappe, S., T. Bruderer, S. Gantt, H. Fujioka, V. Nussenzweig, and R. Ménard. 1999. “Conservation of a Gliding Motility and Cell Invasion Machinery in Apicomplexan Parasites.” *The Journal of Cell Biology* 147 (5): 937–44. https://doi.org/10.1083/jcb.147.5.937.
Kappe, Stefan, Thomas Bruderer, Soren Gantt, Hisashi Fujioka, Victor Nussenzweig, and Robert Ménard. 1999. “Conservation of a Gliding Motility and Cell Invasion Machinery in Apicomplexan Parasites.” *The Journal of Cell Biology* 147 (5): 937–44. https://doi.org/10.1083/jcb.147.5.937.
Kappe, Stefan H. I., Carlos A. Buscaglia, Lawrence W. Bergman, Isabelle Coppens, and Victor Nussenzweig. 2004. “Apicomplexan Gliding Motility and Host Cell Invasion: Overhauling the Motor Model.” *Trends in Parasitology* 20 (1): 13–16. https://doi.org/10.1016/j.pt.2003.10.011.
Kehrer, Jessica, Pauline Formaglio, Julianne Mendi Muthinja, Sebastian Weber, Danny Baltissen, Christopher Lance, Johanna Ripp, et al. 2022. “Plasmodium Sporozoite Disintegration during Skin Passage Limits Malaria Parasite Transmission.” *EMBO Reports* 23 (7): e54719. https://doi.org/10.15252/embr.202254719.
Kehrer, Jessica, Friedrich Frischknecht, and Gunnar R. Mair. 2016. “Proteomic Analysis of the Plasmodium Berghei Gametocyte Egressome and Vesicular bioID of Osmiophilic Body Proteins Identifies Merozoite TRAP-like Protein (MTRAP) as an Essential Factor for Parasite Transmission.” *Molecular & Cellular Proteomics* 15 (9): 2852–62. https://doi.org/10.1074/mcp.M116.058263.

Kehrer, Jessica, Mirko Singer, Leandro Lemgruber, Patricia A. G. C. Silva, Friedrich Frischknecht, and Gunnar R. Mair. 2016. "A Putative Small Solute Transporter Is Responsible for the Secretion of G377 and TRAP-Containing Secretory Vesicles during Plasmodium Gamete Egress and Sporozoite Motility." Edited by Oliver Billker. *PLOS Pathogens* 12 (7): e1005734. https://doi.org/10.1371/journal.ppat.1005734.

Kennedy, Mark, Matthew E Fishbaugher, Ashley M Vaughan, Rapatbhorn Patrapuvich, Rachasak Boonhok, Narathatai Yimamnuaychok, Nastaran Rezakhani, et al. 2012. "A Rapid and Scalable Density Gradient Purification Method for Plasmodium Sporozoites." *Malaria Journal* 11 (1): 421. https://doi.org/10.1186/1475-2875-11-421.

Khater, Emad I., Robert E. Sinden, and Johannes T. Dessens. 2004. "A Malaria Membrane Skeletal Protein Is Essential for Normal Morphogenesis, Motility, and Infectivity of Sporozoites." *The Journal of Cell Biology* 167 (3): 425–32. https://doi.org/10.1083/jcb.200406068.

Kimmel, Jessica, Jessica Kehrer, Friedrich Frischknecht, and Tobias Spielmann. 2022. "Proximity‐dependent Biotinylation Approaches to Study Apicomplexan Biology." *Molecular Microbiology* 117 (3): 553–68. https://doi.org/10.1111/mmi.14815.

Klug, Dennis, and Friedrich Frischknecht. 2017. "Motility Precedes Egress of Malaria Parasites from Oocysts." *eLife* 6 (January):e19157. https://doi.org/10.7554/eLife.19157.

Klug, Dennis, Sarah Goellner, Jessica Kehrer, Julia Sattler, Léanne Strauss, Mirko Singer, Chafen Lu, Timothy A. Springer, and Friedrich Frischknecht. 2020. "Evolutionarily Distant I Domains Can Functionally Replace the Essential Ligand-Binding Domain of Plasmodium TRAP." *eLife* 9 (July):e57572. https://doi.org/10.7554/eLife.57572.

Koreny, Ludek, Mohammad Zeeshan, Konstantin Barylyuk, Eelco C. Tromer, Jolien J. E. Van Hooff, Declan Brady, Huiling Ke, et al. 2021. "Molecular Characterization of the Conoid Complex in Toxoplasma Reveals Its Conservation in All Apicomplexans, Including Plasmodium Species." Edited by Michael Duffy. *PLOS Biology* 19 (3): e3001081. https://doi.org/10.1371/journal.pbio.3001081.

Kozlov, Michael M., and Alex Mogilner. 2007. "Model of Polarization and Bistability of Cell Fragments." *Biophysical Journal* 93 (11): 3811–19. https://doi.org/10.1529/biophysj.107.110411.

Kubota, Hiroshi, Gillian Hynes, and Keith Willison. 1995. "The Chaperonin Containing T-Complex Polypeptide 1 (TCP-1). Multisubunit Machinery Assisting in Protein Folding and Assembly in the Eukaryotic Cytosol." *European Journal of Biochemistry* 230 (1): 3–16. https://doi.org/10.1111/j.1432-1033.1995.tb20527.x.

Kudryashev, Mikhail, Simone Lepper, Rebecca Stanway, Stefan Bohn, Wolfgang Baumeister, Marek Cyrklaff, and Friedrich Frischknecht. 2010. "Positioning of Large Organelles by a Membrane- Associated Cytoskeleton in *Plasmodium* Sporozoites." *Cellular Microbiology* 12 (3): 362–71. https://doi.org/10.1111/j.1462-5822.2009.01399.x.

Kudryashev, Mikhail, Sylvia Münter, Leandro Lemgruber, Georgina Montagna, Henning Stahlberg, Kai Matuschewski, Markus Meissner, Marek Cyrklaff, and Friedrich Frischknecht. 2012. "Structural Basis for Chirality and Directional Motility of Plasmodium Sporozoites." *Cellular Microbiology* 14 (11): 1757–68. https://doi.org/10.1111/j.1462-5822.2012.01836.x.

Kwong, Waldan K., Javier Del Campo, Varsha Mathur, Mark J. A. Vermeij, and Patrick J. Keeling. 2019. "A Widespread Coral-Infecting Apicomplexan with Chlorophyll Biosynthesis Genes." *Nature* 568 (7750): 103–7.

https://doi.org/10.1038/s41586-019-1072-z.
Lamers, Olivia A. C., Blandine M. D. Franke-Fayard, Jan Pieter R. Koopman, Geert V. T. Roozen, Jacqueline J. Janse, Severine C. Chevalley-Maurel, Fiona J. A. Geurten, et al. 2024. “Safety and Efficacy of Immunization with a Late-Liver-Stage Attenuated Malaria Parasite.” *The New England Journal of Medicine* 391 (20): 1913–23. https://doi.org/10.1056/NEJMoa2313892.
Lee, Wenn-Chyau, Bruce Russell, and Laurent Rénia. 2019. “Sticking for a Cause: The Falciparum Malaria Parasites Cytoadherence Paradigm.” *Frontiers in Immunology* 10:1444. https://doi.org/10.3389/fimmu.2019.01444.
Lindner, Scott E., Kristian E. Swearingen, Anke Harupa, Ashley M. Vaughan, Photini Sinnis, Robert L. Moritz, and Stefan H. I. Kappe. 2013. “Total and Putative Surface Proteomics of Malaria Parasite Salivary Gland Sporozoites.” *Molecular & Cellular Proteomics: MCP* 12 (5): 1127–43. https://doi.org/10.1074/mcp.M112.024505.
Lopaticki, Sash, Robyn McConville, Alan John, Niall Geoghegan, Shihab Deen Mohamed, Lisa Verzier, Ryan W. J. Steel, et al. 2022. “Tryptophan C-Mannosylation Is Critical for Plasmodium Falciparum Transmission.” *Nature Communications* 13 (1): 4400. https://doi.org/10.1038/s41467-022-32076-8.
Lopaticki, Sash, Annie S. P. Yang, Alan John, Nichollas E. Scott, James P. Lingford, Matthew T. O’Neill, Sara M. Erickson, et al. 2017. “Protein O-Fucosylation in Plasmodium Falciparum Ensures Efficient Infection of Mosquito and Vertebrate Hosts.” *Nature Communications* 8 (1): 561. https://doi.org/10.1038/s41467-017-00571-y.
Loubens, Manon, Carine Marinach, Clara-Eva Paquereau, Soumia Hamada, Bénédicte Hoareau-Coudert, David Akbar, Jean-François Franetich, and Olivier Silvie. 2023. “The Claudin-like Apicomplexan Microneme Protein Is Required for Gliding Motility and Infectivity of Plasmodium Sporozoites.” *PLoS Pathogens* 19 (3): e1011261. https://doi.org/10.1371/journal.ppat.1011261.
Loubens, Manon, Laetitia Vincensini, Priyanka Fernandes, Sylvie Briquet, Carine Marinach, and Olivier Silvie. 2021. “*Plasmodium* Sporozoites on the Move: Switching from Cell Traversal to Productive Invasion of Hepatocytes.” *Molecular Microbiology* 115 (5): 870–81. https://doi.org/10.1111/mmi.14645.
Lukeš, Julius, Brian S. Leander, and Patrick J. Keeling. 2009. “Cascades of Convergent Evolution: The Corresponding Evolutionary Histories of Euglenozoans and Dinoflagellates.” *Proceedings of the National Academy of Sciences* 106 (supplement_1): 9963–70. https://doi.org/10.1073/pnas.0901004106.
Mantovani, Alberto, Raffaella Bonecchi, and Massimo Locati. 2006. “Tuning Inflammation and Immunity by Chemokine Sequestration: Decoys and More.” *Nature Reviews. Immunology* 6 (12): 907–18. https://doi.org/10.1038/nri1964.
Manzoni, Giulia, Carine Marinach, Selma Topçu, Sylvie Briquet, Morgane Grand, Matthieu Tolle, Marion Gransagne, et al. 2017. “Plasmodium P36 Determines Host Cell Receptor Usage during Sporozoite Invasion.” *eLife* 6 (May):e25903. https://doi.org/10.7554/eLife.25903.
Mathur, Varsha, Martin Kolísko, Elisabeth Hehenberger, Nicholas A. T. Irwin, Brian S. Leander, Árni Kristmundsson, Mark A. Freeman, and Patrick J. Keeling. 2019. “Multiple Independent Origins of Apicomplexan-Like Parasites.” *Current Biology: CB* 29 (17): 2936-2941.e5. https://doi.org/10.1016/j.cub.2019.07.019.
Matsumoto, Y., G. Perry, L. W. Scheibel, and M. Aikawa. 1987. “Role of Calmodulin in

Plasmodium Falciparum: Implications for Erythrocyte Invasion by the Merozoite." *European Journal of Cell Biology* 45 (1): 36–43.
Matuschewski, Kai, Alvaro C. Nunes, Victor Nussenzweig, and Robert Ménard. 2002. "Plasmodium Sporozoite Invasion into Insect and Mammalian Cells Is Directed by the Same Dual Binding System." *The EMBO Journal* 21 (7): 1597–1606. https://doi.org/10.1093/emboj/21.7.1597.
Matz, Joachim M., Benjamin Drepper, Thorsten B. Blum, Eric van Genderen, Alana Burrell, Peer Martin, Thomas Stach, et al. 2020. "A Lipocalin Mediates Unidirectional Heme Biomineralization in Malaria Parasites." *Proceedings of the National Academy of Sciences of the United States of America* 117 (28): 16546–56. https://doi.org/10.1073/pnas.2001153117.
Matz, Joachim M., and Taco W. A. Kooij. 2015. "Towards Genome-Wide Experimental Genetics in the in Vivo Malaria Model Parasite Plasmodium Berghei." *Pathogens and Global Health* 109 (2): 46–60. https://doi.org/10.1179/2047773215Y.0000000006.
Meissner, Markus, Dirk Schlüter, and Dominique Soldati. 2002. "Role of Toxoplasma Gondii Myosin A in Powering Parasite Gliding and Host Cell Invasion." *Science (New York, N.Y.)* 298 (5594): 837–40. https://doi.org/10.1126/science.1074553.
Ménard, Robert, Joana Tavares, Ian Cockburn, Miles Markus, Fidel Zavala, and Rogerio Amino. 2013. "Looking under the Skin: The First Steps in Malarial Infection and Immunity." *Nature Reviews. Microbiology* 11 (10): 701–12. https://doi.org/10.1038/nrmicro3111.
Mendes, António M., Isaie J. Reuling, Carolina M. Andrade, Thomas D. Otto, Marta Machado, Filipa Teixeira, Joana Pissarra, et al. 2018. "Pre-Clinical Evaluation of a P. Berghei-Based Whole-Sporozoite Malaria Vaccine Candidate." *Npj Vaccines* 3 (1): 54. https://doi.org/10.1038/s41541-018-0091-3.
Michinaga, Shotaro, and Yutaka Koyama. 2015. "Pathogenesis of Brain Edema and Investigation into Anti-Edema Drugs." *International Journal of Molecular Sciences* 16 (5): 9949–75. https://doi.org/10.3390/ijms16059949.
Mikolajczak, Sebastian A., Hilda Silva-Rivera, Xinxia Peng, Alice S. Tarun, Nelly Camargo, Vanessa Jacobs-Lorena, Thomas M. Daly, et al. 2008. "Distinct Malaria Parasite Sporozoites Reveal Transcriptional Changes That Cause Differential Tissue Infection Competence in the Mosquito Vector and Mammalian Host." *Molecular and Cellular Biology* 28 (20): 6196–6207. https://doi.org/10.1128/MCB.00553-08.
Miller, Sven, and Jacomine Krijnse-Locker. 2008. "Modification of Intracellular Membrane Structures for Virus Replication." *Nature Reviews Microbiology* 6 (5): 363–74. https://doi.org/10.1038/nrmicro1890.
Milner, Danny A. 2018. "Malaria Pathogenesis." *Cold Spring Harbor Perspectives in Medicine* 8 (1): a025569. https://doi.org/10.1101/cshperspect.a025569.
Minns, Allen M., Kevin J. Hart, Suriyasri Subramanian, Susan Hafenstein, and Scott E. Lindner. 2018. "Nuclear, Cytosolic, and Surface-Localized Poly(A)-Binding Proteins of Plasmodium Yoelii." Edited by William J. Sullivan. *mSphere* 3 (1): e00435-17. https://doi.org/10.1128/mSphere.00435-17.
Montagna, Georgina N., Carlos A. Buscaglia, Sylvia Münter, Christian Goosmann, Friedrich Frischknecht, Volker Brinkmann, and Kai Matuschewski. 2012. "Critical Role for Heat Shock Protein 20 (HSP20) in Migration of Malarial Sporozoites." *The Journal of Biological Chemistry* 287 (4): 2410–22. https://doi.org/10.1074/jbc.M111.302109.
Morahan, Belinda J., Lina Wang, and Ross L. Coppel. 2009. "No TRAP, No Invasion." *Trends in*

Parasitology 25 (2): 77–84. https://doi.org/10.1016/j.pt.2008.11.004.
Moreira, Cristina K., Thomas J. Templeton, Catherine Lavazec, Rhian E. Hayward, Charlotte V. Hobbs, Hans Kroeze, Chris J. Janse, Andrew P. Waters, Photini Sinnis, and Alida Coppi. 2008. "The Plasmodium TRAP/MIC2 Family Member, TRAP-Like Protein (TLP), Is Involved in Tissue Traversal by Sporozoites." *Cellular Microbiology* 10 (7): 1505–16. https://doi.org/10.1111/j.1462-5822.2008.01143.x.
Morrison, David A. 2009. "Evolution of the Apicomplexa: Where Are We Now?" *Trends in Parasitology* 25 (8): 375–82. https://doi.org/10.1016/j.pt.2009.05.010.
Mota, M. M., G. Pradel, J. P. Vanderberg, J. C. Hafalla, U. Frevert, R. S. Nussenzweig, V. Nussenzweig, and A. Rodríguez. 2001. "Migration of Plasmodium Sporozoites through Cells before Infection." *Science (New York, N.Y.)* 291 (5501): 141–44. https://doi.org/10.1126/science.291.5501.141.
Moussaoui, Dihia, James P Robblee, Daniel Auguin, Elena B Krementsova, Silvia Haase, Thomas Ca Blake, Jake Baum, Julien Robert-Paganin, Kathleen M Trybus, and Anne Houdusse. 2020. "Full-Length Plasmodium Falciparum Myosin A and Essential Light Chain PfELC Structures Provide New Anti-Malarial Targets." *eLife* 9 (October):e60581. https://doi.org/10.7554/eLife.60581.
Münter, Sylvia, Benedikt Sabass, Christine Selhuber-Unkel, Mikhail Kudryashev, Stephan Hegge, Ulrike Engel, Joachim P. Spatz, Kai Matuschewski, Ulrich S. Schwarz, and Friedrich Frischknecht. 2009. "Plasmodium Sporozoite Motility Is Modulated by the Turnover of Discrete Adhesion Sites." *Cell Host & Microbe* 6 (6): 551–62. https://doi.org/10.1016/j.chom.2009.11.007.
Muthinja, Julianne Mendi, Johanna Ripp, Timothy Krüger, Andrea Imle, Tamás Haraszti, Oliver T. Fackler, Joachim P. Spatz, Markus Engstler, and Friedrich Frischknecht. 2018. "Tailored Environments to Study Motile Cells and Pathogens." *Cellular Microbiology* 20 (3). https://doi.org/10.1111/cmi.12820.
Nair, Sethu C., Carrie F. Brooks, Christopher D. Goodman, Angelika Sturm, Geoffrey I. McFadden, Sandeep Sundriyal, Justin L. Anglin, Yongcheng Song, Silvia N. J. Moreno, and Boris Striepen. 2011. "Apicoplast Isoprenoid Precursor Synthesis and the Molecular Basis of Fosmidomycin Resistance in Toxoplasma Gondii." *The Journal of Experimental Medicine* 208 (7): 1547–59. https://doi.org/10.1084/jem.20110039.
Neubauer, Emilie-Fleur, Angela Z Poole, Philipp Neubauer, Olivier Detournay, Kenneth Tan, Simon K Davy, and Virginia M Weis. 2017. "A Diverse Host Thrombospondin-Type-1 Repeat Protein Repertoire Promotes Symbiont Colonization during Establishment of Cnidarian-Dinoflagellate Symbiosis." *eLife* 6 (May):e24494. https://doi.org/10.7554/eLife.24494.
Nishi, Manami, Ke Hu, John M. Murray, and David S. Roos. 2008. "Organellar Dynamics during the Cell Cycle of Toxoplasma Gondii." *Journal of Cell Science* 121 (Pt 9): 1559–68. https://doi.org/10.1242/jcs.021089.
Okada, Megan, Krithika Rajaram, Russell P. Swift, Amanda Mixon, John Alan Maschek, Sean T. Prigge, and Paul A. Sigala. 2022. "Critical Role for Isoprenoids in Apicoplast Biogenesis by Malaria Parasites." *eLife* 11 (March):e73208. https://doi.org/10.7554/eLife.73208.
Osoro, Caroline Bonareri, Eleanor Ochodo, Titus K Kwambai, Jenifer Akoth Otieno, Lisa Were, Caleb Kimutai Sagam, Eddy Johnson Owino, Simon Kariuki, Feiko O Ter Kuile, and Jenny Hill. 2024. "Policy Uptake and Implementation of the RTS,S/AS01 Malaria Vaccine in Sub-Saharan African Countries: Status 2 Years Following the WHO

Recommendation." *BMJ Global Health* 9 (4): e014719. https://doi.org/10.1136/bmjgh-2023-014719.
Oxborough, Richard M., Karen C. Figueroa Chilito, Filemon Tokponnon, and Louisa A. Messenger. 2024. "Malaria Vector Control in Sub-Saharan Africa: Complex Trade-Offs to Combat the Growing Threat of Insecticide Resistance." *The Lancet. Planetary Health* 8 (10): e804–12. https://doi.org/10.1016/S2542-5196(24)00172-4.
Pegoraro, Stefano, Maëlle Duffey, Thomas D. Otto, Yulin Wang, Roman Rösemann, Roland Baumgartner, Stefanie K. Fehler, et al. 2017. "SC83288 Is a Clinical Development Candidate for the Treatment of Severe Malaria." *Nature Communications* 8 (January):14193. https://doi.org/10.1038/ncomms14193.
Pradel, G., and U. Frevert. 2001. "Malaria Sporozoites Actively Enter and Pass through Rat Kupffer Cells Prior to Hepatocyte Invasion." *Hepatology (Baltimore, Md.)* 33 (5): 1154–65. https://doi.org/10.1053/jhep.2001.24237.
Pradel, Gabriele, Shivani Garapaty, and Ute Frevert. 2002. "Proteoglycans Mediate Malaria Sporozoite Targeting to the Liver." *Molecular Microbiology* 45 (3): 637–51. https://doi.org/10.1046/j.1365-2958.2002.03057.x.
Pryce, Joseph, Nancy Medley, and Leslie Choi. 2022. "Indoor Residual Spraying for Preventing Malaria in Communities Using Insecticide-Treated Nets." *The Cochrane Database of Systematic Reviews* 1 (1): CD012688. https://doi.org/10.1002/14651858.CD012688.pub3.
Quadt, Katharina A., Martin Streichfuss, Catherine A. Moreau, Joachim P. Spatz, and Friedrich Frischknecht. 2016. "Coupling of Retrograde Flow to Force Production During Malaria Parasite Migration." *ACS Nano* 10 (2): 2091–2102. https://doi.org/10.1021/acsnano.5b06417.
Ramakrishnan, Chandra, Johannes T. Dessens, Rebecca Armson, Sofia B. Pinto, Arthur M. Talman, Andrew M. Blagborough, and Robert E. Sinden. 2011. "Vital Functions of the Malarial Ookinete Protein, CTRP, Reside in the A Domains." *International Journal for Parasitology* 41 (10): 1029–39. https://doi.org/10.1016/j.ijpara.2011.05.007.
Ren, Bingjian, Romuald Haase, Sharon Patray, Quynh Nguyen, Bohumil Maco, Nicolas Dos Santos Pacheco, Yi-Wei Chang, and Dominique Soldati-Favre. 2024. "Architecture of the *Toxoplasma Gondii* Apical Polar Ring and Its Role in Gliding Motility and Invasion." *Proceedings of the National Academy of Sciences* 121 (46): e2416602121. https://doi.org/10.1073/pnas.2416602121.
Richie, Thomas L., L. W. Preston Church, Tooba Murshedkar, Peter F. Billingsley, Eric R. James, Mei-Chun Chen, Yonas Abebe, et al. 2023. "Sporozoite Immunization: Innovative Translational Science to Support the Fight against Malaria." *Expert Review of Vaccines* 22 (1): 964–1007. https://doi.org/10.1080/14760584.2023.2245890.
Ridzuan, Mohd A. Mohd, Robert W. Moon, Ellen Knuepfer, Sally Black, Anthony A. Holder, and Judith L. Green. 2012. "Subcellular Location, Phosphorylation and Assembly into the Motor Complex of GAP45 during Plasmodium Falciparum Schizont Development." *PloS One* 7 (3): e33845. https://doi.org/10.1371/journal.pone.0033845.
Ripp, Johanna, Jessica Kehrer, Xanthoula Smyrnakou, Nathalie Tisch, Joana Tavares, Rogerio Amino, Carmen Ruiz De Almodovar, and Friedrich Frischknecht. 2021. "Malaria Parasites Differentially Sense Environmental Elasticity during Transmission." *EMBO Molecular Medicine* 13 (4): e13933. https://doi.org/10.15252/emmm.202113933.
Ripp, Johanna, Dimitri Probst, Mirko Singer, Ulrich S. Schwarz, and Friedrich Frischknecht. 2024. "Traction Force Generation in Motile Malaria Parasites Is Modulated by the

Plasmodium Adhesin TLP." https://doi.org/10.1101/2024.10.02.616286.
Ripp, Johanna, Xanthoula Smyrnakou, Marie-Therese Neuhoff, Franziska Hentzschel, and Friedrich Frischknecht. 2022. "Phosphorylation of Myosin A Regulates Gliding Motility and Is Essential for Plasmodium Transmission." *EMBO Reports* 23 (7): e54857. https://doi.org/10.15252/embr.202254857.
Risco-Castillo, Veronica, Selma Topçu, Carine Marinach, Giulia Manzoni, Amélie E. Bigorgne, Sylvie Briquet, Xavier Baudin, Maryse Lebrun, Jean-François Dubremetz, and Olivier Silvie. 2015. "Malaria Sporozoites Traverse Host Cells within Transient Vacuoles." *Cell Host & Microbe* 18 (5): 593–603. https://doi.org/10.1016/j.chom.2015.10.006.
Rodriguez, Mario H., and Fidel de la C. Hernández-Hernández. 2004. "Insect-Malaria Parasites Interactions: The Salivary Gland." *Insect Biochemistry and Molecular Biology* 34 (7): 615–24. https://doi.org/10.1016/j.ibmb.2004.03.014.
Saeed, Sadia, Annie Z. Tremp, and Johannes T. Dessens. 2023. "Plasmodium Sporozoite Excystation Involves Local Breakdown of the Oocyst Capsule." *Scientific Reports* 13 (1): 22222. https://doi.org/10.1038/s41598-023-49442-1.
Salomaki, Eric D., Kristina X. Terpis, Sonja Rueckert, Michael Kotyk, Zuzana Kotyková Varadínová, Ivan Čepička, Christopher E. Lane, and Martin Kolisko. 2021. "Gregarine Single-Cell Transcriptomics Reveals Differential Mitochondrial Remodeling and Adaptation in Apicomplexans." *BMC Biology* 19 (1): 77. https://doi.org/10.1186/s12915-021-01007-2.
Santos, Jorge M., Saskia Egarter, Vanessa Zuzarte-Luís, Hirdesh Kumar, Catherine A. Moreau, Jessica Kehrer, Andreia Pinto, et al. 2017. "Malaria Parasite LIMP Protein Regulates Sporozoite Gliding Motility and Infectivity in Mosquito and Mammalian Hosts." *eLife* 6 (May):e24109. https://doi.org/10.7554/eLife.24109.
Sattler, Julia M, Lukas Keiber, Aiman Abdelrahim, Xinyu Zheng, Martin Jäcklin, Luisa Zechel, Catherine A Moreau, et al. 2024. "Experimental Vaccination by Single Dose Sporozoite Injection of Blood-Stage Attenuated Malaria Parasites." *EMBO Molecular Medicine* 16 (9): 2060–79. https://doi.org/10.1038/s44321-024-00101-6.
Sattler, Julia Magdalena, Markus Ganter, Marion Hliscs, Kai Matuschewski, and Herwig Schüler. 2011. "Actin Regulation in the Malaria Parasite." *European Journal of Cell Biology* 90 (11): 966–71. https://doi.org/10.1016/j.ejcb.2010.11.011.
Scarpa, Elena, and Roberto Mayor. 2016. "Collective Cell Migration in Development." *The Journal of Cell Biology* 212 (2): 143–55. https://doi.org/10.1083/jcb.201508047.
Schüler, Herwig, and Kai Matuschewski. 2006. "Plasmodium Motility: Actin Not Actin' like Actin." *Trends in Parasitology* 22 (4): 146–47. https://doi.org/10.1016/j.pt.2006.02.005.
Schüler, Herwig, Ann-Kristin Mueller, and Kai Matuschewski. 2005. "A *Plasmodium* Actin-Depolymerizing Factor That Binds Exclusively to Actin Monomers." *Molecular Biology of the Cell* 16 (9): 4013–23. https://doi.org/10.1091/mbc.e05-02-0086.
Shunmugam, Serena, Christophe-Sébastien Arnold, Sheena Dass, Nicholas J. Katris, and Cyrille Y. Botté. 2022. "The Flexibility of Apicomplexa Parasites in Lipid Metabolism." *PLoS Pathogens* 18 (3): e1010313. https://doi.org/10.1371/journal.ppat.1010313.
Siden-Kiamos, Inga, Markus Ganter, Andreas Kunze, Marion Hliscs, Marion Steinbüchel, Jacqueline Mendoza, Robert E. Sinden, Christos Louis, and Kai Matuschewski. 2011. "Stage-Specific Depletion of Myosin A Supports an Essential Role in Motility of Malarial Ookinetes." *Cellular Microbiology* 13 (12): 1996–2006. https://doi.org/10.1111/j.1462-5822.2011.01686.x.

Sidjanski, S., and J. P. Vanderberg. 1997. “Delayed Migration of Plasmodium Sporozoites from the Mosquito Bite Site to the Blood.” *The American Journal of Tropical Medicine and Hygiene* 57 (4): 426–29. https://doi.org/10.4269/ajtmh.1997.57.426.

Simwela, Nelson V., and Andrew P. Waters. 2022. “Current Status of Experimental Models for the Study of Malaria.” *Parasitology* 149 (6): 1–22. https://doi.org/10.1017/S0031182021002134.

Sinden, R. E., and N. A. Croll. 1975. “Cytology and Kinetics of Microgametogenesis and Fertilization in Plasmodium Yoelii Nigeriensis.” *Parasitology* 70 (1): 53–65. https://doi.org/10.1017/s0031182000048861.

Singer, Mirko, and Friedrich Frischknecht. 2023. “Still Running Fast: Plasmodium Ookinetes and Sporozoites 125 Years after Their Discovery.” *Trends in Parasitology* 39 (12): 991–95. https://doi.org/10.1016/j.pt.2023.09.015.

Singer, Mirko, Sachie Kanatani, Stefano Garcia Castillo, Friedrich Frischknecht, and Photini Sinnis. 2024. “The Plasmodium Circumsporozoite Protein.” *Trends in Parasitology* 40 (12): 1124–34. https://doi.org/10.1016/j.pt.2024.10.017.

Sinha, Abhinav, Katie R. Hughes, Katarzyna K. Modrzynska, Thomas D. Otto, Claudia Pfander, Nicholas J. Dickens, Agnieszka A. Religa, et al. 2014. “A Cascade of DNA-Binding Proteins for Sexual Commitment and Development in Plasmodium.” *Nature* 507 (7491): 253–57. https://doi.org/10.1038/nature12970.

Sinnis, Photini, Alida Coppi, Toshihiko Toida, Hidenao Toyoda, Akiko Kinoshita-Toyoda, Jin Xie, Melissa M. Kemp, and Robert J. Linhardt. 2007. “Mosquito Heparan Sulfate and Its Potential Role in Malaria Infection and Transmission.” *The Journal of Biological Chemistry* 282 (35): 25376–84. https://doi.org/10.1074/jbc.M704698200.

Skillman, Kristen M., Karthikeyan Diraviyam, Asis Khan, Keliang Tang, David Sept, and L. David Sibley. 2011. “Evolutionarily Divergent, Unstable Filamentous Actin Is Essential for Gliding Motility in Apicomplexan Parasites.” *PLoS Pathogens* 7 (10): e1002280. https://doi.org/10.1371/journal.ppat.1002280.

Song, Gaojie, Adem C. Koksal, Chafen Lu, and Timothy A. Springer. 2012. “Shape Change in the Receptor for Gliding Motility in *Plasmodium* Sporozoites.” *Proceedings of the National Academy of Sciences* 109 (52): 21420–25. https://doi.org/10.1073/pnas.1218581109.

Spillman, Natalie J., Josh R. Beck, Suresh M. Ganesan, Jacquin C. Niles, and Daniel E. Goldberg. 2017. “The Chaperonin TRiC Forms an Oligomeric Complex in the Malaria Parasite Cytosol.” *Cellular Microbiology* 19 (6). https://doi.org/10.1111/cmi.12719.

Stamnes, Mark. 2002. “Regulating the Actin Cytoskeleton during Vesicular Transport.” *Current Opinion in Cell Biology* 14 (4): 428–33. https://doi.org/10.1016/s0955-0674(02)00349-6.

Steinbuechel, Marion, and Kai Matuschewski. 2009. “Role for the *Plasmodium* Sporozoite-Specific Transmembrane Protein S6 in Parasite Motility and Efficient Malaria Transmission.” *Cellular Microbiology* 11 (2): 279–88. https://doi.org/10.1111/j.1462-5822.2008.01252.x.

Stuelten, Christina H., Carole A. Parent, and Denise J. Montell. 2018. “Cell Motility in Cancer Invasion and Metastasis: Insights from Simple Model Organisms.” *Nature Reviews. Cancer* 18 (5): 296–312. https://doi.org/10.1038/nrc.2018.15.

Sturm, Angelika, Rogerio Amino, Claudia van de Sand, Tommy Regen, Silke Retzlaff, Annika Rennenberg, Andreas Krueger, Jörg-Matthias Pollok, Robert Menard, and Volker T. Heussler. 2006. “Manipulation of Host Hepatocytes by the Malaria Parasite for Delivery

into Liver Sinusoids." *Science (New York, N.Y.)* 313 (5791): 1287–90. https://doi.org/10.1126/science.1129720.
Suarez, Catherine, Gaëlle Lentini, Raghavendran Ramaswamy, Marjorie Maynadier, Eleonora Aquilini, Laurence Berry-Sterkers, Michael Cipriano, et al. 2019. "A Lipid-Binding Protein Mediates Rhoptry Discharge and Invasion in Plasmodium Falciparum and Toxoplasma Gondii Parasites." *Nature Communications* 10 (1): 4041. https://doi.org/10.1038/s41467-019-11979-z.
Sultan, Ali A, Vandana Thathy, Ute Frevert, Kathryn J.H Robson, Andrea Crisanti, Victor Nussenzweig, Ruth S Nussenzweig, and Robert Ménard. 1997. "TRAP Is Necessary for Gliding Motility and Infectivity of Plasmodium Sporozoites." *Cell* 90 (3): 511–22. https://doi.org/10.1016/S0092-8674(00)80511-5.
Tachibana, Mayumi, Hideyuki Iriko, Minami Baba, Motomi Torii, and Tomoko Ishino. 2021. "PSOP1, Putative Secreted Ookinete Protein 1, Is Localized to the Micronemes of Plasmodium Yoelii and P. Berghei Ookinetes." *Parasitology International* 84 (October):102407. https://doi.org/10.1016/j.parint.2021.102407.
Talman, Arthur M., Céline Lacroix, Sara R. Marques, Andrew M. Blagborough, Raffaella Carzaniga, Robert Ménard, and Robert E. Sinden. 2011. "PbGEST Mediates Malaria Transmission to Both Mosquito and Vertebrate Host: PbGEST Mediates Malaria Transmission." *Molecular Microbiology* 82 (2): 462–74. https://doi.org/10.1111/j.1365-2958.2011.07823.x.
Tan, Benedict, Suat Peng, Siti Maryam J.M. Yatim, Jayantha Gunaratne, Walter Hunziker, and Alexander Ludwig. 2020. "An Optimized Protocol for Proximity Biotinylation in Confluent Epithelial Cell Cultures Using the Peroxidase APEX2." *STAR Protocols* 1 (2): 100074. https://doi.org/10.1016/j.xpro.2020.100074.
Tavares, Joana, Pauline Formaglio, Sabine Thiberge, Elodie Mordelet, Nico Van Rooijen, Alexander Medvinsky, Robert Ménard, and Rogerio Amino. 2013. "Role of Host Cell Traversal by the Malaria Sporozoite during Liver Infection." *The Journal of Experimental Medicine* 210 (5): 905–15. https://doi.org/10.1084/jem.20121130.
Tewari, Rita, Roberta Spaccapelo, Francesco Bistoni, Anthony A. Holder, and Andrea Crisanti. 2002. "Function of Region I and II Adhesive Motifs of Plasmodium Falciparum Circumsporozoite Protein in Sporozoite Motility and Infectivity." *The Journal of Biological Chemistry* 277 (49): 47613–18. https://doi.org/10.1074/jbc.M208453200.
Thathy, V. 2002. "Levels of Circumsporozoite Protein in the Plasmodium Oocyst Determine Sporozoite Morphology." *The EMBO Journal* 21 (7): 1586–96. https://doi.org/10.1093/emboj/21.7.1586.
Thieleke-Matos, Carolina, Kevin Walz, Friedrich Frischknecht, and Mirko Singer. 2024. "Overcoming the Egress Block of Plasmodium Sporozoites Expressing Fluorescently Tagged Circumsporozoite Protein." *Molecular Microbiology* 121 (3): 565–77. https://doi.org/10.1111/mmi.15230.
Tilley, Leann, Matthew W.A. Dixon, and Kiaran Kirk. 2011. "The Plasmodium Falciparum-Infected Red Blood Cell." *The International Journal of Biochemistry & Cell Biology* 43 (6): 839–42. https://doi.org/10.1016/j.biocel.2011.03.012.
Vaglia, J. L., and B. K. Hall. 1999. "Regulation of Neural Crest Cell Populations: Occurrence, Distribution and Underlying Mechanisms." *The International Journal of Developmental Biology* 43 (2): 95–110.
Vahokoski, Juha, Saligram Prabhakar Bhargav, Ambroise Desfosses, Maria Andreadaki,

Esa-Pekka Kumpula, Silvia Muñico Martinez, Alexander Ignatev, et al. 2014. “Structural Differences Explain Diverse Functions of Plasmodium Actins.” *PLoS Pathogens* 10 (4): e1004091. https://doi.org/10.1371/journal.ppat.1004091.

Valleau, Dylan, Saima M. Sidik, Luiz C. Godoy, Yamilex Acevedo-Sánchez, Charisse Flerida A. Pasaje, My-Hang Huynh, Vern B. Carruthers, Jacquin C. Niles, and Sebastian Lourido. 2023. “A Conserved Complex of Microneme Proteins Mediates Rhoptry Discharge in Toxoplasma.” *The EMBO Journal* 42 (23): e113155. https://doi.org/10.15252/embj.2022113155.

Vanderberg, J. P. 1974. “Studies on the Motility of Plasmodium Sporozoites.” *The Journal of Protozoology* 21 (4): 527–37. https://doi.org/10.1111/j.1550-7408.1974.tb03693.x.

———. 1975. “Development of Infectivity by the Plasmodium Berghei Sporozoite.” *The Journal of Parasitology* 61 (1): 43–50.

Vanderberg, J., and J. Rhodin. 1967. “Differentiation of Nuclear and Cytoplasmic Fine Structure during Sporogonic Development of Plasmodium Berghei.” *The Journal of Cell Biology* 32 (3): C7-10. https://doi.org/10.1083/jcb.32.3.c7.

Vanderberg, Jerome P., and Ute Frevert. 2004. “Intravital Microscopy Demonstrating Antibody-Mediated Immobilisation of Plasmodium Berghei Sporozoites Injected into Skin by Mosquitoes.” *International Journal for Parasitology* 34 (9): 991–96. https://doi.org/10.1016/j.ijpara.2004.05.005.

Vincke, I. H., and J. Bafort. 1968. “[Standardization of the inoculum of Plasmodium berghei sporozoites].” *Annales Des Societes Belges De Medecine Tropicale, De Parasitologie, Et De Mycologie* 48 (2): 181–94.

Vincke, I. H., and M. Lips. 1948. “[A new plasmodium from a wild Congo rodent Plasmodium berghei n. sp].” *Annales De La Societe Belge De Medecine Tropicale (1920)* 28 (1): 97–104.

Vinetz, J. M. 2005. “Plasmodium Ookinete Invasion of the Mosquito Midgut.” *Current Topics in Microbiology and Immunology* 295:357–82. https://doi.org/10.1007/3-540-29088-5_14.

Wang, Qian, Hisashi Fujioka, and Victor Nussenzweig. 2005. “Exit of Plasmodium Sporozoites from Oocysts Is an Active Process That Involves the Circumsporozoite Protein.” Edited by Kasturi Haldar. *PLoS Pathogens* 1 (1): e9. https://doi.org/10.1371/journal.ppat.0010009.

Wang, Zhipeng A., and Philip A. Cole. 2020. “The Chemical Biology of Reversible Lysine Post-Translational Modifications.” *Cell Chemical Biology* 27 (8): 953–69. https://doi.org/10.1016/j.chembiol.2020.07.002.

Wasmuth, James, Jennifer Daub, José Manuel Peregrín-Alvarez, Constance A. M. Finney, and John Parkinson. 2009. “The Origins of Apicomplexan Sequence Innovation.” *Genome Research* 19 (7): 1202–13. https://doi.org/10.1101/gr.083386.108.

Wengelnik, K., R. Spaccapelo, S. Naitza, K. J. Robson, C. J. Janse, F. Bistoni, A. P. Waters, and A. Crisanti. 1999. “The A-Domain and the Thrombospondin-Related Motif of Plasmodium Falciparum TRAP Are Implicated in the Invasion Process of Mosquito Salivary Glands.” *The EMBO Journal* 18 (19): 5195–5204. https://doi.org/10.1093/emboj/18.19.5195.

White, Nicholas J. 2018. “Anaemia and Malaria.” *Malaria Journal* 17 (1): 371. https://doi.org/10.1186/s12936-018-2509-9.

Whittaker, Charles A., and Richard O. Hynes. 2002. “Distribution and Evolution of von Willebrand/Integrin A Domains: Widely Dispersed Domains with Roles in Cell Adhesion

and Elsewhere." *Molecular Biology of the Cell* 13 (10): 3369–87. https://doi.org/10.1091/mbc.e02-05-0259.
Yahata, Kazuhide, Melissa N. Hart, Heledd Davies, Masahito Asada, Samuel C. Wassmer, Thomas J. Templeton, Moritz Treeck, Robert W. Moon, and Osamu Kaneko. 2021. "Gliding Motility of *Plasmodium* Merozoites." *Proceedings of the National Academy of Sciences* 118 (48): e2114442118. https://doi.org/10.1073/pnas.2114442118.
Yamauchi, Lucy Megumi, Alida Coppi, Georges Snounou, and Photini Sinnis. 2007. "Plasmodium Sporozoites Trickle out of the Injection Site." *Cellular Microbiology* 9 (5): 1215–22. https://doi.org/10.1111/j.1462-5822.2006.00861.x.
Yan, Ming, Richard F. Collins, Sergio Grinstein, and William S. Trimble. 2005. "Coronin-1 Function Is Required for Phagosome Formation." *Molecular Biology of the Cell* 16 (7): 3077–87. https://doi.org/10.1091/mbc.e04-11-0989.
Yi, Meiqi, Jian Sun, Hanzi Sun, Yifei Wang, Shan Hou, Beibei Jiang, Yuanyuan Xie, et al. 2023. "Identification and Characterization of an Unexpected Isomerization Motif in CDRH2 That Affects Antibody Activity." *mAbs* 15 (1): 2215364. https://doi.org/10.1080/19420862.2023.2215364.

8. Appendix

8.1 TRAP could not be functionally tagged at the C-terminus

The TRAP C-terminus plays a critical role in interacting with the acto-myosin cytoskeleton beneath the parasite plasma membrane. However, its direct interaction partners remain unidentified. To address this, efforts were made to tag TRAP at the C-terminus to gain insights into its binding partners. Previous attempts at C-terminal tagging were unsuccessful, likely due to the essential interactions occurring at this region (S. Kappe et al. 1999; Matuschewski et al. 2002).

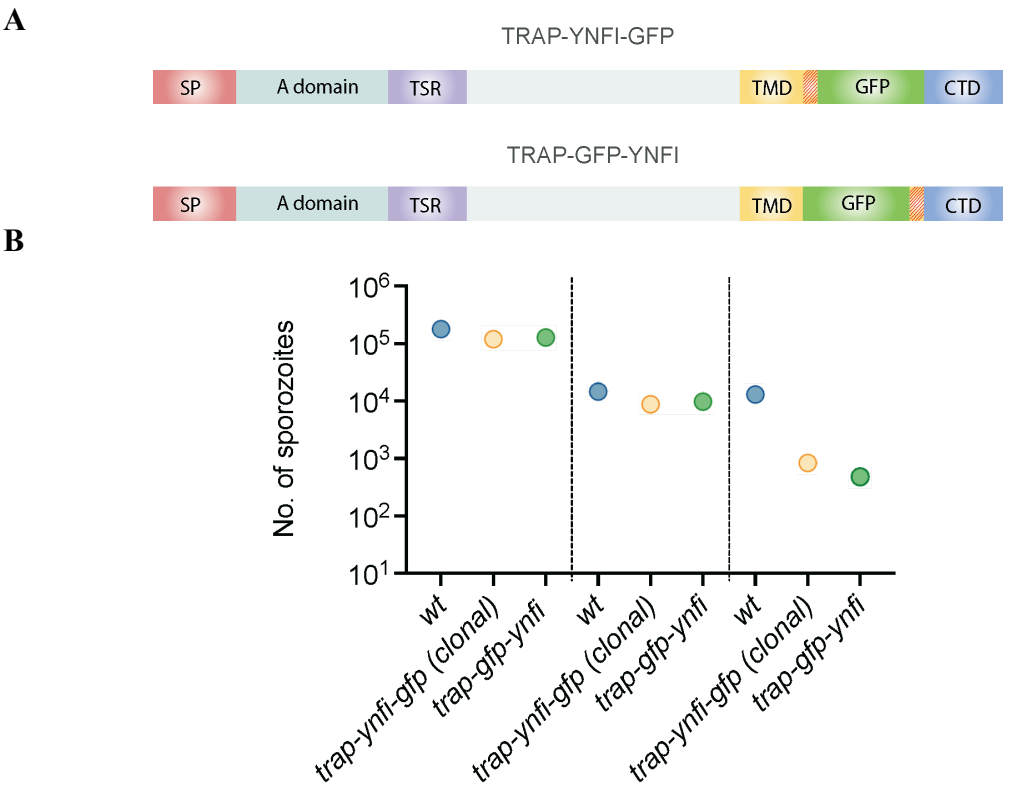

Figure: 8.1. TRAP could not be successfully tagged at the C-terminus.

A. Schematic representation of TRAP-YNFI-GFP and TRAP-GFP-YNFI. The red dashed part downstream of the TMD indicates micronemal sorting sequence YXXφ (φ = hydrophobic residue). B. Total numbers of sporozoites in midgut, hemolymph and salivary gland of various

C-terminus tagged mutants; Each dot represents an average number of sporozoites calculated from mosquitoes dissected from 1 cage feed. (Data from 1 cage)

To overcome the challenges of C-terminal tagging, *trap-ynfi-gfp* and *trap-gfp-ynfi* parasite lines were generated, where a GFP tag was inserted directly upstream of the C-terminal domain. In the *trap-ynfi-gfp* line, the tag was placed downstream of the micronemal sorting sequence (YXXφ, where φ represents a hydrophobic residue), whereas in the *trap-gfp-ynfi* line, the tag was positioned immediately after the sorting sequence with a short linker on both sides of the GFP tag (Fig: 8.1. A). The micronemal sorting sequence is known to be crucial for the correct localization of TRAP and disruption of the signal resulted in decreased infectivity (Matuschewski et al. 2002).

For generating *trap-ynfi-gfp* and *trap-gfp-ynfi* parasite lines, the Pb268_Pbtheo_PbTRAP_transf_Vector, an intermediate vector containing the entire *trap* ORF (borrowed from Kevin Walz) was used with the help of master students Nina Schmidt and Marzia Matejcek. A four fragment gibson assembly was used to clone three PCR amplified fragments entailed either 2665 bp (*trap-gfp-ynfi*) or 2684 bp *trap* ORF (*trap-ynfi-gfp*) depending on whether it contained the micronemal sorting sequence YXXI or not, a 771 bp long *egfp* sequence that was cloned either upstream (*trap-gfp-ynfi*) or downstream(*trap-ynfi-gfp*) of the micronemal sorting sequence and a 1086 bp long sequence encoding the rest of the *trap* ORF and its 3'UTR. The sequence encoding *egfp* was amplified from the Pb238::TRP1 TMD-GFP vector. The final vectors, Pb268_Pbtheo_PbTRAP::YNFI_GFP and Pb268_Pbtheo_PbTRAP::GFP_YNFI were digested (*Sac*II and *Hind*III), purified and transfected into *wt* parasites and isogenic populations were generated for *trap-ynfi-gfp* parasite line while a mixed population was generated for *trap-gfp-ynfi* for further experiments.

However, both attempts at tagging TRAP at the C-terminus were futile since the hemolymph sporozoites from both *trap-ynfi-gfp* and *trap-gfp-ynfi* parasite lines showed severe defects in salivary gland invasion (Fig: 8.1. B). This highlights the importance of the transmembrane domain including the micronemal sorting sequence along with the C-terminus in the function of *Pb*TRAP.

8.2 Expression Profiles of Uncharacterized Proteins Identified by MS Analysis of APEX-Based Proximity Labeling in *trp1-apex* Sporozoites

1. PBANKA_1417200

   AlphaFold3 structure prediction:

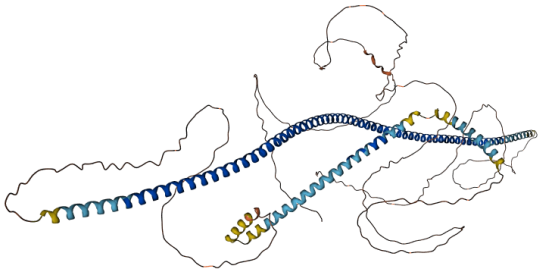

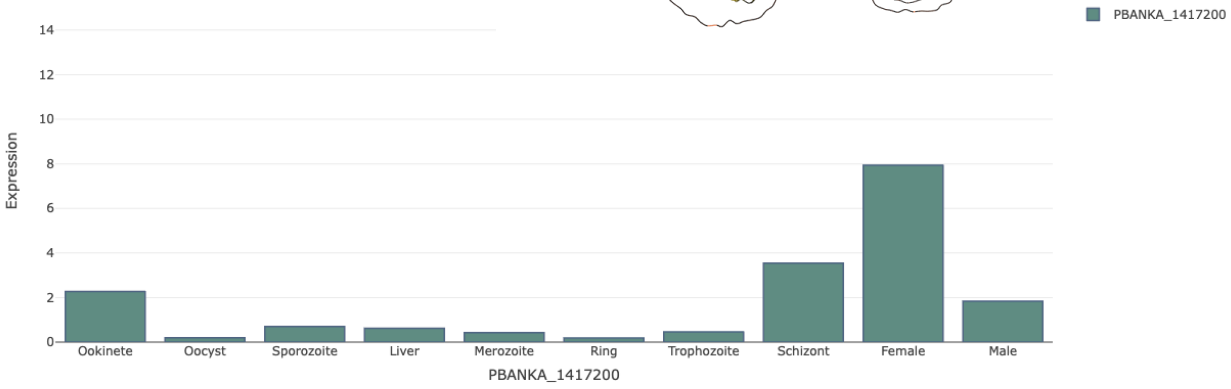

2. PBANKA_0206700

   AlphaFold3 structure prediction:

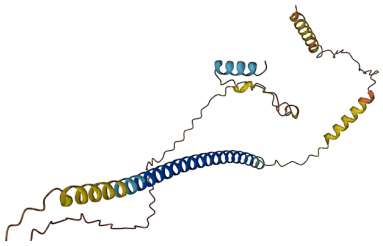

RNAseq Profile

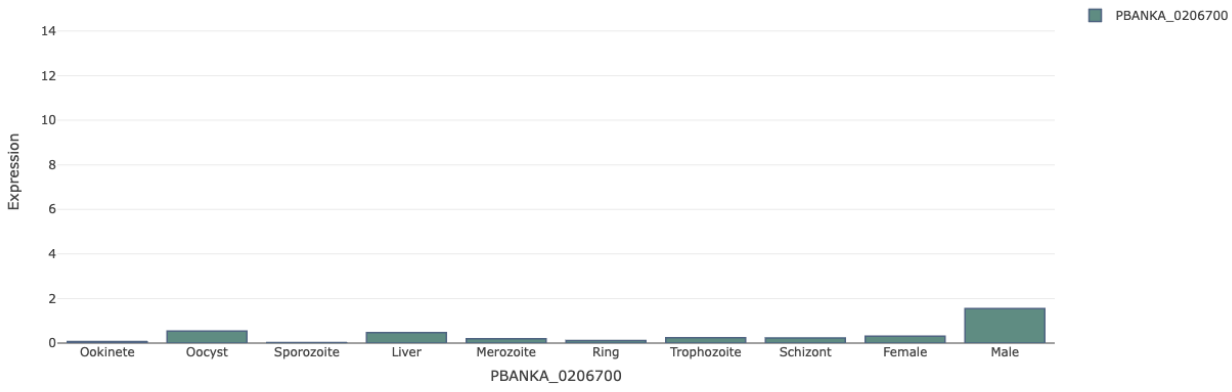

3. PBANKA_0931100

AlphaFold3 structure prediction:

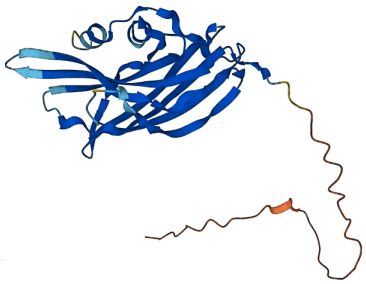

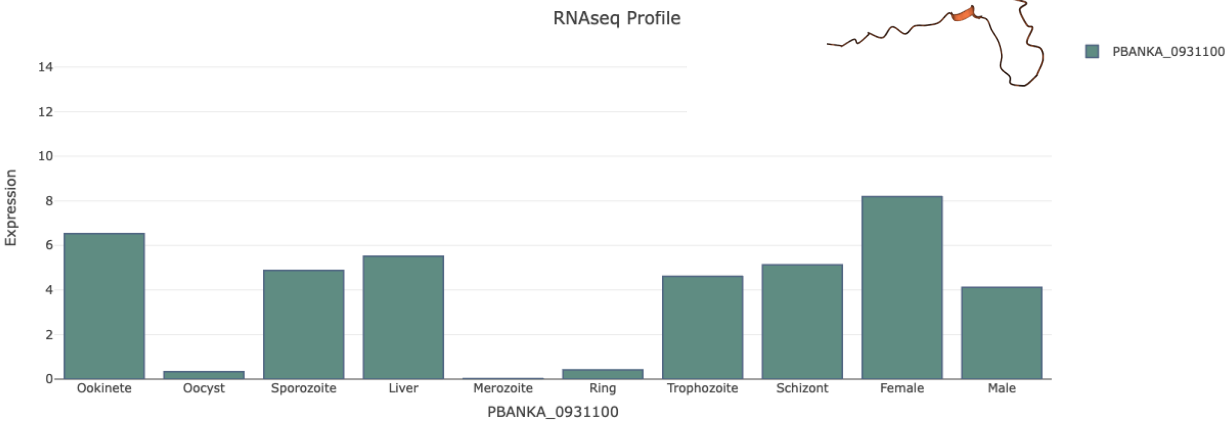

4. PBANKA_1034500

AlphaFold3 structure prediction:

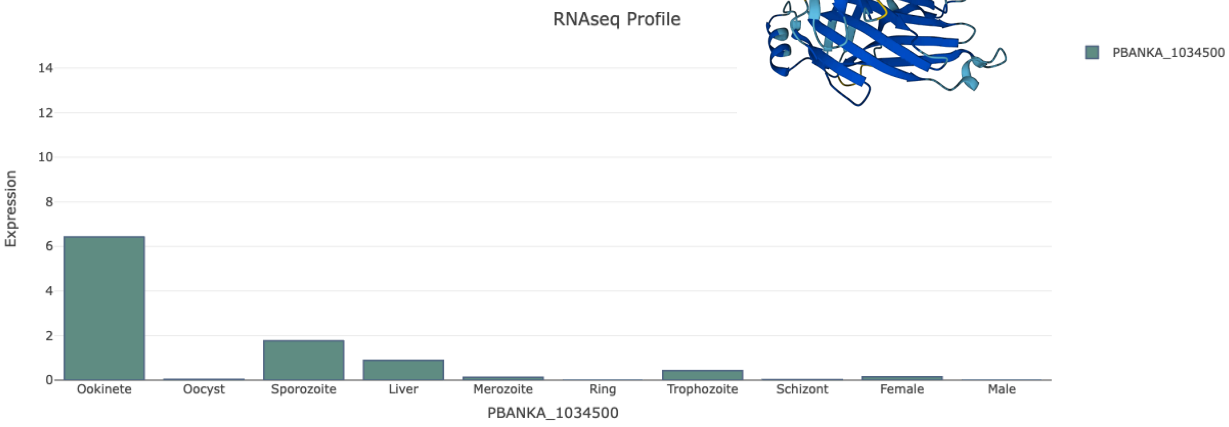

5. PBANKA_1233700

AlphaFold3 structure prediction:

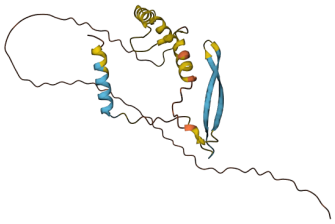

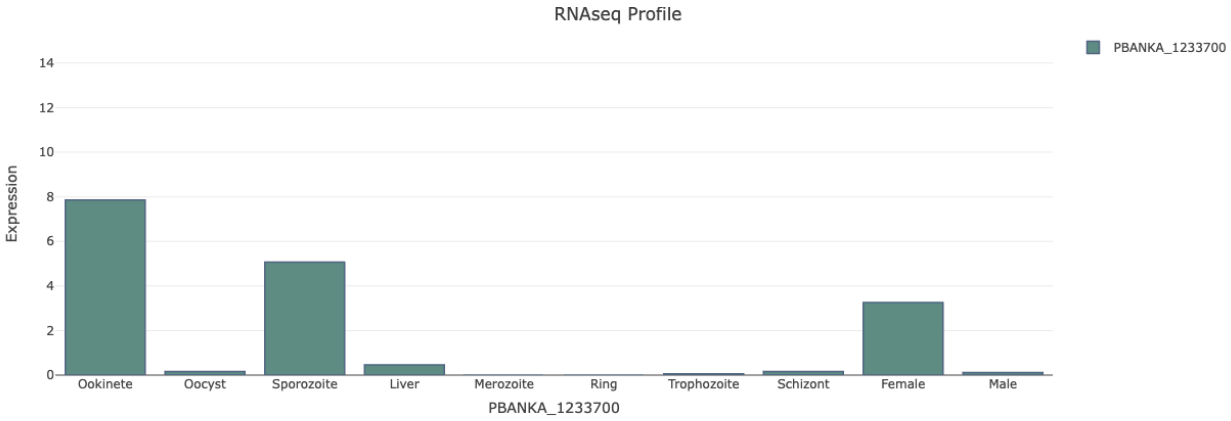

6. PBANKA_0902700

AlphaFold3 structure prediction:

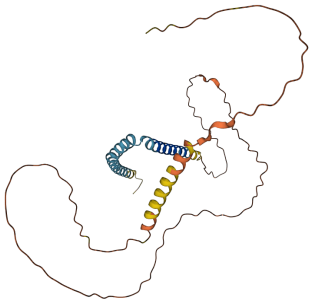

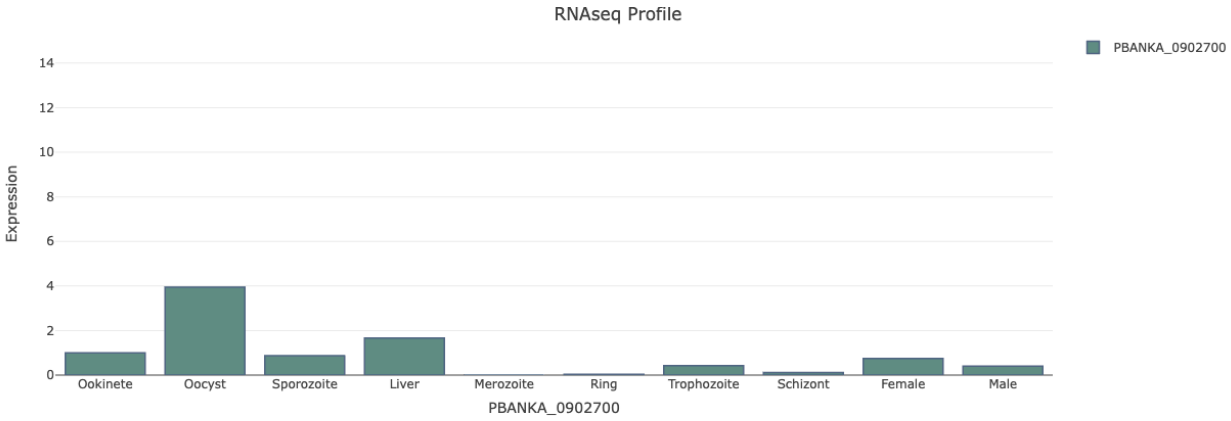

7. PBANKA_0306600

AlphaFold3 structure prediction:

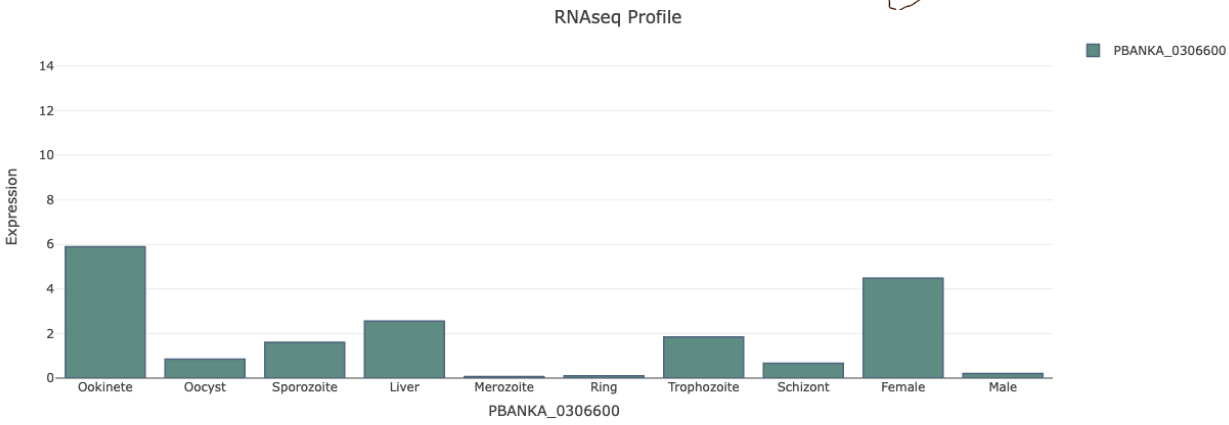

8. PBANKA_0620800

AlphaFold3 structure prediction:

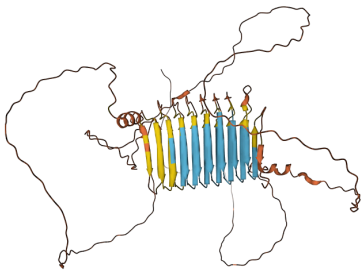

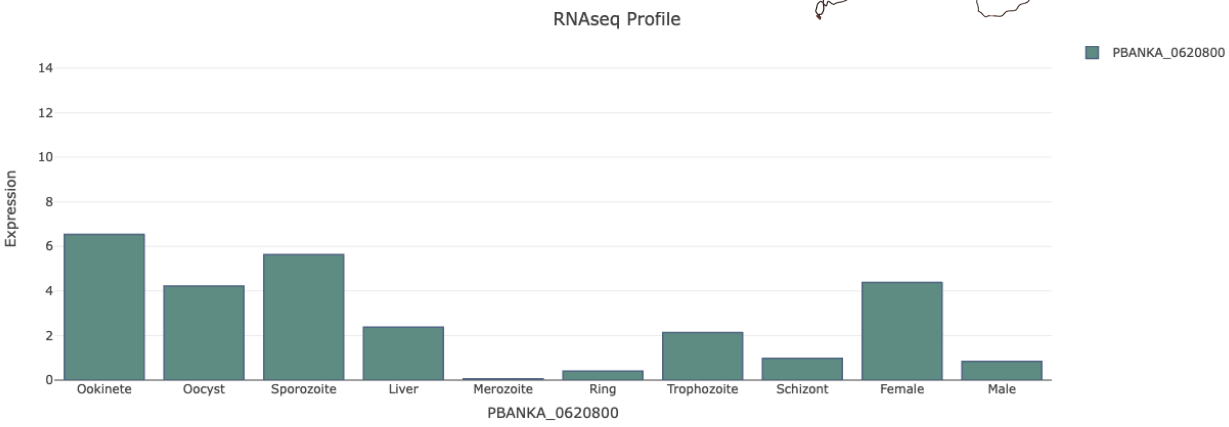

9. PBANKA_1120100

AlphaFold3 structure prediction: N/A

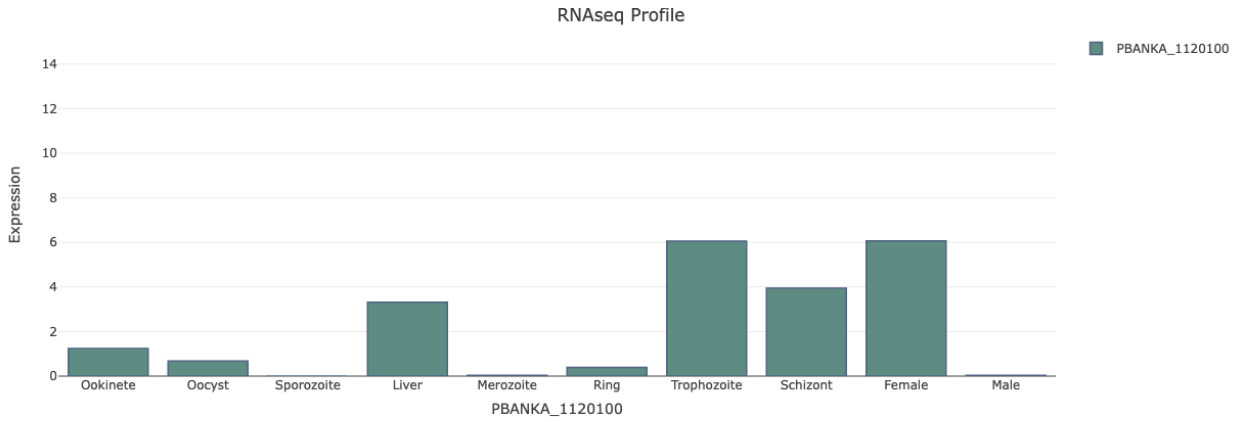

8.3 Primer list

No.	Old Primer name	New Primer name	Primer sequence
1	SacII_TRP1_Fwd	MRC P1	AATTCCGCGGGATGATAATTGCACTTATTTTGAT
2	BamHI_TRP_Del1_Rev	MRC P2	ATTTGGATCCTTATGTTTCAGTTTGTACATATTTTTTTTC
3	P885 DK059 (Dennis)	MRC P3	ATGTATCGAATTATATTCTTCTTTATTTCATTG
4	P1619 PbDHFS AgeI rev (Julia)	MRC P4	CCCACCGGTGCTTTTTCACGTATATTTTTTTGTTAC
5	P234 ef1arev51AgeI	MRC P5	CTTGCACCGGTTTTTATAAAATTTTTATTTATTTATAAGC
6	P609 DK030 (Dennis)	MRC P6	GTAGCTCGAGCATCTACTACTCATAATACACTTAGTGGAAGTACG
7	P1618 PbDHFS NheI for (Julia)	MRC P7	CCCGCTAGCCCTAGCTAAAAGGTGTGCAAG
8	P2031 EcoRI_NcoI_hDHFR_for (Johanna) for complement	MRC P8	CGGGAATTCAAACCATGGTTGGTTCGCT
9	5' HR2	MRC P9	GGAAAAAAATAAAATGATATACAACTATAGCATGG
10	BamHI_TRP1_Del2_Rev	MRC P10	ATTTGGATCCTTATATGGTATCTGTAATTATATCATTTTCAG
11	newdel1rev	MRC P11	ATTGGATCCTTAATATTTTTTTTCATTTTGAG
12	TRP1gDNA_SACII_fwd	MRC P12	AATCCGCGGATGTATCGAATTATATTCTTCTTTATTTCATTG

13	TRP1gDNA_BamH1_rev	MRC P13	AACGGATCCTTAATCTTTCTTTATGGTATCTGTAATTATATC
14	TRP1_gib1_fwd	MRC P14	AATGATATACAACTATAGCATGG
15	TRP1_TMD_iGFP_rev	MRC P15	TTCTCCTTTACTCATTCCTCCGACAATTAAATAAACAAGAT
16	TRP1_TMD_iGFP_gib2fwd	MRC P16	TATCTTGTTTATTTAATTGTCGGAGGAATGAGTAAAGGAGAAGAACTTTTC
17	TRP1_TMD_iGFP_gib2_rev	MRC P17	CTTTATATTTTATAATTTCTTTTCCTCCTTTGTATAGTTCATCCATGCC
18	gibson3	MRC P18	TGTATGAAATTACTTTTAAACG
19	TRP1_TMD_iGFP_gib3fwd	MRC P19	CATGGATGAACTATACAAAGGGGAGGAAAAGAAATTATAAAATATAAAG
20	TRP1-Flag1-F1rev	MRC P20	CCGCATCGTGGTCCTTATAATCGACAATACCATGATTATTTGGA
21	TRP1-Flag1-F2 fwd	MRC P21	TGATCCAAATAATCATGGTATTGTCGATTATAAGGACCACGATGG
22	TRP1-Flag1-F2 rev	MRC P22	ACATTTTATTTTTGTATGTTTACACAACTTATCGTCATCGTCCTTATAA
23	TRP1-Flag1-F3 fwd	MRC P23	CGATTATAAGGACGATGACGATAAGTTGTGTAAACATACAAAAATAAAATGT
24	TRP1 Flag2 F1 rev	MRC P24	CGCCATCGTGGTCCTTATAATCAGTGCAATTATCATCAAAATATTT
25	TRP1 Flag2 F2 fwd	MRC P25	AAATATTTTGATGATAATTGCACTGATTATAAGGACCACGATGG
26	TRP1 Flag2 F2 rev	MRC P26	ACCATGATTATTTGGATCAAAATACTTATCGTCATCGTCCTTATAA
27	TRP1 Flag2 F3 fwd	MRC P27	CGATTATAAGGACGATGACGATAAGTATTTTGATCCAAATAATCATGG
28	Gibfwd1	MRC P28	TAAAATGATATACAACTATAGC
29	gib2	MRC P29	CTACTTCCTGCTATAAAATTTTCTTTGACAATTAAATAAAC
30	Forward_insert	MRC P30	GTTTATTTAATTGTCAAAGAAAATTTTATAGCAGGAAGTAGC
31	Reverse_insertedited	MRC P31	GGGCTTGCACACCTTTTAGCTATTAGTTCCAGTCATTATCTTC
32	gibson4	MRC P32	GAAGATAATGACTGGAACTAATAGCTAAAAGGTGTGCAAG
33	Primer 1	MRC P33	GTTTATTTAATTGTCAAAGAAAAGTGGCATATTTTTAAATTACTC
34	Primer 2	MRC P34	GCTTGCACACCTTTTAGCTATTAGTATGATTTTTTTTTGTTTTG
35	trialgib1rev	MRC P35	TTCTCCTTTACTCATTCCTCCATTACATTTTATTTTTGTATG
36	trialgfpfwd1	MRC P36	CATACAAAAATAAAATGTAATGGAGGAATGAGTAAAGGAGAAGAACTTTTC
37	trial2	MRC P37	CAATCTGACCAAGAACTAAAtcctccTTTGTATAGTTCATCCATGCC
38	TRP1_gib3_fwd	MRC P38	GGAGGATTTAGTTCTTGGTCAGATTG
39	F1 mTurbo TRP1 rev	MRC P39	GTTTAGCGTTCAGCAGCGGGATTCCTCCGACAATTAAATAAACAAG
40	F2 MTurboTRPfwd	MRC P40	GATATATCTTGTTTATTTAATTGTCGGAGGAATCCCGCTGCTGAACGCTAAAC
41	F2 mTurboTRP rev	MRC P41	CTTTATATTTTATAATTTCTTTTCCTCCCTTTTCGGCAGACCGCAGACTG
42	F3 mTurboTRP fwd	MRC P42	CAGTCTGCGGTCTGCCGAAAAGGGAGGAAAAGAAATTATAAAATATAAAG
43	F1 rev apex TRP1	MRC P43	CACAGTTGGGTAAGACTTTCCTCCTCCGACAATTAAATAAACAAGAT
44	F2 fwd APEX TRP1	MRC P44	TATCTTGTTTATTTAATTGTCGGAGGAGGAAAGTCTTACCCAACTGTG
45	F2 rev APEX TRP1	MRC P45	CTTTATATTTTATAATTTCTTTTCCTCCGGCATCAGCAAACCCAAGC
46	F3 fwd TRP1 APEX	MRC P46	GCTTGGGTTTGCTGATGCCGGAGGAAAAGAAATTATAAAATATAAAG
47	TSRp-F1-rev	MRC P47	CATGATTTAGTACATTCTGAGGCATCTGATGCAGAACTAAAATTA

			CATTTTATTTTTGT
48	TSRp-F2-fwd	MRC P48	CAAAAATAAAATGTAATTTTAGTTCTGCATCAGATGCCTCAGAATGTACTAAATCATG
49	TSRs-F3-fwd	MRC P49	GTAAGGTTCGTGATTGCCCAGATATAAATGATTCAAATAAAGAAGTTAC
50	TSRs-F1-rev	MRC P50	CCATTCTTCCCATTTTCCACAATTACATTTTATTTTTGTATGTTTACAC
51	TSRs-F2-fwd	MRC P51	GTGTAAACATACAAAAATAAAATGT AATTGTGGAAAATGGGAAGAATGG
52	TSR Point F1 rev	MRC P52	CATGATTTAGTACATTCTGAGGCATCTGATGCAGAACTAAAATTA CATTTTATTTTTGTTTACATTTTATTTTTG
53	TSR point F2 fwd	MRC P53	CAAAAATAAAATGTAATTTTAGTTCTGCATCAGATGCCTCAGAATGTACTAAATCATG
54	TSR Gib F1 fwd	MRC P54	AATGATATACAACTATAGCATGG
55	TSR Gib F2 fwd	MRC P55	GTGTAAACATACAAAAATAAAATGTAATGATATAAATGAT
56	TSR gib F1 rev	MRC P56	GTAACTTCTTTATTTGAATCATTTATATCATTACATTTTATTTTTGTATGTTTACAC